frontiers | Research Topics

Three-way interactions between host, environment, and microbiome: Importance of microbiology in the one health

Edited by
Ruixin Zhu, Na Li, Yongxu Lu, Weiwei Cui, Dong Li and Yuan Xiao

Published in
Frontiers in Microbiology

ISSN 1664-8714
ISBN 978-2-83252-091-8
DOI 10.3389/978-2-83252-091-8

About Frontiers

Frontiers is more than just an open access publisher of scholarly articles: it is a pioneering approach to the world of academia, radically improving the way scholarly research is managed. The grand vision of Frontiers is a world where all people have an equal opportunity to seek, share and generate knowledge. Frontiers provides immediate and permanent online open access to all its publications, but this alone is not enough to realize our grand goals.

Frontiers journal series

The Frontiers journal series is a multi-tier and interdisciplinary set of open-access, online journals, promising a paradigm shift from the current review, selection and dissemination processes in academic publishing. All Frontiers journals are driven by researchers for researchers; therefore, they constitute a service to the scholarly community. At the same time, the *Frontiers journal series* operates on a revolutionary invention, the tiered publishing system, initially addressing specific communities of scholars, and gradually climbing up to broader public understanding, thus serving the interests of the lay society, too.

Dedication to quality

Each Frontiers article is a landmark of the highest quality, thanks to genuinely collaborative interactions between authors and review editors, who include some of the world's best academicians. Research must be certified by peers before entering a stream of knowledge that may eventually reach the public - and shape society; therefore, Frontiers only applies the most rigorous and unbiased reviews. Frontiers revolutionizes research publishing by freely delivering the most outstanding research, evaluated with no bias from both the academic and social point of view. By applying the most advanced information technologies, Frontiers is catapulting scholarly publishing into
a new generation.

What are Frontiers Research Topics?

Frontiers Research Topics are very popular trademarks of the *Frontiers journals series*: they are collections of at least ten articles, all centered on a particular subject. With their unique mix of varied contributions from Original Research to Review Articles, Frontiers Research Topics unify the most influential researchers, the latest key findings and historical advances in a hot research area.

Find out more on how to host your own Frontiers Research Topic or contribute to one as an author by contacting the Frontiers editorial office:
frontiersin.org/about/contact

Three-way interactions between host, environment, and microbiome: Importance of microbiology in the one health

Topic editors

Ruixin Zhu — Tongji University, China
Na Li — Hainan Medical University, China
Yongxu Lu — University of Cambridge, United Kingdom
Weiwei Cui — Jilin University, China
Dong Li — Jilin University, China
Yuan Xiao — Shanghai Jiao Tong University, China

Citation

Zhu, R., Li, N., Lu, Y., Cui, W., Li, D., Xiao, Y., eds. (2023). *Three-way interactions between host, environment, and microbiome: Importance of microbiology in the one health*. Lausanne: Frontiers Media SA. doi: 10.3389/978-2-83252-091-8

Table of contents

frontiers | Frontiers in Microbiology

TYPE Editorial
PUBLISHED 21 March 2023
DOI 10.3389/fmicb.2023.1177119

OPEN ACCESS

EDITED AND REVIEWED BY
Axel Cloeckaert,
Institut National de recherche pour l'agriculture, l'alimentation et l'environnement (INRAE), France

*CORRESPONDENCE
Weiwei Cui
✉ cuiweiwei@jlu.edu.cn
Na Li
✉ 28914358@qq.com

SPECIALTY SECTION
This article was submitted to Infectious Agents and Disease, a section of the journal Frontiers in Microbiology

RECEIVED 01 March 2023
ACCEPTED 06 March 2023
PUBLISHED 21 March 2023

CITATION
Wu C, Zhu R, Lu Y, Li D, Xiao Y, Cui W and Li N (2023) Editorial: Three-way interactions between host, environment, and microbiome: Importance of microbiology in the One Health. *Front. Microbiol.* 14:1177119. doi: 10.3389/fmicb.2023.1177119

Editorial: Three-way interactions between host, environment, and microbiome: Importance of microbiology in the One Health

Caihong Wu[1], Ruixin Zhu[2], Yongxu Lu[3], Dong Li[4], Yuan Xiao[5], Weiwei Cui[1]* and Na Li[6]*

[1]Department of Nutrition and Food Hygiene, School of Public Health, Jilin University, Changchun, China, [2]Department of Bioinformatics, School of Life Sciences and Technology, Tongji University, Shanghai, China, [3]Department of Pathology, University of Cambridge, Cambridge, United Kingdom, [4]Department of Immunology, College of Basic Medical Sciences, Jilin University, Changchun, China, [5]Department of Pediatrics, Ruijin Hospital, Shanghai Jiao Tong University School of Medicine, Shanghai, China, [6]School of Tropical Medicine, The Second Affiliated Hospital, Hainan Medical University, Haikou, China

KEYWORDS

microbiome, host health and disease, environmental, interactions, One Health

Editorial on the Research Topic
Three-way interactions between host, environment, and microbiome: Importance of microbiology in the One Health

The microbiome is burgeoning as one of the new frontiers in the field of biomedical research. The potential of research is as colossal and varied as the microbes in these communities. Microbes such as viruses, bacteria, prions, and fungi as disease vectors have been intensively studied in recent years, contributing to great advances in medicine. As research on gut microbes has progressed, microbes have generally come to be considered as closely related to hosts and as having a vital role in maintaining human health, ranging from digestive functions to nutrient uptake, and regulating the immune response. However, little research has examined the role of microbes in host health in certain environments. There is a huge knowledge gap as to how the microorganisms, environment, and host interact with each other and what the results are.

Microbiology continues to attract the attention of ecologists and medical scientists, resulting in the stimulation of numerous initiatives to study the effects of the microbiome on host health in different microenvironments. In this Research Topic, "*Three-way interactions between host, environment, and microbiome: Importance of microbiology in the One Health,*" a total of nine articles were published, covering a variety of topics that involve a variety of microbes in different microenvironments, including bacteria in the tumor microenvironment, the microbiota of different anatomical sites (nasopharyngeal, oropharyngeal, lung, and gut), and the discovery of novel, bioactive functional substances such as a microsatellite DNA-derived oligodeoxynucleotide, hypothetical protein FoDbp40, and *Stenotrophomonas maltophilia*. Moreover, the synergy of the microbiome was reported, focusing on the effects of the regulation of intestinal flora in conjunction with drug use on host health.

In recent times, research on the microbiome has evolved from the culture of intestinal and oral microbiota to a mechanistic comprehension of the host–microbiome connection and a microbiome map of all the niches in the body. Xu et al. discussed the diversity and specificity of bacteria in different cancers. The amount and multiformity of bacteria in breast tumor samples were greater than in normal breast samples. In contrast, the microbiome of lung cancer tissue changed less than that of the corresponding normal tissue. A particular bacterium, *Helicobacter pylori*, has been associated with stomach cancer and specified by the World Health Organization as a class I carcinogen; however, no conclusive results on the potential role of other bacterial species in most cancer types have been reported. Many challenges remain in the identification of tumor-specific bacteria. Xu et al. further reviewed the connection between macrophages and bacteria in cancer. Bacteria may multiply in macrophages and control them *via* a variety of interference tactics. Macrophage polarization seems to be an intermediate procedure activated by some signals during tumorigenesis and regression. Macrophages show diverse phenotypes in response to multiple stimuli that act on various receptors and thus play a regulatory role through multiple signaling pathways. Chen et al. also focused on microbiomes at different anatomical sites. Chen et al. analyzed the gut and respiratory tract (oropharynx, nasopharynx, and lung) microflora of normal and influenza A virus (IAV)-infected mice and compared the microflora structure on diverse mucosal surfaces. It was shown that the pulmonary flora of healthy mice was mainly nasopharyngeal, and IAV infection could increase the microbiota similarity between the lungs and nasopharynx. Importantly, *Lactobacillus murinus* was identified as a biomarker for IAV infection, because its abundance was decreased in all ecological niches.

Fusarium oxysporum, a fungus existing in the environment that can infect crops such as cotton, rice, and wheat, is also an important opportunistic pathogen of humans, which seriously affects food safety and human health (Kazan and Gardiner, 2018; Alkatan and Al-Essa, 2019; Zhu et al., 2021). The study of Zhao et al. indicated that the gene encoding isocitrate lyase is a pivotal element that affects the growth of *Fusarium oxysporum*, and FoDbp40 protein could regulate the activity of isocitrate lyase, affect the ATP level and the AMPK/mTOR pathways, and consequently regulate *Fusarium oxysporum* virulence and growth. Dai et al. reviewed various toll-like receptors (TLRs) that are involved in the immunopathogenesis of severe acute respiratory syndrome coronavirus 2 (SARS-CoV-2) infection. Dai et al. made clear the potential application value of the application of TLR immunomodulators in patients with coronavirus disease 2019 (COVID-19). Some viruses and fungi living in the natural environment, and likewise environmental factors such as smoking and exposure to chemicals, may cause changes in the composition and structure of an organism's microbiome that can affect host health. Shen et al. demonstrated an observable augmentation of the genus *Stenotrophomonas* in lung adenocarcinoma (LADC) tissues of non-smoking patients with a primary tumor size greater than 3 cm. Shen et al. further found that *Stenotrophomonas* treatment drove inflammation and upregulated tumor-associated cell signaling in the nitrosamines 4-(methylnitrosamino)-1-(3-pyridyl)-1-butanone-induced lung cancer mouse model. In addition, histone deacetylase 5 gene expression was significantly upregulated in *Stenotrophomonas*-treated groups and was required for *Stenotrophomonas*-induced cell proliferation and migration in LADC cell line A549. Zhang et al. previously designed an oligodeoxynucleotide (named MS19) with six AAAG repeated units based on human microsatellite DNA sequences. Zhang et al. demonstrated that MS19 inhibited pathogen-associated molecular patterns-induced inflammatory responses *in vitro* and *in vivo*. This inhibition is related to nuclear factor kappa B signal transduction but not to mitogen-activated protein kinase transduction. Moreover, Li et al. found that guanylate-binding protein 5 (GBP5) is highly expressed in the colonic immune cells of inflammatory bowel disease (IBD) patients. Induction of GBP5 is required for the stimulated production of proinflammatory cytokines and chemokines, while GBP5 deficiency decreases the expression of the proinflammatory mediators. These results suggest that targeting GBP5 may be an effective strategy for IBD management.

Exposure to radiation, heat and cold stimulation, animal fur, pollen, chemicals, parasites, and other aspects of the environment may cause human skin inflammation and even skin diseases. However, it is not clear whether the progression of skin diseases is connected with the changes in human microbes. Liu et al. analyzed changes of the intestinal flora in stool samples from melasma patients and healthy subjects by 16S rRNA sequencing, observing that many significantly different microbiomes are closely related to beta-glucuronidase production and the regulation of estrogen metabolism. These findings imply that changes of the gut microbiota structure in melasma patients can play an important role in the occurrence and development of melasma by affecting the body's estrogen metabolism.

Either Shugan decoction (SGD) or fecal microbiota transplantation (FMT) can alleviate the symptoms of irritable bowel syndrome (IBS) in patients and animal models. However, the synergistic effect of FMT and SGD on IBS symptoms is not clear. Meng et al. conducted relevant research and found that SGD and FMT had no synergistic effect on water avoidance stress (WAS)-induced IBS model rats. It was suggested that the metabolites of intestinal microbiota may be the main active substances of the FML derived from normal rats to alleviate WAS-induced IBS symptoms.

Taken together, these studies provide crucial insights into the interactions between the microbiota change, environment, and host health and emphasize the potential of a microsatellite DNA-derived oligodeoxynucleotide, hypothetical protein FoDbp40, and *Stenotrophomonas maltophilia*. However, the mechanisms behind these phenomena need to be further studied. Moreover, future research should also focus on the role of extreme environmental conditions, such as extreme temperatures and ultraviolet radiation, in shaping the multiniche microbiome and its consequence to host health. Overall, the studies have provided increasing evidence on the importance of the microbiome and highlighted the need for further research into the interactions between the host, environment, and microbiome.

Author contributions

All authors listed have made a substantial, direct, and intellectual contribution to the work and approved it for publication.

Conflict of interest

The authors declare that the research was conducted in the absence of any commercial or financial relationships that could be construed as a potential conflict of interest.

Publisher's note

References

Alkatan, H. M., and Al-Essa, R. S. (2019). Challenges in the diagnosis of microbial keratitis: a detailed review with update and general guidelines. *Saudi. J. Ophthalmol.* 33, 268–276. doi: 10.1016/j.sjopt.2019.09.002

Kazan, K., and Gardiner, D. M. (2018). Fusarium crown rot caused by *Fusarium pseudograminearum* in cereal crops: recent progress and future prospects. *Mol. Plant. Pathol.* 19, 1547–1562. doi: 10.1111/mpp.12639

Zhu, Y., Abdelraheem, A., Lujan, P., Idowu, J., Sullivan, P., Nichols, R., et al. (2021). Detection and characterization of Fusarium Wilt (*Fusarium oxysporum* f. sp. vasinfectum) race 4 causing fusarium wilt of cotton seedlings in New Mexico. *Plan. Dis.* 105, 3353–3367. doi: 10.1094/PDIS-10-20-2174-RE

frontiers | Frontiers in Microbiology

ORIGINAL RESEARCH
published: 02 June 2022
doi: 10.3389/fmicb.2022.926915

The Proinflammatory Role of Guanylate-Binding Protein 5 in Inflammatory Bowel Diseases

Yichen Li[1†], Xutao Lin[2†], Wenxia Wang[1†], Wenyu Wang[1], Sijing Cheng[1,3], Yibo Huang[1], Yifeng Zou[1], Jia Ke[1‡] and Lixin Zhu[1*‡]*

[1] Guangdong Provincial Key Laboratory of Colorectal and Pelvic Floor Diseases, Department of Colorectal Surgery, The Sixth Affiliated Hospital, Guangdong Institute of Gastroenterology, Sun Yat-sen University, Guangzhou, China, [2] Guangdong Provincial Key Laboratory of Colorectal and Pelvic Floor Diseases, Department of Gastrointestinal Endoscopy, The Sixth Affiliated Hospital, Guangdong Institute of Gastroenterology, Sun Yat-sen University, Guangzhou, China, [3] School of Medicine, Sun Yat-sen University, Shenzhen, China

OPEN ACCESS

Edited by:
Na Li,
Hainan Medical University, China

Reviewed by:
Haiyan Song,
Shanghai University of Traditional Chinese Medicine, China
Jian Lin,
Affiliated Hospital of Putian University, China
Ioanna Aggeletopoulou,
University of Patras, Greece

***Correspondence:**
Jia Ke
kjia@mail.sysu.edu.cn
Lixin Zhu
zhulx6@mail.sysu.edu.cn

[†]These authors have contributed equally to this work and share first authorship

[‡]These authors share last authorship

Specialty section:
This article was submitted to Infectious Agents and Disease, a section of the journal Frontiers in Microbiology

Received: 23 April 2022
Accepted: 09 May 2022
Published: 02 June 2022

Citation:
Li Y, Lin X, Wang W, Wang W, Cheng S, Huang Y, Zou Y, Ke J and Zhu L (2022) The Proinflammatory Role of Guanylate-Binding Protein 5 in Inflammatory Bowel Diseases. Front. Microbiol. 13:926915. doi: 10.3389/fmicb.2022.926915

NLRP3 inflammasome is implicated in the pathogenesis of inflammatory bowel diseases (IBD). Since guanylate-binding protein 5 (GBP5) induces the NLRP3 inflammasome activity, we aim to investigate the potential role of GBP5 in IBD pathogenesis. The expression of GBP5, NLRP3 inflammasome, and related cytokines and chemokines was examined in two cohorts of IBD patients and healthy controls, by microarray transcriptome analysis and quantitative real-time PCR. Cellular localization of GBP5 in colonic biopsies was examined by immunohistochemistry and immunofluorescence with confocal microscopy. For functional studies, *GBP5* was induced by interferon γ or silenced by siRNA or CRISPR/CAS9 technique, and inflammatory activities were evaluated at mRNA and protein levels. We found that the expression of *GBP5* was elevated in colonic mucosa in two geographically and culturally distinct IBD cohorts. In colonic tissues of IBD patients, GBP5 expression was mainly confined to immune cells and the levels of *GBP5* expression were correlated with those of the inflammatory cytokines and chemokines. In cultured T and macrophage cells, the expression of proinflammatory cytokines and chemokines was increased when *GBP5* was induced, while *GBP5* deficiency leads to decreased expression of proinflammatory mediators including gasdermin D, caspase 1, cytokines, and chemokines. We conclude that GBP5 is required in the expression of many proinflammatory cytokines and chemokines in intestinal immune cells. In addition, GBP5 may upregulate inflammatory reactions through an inflammasome-mediated mechanism. Since GBP5 plays a proinflammatory role at the early steps of the inflammatory cascades of IBD pathogenesis, and is implicated in IBD patients of distinct genetic and environmental backgrounds, targeting GBP5 could be an effective strategy for the management of IBD.

Keywords: Crohn's disease, ulcerative colitis, inflammasome, pyroptosis, guanylate binding protein

Abbreviations: AOM, azoxymethane; ASC, apoptosis-associated speck-like protein containing a CARD domain; CD, Crohn's disease; DSS, dextran sodium sulfate; GBP, guanylate-binding protein; GSEA, gene set enrichment analysis; IBD, inflammatory bowel diseases; IFN, interferon; IHC, immunohistochemistry; LPS, lipopolysaccharide; NLRP3, NOD-like receptor family pyrin domain containing 3; PBMCs, peripheral blood mononuclear cells; SES-CD, simple endoscopic score for Crohn's disease; SNP, single-nucleotide polymorphism; TNBS, 2,4,6-trinitrobenzene sulfonic acid; UC, ulcerative colitis; UC-EIS, ulcerative colitis endoscopic index of severity.

INTRODUCTION

Inflammatory bowel diseases (IBD), including Crohn's disease (CD) and ulcerative colitis (UC), are chronic and relapsing inflammatory diseases mainly affecting the intestines. The pathogenesis of IBD is not known, but generally believed to be driven by abnormalities in genetics, environment, gut microbiota, and immunity (Seyed Tabib et al., 2020).

NLRP3 (NOD-like receptor family pyrin domain containing 3) inflammasome comprises the inflammasome sensor NLRP3, the adaptor protein ASC (apoptosis-associated speck-like protein containing a CARD domain), and the effector caspase 1. Activation of NLRP3 inflammasome leads to the production of active form of proinflammatory cytokines IL1β and IL-18. Different groups have reported that colonic mucosa of IBD patients exhibited higher levels of caspase 1 (McAlindon et al., 1998), IL1β (Mahida et al., 1989; Ligumsky et al., 1990; Reinecker et al., 1993; McAlindon et al., 1998), and IL-18 (Kanai et al., 2000), demonstrating an association of elevated NLRP3 inflammasome activity with IBD. Animal studies provided a chain of evidence in support of a key role for NLRP3 inflammasome in colitis. NLRP3 gene knockout mice are protected from dextran sodium sulfate (DSS) (Bauer et al., 2010) or 2,4,6-trinitrobenzene sulfonic acid (TNBS) (Bauer et al., 2012) induced colitis compared to wild-type animals. Similar protection was also observed with pharmacological inhibition of caspase 1 with pralnacasan (Bauer et al., 2010) or with caspase 1 knockout mice (Siegmund et al., 2001; Blazejewski et al., 2017). Along this line, inhibition of IL1β or its receptor suppressed experimental colitis (Seo et al., 2015; Neudecker et al., 2017). Importantly, IL-1 receptor blockade using anakinra resulted in a rapid and sustained improvement in patients with colitis (de Luca et al., 2014).

Further support for a causal role of NLRP3 inflammasome in IBD pathogenesis came from studies on CARD8, an inhibitor for NLRP3. Single-nucleotide polymorphism (SNP) studies found that a loss-of-function mutation in CARD8 is associated with IBD (Fisher et al., 2007; Yang et al., 2011). Without the inhibitory CARD8 activity, the unchecked NLRP3 inflammasome activity leads to elevated IL1β and consequently intestinal inflammation. Patients with CARD8 loss-of-function mutation specifically responded to IL1β blockers, but not to anti-TNFα (Mao et al., 2018), demonstrating the role of CARD8-NLRP3-IL1β axis in IBD.

Guanylate-binding protein 5 (GBP5), a member of the GBP family, is a GTPase highly inducible by interferon (Cheng et al., 1983). GBP5 has an emerging role in mediating cell autonomous defenses against intracellular pathogens including those of *Francisella novicida* (Meunier et al., 2015), *Toxoplasma gondii* (Matta et al., 2018), and HIV-1 (Krapp et al., 2016). Peripheral blood mononuclear cells (PBMCs) from children with decreased GBP5 expression were more susceptible to respiratory syncytial virus compared to adult (Li et al., 2020). Under pathological conditions, abnormal upregulated expression of GBP5 is caused by dysregulated immune responses, such as rheumatoid arthritis-affected synovial tissue (Haque et al., 2021) and some human malignancies including medullary carcinoma (Friedman et al., 2016), gastric adenocarcinomas (Patil et al., 2018), and glioblastoma (Yu et al., 2021). GBP5, but not other members of the GBP family, promotes the assembly of the NLRP3 inflammasome in response to live *L. monocytogenes*, *S. Typhimurium,* and soluble inflammasome priming agents, as demonstrated in *GBP5* knockout mice and cell culture models (Shenoy et al., 2012; Santos et al., 2018). Consistent with its effect on inflammasome assembly, GBP5 was reported to stimulate NF-κB signaling, induce the expression of interferon (IFN) and other proinflammatory factors, and inhibit the replication of influenza A virus in a cell culture model (Feng et al., 2017). The dysregulation of the immune–microbiome axis is an important cause of IBD (Graham and Xavier, 2020). In the presence of microbial ligands, NLRP3 inflammasome is crucial for regulation of intestinal homeostasis (Tourkochristou et al., 2019). Therefore, we hypothesize that GBP5 plays a key role in IBD by regulating NLRP3 inflammasome activity. Here, we show that GBP5 is highly elevated in the colonic mucosa of IBD patients and that GBP5 is required in the stimulated secretion of proinflammatory mediators in cell culture models.

RESULTS

Elevated Guanylate-Binding Protein 5 Expression in the Colonic Mucosa of Inflammatory Bowel Diseases Patients

We first examined *GBP5* mRNA expression in patients with IBD using a published transcriptome dataset generated with colonic biopsies from European patients. The demographic and clinical characteristics of these patients were described previously (Arijs et al., 2009). Elevated *GBP5* expression was observed in both CD and UC patients compared to healthy controls, with fold changes of 8.6 and 8.1, respectively (**Figure 1A**). To confirm these findings, a validation cohort including healthy controls, CD, and UC patients from south China was enrolled (**Supplementary Table 1**) and *GBP5* mRNA levels in colonic mucosa were evaluated by quantitative real-time PCR (qRT-PCR). Similarly, elevated *GBP5* expression was observed in CD and UC patients compared to healthy controls, with fold changes of 13.1 and 3.8, respectively (**Figure 1B**).

To examine the GBP5 expression at protein level, inflamed and adjacent non-inflamed colonic tissues from the same CD patients who underwent colon resection were subjected to immunohistochemistry (IHC) staining. With all the samples examined, GBP5 staining was more intense in the inflamed tissue than in the non-inflamed tissue (**Figures 1C,D**). Interestingly, GBP5 positive cells were mostly found in the lamina propria, with a few exceptions located at the luminal or glandular epithelium (**Figure 1C**).

To understand the potential role of GBP5 in clinical outcome, correlation analysis between mucosal GBP5 expression and disease degree of IBD was performed. We used the simple endoscopic score for Crohn's disease (SES-CD) and the ulcerative colitis endoscopic index of

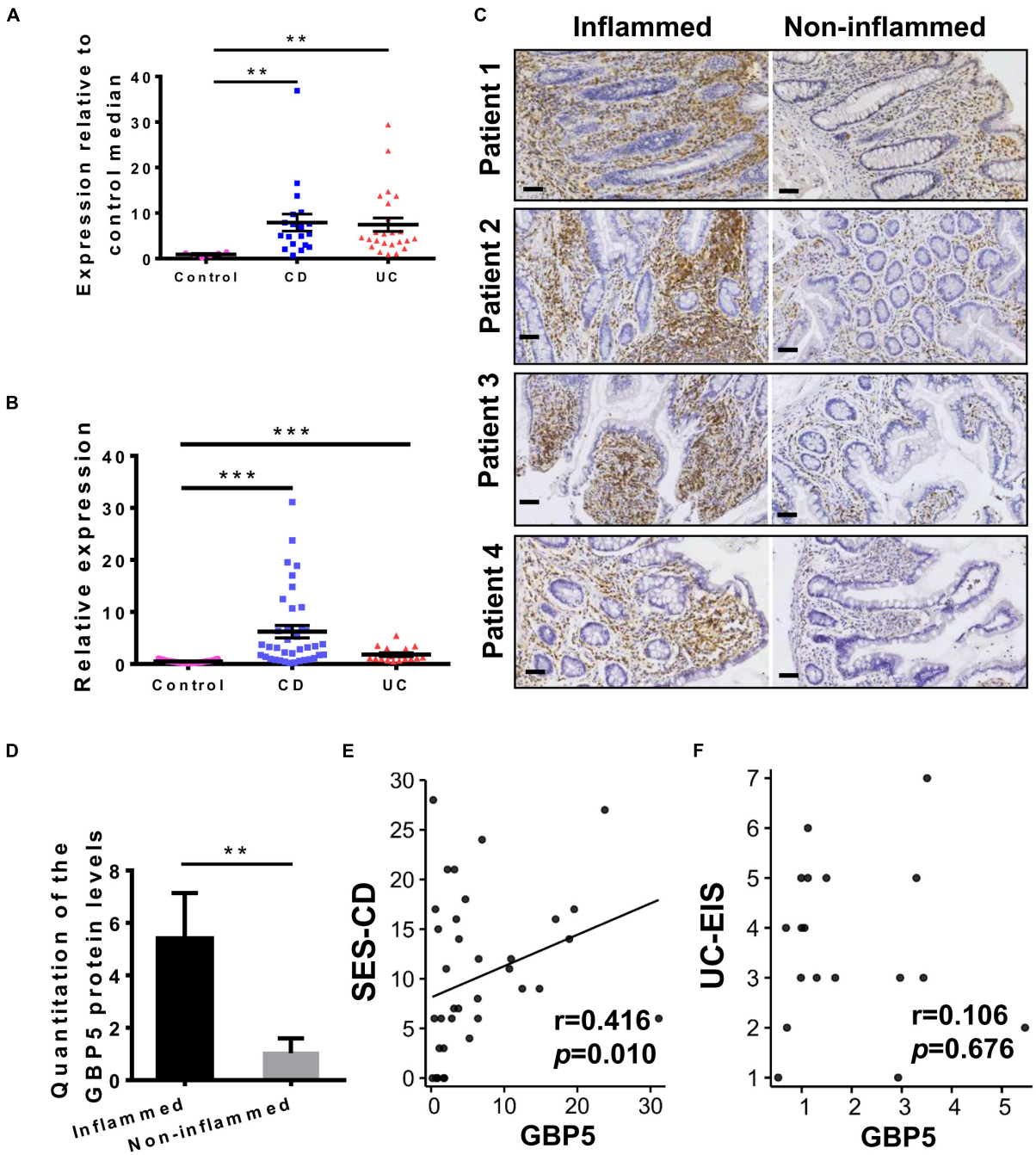

FIGURE 1 | GBP5 is highly expressed in the inflamed intestinal tissue of IBD patients. **(A)** Messenger RNA expression of GBP5 in the colonic mucosa of healthy controls (n = 6), patients with Crohn's disease (CD, n = 19), and ulcerative colitis (UC, n = 24). Data are from a microarray dataset generated from a European cohort. $^{**}P < 0.01$, Dunn's multiple comparison test. **(B)** Quantitative RT-PCR analysis of GBP5 mRNA in colonic mucosa from a Chinese cohort including healthy controls (n = 35), and patients with CD (n = 38) and UC (n = 17). $^{***}P < 0.001$, Dunn's multiple comparison test. **(C)** Immunohistochemical staining of GBP5 in colonic mucosa from four representative patients with CD. Images of inflamed and non-inflamed sites from the same patient are compared side by side. Bar = 50 μm. **(D)** Quantitation of the GBP5 staining in the inflamed and non-inflamed sites in **(C)**. $^{**}P < 0.01$, paired Student's t-test. **(E,F)** Spearman's correlation analysis of the mucosal GBP5 expression levels and endoscopic severities. GBP5 expression levels are from quantitative RT-PCR results. SES-CD, simple endoscopic score for Crohn's disease; UC-EIS, ulcerative colitis endoscopic index of severity.

severity (UC-EIS) to evaluate the severity of CD and UC, respectively. The expression of GBP5 was positively correlated with SES-CD (**Figure 1E**, Spearman's correlation coefficient = 0.416; P = 0.010), but not correlated with UC-EIS (**Figure 1F**, Spearman's correlation coefficient = 0.106; P = 0.676).

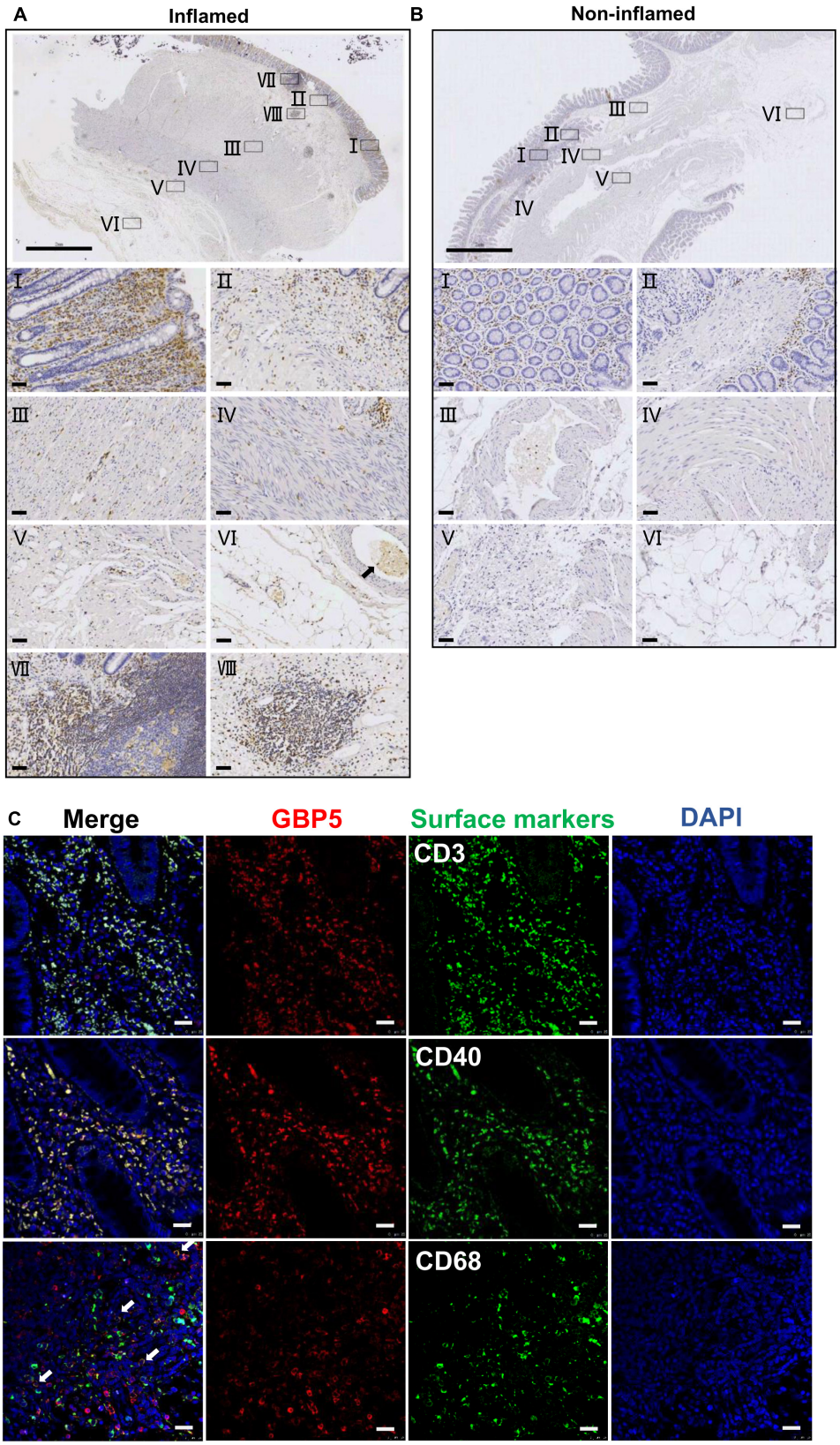

FIGURE 2 | Continued

FIGURE 2 | Immune cell-specific GBP5 expression in patients with CD. **(A)** Immunohistochemical staining of a colonic biopsy section from a representative CD patient with an anti-GBP5 antibody: an inflamed area. The top image shows a panoramic view of the section. Bar = 2 mm. Details are shown for boxed areas representing different anatomic structures. I, mucosa; II, muscularis mucosa and submucosa; III, circular muscle; IV, longitudinal muscle; V, serosa; VI, mesentery, black arrow indicates a blood vessel; VII, Peyer's patch in mucosa; VIII, lymph node in submucosa. Bar = 50μm. **(B)** Immunohistochemical staining of a colonic biopsy section from a representative CD patient with an anti-GBP5 antibody: a non-inflamed area. The top image shows a panoramic view of the section. Bar = 2 mm. Details are shown for boxed areas representing different anatomic structures. I, mucosa; II, lamina propria, muscularis mucosa and submucosa; III, a blood vessel in submucosae layer; IV, circular muscle and longitudinal muscle; V, serosa; VI, mesentery. Bar = 50μm. **(C)** Immunofluorescence staining of inflamed colon tissue from a representative CD patient with antibodies against GBP5, CD3, CD40, and CD68. White arrow indicates the overlap of GBP5 and CD68. Bar = 50 μm.

Immune Cell-Specific Guanylate-Binding Protein 5 Expression in the Colon of Crohn's Disease Patients

To better understand the tissue distribution of GBP5, IHC staining of GBP5 was examined at the entire depth of the inflamed and non-inflamed colonic tissues of CD patients who underwent colon resection. In the inflamed colon, GBP5 positive cells were densely populated in mucosa, mostly lamina propria (**Figure 2AI**). Besides, GBP5 positive cells were frequently observed in other layers of the colonic tissue including submucosa, circular muscle, longitudinal muscle, serosa, and mesentery (**Figures 2AII–VI**). Less GBP5 positive cells were observed in colonic layers of the non-inflamed tissue from the same patient (**Figure 2B**). It is noteworthy that GBP5 was not detected in muscle cell (**Figures 2AIII,IV**) or endothelial cell, but detected in the blood cells (**Figure 2AVI**). Another outstanding observation was the enrichment of GBP5 positive cells in Peyer's patch (mucosa, **Figure 2AVII**) and lymph node (submucosa, **Figure 2AVIII**). The elevated expression of GBP5 across the colonic layers of CD patients is in line with the fact that CD is usually inflicted by transmural inflammation.

To determine the cellular distribution of GBP5, inflamed colon tissues from CD patients were subjected to immunofluorescence staining for GBP5 and immune cell marker proteins. Confocal microscopy showed that most of the CD3 positive cells, most of the CD40 positive cells, and the majority of CD68 positive cells expressed GBP5 (**Figure 2C**). CD3, CD40, and CD68 are marker proteins for T lymphocytes, antigen-presenting cells (dendritic cells, macrophages, and B cells) (Croft and Siegel, 2017), and macrophages, respectively. Thus, the above results demonstrated immune cell-specific expression of GBP5.

Transcriptome Analysis Reveals Association Between Guanylate-Binding Protein 5 and Inflammatory Reaction Pathways

To identify potential links between *GBP5* and IBD pathogenesis, we performed hierarchical clustering of *GBP5* with 102 available cytokine and chemokine genes with the transcriptome dataset generated from colonic mucosa of IBD patients (GSE16879) (Arijs et al., 2009). The clustering result showed that *GBP5* shared a similar expression pattern with gene coding for proinflammatory cytokines and chemokines including *IL1B* and *IL-6*, and they were highly elevated in most of the CD and UC patients compared to the healthy controls (**Figure 3A**). Interestingly, the anti-inflammatory cytokine *IL-10* exhibited a similar expression pattern as *GBP5*. The elevated *IL-10* expression in IBD was observed previously and was thought to reflect a futile effort of patient immune system to control the excessive inflammatory reaction (Autschbach et al., 1998). Next, we performed Pearson's correlation analyses between every two genes based on the transcriptome data (**Figure 3B**). With a threshold of correlation coefficient greater than 0.6, 486 genes were correlated with *GBP5*. In comparison, 226, 123, and 112 genes were correlated with *GBP1*, *GBP2,* and *GBP4*, respectively. Apparently, at the transcription level, *GBP5* had the largest impact on IBD among all *GBP* family genes. We then performed Gene Ontology (GO) enrichment analysis with all 486 genes correlated with *GBP5*. The top "biological process," "cellular compartment," and "molecular function" are listed in **Figure 3C**. The top "biological process," including "leukocyte migration," "response to molecule of bacterial origin," "response to lipopolysaccharide," and "cellular response to molecule of bacterial origin," is related to inflammatory responses to bacterial infection. In addition, the top "cellular compartment" and the top "molecular function," such as "collagen-containing extracellular matrix" and "extracellular matrix structural constituent," are closely related to lymphocyte migration and infiltration. These results are consistent with previous reports that GBP5 plays a critical role in host defense against bacterial pathogens (Meunier et al., 2014; Pilla et al., 2014).

Guanylate-Binding Protein 5 Deficiency Downregulates Proinflammatory Chemokines and Cytokines in Cultured Cells

For further understanding of the association between *GBP5* and inflammatory processes, we performed *GBP5* siRNA knockdown in Jurkat cells to determine the impact of *GBP5* on chemokine and cytokine secretion. Diminished GBP5 expression in Western blot analysis indicated efficient knockdown of *GBP5* gene in Jurkat cells (**Supplementary Figure 1A**). The cell culture supernatants were then subjected to Luminex chemokine and cytokine assay. Compared to cells treated with control RNA, upon stimulation with IFNγ and lipopolysaccharide (LPS), *GBP5* siRNA-treated cells exhibited decreased levels of CCL2, CCL8, CCL13, CCL25, CXCL10, CXCL11, CXCL12, CXCL16, CX3CL1, IL-1β, IL-10, and MIF in the cell culture supernatant (**Supplementary Figure 1B**). In addition, CCL19, CCL20, CCL22, CXCL2, and CXCL13 were not detected in the supernatant after *GBP5* knockdown, but detected in the supernatant of the cells treated with

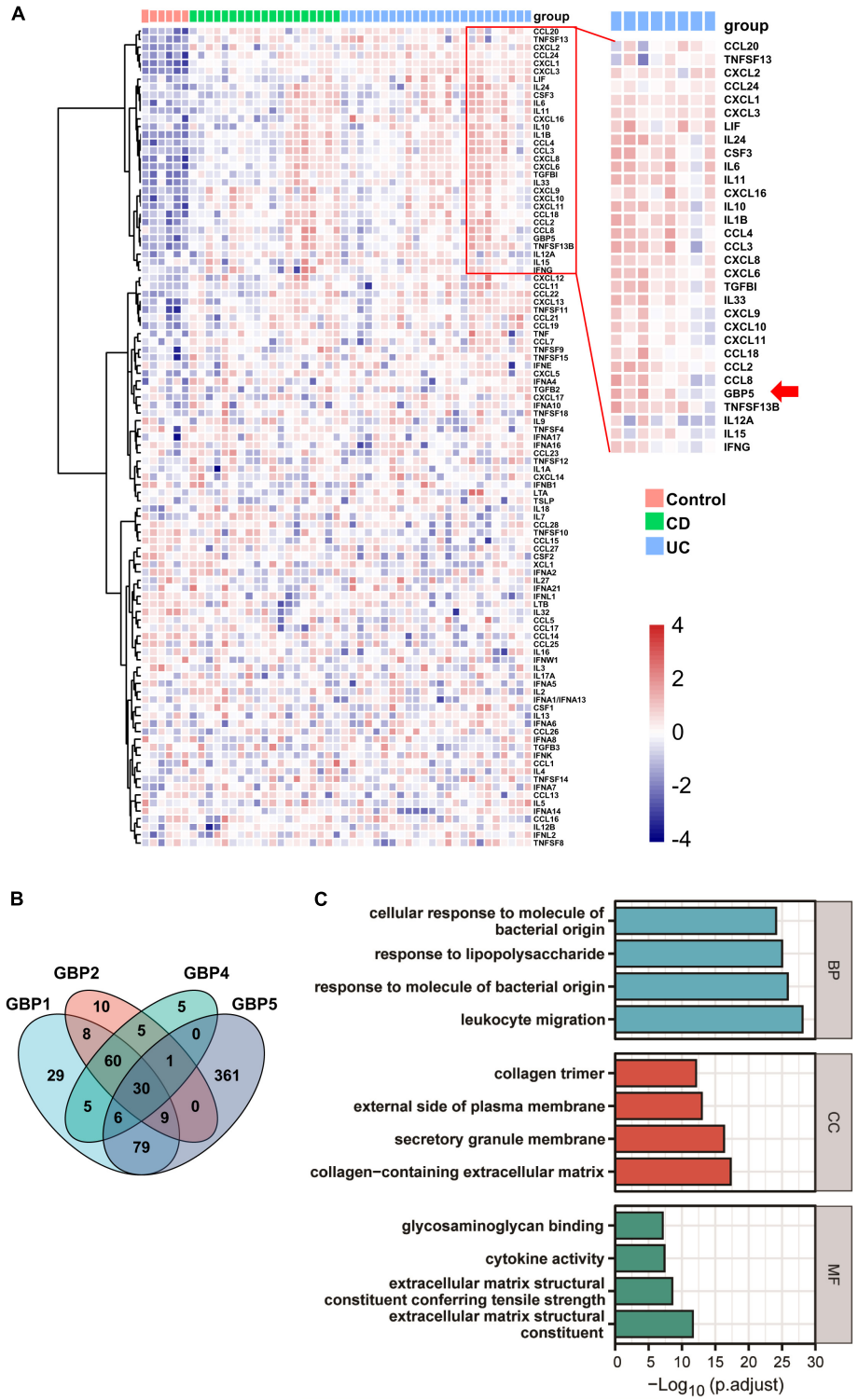

FIGURE 3 | GBP5 is implicated in inflammatory processes in IBD according to transcriptome analysis. **(A)** Heatmap for mRNA expression levels of GBP5 (arrow), available cytokines, and chemokines based on transcriptome data generated from colonic mucosal biopsies of healthy controls (n = 6), patients with Crohn's disease (CD, n = 19), and ulcerative colitis (UC, n = 24). Unsupervised hierarchical clustering of *GBP5*, cytokine, and chemokine genes was performed. Genes in the red box are more closely clustered with GBP5. **(B)** Venn plot of the number of genes associated with GBP1, GBP2, GBP4, and GBP5, based on their mRNA expression levels. Associations with Pearson's correlation coefficient no less than 0.6 are counted. **(C)** Gene Ontology (GO) analysis of GBP5 associated genes. The cutoff value for the input gene list is Pearson's correlation coefficient no less than 0.6. BP, biological process; CC, cellular compartment; MF, molecular function. All samples from GSE16879 are included (n = 90).

control RNA (**Supplementary Figure 1B**). *GBP5* knockdown also caused a trend of decreased levels in some proinflammatory chemokines and cytokines, including CCL1, CCL11, CCL15, CCL21, CCL26, CCL27, CXCL1, CXCL5, IL-16, and TNF-α, but statistical significance was not achieved (**Supplementary Figure 1B**). CCL7, CCL17, CCL23, CXCL6, CXCL9, GM-CSF, IL-2, IL-4, and IL-6 were not detected in any of the samples (**Supplementary Figure 1B**).

For a precise evaluation of *GBP5* impact on chemokine and cytokine secretion, *GBP5* gene was removed from THP-1 cell by CRISPR/CAS9 method and confirmed by Western blot showing no GBP5 expression in $GBP5^{-/-}$ THP-1 cells (**Figure 4A**). Global mRNA expression of the $GBP5^{-/-}$ THP-1 cells was assessed by RNA sequencing. As expected, *GBP5* mRNA was reduced in $GBP5^{-/-}$ THP-1 cells compared to the wild-type controls, with or without induction by IFNγ plus LPS (**Figures 4B,C**). Surprisingly, *GBP5* deficiency greatly reduced the mRNA expressions of many inflammation and immune related genes, including (1) IFNγ response genes such as *AIM2, CASP1, GSDMD*, and *IL1B*, and (2) IFNγ non-response genes such as *NLRP3, CASP4, CASP5,* and *IL-18* (**Figure 4B**).

Comparing the $GBP5^{-/-}$ with wild-type THP-1 cells, many differentially expressed genes, including 2,298 genes upregulated and 2,813 genes downregulated in $GBP5^{-/-}$ cells, were identified (**Figure 4C**). The mRNA expression for most proinflammatory cytokines and chemokines was reduced or undetected in $GBP5^{-/-}$ cells (**Supplementary Figure 2**). We then performed GO enrichment analysis with the list of genes downregulated in $GBP5^{-/-}$ cells. The identified top "biological process," "cellular compartment," and "molecular function" are related to inflammatory signaling, immune cell migration, neutrophil activation, secretion of cytokines and chemokines, and other immune and inflammatory events (**Figure 4D**).

Using a different approach for functional analysis, gene set enrichment analysis (GSEA) identified a similarly broad suppression of immune and inflammatory functions in $GBP5^{-/-}$ THP-1 cells, including antigen processing, chemokine signaling, cytokine signaling, leukocyte migration, and NK cell cytotoxicity (**Figure 4E**). Compared to GO enrichment analysis that uses partial information of the biological pathways (in our case, the downregulated genes), GSEA considers all available information of relevant genes for functional analysis. Thus, both methods identified immune and inflammatory pathways as downregulated pathways in $GBP5^{-/-}$ THP-1 cells.

Next, we examined the altered immune and inflammatory pathways at protein level. Compared to the wild-type controls, THP-1 cells with *GBP5* deficiency exhibited decreased levels of CCL2, CCL8, CCL13, CCL21, CCL25, CCL26, CXCL5, CXCL11, CXCL12, CX3CL1, IL1β, IL-10, and IL-16 in the cell culture supernatant (**Figure 5**). In addition, CCL1, CCL3, CCL7, CCL11, CCL15, CCL19, CCL20, CCL22, CCL23, CCL24, CCL27, CXCL1, CXCL2, CXCL6, CXCL9, CXCL10, CXCL13, CXCL16, IL-2, IL-4, IL-6, CXCL8, TNF-α, and GM-CSF were not detected in the supernatant of *GBP5* knockout cells, but detected in the WT controls (**Figure 5**). CCL17 was again not detected in any of the samples (**Figure 5**). Therefore, *GBP5* deficiency led to decreased secretion for most of the inflammatory mediators analyzed.

Given the close relation among GBP5, inflammasomes, and IL1β, we examined the intracellular protein expression of some related molecules. Western blots showed that *GBP5* deficiency greatly decreased the expression of gasdermin D, caspase 1, and pro-IL1β (**Figure 6**). Since the active form for gasdermin D or caspase 1 was not observed in any of the samples, the decreased production of IL1β is not likely due to impaired proteolytic activation by inflammasomes in *GBP5* deficiency. Rather, the transcription and expression analyses indicate that the decreased IL1β production is part of the consequence of broad inhibition of inflammatory gene expression in *GBP5* deficiency.

DISCUSSION

Here, we show for the first time the elevated expression of *GBP5* in colonic mucosa of patients with IBD and that *GBP5* is required for the stimulated secretion of inflammatory cytokines and chemokines, including IL1β, from T lymphocytes and macrophages. In colonic tissues of IBD patients, the expression of GBP5 was mainly confined to immune cells and the levels of *GBP5* expression were correlated with those of the inflammatory markers. Importantly, the expression of proinflammatory cytokines and chemokines was increased when *GBP5* was induced, while *GBP5* deficiency leads to decreased production of the proinflammatory mediators in T and macrophage cells. Thus, the specific role of GBP5 in IBD pathogenesis is to facilitate the stimulated production of inflammatory mediators in intestinal immune cells. Our observation of highly elevated *GBP5* expression at the inflamed colonic mucosa in two geographically and culturally distinct IBD cohorts indicates that GBP5 plays a common and important role in the early steps of IBD pathogenesis and, therefore, is a potential therapeutic target for the management of IBD patients of various genetic and environmental backgrounds.

Our results suggest that GBP5 may promote inflammation through two mechanisms. First, gene knockout studies indicated that *GBP5* is required for the stimulated expression of many inflammatory cytokines, such as IL1β, and is required for the expression of many IFNγ non-response cytokines, such as IL-18. Studies at both mRNA and protein levels indicated that GBP5 had a large impact on the expression of these proinflammatory cytokines and chemokines. Once IL1β is induced, in turn, IL1β may stimulate the production of other proinflammatory cytokines and chemokines including IL-6, IL8, CCL2, CCL5, CXCL1, CXCL2, CXCL3, CXCL6, and IFNγ (Cooper et al., 2001; Hengartner et al., 2015). The outstanding knowledge gap is how the cytoplasmic inflammasome interacting GBP5 regulates gene expression? Second, since GBP5 promotes NLRP3 inflammasome activity (Shenoy et al., 2012), and NLRP3 inflammasome is required for the excessive inflammatory reactions in IBD (reviewed in Yuan et al., 2018), it is expected that NLRP3 inflammasome may mediate the proinflammatory effect of GBP5. This is supported by our observation that the expression of caspase 1, gasdermin D, and IL1β was elevated when *GBP5* is induced and was reduced when *GBP5* was downregulated by siRNA or gene knockout. The puzzle here is the observation

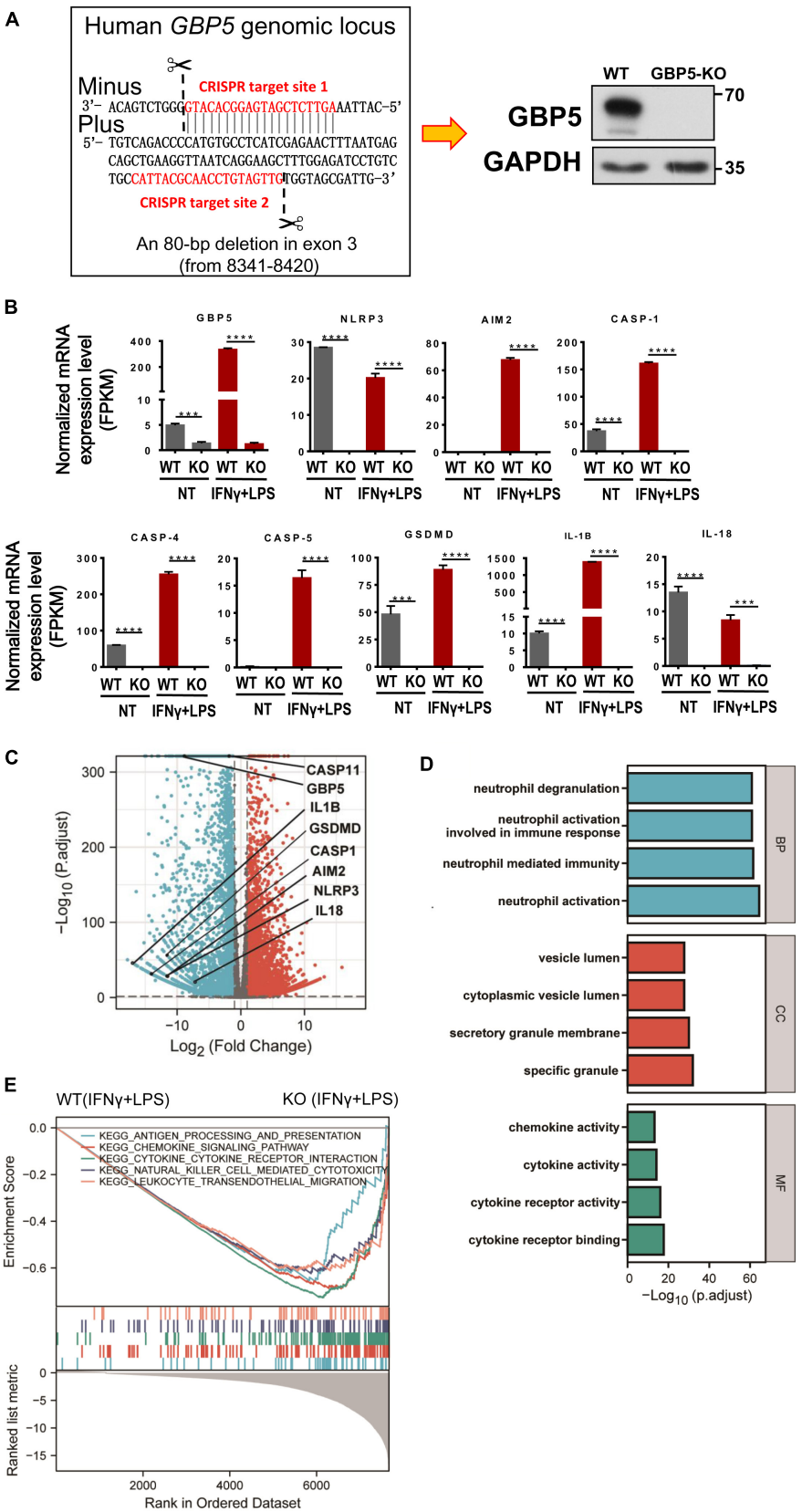

FIGURE 4 | Continued

FIGURE 4 | *GBP5* knockout downregulated the expression of proinflammatory mediator genes in THP-1 cells. The transcriptomes of wild-type and *GBP5*$^{-/-}$ THP-1 cells, with or without stimulation [IFNγ and lipopolysaccharide (LPS)], respectively, were analyzed by RNAseq technique. N = 3 for each treatment group. **(A)** Generation of *GBP5* knockout (*GBP5*$^{-/-}$). THP-1 cell line by CRISPR/Cas9-mediated genome editing. The two CRISPR target sites are highlighted in red. Loss of GBP5 was confirmed by Western blot. WT, wild-type control. **(B)** Messenger RNA expression of *GBP5* and related genes in wild-type and *GBP5*$^{-/-}$ THP-1 cells (clone B2), with or without stimulation (IFNγ and LPS), respectively. FPKM, fragments per kilobase million. ***$P < 0.001$; ****$P < 0.0001$; unpaired Student's *t*-test. **(C)** Differential gene expression between wild-type and *GBP5*$^{-/-}$ THP-1 cells: volcano plot. Vertical and horizontal dashed lines indicate the cutoff values for differentially expressed genes:$|\text{Log}_2\text{ (Fold Change)}| > 1$ and p.adjust < 0.05. **(D)** GO (Gene Ontology) analysis of downregulated genes in *GBP5* knockout cells. The cutoff values for selecting differentially expressed genes for the input gene list: Log_2(Fold Change) < -2, and p. adjust < 0.05. BP, biological process; CC, cellular compartment; MF, molecular function. **(E)** Gene set enrichment analysis (GSEA) of *GBP5*$^{-/-}$ THP-1 cells (clone B2) transcriptome compared to wild-type THP-1 cells. Upper panel: the enrichment score curves of the top KEGG (Kyoto Encyclopedia of Genes and Genomes) pathways exhibiting decreased expression in *GBP5*$^{-/-}$ THP-1 cells: immune related pathways. Middle panel: distribution of the genes related to the pathways indicated in the upper panel. The genes were ranked according to their differential expression between wild-type and *GBP5*$^{-/-}$ THP-1 cells. Genes of higher rank (left) exhibit relatively higher expression in wild-type THP-1 cells. Lower panel: Graphical representation of the correlations of the gene expression levels with the phenotypes: wild-type or *GBP5* knockout. Genes on the right are more negatively correlated with *GBP5* deficiency.

that the active forms of caspase 1 and gasdermin D were not observed in IFNγ primed THP-1 cells. For both mechanisms, future efforts are needed to unravel the puzzles and to join the knowledge gaps.

One major challenge for the interpretation of our data came from a few studies that reported protective role for NLRP3 inflammasome in mouse models of colitis, that is, mice lacking NLRP3, ASC, or caspase 1 were more susceptible for colitis in DSS and azoxymethane (AOM) models (Allen et al., 2010; Dupaul-Chicoine et al., 2010; Zaki et al., 2010a,b; Hirota et al., 2011). The discrepancies regarding the role of NLRP3 inflammasome in colitis may be explained by environmental factors including microbiota (Bauer et al., 2012) and diet (Youm et al., 2015). In addition, Zaki et al. (2010a) argued that the protective role of NLRP3 inflammasome is due to its beneficial effect on epithelial barrier function via induction of IL-18 in epithelial cells. However, this argument does not reconcile with the facts that little NLRP3 inflammasome activity presents in the intestinal epithelial cells and that IL-18 production by these cells is independent of NLRP3 inflammasome (Yao et al., 2017).

Besides the conventional NLRP3 inflammasome-mediated mechanism, a caspase-11-dependent pathway may relay the inflammatory signal from GBP5. Mice and cell culture studies suggested that, upon detection of cytoplasmic LPS, GBP proteins encoded on mouse chromosome 3 activate caspase-11-dependent cell autonomous immune responses (Pilla et al., 2014). This is consistent with current knowledge that structural and functional alterations in the gut microbiota, especially in gram-negative bacteria (Palmela et al., 2018), and their cell wall component LPS (Caradonna et al., 2000), are implicated in the pathogenesis of IBD. In support of a causal role for bacteria and LPS in IBD, we identified the following pathways as the top features of the GBP5 associated colonic mucosal transcriptome in IBD: "response to molecule of bacterial origin," "response to lipopolysaccharide," and "cellular response to molecule of bacterial origin." On the contrary, it is noteworthy that virus infection is implicated in IBD pathogenesis (Yang et al., 2019), and GBP5 has been identified as an IFN-induced virus restriction factor that interferes with virus assembly (Krapp et al., 2016), or through induction of innate immune mediators (Feng et al., 2017). Further study is required to clarify potential collaborative roles of caspase-11 and GBP5 in IBD pathogenesis, and whether viral or bacterial infection triggers elevated GBP5 expression in the intestines of IBD.

The limitations of our study include lack of *in vivo* study and small sample size. Therefore, further experimentations have been planned to validate our findings. In addition, other interesting questions emerged from our study. For example, GBP5 seemed to play a more important role in CD than in UC. With the prospective cohort enrolled in our hospital, the expression level of GBP5 was more elevated in CD than in UC. Consistently, the expression levels of GBP5 were correlated with the disease severities of CD, but not that of UC. However, the differential expression of GBP5 was not observed with treatment-naive patients with IBD (**Figure 1A**). Therefore, the differential expression of GBP5 in CD and UC may be a consequence of different treatments.

In summary, GBP5 is highly expressed in the colonic immune cells of IBD patients. Induction of GBP5 is required for the stimulated production of proinflammatory cytokines and chemokines, while GBP5 deficiency decreases the expression of the proinflammatory mediators. Since GBP5 plays a proinflammatory role at the early steps of the inflammatory cascades of IBD pathogenesis, and is implicated in IBD patients of distinct genetic and environmental backgrounds, targeting GBP5 could be an effective strategy for the management of IBD.

MATERIALS AND METHODS

Human Samples

Colonic pinch biopsies were obtained from patients with IBD at the Sixth Affiliated Hospital of Sun Yat-sen University, Guangzhou, China. Healthy control colonic biopsy samples were from patients suspected of intestinal diseases but diagnosed normal according to biopsy. The simple endoscopic score for Crohn's disease (SES-CD) and the ulcerative colitis endoscopic index of severity (UC-EIS) were used to evaluate the endoscopic severity of CD and UC, respectively, by endoscopist as previously described (Daperno et al., 2004; Travis et al., 2013). Colon resections were obtained from patients with IBD who underwent colectomy. Non-inflamed control specimens were obtained 5 cm away from the inflamed lesion. Written informed consents were obtained from all donors. This study was approved by the

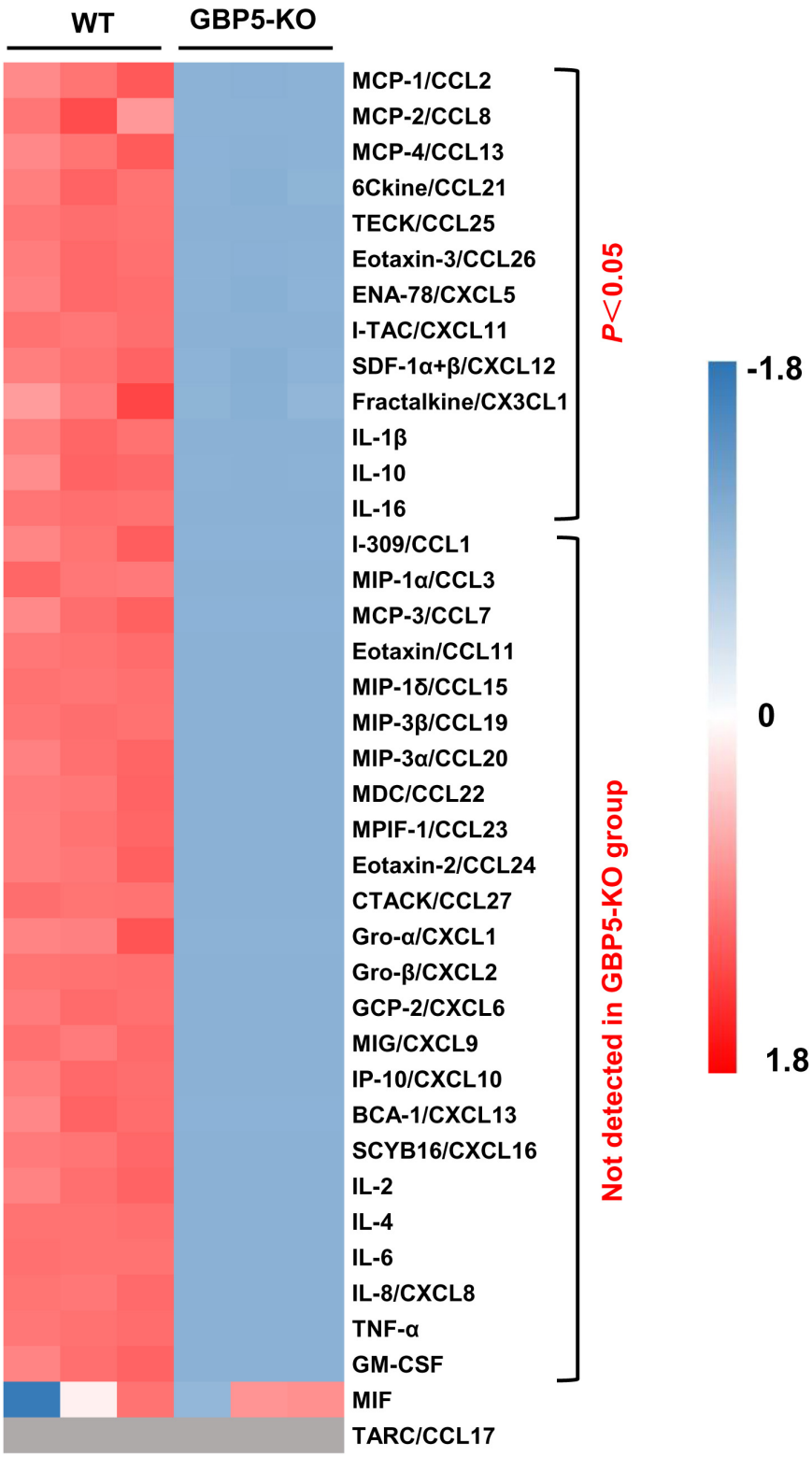

FIGURE 5 | Decreased chemokine and cytokine secretion in *GBP5* knockout THP-1 cells. The protein levels of chemokines and cytokines in the cell culture supernatant of wild-type (WT) and *GBP5* knockout (KO) THP-1 cells are plotted. Cells were primed with IFNγ and LPS before sample collection. The concentrations of cytokines and chemokines were determined by Luminex liquid suspension chip. Data were normalized as (x-mean)/SD. Gray blocks indicate no detection. *P*-values were from Student's *t*-tests.

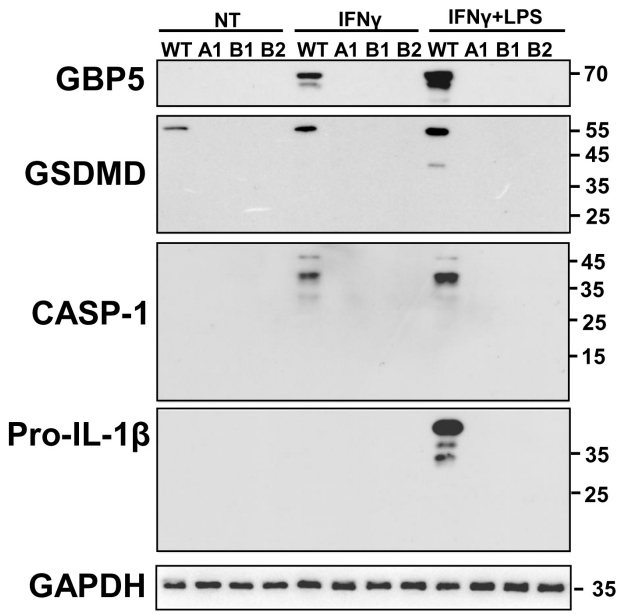

FIGURE 6 | Diminished expression of inflammasome related proteins in *GBP5* knockout THP-1 cells was subjected to wild-type THP-1 cells, and *GBP5* knockout THP-1 cell clones (A1, B1, and B2) were left untreated (NT), treated with IFNγ (25 ng/ml) only, or treated with IFNγ (25 ng/ml) plus LPS (500 ng/ml) for 16 h, before Western blot analysis with antibodies against GBP5, gasdermin D (GSDMD), caspase 1 (CASP1), pro-IL1β, and GAPDH, respectively.

Institutional Review Board of the Sixth Affiliated Hospital of Sun Yat-sen University.

RNA Extraction, Complementary DNA Synthesis, and Quantitative Real-Time PCR

Total RNA from cultured cells was isolated using TRIzol (Invitrogen, United States). For RNA isolation from clinical samples, colonic tissues were disrupted with lysis beads (Luka, China) before RNA isolation with AllPrep® DNA/RNA Micro Kits (Qiagen, United States). Using total RNA as template, Complementary DNA (cDNA) was synthesized with Fast Reverse Transcription kits (ES Science, China). For the gene expression analysis, qRT-PCR was performed with FastStart Essential DNA Green Master (Roche, United Kingdom) on LightCycler® 96 (Roche, United Kingdom). The gene expression levels were normalized with β-actin gene as the reference gene according to the $2^{-\Delta\Delta CT}$ method. The sequences of the qRT-PCR primers are as follows: GBP5, forward: 5′-CCTGATGATGAGCTAGAGCCTG-3′, and reverse: 5′-GCACCAGGTTCTTTAGACGAGA; β-actin, forward: 5′-TTGTTACAGGAAGTCCCTTGCC-3′, and reverse: 5′-ATGCTATCACCTCCCCTGTGTG-3′.

Transcriptome Analysis

Global transcriptome analysis of the colonic tissue from IBD patients used the published microarray dataset generated from the colonic mucosa of IBD patients and healthy controls (GSE16879)[1] (Arijs et al., 2009). Data were normalized by MAS5 method before further analysis. Unsupervised hierarchical clustering and Gene Ontology (GO) enrichment were performed with R (3.6.3).

For transcriptome analysis of the wild-type and *GBP5* knockout THP-1 cells, total RNA from parental THP-1 cells and *GBP5* knockout THP-1 clone B2, with and without stimulation (IFNγ and LPS) for 16 h, respectively, was isolated as described above. The RNA preparation was qualified with an Agilent 2100 Bioanalyzer (Thermo Fisher Scientific, United States). Oligo (dT)-attached magnetic beads were used to purify mRNA, which served as templates for cDNA synthesis. Libraries were constructed with the cDNA preparations at BGI-Shenzhen, China, amplified with phi29 to make DNA nanoball (DNB) which had more than 300 copies of one molecular, and sequenced on a BGIseq500 platform (BGI-Shenzhen, China). The sequencing data were filtered with SOAPnuke (v1.5.2) to remove sequences of adapters, to remove reads with low-quality base percentage (base quality less than or equal to 5) higher than 20%, and to remove reads whose unknown base ("N" base) percentage is higher than 5%. The clean reads were mapped to the reference genome using HISAT2 (v2.0.4). After that, EricScript (v0.5.5) and rMATS (V3.2.5) were used to identify fusion genes and differentially spliced genes (DSGs), respectively. Bowtie2 (v2.2.5) was applied to align the clean reads to a human mRNA database built by BGI (Shenzhen, China), and the expression level of gene was calculated by RSEM (v1.2.12). The heatmap was drawn by pheatmap (v1.0.8) according to the gene expression levels. Differential expression analysis was performed using the DESeq2 (v1.4.5) with Q-value $\leq$ 0.05. GO[2] and KEGG[3] enrichment analysis of differentially expressed genes was performed by phyper[4] based on Hypergeometric test. The statistical significance for multiple tests was adjusted by Bonferroni method. Transcriptome data for wild-type and *GBP5* knockout THP-1 cells are available at https://www.biosino.org/node/, accession ID: OEP002938.

Immunohistochemistry

Formalin-fixed paraffin-embedded intestine tissues from inflamed and non-inflamed sites of IBD patients were sectioned and collected onto glass slides. Antigen retrieval was performed in 10 mM sodium citrate (pH6.0) at 100°C for 15 min. GBP5 was stained with PV-6000 immunohistochemistry (IHC) kit (ZSGB-BIO, China) according to the protocol of the manufacturer, with the GBP5 antibody (Catalog #: 67798) from Cell Signaling (United States). The images were collected with Slide Scanning System SQS-1000 (TEKSQRAY, China). Quantitation of the GBP5 signals was performed with ImageJ with IHC-Toolbox plugins.

[1]http://www.ncbi.nlm.nih.gov/geo/

[2]http://www.geneontology.org/

[3]https://www.kegg.jp/

[4]https://en.wikipedia.org/wiki/Hypergeometric_distribution

Immunofluorescence

The tissue section was prepared as in IHC method. Primary antibodies include anti-GBP5 (Cat. #: 67798, Cell Signaling, United States), anti-CD3 (Cat. #: 60181-1-Ig, Proteintech, China), anti-CD40 (Cat. #: ab280207, Abcam, United States), and anti-CD68 (Cat. #: ARG10514, Arigo, China). Secondary antibodies include Alexa Fluor647 or 488 conjugated goat anti-rabbit or goat anti-mouse antibodies (Invitrogen, United States). Cell nuclei were stained with 4′,6-diamidine-2′-phenylindole dihydrochloride (DAPI, Sigma-Aldrich, United States). Slides were visualized with a TCS-SP8 confocal microscope (Leica, Germany).

Cell Culture and Gene Knockdown With siRNA

Human cell lines Jurkat, THP-1, and 293T cells were purchased from American Type Culture Collection (ATCC, United States). Cells were cultured in RPMI 1640 medium (Gibco, United States) supplemented with 10% fetal bovine serum (Gibco, United States) maintained at 37°C and 5% CO2. To knockdown GBP5 in Jurkat cells, a pool of two different siRNAs (1, 5′-GCCATAATCTCTTCATTCA-3′; and 2, 5′-GCTCGGCTTTACTTAAGGA-3′) were used. Scrambled sequence of the siRNA was used as control. RNA was synthesized at Ribo-Bio (China) and provided lyophilized. RNA was reconstituted with nuclease-free water to reach a final concentration of 20μM, before transfection using Lipofectamine RNAiMAX (Life technologies, United States) following the manufacturer's instructions. At 48 h post-transfection, cells were stimulated with human interferon γ (IFNγ, 25μg/ml, Novoprotein, China) and lipopolysaccharides from Escherichia coli O55:B5 (LPS, 500 ng/ml, Sigma-Aldrich, United States) for 16 h before harvest.

Western Blot

Cells were lysed in RIPA (Radio-Immunoprecipitation Assay) buffer (P0013B, Beyotime, China) supplemented with protease inhibitors (Cat. #: HY-K0011, MedChemExpress, China) and phosphatase inhibitors (Cat. #: HY-K0021 and HY-K0022, MedChemExpress, China). Lysates were mixed with loading buffer containing SDS and DTT and heated at 95°C for 5 min. Proteins of interest were probed with the following antibodies: anti-GBP5 antibody as described above, anti-GSDMD (Cat. #: 97558, Cell Signaling, United States), anti-caspase 1 (Cat. #: 3866, Cell Signaling, United States), anti-pro-IL1β (Cat. #: 12703, Cell Signaling, United States), and anti-GAPDH (Cat. #: 60004-1-Ig, Proteintech, China). HRP-conjugated secondary antibodies, anti-rabbit IgG and anti-mouse IgG, were from Proteintech, China.

Guanylate-Binding Protein 5 Knockout Cell Line

Two all-in-one sgRNA plasmids (HCP260159-CG04-3-10-a and HCP260159-CG04-3-10-b) for human *GBP5* were purchased from GeneCopoeia (China). In addition to DNA elements required for the generation of recombinant lentivirus, these plasmids carry Cas9 sequence and one of the following sgRNAs targeting the exon 3 of *GBP5*: gRNA1, 5′-AGTTCTCGATGAGGCACATG-3′; gRNA2, 5′-CATTACGCAACCTGTAGTTG-3′. Recombinant lentivirus was produced by transfecting 293T cells with the two sgRNA plasmids together with lentiviral packaging plasmids psPAX2 and pMD2. *GBP5* knockout THP-1 cells were generated by infecting THP-1 cells with the recombinant lentiviruses followed by G418 selection. After obtaining single-cell colonies from limiting dilution, three THP-1 clones (A1, B1, and B2) harboring all-allelic deletion of the 80-bp in exon 3 of *GBP5* locus were identified by PCR and validated by DNA sequencing of the PCR products. The primers used for PCR screening are as follows: forward, 5′- AGTAGTATGTCCCCAGGTTC-3′, and reverse, 5′-AAGACCAGCTGTAGCCTAAA -3′.

Luminex-Based Assays

The cell culture supernatant was collected after IFNγ + LPS stimulation. Multiple cytokines and chemokines were examined with Luminex liquid suspension chip at Wayen Biotechnologies Shanghai, Inc. (China). The Bio-Plex Pro Human Chemokine Panel 40-Plex kit (Cat. #: 171AK99MR2, Bio-Rad, United States) was used following the manufacturer's instructions.

Statistical Analysis

Data were analyzed by either one-way ANOVA and Dunn's test or two-tailed Student's *t*-test using GraphPad Prism (v7.0). Data are represented as the mean ± s.e.m (standard error of the mean). All *in vitro* experiments were performed in triplicate. Correlation analyses were evaluated by Spearman. The number of independent samples and statistical methods used in each experiment is reported in the figure legends. $P < 0.05$ was considered to be statistically significant.

DATA AVAILABILITY STATEMENT

The datasets presented in this study can be found in online repositories. The names of the repository/repositories and accession number(s) can be found below: https://www.biosino.org/node/, OEP002938; https://www.ncbi.nlm.nih.gov/geo/, GSE16879.

ETHICS STATEMENT

The studies involving human participants were reviewed and approved by the Institutional Review Board of the Sixth Affiliated Hospital of Sun Yat-sen University. The patients/participants provided their written informed consent to participate in this study.

AUTHOR CONTRIBUTIONS

LZ and JK conceived and designed the study. XL, YL, SC, YH, YZ, WXW, and JK collected patient samples and clinical data.

YL, SC, and YH performed the experiments. YL, XL, LZ, and JK analyzed the data. YL and LZ prepared the manuscript. All authors critically revised the manuscript, had access to the study data, reviewed, and approved the final manuscript.

FUNDING

This work was supported by the Guangdong Province "Pearl River Talent Plan" Innovation and Entrepreneurship Team Project 2019ZT08Y464 (LZ) and the National Natural Science Foundation of China 81770571 (LZ).

SUPPLEMENTARY MATERIAL

The Supplementary Material for this article can be found online at: https://www.frontiersin.org/articles/10.3389/fmicb.2022.926915/full#supplementary-material

REFERENCES

Allen, I. C., TeKippe, E. M., Woodford, R. M., Uronis, J. M., Holl, E. K., Rogers, A. B., et al. (2010). The NLRP3 inflammasome functions as a negative regulator of tumorigenesis during colitis-associated cancer. *J. Exp. Med.* 207, 1045–1056. doi: 10.1084/jem.20100050

Arijs, I., De Hertogh, G., Lemaire, K., Quintens, R., Van Lommel, L., Van Steen, K., et al. (2009). Mucosal gene expression of antimicrobial peptides in inflammatory bowel disease before and after first infliximab treatment. *PLoS One* 4:e7984. doi: 10.1371/journal.pone.0007984

Autschbach, F., Braunstein, J., Helmke, B., Zuna, I., Schurmann, G., Niemir, Z. I., et al. (1998). In situ expression of interleukin-10 in noninflamed human gut and in inflammatory bowel disease. *Am. J. Pathol.* 153, 121–130. doi: 10.1016/S0002-9440(10)65552-6

Bauer, C., Duewell, P., Lehr, H. A., Endres, S., and Schnurr, M. (2012). Protective and aggravating effects of Nlrp3 inflammasome activation in IBD models: influence of genetic and environmental factors. *Dig. Dis.* 30(Suppl. 1), 82–90. doi: 10.1159/000341681

Bauer, C., Duewell, P., Mayer, C., Lehr, H. A., Fitzgerald, K. A., Dauer, M., et al. (2010). Colitis induced in mice with dextran sulfate sodium (DSS) is mediated by the NLRP3 inflammasome. *Gut* 59, 1192–1199. doi: 10.1136/gut.2009.197822

Blazejewski, A. J., Thiemann, S., Schenk, A., Pils, M. C., Galvez, E. J. C., Roy, U., et al. (2017). Microbiota normalization reveals that canonical caspase-1 activation exacerbates chemically induced intestinal inflammation. *Cell Rep.* 19, 2319–2330. doi: 10.1016/j.celrep.2017.05.058

Caradonna, L., Amati, L., Magrone, T., Pellegrino, N. M., Jirillo, E., and Caccavo, D. (2000). Enteric bacteria, lipopolysaccharides and related cytokines in inflammatory bowel disease: biological and clinical significance. *J. Endotoxin Res.* 6, 205–214. doi: 10.1179/096805100101532063

Cheng, Y. S., Colonno, R. J., and Yin, F. H. (1983). Interferon induction of fibroblast proteins with guanylate binding activity. *J. Biol. Chem.* 258, 7746–7750. doi: 10.1016/S0021-9258(18)32242-7

Cooper, M. A., Fehniger, T. A., Ponnappan, A., Mehta, V., Wewers, M. D., and Caligiuri, M. A. (2001). Interleukin-1beta costimulates interferon-gamma production by human natural killer cells. *Eur. J. Immunol.* 31, 792–801. doi: 10.1002/1521-4141(200103)31:3<792::AID-IMMU792>3.0.CO;2-U

Croft, M., and Siegel, R. M. (2017). Beyond TNF: TNF superfamily cytokines as targets for the treatment of rheumatic diseases. *Nat. Rev. Rheumatol.* 13, 217–233. doi: 10.1038/nrrheum.2017.22

Daperno, M., D'Haens, G., Van Assche, G., Baert, F., Bulois, P., Maunoury, V., et al. (2004). Development and validation of a new, simplified endoscopic activity score for Crohn's disease: the SES-CD. *Gastrointest. Endosc.* 60, 505–512. doi: 10.1016/S0016-5107(04)01878-4

de Luca, A., Smeekens, S. P., Casagrande, A., Iannitti, R., Conway, K. L., Gresnigt, M. S., et al. (2014). IL-1 receptor blockade restores autophagy and reduces inflammation in chronic granulomatous disease in mice and in humans. *Proc. Natl. Acad. Sci. U.S.A.* 111, 3526–3531. doi: 10.1073/pnas.1322831111

Dupaul-Chicoine, J., Yeretssian, G., Doiron, K., Bergstrom, K. S., McIntire, C. R., LeBlanc, P. M., et al. (2010). Control of intestinal homeostasis, colitis, and colitis-associated colorectal cancer by the inflammatory caspases. *Immunity* 32, 367–378. doi: 10.1016/j.immuni.2010.02.012

Feng, J., Cao, Z., Wang, L., Wan, Y., Peng, N., Wang, Q., et al. (2017). Inducible GBP5 mediates the antiviral response via interferon-related pathways during influenza a virus infection. *J. Innate Immun.* 9, 419–435. doi: 10.1159/000460294

Fisher, S. A., Mirza, M. M., Onnie, C. M., Soars, D., Lewis, C. M., Prescott, N. J., et al. (2007). Combined evidence from three large British association studies rejects TUCAN/CARD8 as an IBD susceptibility gene. *Gastroenterology* 132, 2078–2080. doi: 10.1053/j.gastro.2007.03.086

Friedman, K., Brodsky, A. S., Lu, S., Wood, S., Gill, A. J., Lombardo, K., et al. (2016). Medullary carcinoma of the colon: a distinct morphology reveals a distinctive immunoregulatory microenvironment. *Mod. Pathol.* 29, 528–541. doi: 10.1038/modpathol.2016.54

Graham, D. B., and Xavier, R. J. (2020). Pathway paradigms revealed from the genetics of inflammatory bowel disease. *Nature* 578, 527–539. doi: 10.1038/s41586-020-2025-2

Haque, M., Singh, A. K., Ouseph, M. M., and Ahmed, S. (2021). Regulation of synovial inflammation and tissue destruction by guanylate binding protein 5 in synovial fibroblasts from patients with rheumatoid arthritis and rats with adjuvant-induced arthritis. *Arthritis Rheumatol.* 73, 943–954. doi: 10.1002/art.41611

Hengartner, N. E., Fiedler, J., Schrezenmeier, H., Huber-Lang, M., and Brenner, R. E. (2015). Crucial role of IL1beta and C3a in the in vitro-response of multipotent mesenchymal stromal cells to inflammatory mediators of polytrauma. *PLoS One* 10:e0116772. doi: 10.1371/journal.pone.0116772

Hirota, S. A., Ng, J., Lueng, A., Khajah, M., Parhar, K., Li, Y., et al. (2011). NLRP3 inflammasome plays a key role in the regulation of intestinal homeostasis. *Inflamm. Bowel Dis.* 17, 1359–1372. doi: 10.1002/ibd.21478

Kanai, T., Watanabe, M., Okazawa, A., Nakamaru, K., Okamoto, M., Naganuma, M., et al. (2000). Interleukin 18 is a potent proliferative factor for intestinal mucosal lymphocytes in Crohn's disease. *Gastroenterology* 119, 1514–1523. doi: 10.1053/gast.2000.20260

Krapp, C., Hotter, D., Gawanbacht, A., McLaren, P. J., Kluge, S. F., Sturzel, C. M., et al. (2016). Guanylate Binding Protein (GBP) 5 is an interferon-inducible inhibitor of HIV-1 infectivity. *Cell Host Microbe* 19, 504–514. doi: 10.1016/j.chom.2016.02.019

Li, Z., Qu, X., Liu, X., Huan, C., Wang, H., Zhao, Z., et al. (2020). GBP5 is an interferon-induced inhibitor of respiratory syncytial virus. *J. Virol.* 94, e01407-20. doi: 10.1128/JVI.01407-20

Ligumsky, M., Simon, P. L., Karmeli, F., and Rachmilewitz, D. (1990). Role of interleukin 1 in inflammatory bowel disease–enhanced production during active disease. *Gut* 31, 686–689. doi: 10.1136/gut.31.6.686

Mahida, Y. R., Wu, K., and Jewell, D. P. (1989). Enhanced production of interleukin 1-beta by mononuclear cells isolated from mucosa with active ulcerative colitis of Crohn's disease. *Gut* 30, 835–838. doi: 10.1136/gut.30.6.835

Mao, L., Kitani, A., Similuk, M., Oler, A. J., Albenberg, L., Kelsen, J., et al. (2018). Loss-of-function CARD8 mutation causes NLRP3 inflammasome activation and Crohn's disease. *J. Clin. Investig.* 128, 1793–1806. doi: 10.1172/JCI98642

Matta, S. K., Patten, K., Wang, Q., Kim, B. H., MacMicking, J. D., and Sibley, L. D. (2018). NADPH oxidase and guanylate binding protein 5 restrict survival of avirulent type III strains of *Toxoplasma gondii* in naive macrophages. *mBio* 9, e01393-18. doi: 10.1128/mBio.01393-18

McAlindon, M. E., Hawkey, C. J., and Mahida, Y. R. (1998). Expression of interleukin 1 beta and interleukin 1 beta converting enzyme by intestinal macrophages in health and inflammatory bowel disease. *Gut* 42, 214–219. doi: 10.1136/gut.42.2.214

Meunier, E., Dick, M. S., Dreier, R. F., Schurmann, N., Kenzelmann Broz, D., Warming, S., et al. (2014). Caspase-11 activation requires lysis of pathogen-containing vacuoles by IFN-induced GTPases. *Nature* 509, 366–370. doi: 10.1038/nature13157

Meunier, E., Wallet, P., Dreier, R. F., Costanzo, S., Anton, L., Ruhl, S., et al. (2015). Guanylate-binding proteins promote activation of the AIM2 inflammasome during infection with *Francisella novicida*. *Nat. Immunol.* 16, 476–484. doi: 10.1038/ni.3119

Neudecker, V., Haneklaus, M., Jensen, O., Khailova, L., Masterson, J. C., Tye, H., et al. (2017). Myeloid-derived miR-223 regulates intestinal inflammation via repression of the NLRP3 inflammasome. *J. Exp. Med.* 214, 1737–1752. doi: 10.1084/jem.20160462

Palmela, C., Chevarin, C., Xu, Z., Torres, J., Sevrin, G., Hirten, R., et al. (2018). Adherent-invasive *Escherichia coli* in inflammatory bowel disease. *Gut* 67, 574–587. doi: 10.1136/gutjnl-2017-314903

Patil, P. A., Blakely, A. M., Lombardo, K. A., Machan, J. T., Miner, T. J., Wang, L. J., et al. (2018). Expression of PD-L1, indoleamine 2,3-dioxygenase and the immune microenvironment in gastric adenocarcinoma. *Histopathology* 73, 124–136. doi: 10.1111/his.13504

Pilla, D. M., Hagar, J. A., Haldar, A. K., Mason, A. K., Degrandi, D., Pfeffer, K., et al. (2014). Guanylate binding proteins promote caspase-11-dependent pyroptosis in response to cytoplasmic LPS. *Proc. Natl. Acad. Sci. U.S.A.* 111, 6046–6051. doi: 10.1073/pnas.1321700111

Reinecker, H. C., Steffen, M., Witthoeft, T., Pflueger, I., Schreiber, S., MacDermott, R. P., et al. (1993). Enhanced secretion of tumour necrosis factor-alpha, IL-6, and IL-1 beta by isolated lamina propria mononuclear cells from patients with ulcerative colitis and Crohn's disease. *Clin. Exp. Immunol.* 94, 174–181. doi: 10.1111/j.1365-2249.1993.tb05997.x

Santos, J. C., Dick, M. S., Lagrange, B., Degrandi, D., Pfeffer, K., Yamamoto, M., et al. (2018). LPS targets host guanylate-binding proteins to the bacterial outer membrane for non-canonical inflammasome activation. *EMBO J.* 37:e98089. doi: 10.15252/embj.201798089

Seo, S. U., Kamada, N., Munoz-Planillo, R., Kim, Y. G., Kim, D., Koizumi, Y., et al. (2015). Distinct commensals induce interleukin-1beta via NLRP3 inflammasome in inflammatory monocytes to promote intestinal inflammation in response to injury. *Immunity* 42, 744–755. doi: 10.1016/j.immuni.2015.03.004

Seyed Tabib, N. S., Madgwick, M., Sudhakar, P., Verstockt, B., Korcsmaros, T., and Vermeire, S. (2020). Big data in IBD: big progress for clinical practice. *Gut* 69, 1520–1532. doi: 10.1136/gutjnl-2019-320065

Shenoy, A. R., Wellington, D. A., Kumar, P., Kassa, H., Booth, C. J., Cresswell, P., et al. (2012). GBP5 promotes NLRP3 inflammasome assembly and immunity in mammals. *Science* 336, 481–485. doi: 10.1126/science.1217141

Siegmund, B., Lehr, H. A., Fantuzzi, G., and Dinarello, C. A. (2001). IL-1 beta -converting enzyme (caspase-1) in intestinal inflammation. *Proc. Natl. Acad. Sci. U.S.A.* 98, 13249–13254. doi: 10.1073/pnas.231473998

Tourkochristou, E., Aggeletopoulou, I., Konstantakis, C., and Triantos, C. (2019). Role of NLRP3 inflammasome in inflammatory bowel diseases. *World J. Gastroenterol.* 25, 4796–4804. doi: 10.3748/wjg.v25.i33.4796

Travis, S. P., Schnell, D., Krzeski, P., Abreu, M. T., Altman, D. G., Colombel, J. F., et al. (2013). Reliability and initial validation of the ulcerative colitis endoscopic index of severity. *Gastroenterology* 145, 987–995. doi: 10.1053/j.gastro.2013.07.024

Yang, L., Tang, S., Baker, S. S., Arijs, I., Liu, W., Alkhouri, R., et al. (2019). Difference in pathomechanism between crohn's disease and ulcerative colitis revealed by colon transcriptome. *Inflamm. Bowel Dis.* 25, 722–731. doi: 10.1093/ibd/izy359

Yang, S. K., Kim, H., Hong, M., Lim, J., Choi, E., Ye, B. D., et al. (2011). Association of CARD8 with inflammatory bowel disease in Koreans. *J. Hum. Genet.* 56, 217–223. doi: 10.1038/jhg.2010.170

Yao, X., Zhang, C., Xing, Y., Xue, G., Zhang, Q., Pan, F., et al. (2017). Remodelling of the gut microbiota by hyperactive NLRP3 induces regulatory T cells to maintain homeostasis. *Nat. Commun.* 8:1896. doi: 10.1038/s41467-017-01917-2

Youm, Y. H., Nguyen, K. Y., Grant, R. W., Goldberg, E. L., Bodogai, M., Kim, D., et al. (2015). The ketone metabolite beta-hydroxybutyrate blocks NLRP3 inflammasome-mediated inflammatory disease. *Nat. Med.* 21, 263–269. doi: 10.1038/nm.3804

Yu, X., Jin, J., Zheng, Y., Zhu, H., Xu, H., Ma, J., et al. (2021). GBP5 drives malignancy of glioblastoma via the Src/ERK1/2/MMP3 pathway. *Cell Death Dis.* 12:203. doi: 10.1038/s41419-021-03492-3

Yuan, Y. Y., Xie, K. X., Wang, S. L., and Yuan, L. W. (2018). Inflammatory caspase-related pyroptosis: mechanism, regulation and therapeutic potential for inflammatory bowel disease. *Gastroenterol. Rep.* 6, 167–176. doi: 10.1093/gastro/goy011

Zaki, M. H., Boyd, K. L., Vogel, P., Kastan, M. B., Lamkanfi, M., and Kanneganti, T. D. (2010a). The NLRP3 inflammasome protects against loss of epithelial integrity and mortality during experimental colitis. *Immunity* 32, 379–391. doi: 10.1016/j.immuni.2010.03.003

Zaki, M. H., Vogel, P., Body-Malapel, M., Lamkanfi, M., and Kanneganti, T. D. (2010b). IL-18 production downstream of the Nlrp3 inflammasome confers protection against colorectal tumor formation. *J. Immunol.* 185, 4912–4920. doi: 10.4049/jimmunol.1002046

Conflict of Interest: The authors declare that the research was conducted in the absence of any commercial or financial relationships that could be construed as a potential conflict of interest.

Publisher's Note: All claims expressed in this article are solely those of the authors and do not necessarily represent those of their affiliated organizations, or those of the publisher, the editors and the reviewers. Any product that may be evaluated in this article, or claim that may be made by its manufacturer, is not guaranteed or endorsed by the publisher.

frontiers | Frontiers in Microbiology

REVIEW
published: 27 June 2022
doi: 10.3389/fmicb.2022.948770

Toll-Like Receptor Signaling in Severe Acute Respiratory Syndrome Coronavirus 2-Induced Innate Immune Responses and the Potential Application Value of Toll-Like Receptor Immunomodulators in Patients With Coronavirus Disease 2019

Jiayu Dai[1,2†], Yibo Wang[1,2†], Hongrui Wang[1], Ziyuan Gao[1,2], Ying Wang[1,2], Mingli Fang[1], Shuyou Shi[1], Peng Zhang[3], Hua Wang[1], Yingying Su[4] and Ming Yang[1]**

[1] Department of Molecular Biology, College of Basic Medical Sciences, Jilin University, Changchun, China, [2] College of Clinical Medicine, Jilin University, Changchun, China, [3] Department of Thoracic Surgery, The First Affiliated Hospital of Jilin University, Changchun, China, [4] Department of Anatomy, College of Basic Medical Sciences, Jilin University, Jilin, China

Toll-like receptors (TLRs) are key sensors that recognize the pathogen-associated molecular patterns (PAMPs) of severe acute respiratory syndrome coronavirus 2 (SARS-CoV-2) to activate innate immune response to clear the invading virus. However, dysregulated immune responses may elicit the overproduction of proinflammatory cytokines and chemokines, resulting in the enhancement of immune-mediated pathology. Therefore, a proper understanding of the interaction between SARS-CoV-2 and TLR-induced immune responses is very important for the development of effective preventive and therapeutic strategies. In this review, we discuss the recognition of SARS-CoV-2 components by TLRs and the downstream signaling pathways that are activated, as well as the dual role of TLRs in regulating antiviral effects and excessive inflammatory responses in patients with coronavirus disease 2019 (COVID-19). In addition, this article describes recent progress in the development of TLR immunomodulators including the agonists and antagonists, as vaccine adjuvants or agents used to treat hyperinflammatory responses during SARS-CoV-2 infection.

Keywords: SARS-CoV-2, COVID-19, innate immune response, Toll-like receptor, immunomodulator

OPEN ACCESS

Edited by:
Na Li,
Hainan Medical University, China

Reviewed by:
Pan Liu,
Northwestern University, United States
Guopeng Wang,
Peking University, China

***Correspondence:**
Yingying Su
suyingying@jlu.edu.cn
Ming Yang
myang48@jlu.edu.cn

† These authors have contributed equally to this work

Specialty section:
This article was submitted to Infectious Agents and Disease, a section of the journal Frontiers in Microbiology

Received: *20 May 2022*
Accepted: *06 June 2022*
Published: *27 June 2022*

Citation:
Dai J, Wang Y, Wang H, Gao Z, Wang Y, Fang M, Shi S, Zhang P, Wang H, Su Y and Yang M (2022) Toll-Like Receptor Signaling in Severe Acute Respiratory Syndrome Coronavirus 2-Induced Innate Immune Responses and the Potential Application Value of Toll-Like Receptor Immunomodulators in Patients With Coronavirus Disease 2019. Front. Microbiol. 13:948770. doi: 10.3389/fmicb.2022.948770

INTRODUCTION

Toll-like receptors (TLRs) are members of the pattern recognition receptor (PRR) family, and they play pivotal roles in the activation of innate immune responses and the regulation of cytokine expression (Hedayat et al., 2011; Birra et al., 2020; Debnath et al., 2020). TLRs perform their functions by recognizing distinguishing molecules of invading pathogens, called pathogen-associated molecular patterns (PAMPs), and then initiate innate immune responses *via* several distinct signaling pathways, thereby limiting infection and promoting adaptive immune responses

(Kawai and Akira, 2011). Generally, myeloid differentiation primary response 88 (MyD88) and Toll-IL-1R (TIR)-domain containing adaptor-inducing interferon-β (TRIF) are the two main pathways by which TLRs transduce signals after activation (Kim et al., 2018).

The innate immune system acts as the first line of defense against invading pathogens, including the severe acute respiratory syndrome coronavirus 2 (SARS-CoV-2). SARS-CoV-2 is the causative viral pathogen of the coronavirus disease 2019 (COVID-19), and the COVID-19 pandemic began in March 2020 (Tabary et al., 2020). The characteristics of COVID-19 are extremely variable, and the disease ranges from an asymptomatic form lasting for a few days or mild to severe forms of interstitial pneumonia which requires ventilation therapy and can lead to death (Khan et al., 2020). TLRs recognize SARS-CoV-2-derived molecules and activate innate immune responses. Many studies have shown that SARS-CoV-2 activates the innate immune system *via* TLRs, and mediates the upregulation of TLR expression, which contribute to the elimination of the virus (Aboudounya and Heads, 2021; Bortolotti et al., 2021; Sariol and Perlman, 2021). However, TLR activation may act as a double-edged sword, and dysregulated TLR responses may lead to persistent inflammation and tissue destruction (Yokota et al., 2010; Ebermeyer et al., 2021). For instance, the severity of COVID-19 is associated with cytokine storms in patients which could be produced by overactivation of TLR pathways (Tang et al., 2020; Manik and Singh, 2021). Therefore, a better understanding of the relationship between TLRs and SARS-CoV-2 is critical for understanding the immunopathogenesis involved in COVID-19 and for the preventive and therapeutic application of TLR immunomodulators to combat the disease. In this review, we provide an overview of our recent understanding of the roles of TLRs in SARS-CoV-2-induced immune responses, and we discuss the potential prophylactic and/or therapeutic value of TLR agonists or antagonists in COVID-19 patients.

STRUCTURE AND CLASSIFICATION OF TOLL-LIKE RECEPTORS

All TLRs are type I transmembrane proteins that consist of a leucine-rich repeat (LRR) module, a transmembrane region, and a TIR domain. The LRR motif includes 19–25 tandem sequences containing leucine and is responsible for the recognition of PAMPs, while the TIR endodomain functions to initiate intracellular signaling events *via* downstream adaptors. According to the composition of their subunits, TLRs operate as heterodimers or homodimers. The classification and expression of TLRs differs between species. Thirteen TLRs have been discovered in mice. However, TLR11 has no function, and the TLR12 and TLR13 genes are absent in the human genome. Generally, the TLR family can be divided into two subgroups based on their localization: cell surface TLRs and intracellular TLRs (Kawasaki and Kawai, 2014). Cell surface TLRs reside on the cell membrane and mainly contain TLR1, TLR2, TLR4, TLR5, TLR6, and TLR10, while intracellular TLRs include TLR3, TLR7, TLR8, TLR9, TLR11, TLR12, and TLR13 (**Table 1**). Intracellular TLRs localize to intracellular compartments, such as the endosomes, endoplasmic reticulum, and lysosomes.

Cell surface TLRs mainly recognize microbial membrane components such as lipoproteins, lipids, and proteins. TLR2 forms heterodimers with either TLR1 or TLR6. It recognizes a wide variety of PAMPs including lipoproteins, lipopeptides, peptidoglycans, and zymosan (Yu and Feng, 2018). TLR4 is mainly expressed on cells of the immune system, including macrophages, monocytes, and dendritic cells (DCs). TLR4 recognizes bacterial lipopolysaccharide (LPS) and its activation leads to the synthesis of proinflammatory cytokines and chemokines (Vaure and Liu, 2014). TLR5 is known to specifically sense and recognize bacterial flagellins (Yang and Yan, 2017). The ligands of TLR10 remain unclear but it is believed that human TLR10 collaborates with TLR2 to recognize ligands from *Listeria* and senses influenza A virus during infection; however, TLR10 has no function in mice due to an insertion of a stop codon (Kawasaki and Kawai, 2014).

Intracellular TLRs can recognize nucleic acids derived from foreign pathogens and self-derived nucleic acids in the context of some autoimmune diseases (Schlee and Hartmann, 2016). TLR3 is widely distributed in various epithelial cells, fibroblasts, nerve cells and immune cells. TLR3 mainly recognizes viral double-stranded RNA (dsRNA), self-RNAs derived from damaged cells and the replication intermediates generated during the life cycle of single-stranded RNA (ssRNA) viruses and DNA viruses (Turton et al., 2020). TLR7 is localized to endosomes and is mainly expressed by B cells, monocytes and plasmacytoid DCs (pDCs), while TLR8 expression is closely associated with conventional DCs (cDCs). TLR7/8 can recognize ssRNA and activate MyD88-dependent pathways, which lead to the subsequent production of type I interferons (IFNs) and inflammatory cytokines (Kawai and Akira, 2011; Jung and Lee, 2021). TLR9 recognizes unmethylated CpG-DNA motifs which are frequently presented in viral and bacterial DNA, and activates the innate immune response to eliminate these pathogens. In addition, TLR9 also binds to the DNA sequences that contain cytosine in the second position from the 5′ end (5′-xCx DNA), which cooperatively promotes dimerization and activation of TLR9 in the presence of CpG DNA (Ohto et al., 2018). TLR11 is located to endolysosomes, and TLR12 is predominantly expressed in myeloid cells. These TLRs function in recognizing profilin from the parasites (Lester and Li, 2014). TLR13, the orphan receptor in mice, was found to recognize a conserved 23S ribosomal RNA (rRNA) sequence in bacteria (Wang et al., 2016).

TOLL-LIKE RECEPTOR RECOGNITION OF SEVERE ACUTE RESPIRATORY SYNDROME CORONAVIRUS 2 COMPONENTS

Structure of Severe Acute Respiratory Syndrome Coronavirus 2

Viral proteins and nucleic acids can serve as PAMPs, which are sensed by TLRs to induce the production of antiviral

TABLE 1 | Human and murine TLR classification and their natural ligands.

Classification	TLR name	Gene location	Ligands	References
Cell surface TLRs	TLR1	5C3.1 (mouse)/4p14 (human)	Triacylated lipopeptides, lipoarabinomannan	Yu and Feng, 2018; Su et al., 2019
	TLR2	3E3 (mouse)/4q31.3 (human)	Zymosan, peptidoglycan, lipoteichoic acid, endogenous HSP, HMGB1, gp96	Patidar et al., 2018; Yu and Feng, 2018
	TLR4	4C1 (mouse)/9q33.1 (human)	LPS, endogenous HSP, HMGB1, β-defensin 2	Vaure and Liu, 2014; Patidar et al., 2018
	TLR5	1H5 (mouse)/1q41 (human)	Flagellin	Yang and Yan, 2017
	TLR6	5C3.1 (mouse)/4p14 (human)	Diacylated lipopeptides, zymosan, lipoteichoic acid	Yu and Feng, 2018
	TLR10	4p14 (human)	Unknown	Kawasaki and Kawai, 2014
Intracellular TLRs	TLR3	8B1.1 (mouse)/4q35.1 (human)	dsRNA	Turton et al., 2020
	TLR7	XF5 (mouse)/Xp22.2 (human)	ssRNA	Tanji et al., 2013
	TLR8	XF5 (mouse)/Xp22.2 (human)	ssRNA	Tanji et al., 2013
	TLR9	9F1 (mouse)/3p21.2 (human)	Unmethylated CpG DNA, 5′-xCx DNA	Ohto et al., 2018
	TLR11	11C1 (mouse)	Profilin of *Toxoplasma gondii*	Lester and Li, 2014
	TLR12	4D2.2 (mouse)	Profilin of *Toxoplasma gondii*	Lester and Li, 2014
	TLR13	XD (mouse)	Bacterial 23S rRNA	Oldenburg et al., 2012

and inflammatory cytokines. Thus, it is quite necessary to understand the nucleic acid composition and protein structure of SARS-CoV-2. Similar to other coronaviruses, SARS-CoV-2 is a positive-sense single-stranded RNA (+ssRNA) virus and its genome is approximately 29.9 kb in size; this genome mainly encodes four major structural proteins, including the spike (S), nucleocapsid (N), membrane (M), and envelope (E) proteins. The S protein consists of the receptor binding subunit S1 and the membrane fusing subunit S2. S1 includes a N-terminal domain (NTD), receptor-binding domain (RBD), subdomain 1 (SD1) and subdomain 2 (SD2). S2 includes a fusion peptide (FP), heptad repeat 1 (HR1), heptad repeat 2 (HR2), and transmembrane (TM). The rest of the genome includes two major open reading frames (ORFs)-ORF1a and ORF1b, which can be translated to pp1a and pp1b polypeptides, and then cleaved to form 16 non-structural proteins (Zhang et al., 2021).

Toll-Like Receptors Recognize Viral Proteins and RNA of Severe Acute Respiratory Syndrome Coronavirus 2

When an infection occurs, viruses enter the body and adhere to cell surfaces. Cell surface TLRs are most likely to be involved in recognizing molecular patterns from SARS-CoV-2 to induce immune responses. The S protein is a major structural protein and is essential for the interaction of SARS-CoV-2 with host cell receptors. In addition to its direct binding to angiotensin-converting enzyme II (ACE2), the S protein is a potent viral PAMP that is sensed by TLR2 in macrophages, monocytes, and lung epithelial cells. Then TLR2 forms heterodimers with TLR1 or TLR6, promoting formation of a complex containing MyD88 with IRAK kinase family members, activating nuclear factor-κB (NF-κB) and mitogen-activated protein kinase (MAPK) signaling, and ultimately leading to the production of inflammatory cytokines and chemokines (Khan et al., 2021). SARS-CoV-2 infection also increases the expression of TLR2 and other molecules, such as melanoma differentiation-associated gene 5 (MDA5), ACE2 and interferon regulatory factor 3 (IRF3) (Mohanty et al., 2021; Yang et al., 2022), and the expression of TLR2 is positively associated with the severity of COVID-19 (Zheng et al., 2021). In addition to the S protein, the immunogenic properties of other structural proteins have also been investigated. Recent reports have found that TLR2 binds to the SARS-CoV-2 E and N proteins, but only the SARS-CoV-2 N protein induces TLR2 activation, which was not observed with other coronavirus-derived N proteins (Qian et al., 2021; Zheng et al., 2021). TLR4 is well known to recognize bacterial LPS. Actually, TLR4 was found to exhibit a very strong ability to bind to the S protein of SARS-CoV-2 by molecular docking studies (Choudhury and Mukherjee, 2020), and a surface plasmon resonance (SPR) assay confirmed that trimeric SARS-CoV-2 S protein, which is presented on the surface of viral particles, directly binds to TLR4 with a high affinity of ∼300 nM (Zhao et al., 2021). These findings suggest that TLR4 also plays a potential role in the recognition of SARS-CoV-2. This hypothesis has been supported by other evidence demonstrating that the S1 subunit of S protein elicits inflammatory responses *in vitro* and signals through TLR4. The direct exposure of microglia, macrophages, or TLR4 signaling transgenic HEK293 cells to S1 could activate the MyD88-dependent pathway, resulting in the upregulated expression of proinflammatory cytokines (Shirato and Kizaki, 2021; Frank et al., 2022). Moreover, the responses induced by S1 could be blocked by the TLR4-specific inhibitor Resatorvid or TLR4 siRNA (Shirato and Kizaki, 2021; Zhao et al., 2021). Taken together, these findings suggested that the TLR2 and TLR4 can sense SARS-CoV-2 structural proteins, and they may function independently to induce inflammatory processes (**Figure 1**).

When the SARS-CoV-2 binds to a host cell receptor such as ACE2, it fuses to the host cell membrane and releases its contents into the cell. Viral ssRNA and its replication intermediate dsRNA, are likely to be initially detected by host cells *via* TLR7/8 and TLR3 in endosomes. Previous studies showed that SARS-CoV-2 infection of Calu-3/MRC-5 multicellular spheroids induced the

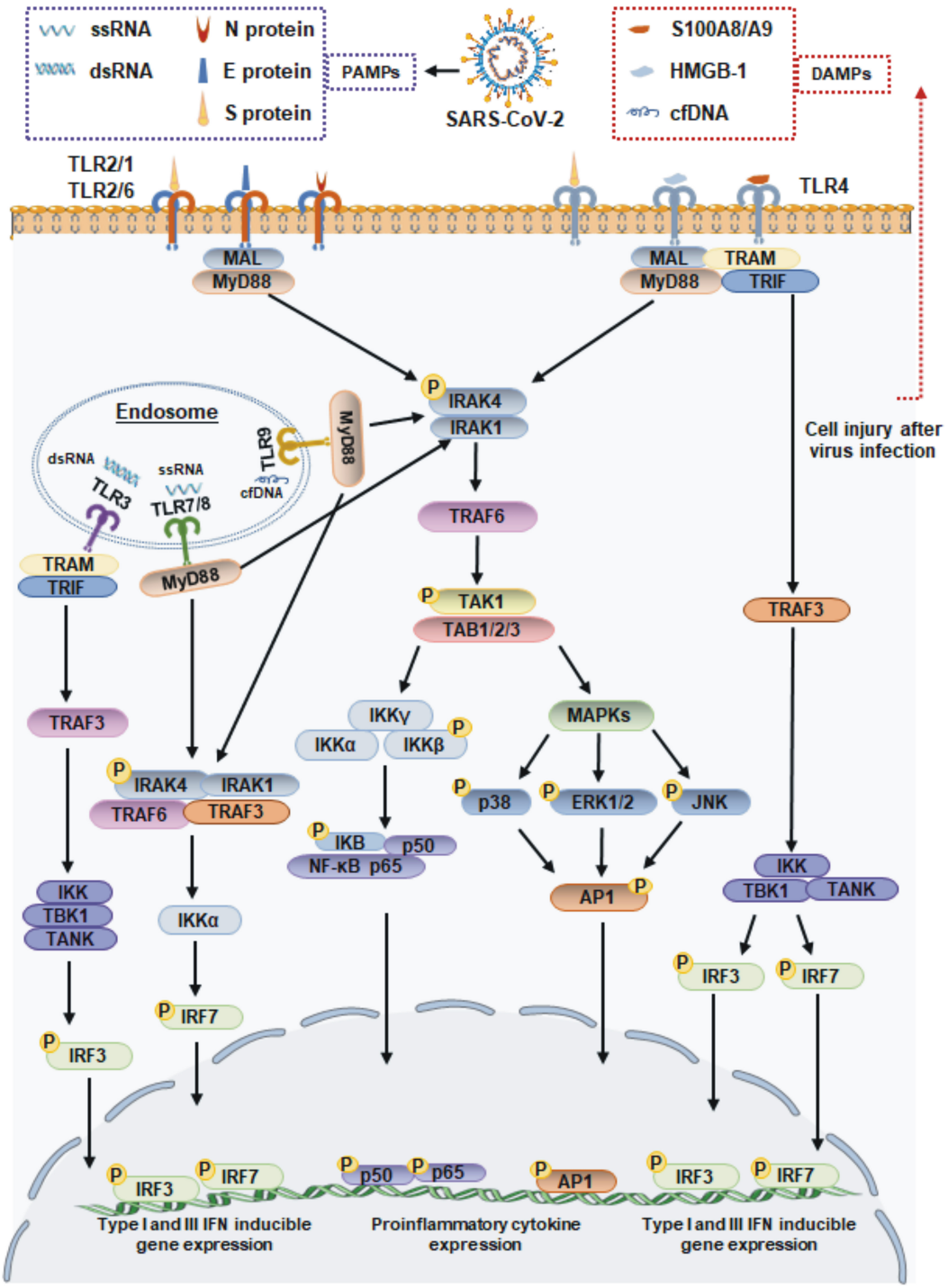

FIGURE 1 | Toll-like receptor-mediated antiviral and inflammatory responses during SARS-CoV-2 infection. TLR1/2/6 and 4 localize to cell membrane, and TLR3, TLR7/8, and 9 localize to endosome surface. The viral proteins of SARS-CoV-2 signal through TLR2 and TLR4 to activate the adaptor MyD88, which subsequently signals *via* NF-κB and MAPK to promote the expression of proinflammatory cytokines. TLR4 also recruits the adapter protein TRIF, which activates the TRAF3, resulting the IRF3 activation to lead the production of type I and III IFN. The ssRNA or dsRNA replication intermediates of SARS-CoV-2 are recognized by TLR3 and TLR7/8, respectively. The TLR7/8 recruit MyD88, and TLR3 *via* TRIF molecule. The proinflammatory cytokines induced by DAMPs accumulating during SARS-CoV-2 infection are driven by the transcription factor NF-κB. MAL, MyD88 adapter-like; TRAF, tumor necrosis factor receptor-associated factor; TRIF, TIR-domain-containing adapter-inducing interferon-β; TRAM, TRIF-related adaptor molecule; IRAK1/4, interleukin-1 receptor associated kinase 1/4; TAK1, transforming growth factor β-activated kinase 1; TAB, TAK1-binding proteins; IKK, IkB kinase; TBK1, TANK-binding kinase 1; ERK1/2, extracellular signal-regulated kinases 1/2; JNK, c-Jun N-terminal kinase; AP-1, activating protein-1.

activation of both the TLR3 and TLR7/8 RNA sensor pathways (Bortolotti et al., 2021). Subsequently, TLR7/8 signaling engages the IRF-7 and MyD88-NF-κB signaling pathways, leading to the increased production of type I IFNs and proinflammatory cytokines (Jung and Lee, 2021). In particular, TLR3 signaling relies on the TRIF adaptor protein but not the MyD88 adaptor protein. TRIF interacts with TRAF6 and TRAF3, leading to the activation of IRF3, which results in the release of IFN-α and IFN-β (Kawasaki and Kawai, 2014; **Figure 1**).

TOLL-LIKE RECEPTOR-MEDIATED ANTIVIRAL AND INFLAMMATORY RESPONSES AGAINST SEVERE ACUTE RESPIRATORY SYNDROME CORONAVIRUS 2: A DOUBLE-EDGED SWORD

It is well-known that TLR signaling plays a key role in host defense against many pathogens including SARS-CoV-2. However, TLR activation can act as a double-edged sword, and it may activate immune-mediated pathogenesis instead of inducing an immune response that defends against pathogens.

Toll-Like Receptor Signaling as an Antiviral Mechanism During Severe Acute Respiratory Syndrome Coronavirus 2 Infection

The IFN signaling cascade induced by TLR activation is crucial for controlling SARS-CoV-2 infection. As mentioned above, during SARS-CoV-2 infection, the expression of TLRs, such as TLR3 and TLR7, is elevated (Jung and Lee, 2021), and activated TLR3, TLR4 and TLR7/8 can interact with the signaling adaptor TRIF, inducing the phosphorylation and translocation of IRF3 and IRF7 and the transcription of type I and III IFN genes. Mice lacking the TLR3 gene are prone to SARS-CoV-2 infection and have increased mortality rates (Totura et al., 2015). Additionally, TLR copy numbers also play a role in the production of IFN; for example, the TLR7 and TLR8 genes are located on the X chromosome. Therefore, TLR7/8 copy numbers are higher in women than in men and their biallelic expression leads to the stronger activation of TLR7/8 and more production of type I IFN. These phenomena are correlated with higher resistance to SARS-CoV-2 infection and better prognosis in women (Viveiros et al., 2021). Moreover, loss-of-function variants of TLR7 have recently been reported to underlie a strong predisposition to severe COVID-19 in a small number of males (Fallerini et al., 2021). Both type I and III IFNs can induce an antiviral transcriptional program (Park and Iwasaki, 2020), thus, dysregulation of host IFN responses has been shown to be associated with severe disease progression in COVID-19 patients. For example, pDCs use TLR7 to sense ssRNA fragments from viruses that are rich in guanine and uracil (GU rich), and TLR7 seems to mainly act *via* the MyD88-TRAF3/6 pathway, inducing the production of type I IFN, IFN-γ, and IFN-λ3 and the upregulation of CD86 expression (Bortolotti et al., 2021; Salvi et al., 2021). However, the pDCs response of COVID-19-infected patients is functionally impaired (Choi and Shin, 2021).

In addition, peripheral blood immune cells from severe COVID-19 patients exhibit diminished type I and III IFN responses but enhanced proinflammatory IL-6 and TNF-α responses (Blanco-Melo et al., 2020; Hadjadj et al., 2020). Analysis of the serum from critical COVID-19 patients showed the levels of proinflammatory cytokines and chemokines are strongly elevated while the levels of type I and III IFNs are undetectable (Park and Iwasaki, 2020). Notably, SARS-CoV-2 also possesses some strategies to escape the innate immune response due to a wide range of viral proteins, such as the M, NSP6, NSP13, NSP15, ORF3b, ORF6, ORF8, and ORF9b proteins, that affect the IFN-mediated antiviral responses (Jiang et al., 2020; Konno et al., 2020; Lei et al., 2020; Han et al., 2021; Sui L. et al., 2021). Therefore, future investigations are still required to obtain a clear understanding of the inhibition of TLR signaling by SARS-CoV-2.

Toll-Like Receptor Signaling as a Part of the Inflammatory Response During Severe Acute Respiratory Syndrome Coronavirus 2 Infection

The activation of TLRs plays a dual role in the progression of COVID-19. It is thought that the production of proinflammatory cytokines is induced by the activation of different TLRs, such as TLR2, TLR4, and TLR7/8, which greatly contributes to the pathogenesis of COVID-19 and its severity. Immunopathological processes that cause death in COVID-19 patients occur due to the interaction of TLRs with virus particles (Patra et al., 2021). TLR2 and TLR4 sense viral proteins, and the expression levels of molecules related to the TLR2- and TLR4-inflammatory signaling molecules are upregulated in in COVID-19 patients, which suggest the involvement of TLR2 and TLR4 signaling in the induction of pathological inflammation during COVID-19 (Sohn et al., 2020). Moreover, several studies have shown that an overwhelming TLR7 response may promote the development of severe COVID-19 (Fallerini et al., 2021; Kayesh et al., 2021), highlighting the clinical importance of the TLR-mediated immune response during SARS-CoV-2 infection. Moreover, other studies on SARS-CoV-2 have revealed the pathological role of TLR4 and TLR7/8 in excessive inflammatory response in COVID-19 patients as it leads to the formation of neutrophil extracellular traps (NETs) and the activation of inflammasomes, leading to acute lung injury (Khadke et al., 2020; Sohn et al., 2020; Veras et al., 2020).

Additionally, obese and overweight individuals exhibit significantly increased TLR expression, which impacts the severity of COVID-19. It is hypothesized that desensitization of TLR signaling may occur due to chronic stimulation in obese and elderly people. TLR/MyD88 signaling, which is enhanced in obese individuals, may contribute to the excessive inflammatory response observed during severe infection with SARS-CoV-2 (Cuevas et al., 2021). Similarly, significantly elevated expression of IL-6 and TNF-α was observed to be associated with TLR

expression in obese individuals but not in controls (Kayesh et al., 2021). Moreover, delayed IFN responses fail to control the virus and can cause inflammation and tissue damage. Delayed but considerable type I IFN responses in SARS-CoV-2 infected BALB/c mice trigger the accumulation of monocytes and macrophages as well as the production of proinflammatory cytokines, resulting in lethal pneumonia, vascular leakage, and insufficient T-cell responses (Channappanavar et al., 2016).

Furthermore, damage to host cell caused by SARS-CoV-2 infection can also lead to the release of endogenous danger-associated molecular patterns (DAMPs). These endogenous self-antigens, such as high-mobility group box 1 (HMGB1) and heat shock proteins (HSPs), activate MAPK and NF-κB signaling, which triggers an inflammatory response. In COVID-19 patients, HMGB1 can be released from dying cells and functions as a pro-inflammatory inducer to bind with TLR4, leading to the production of IL-1β, IL-6, and TNF-α (Yang et al., 2015; Cicco et al., 2020). Another DAMP shown to regulate inflammation during SARS-CoV-2 infection is the S100A8/A9 complex, which is released from host neutrophils and has been proposed to be a potential biomarker in COVID-19 patients. Mechanistically, the S100A8/A9 complex is also an endogenous ligand of TLR4 on DCs and mediates host proinflammatory responses (Mellett and Khader, 2022). TLR9 is not directly involved in recognition of SARS-CoV-2. However, cell-free DNA (cfDNA) production that is triggered by tissue injury during virus infection, cfDNA can subsequently act as a DAMP and exacerbates inflammation *via* TLR9. Recent studies have reported that elevated levels of cfDNA in COVID-19 patients are strongly correlated with COVID-19 disease severity (Andargie et al., 2021; Cavalier et al., 2021). Moreover, the increased cfDNA levels in COVID-19 patients generates excessive mitochondrial ROS (mtROS) production in a concentration-dependent manner (Andargie et al., 2021). Taken together, these findings suggest that host molecules that are released during SARS-CoV-2 infection may function independently as DAMPs, resulting in a more severe inflammatory response (**Figure 1**).

TOLL-LIKE RECEPTOR AGONISTS AS ADJUVANTS FOR CORONAVIRUS DISEASE 2019 VACCINES

More efficient and safe vaccines are still a critical need for combating COVID-19. In vaccine development, adjuvants are required to increase antigen recognition and enhance the magnitude and durability of the elicited immune responses. TLR agonists are considered important molecules for triggering and enhancing rapid and long-term innate immune responses, and they have been extensively studied for use as vaccine adjuvants against cancer and microbial infections. Compared to the first-generation adjuvants, such as aluminum adjuvant, TLR agonist adjuvants could guide DC maturation to elicit a stronger T-cell response. Various TLR agonists, including Pam3CSK4, poly(I:C), monophosphoryl lipid A (MPLA), resiquimod (R848), and CpG oligonucleotide (ODN), are currently under investigation for use as vaccine adjuvants to prevent SARS-CoV-2 infection. The TLR agonists currently under development for COVID-19 vaccines are listed in **Table 2**.

Toll-Like Receptor 1/2 Agonists

The TLR1/TLR2 ligand Pam3CSK4 is a synthetic triacylated lipopeptide and can activate the proinflammatory transcription factor NF-κB. A new water-soluble synthetic Pam3CSK4-derivative, named XS15, is being used in combination with peptides from the SARS-CoV-2 spike protein to develop a vaccine format that induces $CD4^+$ T-cell responses against peptides predicted to bind to HLA-DR (Rammensee et al., 2021). In a phase I open-label trial, a peptide-based vaccine CoVac-1, which is composed of T-cell epitopes derived from various SARS-CoV-2 proteins, was combined with XS15 and emulsified in Montanide ISA 51 VG. This vaccine induced profound SARS-CoV-2-specific T-cell responses targeting multiple vaccine peptides in all the study participants. Moreover, the interferon (IFN)-γ T-cell responses induced by CoVac-1 persisted in the follow-up analyses and surpassed those detected after vaccination with approved vaccines (Heitmann et al., 2022). In addition, in a study of a SARS-CoV-2 subunit vaccine, a combination of TLR1/2 and TLR3 agonists (L-pampo) was found to be a potent adjuvant for eliciting a neutralization antibody response and an antigen-specific cellular immune response against SARS-CoV-2, resulting in a substantially decreased viral load in a ferret model (Jeong et al., 2021).

Toll-Like Receptor 4 Agonists

The TLR4 ligand LPS can regulate inflammation and effector T-cell differentiation. MPLA is a modified form of LPS that exhibits strong immune stimulatory activity but avoids most inflammatory toxicity. It has been approved for utilization as an adjuvant in vaccines against human papilloma virus and hepatitis B virus. In a previous vaccine study, MPLA-adjuvanted truncated spike protein fused with Fc of human IgG (S377-588-Fc) induced a significantly higher titer of specific IgG antibodies against Middle East respiratory syndrome coronavirus than did the alum-adjuvanted protein. In particular, MPLA-adjuvanted S377-588-Fc protein elicited a stronger Th2 (IgG1)-biased response (Zhang et al., 2016). Recently, a biomaterial COVID-19 vaccine based on mesoporous silica rods (MSRs) and loaded with MPLA, granulocyte-macrophage colony-stimulating factor (GM-CSF), and SARS-CoV-2 viral protein antigens was shown to slowly release their cargo and form subcutaneous scaffolds that recruited and activated antigen-presenting cells (APCs) at the local site to generate adaptive immune responses (Langellotto et al., 2021). The SARS-CoV-2 is still mutating; however, the MPLA-adjuvanted antigens like S-trimer/MPLA, RBD/MPLA, and S1/MPLA remain to induce a strong humoral and cellular immune responses against spike variants, including alpha, beta, gamma, delta, and omicron (Wang et al., 2022). Another TLR4 agonist, inulin acetate (InAc), which is a plant-based polymer, has been reported to induce high IgG1, IgG2a, and sIgA titers against antigens in serum after intranasal immunization using antigen-loaded InAc nanoparticles (InAc-NPs); this approach resulted in a strong memory response indicative of both humoral

TABLE 2 | Toll-like receptor agonists as vaccine adjuvants in COVID-19 vaccine formulation.

TLR agonists	Platform	Adjuvant	Antigen	Formulation	Immunological response			Route	Animal model or clinical trial	References
					Nab	sIgA	T-cell response			
TLR 1/2	Peptide vaccine	XS15	T-cell epitopes from viral protein	Montanide ISA 51 VG	Weak	NA	$CD4^+$ T and IFN-γ response	SC	Phase II trial	Rammensee et al., 2021; Heitmann et al., 2022
TLR 1/2 and TLR3	Subunit vaccine	L-pampo	RBD and S1 antigens	NA	Strong	NA	IFN-γ response	IM	BALB/c and ferret	Jeong et al., 2021
TLR3	Adenovirus-based vaccine	dsRNA	SARS-CoV-2 S and N gene	Adenovirus	Strong	Moderate	NA	Oral	Hamsters and phase I trial	Tiboni et al., 2021
TLR3	Subunit vaccine	PIKA	Trimeric S antigen	NA	Strong	NA	Balanced Th1/Th2 and IFN-γ response	IM	Rabbits, mice, and non-human primates	Liu Y. et al., 2021
TLR3 and TLR9	Subunit vaccine	CpG ODN + poly I:C + IL-15	S1 protein	PLGA or DOTAP	Weak	Strong	$CD4^+$ T response	IM, IN	Rhesus macaques	Sui Y. et al., 2021
TLR4	Subunit vaccine	MPLA + PUUC	S1 protein	Polymer nanoparticles	Strong	Strong	Memory T-cell response	IN, IM	BALB/c	Atalis et al., 2022
TLR-4	Subunit vaccine	MPLA + GM-CSF	SARS-CoV-2 N/S1/S2 proteins	MSRs	Strong	NA	$CD4^+$ and $CD8^+$ T response	SC	BALB/c	Langellotto et al., 2021
TLR7/8	Subunit vaccine	Alhydroxiquim-II	Trimeric spike antigen	NA	Strong	NA	$CD4^+$ T	IM	C57BL/6, rabbits, horses	Counoupas et al., 2022
TLR7/8	Subunit vaccine	R848	S1 protein	Nanoparticle decorated erythrocytes	Strong	NA	$CD4^+$ T response	IV	C57BL/6	Wang et al., 2021
TLR7/8	Inactivated vaccine	Chemisorbed Algel	Inactivated antigen	NA	Strong	NA	$CD4^+$ T and Th1-biased responses	IM	Mice, rats, and rabbits	Ganneru et al., 2021
TLR-7 or TLR-9	Subunit vaccine	AS37-Alum or CpG 1018-Alum	RBD antigen	Self-assembling protein nanoparticle	Strong	NA	$CD4^+$ T response	IM	Rhesus macaques and phase II trial	Arunachalam et al., 2021; Richmond et al., 2021
TLR9	mRNA vaccine	CpG SD-101	RBD mRNA	CART	Strong	NA	$CD4^+$ and $CD8^+$ T	IV, IM	BALB/c	Haabeth et al., 2021
TLR-9	Subunit vaccine	CpG 7909-Alum	Trimeric S antigen	NA	Strong	NA	$CD4^+$ T response	IM	BALB/c and monkeys	Liu H. et al., 2021

NA, not available; Nab, naturalization antibody; SC, subcutaneous; IM, intramuscular; IV, intravenous; IN, intranasal; PUUC, RIG-I agonist; PLGA, poly(lactic-co-glycolic acid); DOTAP, 1,2-dioleoyl-3-trimethylammonium-propane; CART, charge-altering releasable transporters.

and cellular immune activation, and may be useful in the development of a COVID-19 vaccine (Bakkari et al., 2021).

Toll-Like Receptor 7/8 Agonists

Toll-Like Receptor 7/8 activation may be investigated as an additional strategy for anti-SARS-CoV-2 vaccines address the current challenge of viral escape. TLR7 stimulation may help viral clearance through Th1 antiviral responses as well as exert beneficial broncho-vasodilatory activity (Khalifa and Ghoneim, 2021). As a synthetic and selective ligand for TLR7, imiquimod has been approved for human-papillomavirus-induced genital and perianal warts. An imiquimod analog, resiquimod (R848), was proven to be a dual TLR7 and TLR8 synthetic agonist that elicits prominent IFN-α/β and IL-6 responses and robust cytotoxic T-cell (CTL) and B-cell proliferation; thus, it is particularly suited for antiviral immune responses. Indeed, the cytokine profiles induced by R848, are almost identical to the profiles induced by the licensed mRNA vaccines against COVID-19 (Rossmann et al., 2021). In a SARS-CoV-2 virus-mimetic nanoparticle vaccine, the SARS-CoV-2 spike protein S1 subunit and R848 were attached to erythrocytes and injected into mice, resulting in greater maturation and activation of APCs, production of specific IgG antibodies, and systemic antiviral T-cell responses than the nanoparticles alone (Wang et al., 2021). However, R848 adjuvanticity should stress more on vaccine formulation. A recent study showed that R848 conjugated to multilamellar liposomes rather than forming a linear structure, resulting in stronger immunostimulatory activity (Liang et al., 2020). Moreover, an R848-encapsulating poly lactic-co-glycolic acid (PLGA) nanoparticle can reduce the

excessive level of inflammatory cytokines induced by free R848 (Chen et al., 2021), which could be beneficial for providing an appropriate immune response and long-term safety in vaccine development.

Toll-Like Receptor 3/9 Agonists

Optimal protection against coronavirus probably involves neutralizing antibodies and $CD8^+$ T cells. Among the TLR agonists, the TLR3 and TLR9 ligands, poly(I:C) and CpG ODN significantly augment the $CD8^+$ T-cell responses to a greater extent than other adjuvants. Thus, CpG ODN and poly(I:C) have been utilized as adjuvants in influenza vaccines. Studies have demonstrated that CpG ODN or PIKA [a stabilized derivative of poly(I:C)] can stimulate enhanced IgG production in animals have been used in the context of immunization with an inactivated SARS-CoV-2 vaccine (Gai et al., 2008; Gupta and Gupta, 2020). Moreover, compared with the alum adjuvanted SARS-CoV-2 S1 vaccine, intranasal boosting with nanoparticles, formulating with CpG 1018 and poly(I:C), elicits higher dimeric IgA production, IFN-α production, and T-cell activation in rhesus macaques (Sui Y. et al., 2021). In another study, a recombinant S trimeric protein adjuvanted with PIKA was reported to induce high titers of SARS-CoV-2 neutralizing antibodies and to protect non-human primates from virus challenge (Liu Y. et al., 2021). Another CpG ODN 7909-adjuvanted SARS-CoV-2 vaccine, 202-COV, is a S-protein subunit vaccine formulated with aluminum hydroxide; that elicits robust neutralizing antibody responses and substantial $CD4^+$ T-cell responses in both mice and non-human primates; this vaccine is currently being investigated in phase II studies of COVID-19 (Liu H. et al., 2021). CpG ODN is capable of inducing both cellular and humoral immune responses, and it preferentially induces Th1-biased responses. Mice that were immunized with mRNA encoding the spike protein of SARS-CoV-2, co-formulated with CpG ODN, developed therapeutically relevant levels of RBD-specific neutralizing antibodies in both circulation and lung bronchial fluids. In addition, vaccination elicited strong and long-lasting RBD-specific Th1 T-cell responses including $CD4^+$ and $CD8^+$ T-cell memory responses (Haabeth et al., 2021).

TOLL-LIKE RECEPTOR SIGNALING INHIBITORS PROTECT AGAINST HYPERINFLAMMATORY RESPONSE IN SEVERE ACUTE RESPIRATORY SYNDROME CORONAVIRUS 2 INFECTION

Uncontrolled TLR-mediated inflammation has been suggested to contribute to immunopathological consequences in COVID-19 patients. It is quite obvious that targeted manipulation of TLR signaling decreases excessive inflammatory responses. TLR4 is one of the major contributors to SARS-CoV-2 infectivity and pathogenesis, and its antagonists are capable of inhibiting the harmful effects of TLR4 signaling. For example, Lipid X is a Lipid A biosynthetic precursor that can competitively bind to TLR4 to block cytokine production *via* the downstream signaling pathways. Therefore, many TLR4 modulators, both natural and synthetic, can be investigated in the context of COVID-19 treatment. TAK242 is a potent and selective TLR4 antagonist that inhibits the release of inflammatory cytokines from human THP-1 cells after exposure to SARS-CoV-2. Therefore, it is postulated that TAK242 may improve patient outcomes by dampening the inflammatory response and preventing systemic infection in patients with COVID-19 (Kate Gadanec et al., 2021).

The intracellular RNA sensors TLR3 and TLR7/8 are thought to be involved in the hyperinflammatory responses induced by SARS-CoV-2 infection. A TLR7/8 antagonist, Enpatoran (M5049), is a potent dual TLR7/8 inhibitor that is expected to cease the hyperinflammatory milieu in symptomatic patients with COVID-19. Furthermore, Merck has already initiated a phase II randomized, controlled clinical study evaluating the efficacy and safety of M5049 in the COVID-19 patient population (Khalifa and Ghoneim, 2021; Port et al., 2021). Similarly, famotidine, a specific histamine H2 receptor antagonist, can inhibit TLR3 expression in SARS-CoV-2 infected cells and reduce TLR3-dependent NF-κB and IRF3 signaling, subsequently controlling antiviral and inflammatory responses (Mukherjee et al., 2021) and reducing the risk of intubation and death in hospitalized patients with COVID-19 (Freedberg et al., 2020). Another TLR signaling inhibitor, the PPARα agonist oleoylethanolamide (OEA), was reported to attenuate TLR3-induced hyperthermia and reduce the expression of hyperthermia-related genes including IL-1β, iNOS, COX2, and m-PGES in the hypothalamus (Flannery et al., 2021).

Toll-like receptor antagonists are not only used as individual drugs but may also be used in combination with immunomodulatory drugs in severe cases of COVID-19 to enhance potential synergistic effects and possibly reduce adverse effects. Currently, most TLR antagonists are being investigated in clinical trials to evaluate their efficacy in reducing detrimental immune effects without causing a drastic change in their basal levels to maintain the immune homeostasis.

CONCLUSION

Toll-like receptors are important constituents of the innate immune system and can recognize a wide variety of PAMPs from viruses. This review has described the various TLRs that are involved in the immunopathogenesis of SARS-CoV-2 infection and the effects of application of TLR immunomodulators in patients with COVID-19. Of the TLRs that have been identified, TLR7/TLR8 and TLR3 are intracellular receptor that sense viral ssRNA, and dsRNA replication intermediates, respectively. TLR2 and TLR4 reside on the cell surface and are activated by SARS-CoV-2 glycoproteins. TLR signaling elicits antiviral and proinflammatory cytokine production through

MyD88-dependent and/or TRIF-dependent pathways. The activation of the innate immune response often contributes to viral clearance and disease resolution. Therefore, TLR agonists could be formulated as adjuvants for use with the S protein or RBD to enhance neutralizing antibody production and T-cell responses against SARS-CoV-2 infection since they elicit timely and optimal TLR responses. However, dysregulated immune signaling may lead to the detrimental production of proinflammatory cytokines and chemokines that cause severe disease. Thus, the use of TLR antagonists might exert a beneficial effect, by attenuating deleterious hyperinflammatory responses in severe COVID-19 patients. However, most of these new therapeutics or combination strategies for anti-SARS-CoV-2 infection are currently being studied in clinical trials of various phases.

AUTHOR CONTRIBUTIONS

JD, YBW, and HRW contributed to the writing of the manuscript. MY and YS provided the ideas and revised the draft manuscript. ZG, YW, MF, SS, PZ, and HW approved the version to be published. MF provided a professional English language revision. All authors read and approved the final manuscript.

FUNDING

This work was supported by the National Natural Science Foundation of China (grant number 81902111) and the Department of Finance of Jilin Province (grant number JLSWSRCZX2020-00107).

REFERENCES

Aboudounya, M. M., and Heads, R. J. (2021). COVID-19 and Toll-Like Receptor 4 (TLR4): SARS-CoV-2 May Bind and Activate TLR4 to Increase ACE2 Expression, Facilitating Entry and Causing Hyperinflammation. *Mediators Inflamm.* 2021:8874339. doi: 10.1155/2021/8874339

Andargie, T. E., Tsuji, N., Seifuddin, F., Jang, M. K., Yuen, P. S., Kong, H., et al. (2021). Cell-free DNA maps COVID-19 tissue injury and risk of death and can cause tissue injury. *JCI Insight* 6:e147610. doi: 10.1172/jci.insight.147610

Arunachalam, P. S., Walls, A. C., Golden, N., Atyeo, C., Fischinger, S., Li, C., et al. (2021). Adjuvanting a subunit COVID-19 vaccine to induce protective immunity. *Nature* 594, 253–258. doi: 10.1038/s41586-021-03530-2

Atalis, A., Keenum, M. C., Pandey, B., Beach, A., Pradhan, P., Vantucci, C., et al. (2022). Nanoparticle-delivered TLR4 and RIG-I agonists enhance immune response to SARS-CoV-2 subunit vaccine. *bioRxiv*[Preprint]. doi: 10.1101/2022.01.31.478507

Bakkari, M. A., Valiveti, C. K., Kaushik, R. S., and Tummala, H. (2021). Toll-like Receptor-4 (TLR4) Agonist-Based Intranasal Nanovaccine Delivery System for Inducing Systemic and Mucosal Immunity. *Mol. Pharm.* 18, 2233–2241. doi: 10.1021/acs.molpharmaceut.0c01256

Birra, D., Benucci, M., Landolfi, L., Merchionda, A., Loi, G., Amato, P., et al. (2020). COVID 19: a clue from innate immunity. *Immunol. Res.* 68, 161–168. doi: 10.1007/s12026-020-09137-5

Blanco-Melo, D., Nilsson-Payant, B. E., Liu, W. C., Uhl, S., Hoagland, D., and Moller, R. (2020). Imbalanced Host Response to SARS-CoV-2 Drives Development of COVID-19. *Cell* 181, 1036–1045.e9. doi: 10.1016/j.cell.2020.04.026

Bortolotti, D., Gentili, V., Rizzo, S., Schiuma, G., Beltrami, S., Strazzabosco, G., et al. (2021). TLR3 and TLR7 RNA Sensor Activation during SARS-CoV-2 Infection. *Microorganisms* 9:1820. doi: 10.3390/microorganisms9091820

Cavalier, E., Guiot, J., Lechner, K., Dutsch, A., Eccleston, M., Herzog, M., et al. (2021). Circulating Nucleosomes as Potential Markers to Monitor COVID-19 Disease Progression. *Front. Mol. Biosci.* 8:600881. doi: 10.3389/fmolb.2021.600881

Channappanavar, R., Fehr, A. R., Vijay, R., Mack, M., Zhao, J., Meyerholz, D. K., et al. (2016). Dysregulated Type I Interferon and Inflammatory Monocyte-Macrophage Responses Cause Lethal Pneumonia in SARS-CoV-Infected Mice. *Cell Host Microbe* 19, 181–193. doi: 10.1016/j.chom.2016.01.007

Chen, L., Huang, Q., Zhao, T., Sui, L., Wang, S., Xiao, Z., et al. (2021). Nanotherapies for sepsis by regulating inflammatory signals and reactive oxygen and nitrogen species: new insight for treating COVID-19. *Redox Biol.* 45:102046. doi: 10.1016/j.redox.2021.102046

Choi, H., and Shin, E. C. (2021). Roles of Type I and III Interferons in COVID-19. *Yonsei Med. J.* 62, 381–390. doi: 10.3349/ymj.2021.62.5.381

Choudhury, A., and Mukherjee, S. (2020). In silico studies on the comparative characterization of the interactions of SARS-CoV-2 spike glycoprotein with ACE-2 receptor homologs and human TLRs. *J. Med. Virol.* 92, 2105–2113. doi: 10.1002/jmv.25987

Cicco, S., Cicco, G., Racanelli, V., and Vacca, A. (2020). Neutrophil Extracellular Traps (NETs) and Damage-Associated Molecular Patterns (DAMPs): two Potential Targets for COVID-19 Treatment. *Mediators Inflamm.* 2020:7527953. doi: 10.1155/2020/7527953

Counoupas, C., Pino, P., Stella, A. O., Ashley, C., Lukeman, H., Bhattacharyya, N. D., et al. (2022). High-Titer Neutralizing Antibodies against the SARS-CoV-2 Delta Variant Induced by Alhydroxyquim-II-Adjuvanted Trimeric Spike Antigens. *Microbiol. Spectr.* 10:e0169521. doi: 10.1128/spectrum.01695-21

Cuevas, A. M., Clark, J. M., and Potter, J. J. (2021). Increased TLR/MyD88 signaling in patients with obesity: is there a link to COVID-19 disease severity? *Int. J. Obes.* 45, 1152–1154. doi: 10.1038/s41366-021-00768-8

Debnath, M., Banerjee, M., and Berk, M. (2020). Genetic gateways to COVID-19 infection: implications for risk, severity, and outcomes. *FASEB J.* 34, 8787–8795. doi: 10.1096/fj.202001115R

Ebermeyer, T., Cognasse, F., Berthelot, P., Mismetti, P., Garraud, O., and Hamzeh-Cognasse, H. (2021). Platelet Innate Immune Receptors and TLRs: a Double-Edged Sword. *Int. J. Mol. Sci.* 22:7894. doi: 10.3390/ijms22157894

Fallerini, C., Daga, S., Mantovani, S., Benetti, E., Picchiotti, N., Francisci, D., et al. (2021). Association of Toll-like receptor 7 variants with life-threatening COVID-19 disease in males: findings from a nested case-control study. *eLife* 10:e67569. doi: 10.7554/eLife.67569

Flannery, L. E., Kerr, D. M., Hughes, E. M., Kelly, C., Costello, J., Thornton, A. M., et al. (2021). N-acylethanolamine regulation of TLR3-induced hyperthermia and neuroinflammatory gene expression: a role for PPARalpha. *J. Neuroimmunol.* 358:577654. doi: 10.1016/j.jneuroim.2021.577654

Frank, M. G., Nguyen, K. H., Ball, J. B., Hopkins, S., Kelley, T., Baratta, M. V., et al. (2022). SARS-CoV-2 spike S1 subunit induces neuroinflammatory, microglial and behavioral sickness responses: evidence of PAMP-like properties. *Brain Behav. Immun.* 100, 267–277. doi: 10.1016/j.bbi.2021.12.007

Freedberg, D. E., Conigliaro, J., Wang, T. C., Tracey, K. J., Callahan, M. V., Abrams, J. A., et al. (2020). Famotidine Use Is Associated With Improved Clinical Outcomes in Hospitalized COVID-19 Patients: a Propensity Score Matched Retrospective Cohort Study. *Gastroenterology* 159, 1129–1131.e3. doi: 10.1053/j.gastro.2020.05.053

Gai, W., Zou, W., Lei, L., Luo, J., Tu, H., Zhang, Y., et al. (2008). Effects of different immunization protocols and adjuvant on antibody responses to inactivated SARS-CoV vaccine. *Viral Immunol.* 21, 27–37. doi: 10.1089/vim.2007.0079

Ganneru, B., Jogdand, H., Daram, V. K., Das, D., Molugu, N. R., Prasad, S. D., et al. (2021). Th1 skewed immune response of whole virion inactivated SARS CoV 2 vaccine and its safety evaluation. *iScience* 24:102298. doi: 10.1016/j.isci.2021.102298

Gupta, T., and Gupta, S. K. (2020). Potential adjuvants for the development of a SARS-CoV-2 vaccine based on experimental results from similar coronaviruses. *Int. Immunopharmacol.* 86:106717. doi: 10.1016/j.intimp.2020.106717

Haabeth, O. A. W., Lohmeyer, J. J. K., Sallets, A., Blake, T. R., Sagiv-Barfi, I., Czerwinski, D. K., et al. (2021). An mRNA SARS-CoV-2 Vaccine Employing Charge-Altering Releasable Transporters with a TLR-9 Agonist Induces

Neutralizing Antibodies and T Cell Memory. *ACS Cent. Sci.* 7, 1191–1204. doi: 10.1021/acscentsci.1c00361

Hadjadj, J., Yatim, N., Barnabei, L., Corneau, A., Boussier, J., Smith, N., et al. (2020). Impaired type I interferon activity and inflammatory responses in severe COVID-19 patients. *Science* 369, 718–724. doi: 10.1126/science.abc6027

Han, L., Zhuang, M. W., Deng, J., Zheng, Y., Zhang, J., Nan, M. L., et al. (2021). SARS-CoV-2 ORF9b antagonizes type I and III interferons by targeting multiple components of the RIG-I/MDA-5-MAVS, TLR3-TRIF, and cGAS-STING signaling pathways. *J. Med. Virol.* 93, 5376–5389. doi: 10.1002/jmv.27050

Hedayat, M., Netea, M. G., and Rezaei, N. (2011). Targeting of Toll-like receptors: a decade of progress in combating infectious diseases. *Lancet Infect. Dis.* 11, 702–712. doi: 10.1016/s1473-3099(11)70099-8

Heitmann, J. S., Bilich, T., Tandler, C., Nelde, A., Maringer, Y., Marconato, M., et al. (2022). A COVID-19 peptide vaccine for the induction of SARS-CoV-2 T cell immunity. *Nature* 601, 617–622. doi: 10.1038/s41586-021-04232-5

Jeong, S. K., Heo, Y. K., Jeong, J. H., Ham, S. J., Yum, J. S., Ahn, B. C., et al. (2021). COVID-19 Subunit Vaccine with a Combination of TLR1/2 and TLR3 Agonists Induces Robust and Protective Immunity. *Vaccines* 9:957.

Jiang, H. W., Zhang, H. N., Meng, Q. F., Xie, J., Li, Y., Chen, H., et al. (2020). SARS-CoV-2 Orf9b suppresses type I interferon responses by targeting TOM70. *Cell. Mol. Immunol.* 17, 998–1000. doi: 10.1038/s41423-020-0514-8

Jung, H. E., and Lee, H. K. (2021). Current Understanding of the Innate Control of Toll-like Receptors in Response to SARS-CoV-2 Infection. *Viruses* 13:2132. doi: 10.3390/v13112132

Kate Gadanec, L., Qaradakhi, T., McSweeney, K., Ashiana Ali, B., Zulli, A., and Apostolopoulos, V. (2021). Dual targeting of Toll-like receptor 4 and angiotensin-converting enzyme 2: a proposed approach to SARS-CoV-2 treatment. *Future Microbiol.* 16, 205–209. doi: 10.2217/fmb-2021-0018

Kawai, T., and Akira, S. (2011). Toll-like receptors and their crosstalk with other innate receptors in infection and immunity. *Immunity* 34, 637–650. doi: 10.1016/j.immuni.2011.05.006

Kawasaki, T., and Kawai, T. (2014). Toll-like receptor signaling pathways. *Front. Immunol.* 5:461. doi: 10.3389/fimmu.2014.00461

Kayesh, M. E. H., Kohara, M., and Tsukiyama-Kohara, K. (2021). An Overview of Recent Insights into the Response of TLR to SARS-CoV-2 Infection and the Potential of TLR Agonists as SARS-CoV-2 Vaccine Adjuvants. *Viruses* 13:2302. doi: 10.3390/v13112302

Khadke, S., Ahmed, N., Ahmed, N., Ratts, R., Raju, S., Gallogly, M., et al. (2020). Harnessing the immune system to overcome cytokine storm and reduce viral load in COVID-19: a review of the phases of illness and therapeutic agents. *Virol. J.* 17:154. doi: 10.1186/s12985-020-01415-w

Khalifa, A. E., and Ghoneim, A. I. (2021). Potential value of pharmacological agents acting on toll-like receptor (TLR) 7 and/or TLR8 in COVID-19. *Curr. Res. Pharmacol. Drug Discov.* 2:100068. doi: 10.1016/j.crphar.2021.100068

Khan, S., Shafiei, M. S., Longoria, C., Schoggins, J., Savani, R. C., and Zaki, H. (2021). SARS-CoV-2 spike protein induces inflammation via TLR2-dependent activation of the NF-κB pathway. *bioRxiv* [Preprint]. doi: 10.1101/2021.03.16.435700.

Khan, S., Siddique, R., Shereen, M. A., Ali, A., Liu, J., Bai, Q., et al. (2020). Emergence of a Novel Coronavirus, Severe Acute Respiratory Syndrome Coronavirus 2: biology and Therapeutic Options. *J. Clin. Microbiol.* 58:e00187–20. doi: 10.1128/jcm.00187-20

Kim, A. Y., Shim, H. J., Kim, S. Y., Heo, S., and Youn, H. S. (2018). Differential regulation of MyD88- and TRIF-dependent signaling pathways of Toll-like receptors by cardamonin. *Int. Immunopharmacol.* 64, 1–9. doi: 10.1016/j.intimp.2018.08.018

Konno, Y., Kimura, I., Uriu, K., Fukushi, M., Irie, T., Koyanagi, Y., et al. (2020). SARS-CoV-2 ORF3b Is a Potent Interferon Antagonist Whose Activity Is Increased by a Naturally Occurring Elongation Variant. *Cell Rep.* 32:108185. doi: 10.1016/j.celrep.2020.108185

Langellotto, F., Dellacherie, M. O., Yeager, C., Ijaz, H., Yu, J., Cheng, C. A., et al. (2021). A Modular Biomaterial Scaffold-Based Vaccine Elicits Durable Adaptive Immunity to Subunit SARS-CoV-2 Antigens. *Adv. Healthc. Mater.* 10:e210137. doi: 10.1002/adhm.202101370

Lei, X., Dong, X., Ma, R., Wang, W., Xiao, X., Tian, Z., et al. (2020). Activation and evasion of type I interferon responses by SARS-CoV-2. *Nat. Commun.* 11:3810. doi: 10.1038/s41467-020-17665-9

Lester, S. N., and Li, K. (2014). Toll-like receptors in antiviral innate immunity. *J. Mol. Biol.* 426, 1246–1264. doi: 10.1016/j.jmb.2013.11.024

Liang, Z., Zhu, H., Wang, X., Jing, B., Li, Z., Xia, X., et al. (2020). Adjuvants for Coronavirus Vaccines. *Front. Immunol.* 11:589833. doi: 10.3389/fimmu.2020.589833

Liu, H., Zhou, C., An, J., Song, Y., Yu, P., Li, J., et al. (2021). Development of recombinant COVID-19 vaccine based on CHO-produced, prefusion spike trimer and alum/CpG adjuvants. *Vaccine* 39, 7001–7011. doi: 10.1016/j.vaccine.2021.10.066

Liu, Y., Dai, L., Feng, X., Gao, R., Zhang, N., Wang, B., et al. (2021). Fast and long-lasting immune response to S-trimer COVID-19 vaccine adjuvanted by PIKA. *Mol. Biomed.* 2:29. doi: 10.1186/s43556-021-00054-z

Manik, M., and Singh, R. K. (2021). Role of toll-like receptors in modulation of cytokine storm signaling in SARS-CoV-2-induced COVID-19. *J. Med. Virol.* 94, 869–877. doi: 10.1002/jmv.27405

Mellett, L., and Khader, S. A. (2022). S100A8/A9 in COVID-19 pathogenesis: impact on clinical outcomes. *Cytokine Growth Factor Rev.* 63, 90–97. doi: 10.1016/j.cytogfr.2021.10.004

Mohanty, M. C., Varose, S. Y., Sawant, U. P., and Fernandes, M. M. (2021). Expression of innate immune response genes in upper airway samples of SARS-CoV-2 infected patients: a preliminary study. *Indian J. Med. Res.* 153, 677–683. doi: 10.4103/ijmr.IJMR_131_21

Mukherjee, R., Bhattacharya, A., Bojkova, D., Mehdipour, A. R., Shin, D., Khan, K. S., et al. (2021). Famotidine inhibits toll-like receptor 3-mediated inflammatory signaling in SARS-CoV-2 infection. *J. Biol. Chem.* 297:100925. doi: 10.1016/j.jbc.2021.100925

Ohto, U., Ishida, H., Shibata, T., Sato, R., Miyake, K., and Shimizu, T. (2018). Toll-like Receptor 9 Contains Two DNA Binding Sites that Function Cooperatively to Promote Receptor Dimerization and Activation. *Immunity* 48, 649-658.e4. doi: 10.1016/j.immuni.2018.03.013

Oldenburg, M., Krüger, A., Ferstl, R., Kaufmann, A., Nees, G., Sigmund, A., et al. (2012). TLR13 recognizes bacterial 23S rRNA devoid of erythromycin resistance-forming modification. *Science* 337, 1111–1115. doi: 10.1126/science.1220363

Park, A., and Iwasaki, A. (2020). Type I and Type III Interferons - Induction, Signaling, Evasion, and Application to Combat COVID-19. *Cell Host Microbe.* 27, 870–878. doi: 10.1016/j.chom.2020.05.008

Patidar, A., Selvaraj, S., Sarode, A., Chauhan, P., Chattopadhyay, D., and Saha, B. (2018). DAMP-TLR-cytokine axis dictates the fate of tumor. *Cytokine* 104, 114–123. doi: 10.1016/j.cyto.2017.10.004

Patra, R., Chandra Das, N., and Mukherjee, S. (2021). Targeting human TLRs to combat COVID-19: a solution? *J. Med. Virol.* 93, 615–617. doi: 10.1002/jmv.26387

Port, A., Shaw, J. V., Klopp-Schulze, L., Bytyqi, A., Vetter, C., Hussey, E., et al. (2021). Phase 1 study in healthy participants of the safety, pharmacokinetics, and pharmacodynamics of enpatoran (M5049), a dual antagonist of toll-like receptors 7 and 8. *Pharmacol. Res. Perspect.* 9:e00842. doi: 10.1002/prp2.842

Qian, Y., Lei, T., Patel, P. S., Lee, C. H., Monaghan-Nichols, P., Xin, H. B., et al. (2021). Direct Activation of Endothelial Cells by SARS-CoV-2 Nucleocapsid Protein Is Blocked by Simvastatin. *J. Virol.* 95:e0139621. doi: 10.1128/JVI.01396-21

Rammensee, H. G., Gouttefangeas, C., Heidu, S., Klein, R., Preuss, B., Walz, J. S., et al. (2021). Designing a SARS-CoV-2 T-Cell-Inducing Vaccine for High-Risk Patient Groups. *Vaccines* 9:428. doi: 10.3390/vaccines9050428

Richmond, P., Hatchuel, L., Dong, M., Ma, B., Hu, B., Smolenov, I., et al. (2021). Safety and immunogenicity of S-Trimer (SCB-2019), a protein subunit vaccine candidate for COVID-19 in healthy adults: a phase 1, randomised, double-blind, placebo-controlled trial. *Lancet* 397, 682–694. doi: 10.1016/s0140-6736(21)00241-5

Rossmann, L., Bagola, K., Stephen, T., Gerards, A. L., Walber, B., Ullrich, A., et al. (2021).). Distinct single-component adjuvants steer human DC-mediated T-cell polarization via Toll-like receptor signaling toward a potent antiviral immune response. *Proc. Natl. Acad. Sci. U.S..A.* 118:e2103651118. doi: 10.1073/pnas.2103651118

Salvi, V., Nguyen, H. O., Sozio, F., Schioppa, T., Gaudenzi, C., Laffranchi, M., et al. (2021). SARS-CoV-2-associated ssRNAs activate inflammation and immunity via TLR7/8. *JCI Insight* 6:e150542.

Sariol, A., and Perlman, S. (2021). SARS-CoV-2 takes its Toll. *Nat. Immunol.* 22, 801–802. doi: 10.1038/s41590-021-00962-w

Schlee, M., and Hartmann, G. (2016). Discriminating self from non-self in nucleic acid sensing. *Nat Rev. Immunol.* 16, 566–580. doi: 10.1038/nri.2016.78

Shirato, K., and Kizaki, T. (2021). SARS-CoV-2 spike protein S1 subunit induces pro-inflammatory responses via toll-like receptor 4 signaling in murine and human macrophages. *Heliyon* 7:e06187. doi: 10.1016/j.heliyon.2021.e06187

Sohn, K. M., Lee, S. G., Kim, H. J., Cheon, S., Jeong, H., Lee, J., et al. (2020). COVID-19 Patients Upregulate Toll-like Receptor 4-mediated Inflammatory Signaling That Mimics Bacterial Sepsis. *J. Korean Med. Sci.* 35:e343. doi: 10.3346/jkms.2020.35.e343

Su, L., Wang, Y., Wang, J., Mifune, Y., Morin, M. D., Jones, B. T., et al. (2019). Structural Basis of TLR2/TLR1 Activation by the Synthetic Agonist Diprovocim. *J. Med. Chem.* 62, 2938–2949. doi: 10.1021/acs.jmedchem.8b01583

Sui, L., Zhao, Y., Wang, W., Wu, P., Wang, Z., Yu, Y., et al. (2021). SARS-CoV-2 Membrane Protein Inhibits Type I Interferon Production Through Ubiquitin-Mediated Degradation of TBK1. *Front. Immunol.* 12:662989. doi: 10.3389/fimmu.2021.662989

Sui, Y., Li, J., Zhang, R., Prabhu, S. K., Andersen, H., Venzon, D., et al. (2021). Protection against SARS-CoV-2 infection by a mucosal vaccine in rhesus macaques. *JCI Insight* 6:e148494. doi: 10.1172/jci.insight.148494

Tabary, M., Khanmohammadi, S., Araghi, F., Dadkhahfar, S., and Tavangar, S. M. (2020). Pathologic features of COVID-19: a concise review. *Pathol. Res. Pract.* 216:153097. doi: 10.1016/j.prp.2020.153097

Tang, Y., Liu, J., Zhang, D., Xu, Z., Ji, J., and Wen, C. (2020). Cytokine Storm in COVID-19: the Current Evidence and Treatment Strategies. *Front. Immunol.* 11:1708. doi: 10.3389/fimmu.2020.01708

Tanji, H., Ohto, U., Shibata, T., Miyake, K., and Shimizu, T. (2013). Structural reorganization of the Toll-like receptor 8 dimer induced by agonistic ligands. *Science* 339, 1426–1429. doi: 10.1126/science.1229159

Tiboni, M., Casettari, L., and Illum, L. (2021). Nasal vaccination against SARS-CoV-2: synergistic or alternative to intramuscular vaccines? *Int. J. Pharm.* 603:120686. doi: 10.1016/j.ijpharm.2021.120686

Totura, A. L., Whitmore, A., Agnihothram, S., Schafer, A., Katze, M. G., Heise, M. T., et al. (2015). Toll-Like Receptor 3 Signaling via TRIF Contributes to a Protective Innate Immune Response to Severe Acute Respiratory Syndrome Coronavirus Infection. *mBio* 6:e00638-15. doi: 10.1128/mBio.00638-15

Turton, H. A., Thompson, A. A. R., and Farkas, L. (2020). RNA Signaling in Pulmonary Arterial Hypertension-A Double-Stranded Sword. *Int. J. Mol. Sci.* 21:3124. doi: 10.3390/ijms21093124

Vaure, C., and Liu, Y. (2014). A comparative review of toll-like receptor 4 expression and functionality in different animal species. *Front. Immunol.* 5:316. doi: 10.3389/fimmu.2014.00316

Veras, F. P., Pontelli, M. C., Silva, C. M., Toller-Kawahisa, J. E., de Lima, M., Nascimento, D. C., et al. (2020). SARS-CoV-2-triggered neutrophil extracellular traps mediate COVID-19 pathology. *J. Exp. Med.* 217:e20201129. doi: 10.1084/jem.20201129

Viveiros, A., Rasmuson, J., Vu, J., Mulvagh, S. L., Yip, C. Y. Y., Norris, C. M., et al. (2021). Sex differences in COVID-19: candidate pathways, genetics of ACE2, and sex hormones. *Am. J. Physiol. Heart Circ. Physiol.* 320, H296–H304. doi: 10.1152/ajpheart.00755.2020

Wang, J., Chai, J., and Wang, H. (2016). Structure of the mouse Toll-like receptor 13 ectodomain in complex with a conserved sequence from bacterial 23S ribosomal RNA. *FEBS J.* 283, 1631–1635. doi: 10.1111/febs.13628

Wang, J., Yin, X. G., Wen, Y., Lu, J., Zhang, R. Y., Zhou, S. H., et al. (2022). MPLA-Adjuvanted Liposomes Encapsulating S-Trimer or RBD or S1, but Not S-ECD, Elicit Robust Neutralization Against SARS-CoV-2 and Variants of Concern. *J. Med. Chem.* 65, 3563–3574. doi: 10.1021/acs.jmedchem.1c02025

Wang, L., Wang, X., Yang, F., Liu, Y., Meng, L., Pang, Y., et al. (2021). Systemic antiviral immunization by virus-mimicking nanoparticles-decorated erythrocytes. *Nano Today* 40:101280. doi: 10.1016/j.nantod.2021.101280

Yang, C. A., Huang, Y. L., and Chiang, B. L. (2022). Innate immune response analysis in COVID-19 and kawasaki disease reveals MIS-C predictors. *J. Formos Med. Assoc.* 121, 623–632. doi: 10.1016/j.jfma.2021.06.009

Yang, H., Wang, H., Ju, Z., Ragab, A. A., Lundback, P., Long, W., et al. (2015). MD-2 is required for disulfide HMGB1-dependent TLR4 signaling. *J. Exp. Med.* 212, 5–14. doi: 10.1084/jem.20141318

Yang, J., and Yan, H. (2017). TLR5: beyond the recognition of flagellin. *Cell Mol. Immunol.* 14, 1017–1019. doi: 10.1038/cmi.2017.122

Yokota, S., Okabayashi, T., and Fujii, N. (2010). The battle between virus and host: modulation of Toll-like receptor signaling pathways by virus infection. *Mediators Inflamm.* 2010:184328. doi: 10.1155/2010/184328

Yu, L., and Feng, Z. (2018). The Role of Toll-Like Receptor Signaling in the Progression of Heart Failure. *Mediators Inflamm.* 2018:9874109. doi: 10.1155/2018/9874109

Zhang, N., Channappanavar, R., Ma, C., Wang, L., Tang, J., Garron, T., et al. (2016). Identification of an ideal adjuvant for receptor-binding domain-based subunit vaccines against Middle East respiratory syndrome coronavirus. *Cell. Mol. Immunol.* 13, 180–190. doi: 10.1038/cmi.2015.03

Zhang, Q., Xiang, R., Huo, S., Zhou, Y., Jiang, S., Wang, Q., et al. (2021). Molecular mechanism of interaction between SARS-CoV-2 and host cells and interventional therapy. *Signal Transduct. Target. Ther.* 6:233. doi: 10.1038/s41392-021-00653-w

Zhao, Y., Kuang, M., Li, J., Zhu, L., Jia, Z., Guo, X., et al. (2021). SARS-CoV-2 spike protein interacts with and activates TLR41. *Cell Res.* 31, 818–820. doi: 10.1038/s41422-021-00495-9

Zheng, M., Karki, R., Williams, E. P., Yang, D., Fitzpatrick, E., Vogel, P., et al. (2021). TLR2 senses the SARS-CoV-2 envelope protein to produce inflammatory cytokines. *Nat. Immunol.* 22, 829–838. doi: 10.1038/s41590-021-00937-x

Conflict of Interest: The authors declare that the research was conducted in the absence of any commercial or financial relationships that could be construed as a potential conflict of interest.

frontiers | Frontiers in Microbiology

TYPE Original Research
PUBLISHED 04 August 2022
DOI 10.3389/fmicb.2022.964112

OPEN ACCESS

EDITED BY
Na Li,
Hainan Medical University, China

REVIEWED BY
Wei Sun,
Albany Medical College, United States
Xiao Wang,
Inner Mongolia University, China

*CORRESPONDENCE
Mingli Fang
fangml@jlu.edu.cn
Ming Yang
myang48@jlu.edu.cn

SPECIALTY SECTION
This article was submitted to Infectious Agents and Disease, a section of the journal Frontiers in Microbiology

RECEIVED 08 June 2022
ACCEPTED 30 June 2022
PUBLISHED 04 August 2022

CITATION
Zhang C, Wang H, Wang H, Shi S, Zhao P, Su Y, Wang H, Yang M and Fang M (2022) A microsatellite DNA-derived oligodeoxynucleotide attenuates lipopolysaccharide-induced acute lung injury in mice by inhibiting the HMGB1-TLR4-NF-κB signaling pathway.
Front. Microbiol. 13:964112.
doi: 10.3389/fmicb.2022.964112

A microsatellite DNA-derived oligodeoxynucleotide attenuates lipopolysaccharide-induced acute lung injury in mice by inhibiting the HMGB1-TLR4-NF-κB signaling pathway

Chenghua Zhang[1,2], Hui Wang[1], Hongrui Wang[1], Shuyou Shi[1], Peiyan Zhao[1], Yingying Su[3], Hua Wang[1], Ming Yang[1]* and Mingli Fang[1]*

[1]Department of Molecular Biology, College of Basic Medical Sciences, Jilin University, Changchun, China, [2]Department of Endoscopy, Jilin Provincial Cancer Hospital, Changchun, China, [3]Department of Anatomy, College of Basic Medical Sciences, Jilin University, Changchun, China

Acute lung injury (ALI) with uncontrolled inflammatory response has high morbidity and mortality rates in critically ill patients. Pathogen-associated molecular patterns (PAMPs) are involved in the development of uncontrolled inflammatory response injury and associated lethality. In this study, we investigated the inhibit effect of MS19, a microsatellite DNA-derived oligodeoxynucleotide (ODN) with AAAG repeats, on the inflammatory response induced by various PAMPs *in vitro* and *in vivo*. In parallel, a microsatellite DNA with AAAC repeats, named as MS19-C, was used as controls. We found that MS19 extensively inhibited the expression of inflammatory cytokines interleukin (IL)-6 and tumor necrosis factor (TNF)-α induced by various PAMPs stimulation, including DNA viruses, RNA viruses, bacterial components lipopolysaccharide (LPS), and curdlan, as well as the dsDNA and dsRNA mimics, in primed bone marrow-derived macrophage (BMDM). Other than various PAMPs, MS19 also demonstrated obvious effects on blocking the high mobility group box1 (HMGB1), a representative damage-associated-molecular pattern (DAMP), nuclear translocation and secretion. With the base substitution from G to C, MS19-C has been proved that it has lost the inhibitory effect. The inhibition is associated with nuclear factor kappa B (NF-κB) signaling but not the mitogen-activated protein kinase (MAPK) transduction. Moreover, MS19 capable of inhibiting the IL-6 and TNF-α production and blocking the HMGB1 nuclear translocation and secretion in LPS-stimulated cells was used to treat mice ALI induced by LPS *in vivo*. In the

ALI mice model, MS19 significantly inhibited the weight loss and displayed the dramatic effect on lessening the ALI by reducing consolidation, hemorrhage, intra-alveolar edema in lungs of the mice. Meanwhile, MS19 could increase the survival rate of ALI by downregulating the inflammation cytokines HMGB1, TNF-a, and IL-6 production in the bronchoalveolar lavage fluid (BALF). The data suggest that MS19 might display its therapeutic role on ALI by inhibiting the HMGB1-TLR4-NF-κB signaling pathway.

KEYWORDS

inflammation, NF-κB – nuclear factor kappa B, acute lung injury (ALI), high-mobility group box 1 (HMGB1), oligodeoxynucleotide (ODN), pathogen-associated molecular patterns (PAMPs)

Introduction

The innate immune system plays an important role in the control of pathogens, and it can be activated to produce a proinflammatory response by the recognition of pathogen-associated molecular patterns (PAMPs) *via* pattern recognition receptors (PRRs) (Li and Chang, 2021). The best-known examples of PAMPs include lipopolysaccharide (LPS) of Gram-negative bacteria and nucleic acids of pathogens. Among all the PRRs, Toll-like receptors (TLRs) have been studied most extensively. For example, it is known that TLR4 senses the LPS from bacteria, TLR2 recognizes polysaccharide and lipoproteins, TLR3 and TLR7/8 recognize viral double-stranded RNA (dsRNA) and single-stranded RNA (ssRNA), and TLR9 responds to microbial DNA rich in non-methylated CG motifs (CpGs), respectively (Mu and Hur, 2021). Upon activation, TLRs recruit a cytoplasmic protein, myeloid differentiation primary response protein 88 (MyD88), and subsequently bind the interleukin 1R-associated kinase (IRAK) complex. In turn, IRAK dissociates from the receptor–adapter complex upon phosphorylation and interacts with TNFR-associated factor 6 (TRAF6). Then, TRAF6 activates transforming growth factor activated kinase-1 (TAK1) and subsequently leads to the activation of two major pathways involving the Rel family transcription factor NF-κB and the mitogen-activated protein kinase (MAPK) family. The MAPKs mainly include the extracellular signal-regulated kinase (ERK) and p38. Activation of the MAPKs and NF-kB signaling pathways promotes inflammation by inducing the expression of interleukin (IL)-6, tumor necrosis factor-α (TNF-α), IL-1β, and some inflammatory chemokines (Park et al., 2022; Yue et al., 2022). In addition, interferon regulatory factor 5 (IRF5) is another downstream transcription factor in TLRs/MyD88 signaling pathways. TLRs activation triggers the formation of MyD88-IRF5-TRAF6 complexes and then activates IRF5, which leads to the IRF5 nuclear translocation to initial the transcription of proinflammatory cytokines (Tang et al., 2021).

Although inflammation can defend against invading pathogens, it is also a double-edged sword. Usually, deregulated or severe inflammation induced by PAMPs has been linked to tissue injury and inflammatory diseases, such as acute lung inflammatory injury, septic peritonitis, and multiple sclerosis (Zheng et al., 2019; Sun et al., 2022). Moreover, some endogenous molecules called damage-associated molecular patterns (DAMPs) could be passively released from the damaged cells of tissue injury (Zhou et al., 2021). High-mobility group box 1 (HMGB1) is a nuclear DNA-binding protein and acts as a typical DAMP molecule, which plays an important role in sterile inflammatory responses. HMGB1 can also be actively released from the nucleus to the extracellular space in response to different stimuli. The active secretion always requires the translocation of nuclear HMGB1 to the cytoplasm and the secretion of cytoplasmic HMGB1 to reach the extracellular space (Ding et al., 2021). Inside the nucleus, HMGB1 has been found to increase the binding affinity of many transcription factors to their cognate DNA sequences, such as NF−κB (Xue et al., 2021). More importantly, HMGB1 is also involved in extracellular activity as an endogenous danger signal, which participates in cell–cell interactions including the production of proinflammatory cytokines. For example, HMGB1 protein can interact with multiple cell surface receptors, including TLR2, TLR4, and TLR9, and subsequently activate NF−κB and IFN regulatory factor pathways, stimulating more production of cytokines and chemokines, aggravating the inflammatory response and tissue damage (Ge et al., 2021). Therefore, there is a need to precisely control and tightly regulate the TLRs-mediated signaling pathways induced by PAMPs and DAMPs for preventing the inflammation-induced pathology. Medicines that inhibit the activation of the TLRs signaling pathway are potential anti-inflammatory agents and may prevent tissue inflammatory damage.

In contrast to microbial DNA, host-derived DNA contents are usually considered as anti-inflammatory agents that

could negatively regulate pathologic inflammatory responses (Hu et al., 2009; Bode et al., 2014; Herzner et al., 2016). In our previous study, an oligodeoxynucleotide (ODN) named as MS19, designed based on the sequence of human microsatellite DNA (MS DNA), with six AAAG repeated units. It could not only rescue mice from bacterial septic peritonitis (Gao et al., 2017) but also attenuate the acute lung injury (ALI) and myocarditis in virus-infected mice (Fang et al., 2011; Nie et al., 2019). It was confirmed that MS19 could reduce the expression of IRF5 and inhibit the nuclear translocation of IRF5 in RAW264.7 cells, since the sequence of AAAG unit is in consensus with the DNA-binding site of IRF5 (Gao et al., 2017). Moreover, MS19 also decreased the expression of IRF5 in the burn injury skin and the myocardial tissues of coxsackievirus B3-infected mice (Xiao et al., 2017; Nie et al., 2019). However, there are still more inflammatory signaling pathways that are involved in the regulation of TLR-induced inflammation, such as the NF-κB and MAPK signaling. Thus, it is necessary to explore the other potential anti-inflammatory mechanisms of MS19 except for the IRF5.

In this study, we assessed the inflammation inhibitory effect of MS19 against different pathogens and their component mimics, in parallel, an ODN with special base substitution, named as MS19-C, was used as a control. Moreover, the role of MS19 in the NF-κB and MAPK signaling, and the nucleocytoplasmic translocation and secretion of HMGB1 were evaluated in LPS-stimulated macrophages. Furthermore, a mouse model with LPS-induced ALI was established and used for observing the interfering effect of MS19 on inflammatory injury *in vivo*. The data obtained suggest that MS19 could drive the suppression of the NF-κB but not the MAPK signaling in PAMPs-induced inflammation, which provides a new insight into the mechanisms on how MS19 reduces the excessive inflammatory responses.

Materials and methods

Oligodeoxynucleotides

All oligodeoxynucleotides (ODNs) with nuclease-resistant phosphorothioate-modified, including the MS19 (5′-AAAGAAAGAAAGAAAGAAAGAAAG-3′) and the control ODN MS19-C (5′-AAACAAACAAACAAACAAACAAAC-3′), were synthesized in the Takara Biotechnology Company (Dalian, China).

Virus, cell isolation, and culture

A mouse-adapted H1N1 influenza virus PR8 and a plaque-purified herpes simplex virus-1 (HSV-1) strain were obtained from the Department of Microbiology, Jilin University, Changchun, China. Virus stocks were propagated in Vero cells, which were then aliquoted and stored at −80°C. All experiments involving pathogens were handled at the laboratory with biosafety level 2 (BSL-2).

Mouse bone marrow-derived macrophages (BMDMs) were isolated as previously described (Bailey et al., 2020). Briefly, mice legs were cut to access the femur and tibia, and muscle and tissue were removed in sterile environment. The bone marrow content was washed out using a syringe with complete RPMI 1640 (GIBCO, Shanghai, China). The cells were centrifuged at 1,000 rpm for 5 min, and the pellet was resuspended in complete RPMI 1640 with 20% L929 culture supernatant. The media was replaced every 3 days. The experiment was performed on the 7th day of differentiation. The RAW264.7 cell line was obtained from the Cell Bank of Chinese Academy of Sciences (Shanghai, China). Cells were cultured at 37°C in a 5% CO_2 humidified incubator and maintained in RPMI 1640 medium supplemented with 10% fetal bovine serum (HyClone, Logan, UT, United States) and antibiotics (100 IU/ml penicillin and streptomycin).

Pathogen-associated molecular patterns stimulation and oligodeoxynucleotide transfection in cells

Bone marrow-derived macrophage and RAW264.7 cells were planted into 6-well plates at a density of 3×10^5 cells per well and then treated with 1 μg/ml LPS (Sigma-Aldrich, St. Louis, MO, United States), 5 μg/ml VACV-70 (InvivoGen, Hong Kong), 25 μg/ml long polyI:C (LPIC), 20 μg/ml curdlan, or infected with PR8 or HSV-1virus at MOI 10:1 in the presence or absence of 2 μg/ml ODNs, respectively. Transfection of ODNs was performed using Lipofectamine 3000 (Thermo Fisher Scientific, Carlsbad, CA, United States) according to the manufacturer's instructions. After 30 min of treatment, the cells were harvested to analyze the total expression and phosphorylation analysis of proteins in the cells, which were detected using Western blot. After 16 h of treatment, the cell supernatants were harvested for TNF-α, IL-6 and HMGB1 expression analysis by enzyme-linked immunosorbent assay (ELISA) kits (R&D Systems, Minneapolis, MN, United States) according to the manufacturer's instructions.

Western blot analysis

Protein extraction solution (Beyotime Biotechnology, Shanghai, China) was added to the cultured cells. The protein

concentration was determined using a BCA Protein Assay Kit (Solarbio). Equivalent amounts of protein (20 μg) were loaded onto a gel and separated by sodium dodecyl-sulfate polyacrylamide gel electrophoresis (SDS-PAGE) and then transferred to nitrocellulose membranes (Thermo fisher scientific). The membranes were blocked in 5% bovine serum albumin (BSA) in Tris-buffered saline/Tween 20 at room temperature for 1 h, followed by incubation overnight at 4°C with rabbit polyclonal antibodies against p-p65, p65, p-p38, p38, p-ERK, ERK, p-TAK1, TAK1, and β-actin, all antibodies were obtained from the Cell Signaling (Beverly, MA, United States). After washing, the membrane was incubated with horseradish peroxidase-conjugated goat anti-rabbit IgG (Beyotime; 1:3,000 dilution). Immunoreactivity was visualized by enhanced chemiluminescence (Thermo fisher scientific), and signals were quantified using the ImageJ software (National Institutes of Health, Bethesda, MD, United States) or film autoradiography.

Immunofluorescence

RAW264.7 cells were seeded in 4-well chambered glass slides coated with poly-L-lysine (Sigma-Aldrich). Treatment dosage for LPS and/or MS19 was adjusted to facilitate visualization *via* immunofluorescence. After washing with ice-cold PBS (pH 7.4), the cells were fixed using 4% paraformaldehyde for 30 min. Subsequently, the cells were further washed three times in PBS containing 0.1% Triton X-100, followed by incubation with 3% BSA in PBS for 30 min. Thereafter, the cells were incubated with primary rabbit antibodies against HMGB1 (1:200; Abcam, Shanghai, China) at 4°C overnight. After washing with PBS, cells were incubated with goat anti-rabbit IgG against HMGB1 conjugated with FITC (1:200; Beyotime) for 1 h at room temperature. Finally, the nuclei were counterstained with 4,6-diamidino-2-phenylindole (DAPI), and the coverslips were placed. Immunostaining was analyzed using a fluorescence microscope (Nikon) interfaced with a digital charge-coupled device camera and an image analysis system. The nucleocytoplasmic translocation percentage in each group was calculated under three fields of vision in fluorescence microscope.

Lipopolysaccharide-induced acute lung injury mouse model

Eight-week-old specific pathogen-free female BALB/c mice (18 ± 2 g) were obtained from the Vital River Laboratory Animal Technology Co., Ltd. (Beijing, China). The mice were maintained at 22 ± 2°C with a 12 h light/dark cycle and had free access to food and water for experiments in accordance with the National Institute of Health Guide for the Care and Use of Laboratory Animals. All mouse experiments were approved by the ethics committee of the College of Basic Medical Sciences of Jilin University. Briefly, mice were randomly assigned to three study groups, namely, PBS, LPS, and LPS plus MS19, with 11 mice in each group. To study the inhibitory effect of MS19 on the LPS-induced lung inflammation, LPS was administered *via* intranasal injection. Mice were intraperitoneally anesthetized with pentobarbital sodium (50 mg/kg) and then were injected *via* the tail vein with PBS or MS19 (25 μg/mouse) at 6 h before LPS (20 mg/kg) inoculation. It was worth noting that MS19 was encapsulated in N-[1-(2,3-dioleoyloxy) propyl]-N, N, N-trimethylammonium methyl-sulfate (DOTAP) (Roche) in animal experiments. Part of the mice (three mice per group) were euthanized using CO_2 at 1 day after exposure to LPS, and then the bronchoalveolar lavage fluid (BALF) samples were collected; after centrifuging at 3,000 rpm for 10 min at 4°C, the supernatant of the BALF samples were used for the ELISA analysis. Subsequently, the lungs were isolated for histopathological examination. Finally, the survival and weight of the rest mice (six mice per group) were recorded daily for 15 days after LPS injection.

Lung histological assessments

The lung tissues with 4% paraformaldehyde were embedded in paraffin. Paraffin sections, 8 μm thick, were deparaffinized, rehydrated, stained with hematoxylin and eosin (H&E), and viewed under a microscope. A pathologist who was blinded to the data performed the histological assessments based on a method described previously (Jiang et al., 2021). The assessment was scored on a scale of 1 (i.e., normal) to 5 (i.e., maximal). The degree of leukocyte infiltration in peribronchiolar areas was judged by the number of infiltrated leukocytes. The sum of the score of cell infiltration and damage levels, including the thickening of the alveolar walls and epithelium, yielded the lung inflammatory score.

Statistical analysis

Statistical analyses were performed using the SPSS v.19.0 software (IBM, Armonk, NY, United States). Quantitative data are presented as the means ± SEMs. All data were tested for normality and homoscedasticity. Differences between groups were evaluated using the Student's *t*-test and one-way analysis of variance (ANOVA) followed by the Tukey–Kramer's multiple range test. Survival rates of mice were compared using the Kaplan–Meier test. $P < 0.05$ was considered significant.

10.3389/fmicb.2022.964112

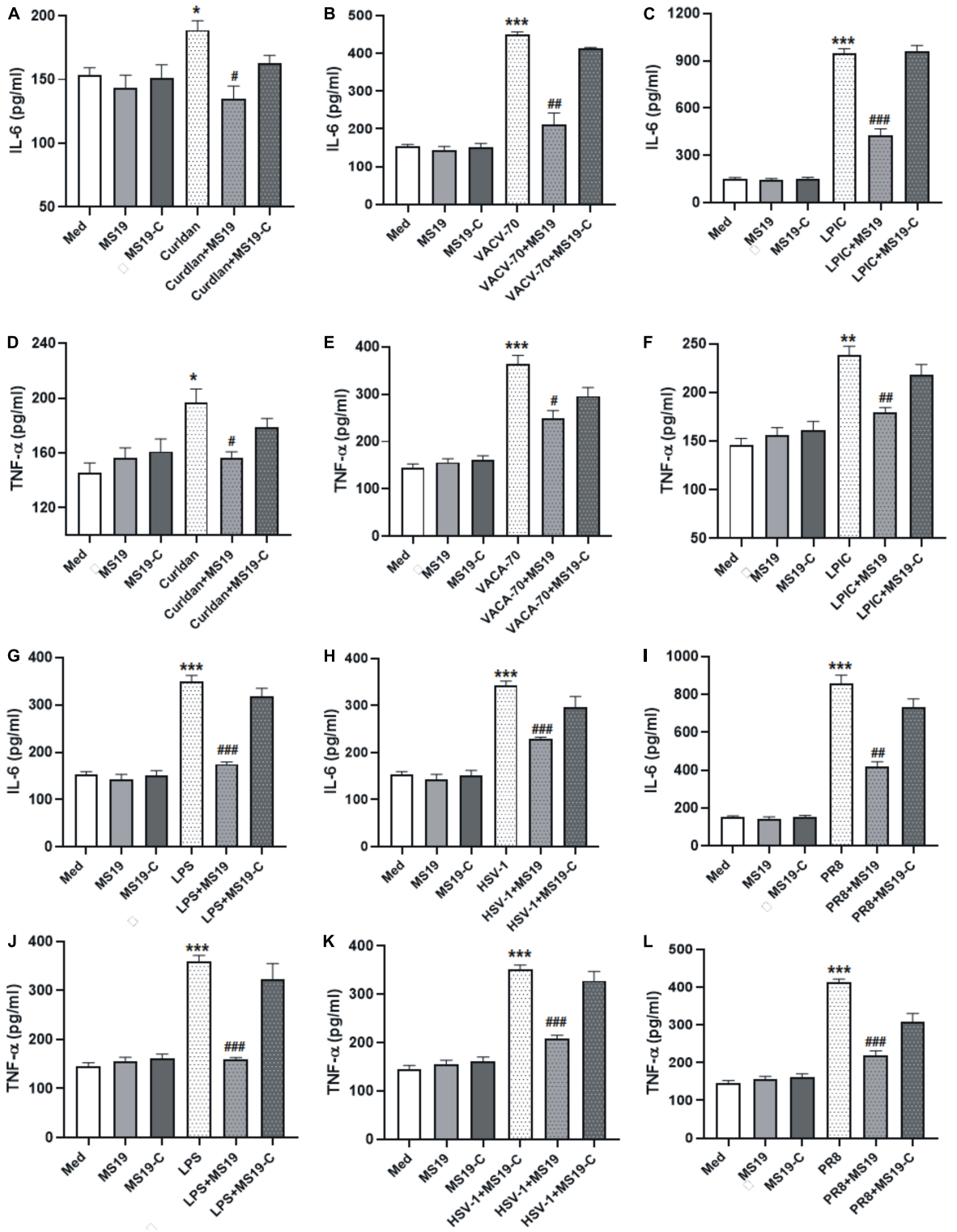

FIGURE 1
MS19 plays an inhibitory role on regulating interleukin 6 (IL-6) and tumor necrosis factor-α (TNF-α) production in bone marrow-derived macrophage (BMDM) cells upon various pathogen-associated molecular patterns (PAMPs) stimulation. BMDMs were treated with different stimulators in the presence or absence of MS19, and then culture supernatants were collected to evaluate the expression of IL-6 and TNF-α level using ELISA. The cytokine levels of IL-6 in BMDM supernatants with the stimulation of bacterium components curdlan, dsDNA virus mimic VACV-70, and RNA virus mimic LPIC **(A–F)**. The cytokine levels of IL-6 and TNF-α in BMDM supernatants with the stimulation of LPS **(G,J)**, DNA virus HSV-1 **(H,K)**, and RNA virus PR8 **(I,L)**. The values are presented as the means ± SEM of three independent experiments. *$p < 0.05$, **$p < 0.01$, and ***$p < 0.001$, vs. medium group; $^{\#}p < 0.05$, $^{\#\#}p < 0.01$, and $^{\#\#\#}p < 0.001$, vs. curdlan, VACV-70, LPIC, LPS, HSV-1, or PR8.

10.3389/fmicb.2022.964112

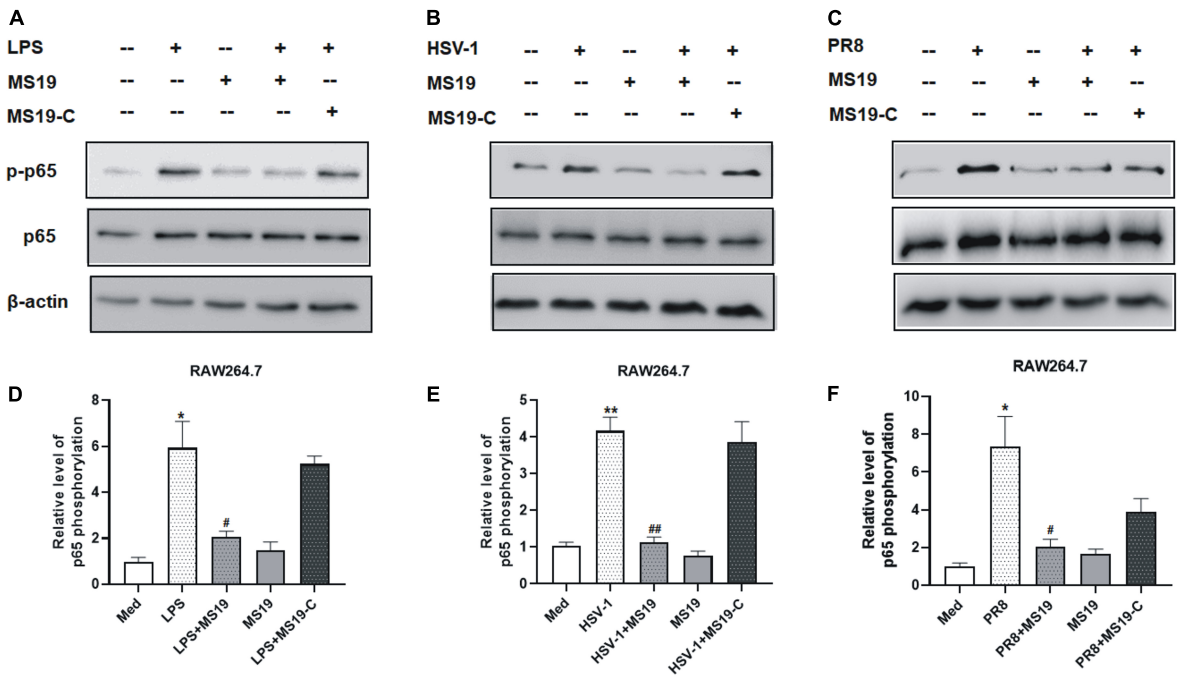

FIGURE 2
Inhibitory effect of MS19 on the expression of NF-κB signaling pathway in different PAMPs-stimulated RAW264.7 cells. The protein expression of p-P65, p65, and β-actin in RAW264.7 cells stimulated by LPS, HSV-1, and PR8 were detected by Western blot **(A–C)**. Band intensity was measured using an imaging densitometer, and the expression of the proteins was calculated relative to the intensity of β-actin protein **(D–F)**. Western blot analysis was assayed in triplicate for each sample. Data represent the mean ± SEM. $^{*}p < 0.05$, $^{**}p < 0.01$, vs. medium group; $^{\#}p < 0.05$, $^{\#\#}p < 0.01$, vs. LPS, HSV-1, or PR8 group.

Results

MS19 inhibited the expression of inflammatory cytokines induced by various pathogen-associated molecular patterns

Pathogen-associated molecular patterns (PAMPs) that are present during infection can induce lung inflammatory responses and injuries. To evaluate the inhibitory effect of MS19 on different PAMPs-induced inflammation, the production of IL-6 and TNF-α in BMDM stimulated with various different PAMPs stimulants were analyzed using ELISA. We chose the bacterial components (i.e., LPS and Gram-positive bacteria cell wall component Curdlan), DNA viruses Herpes simplex virus (HSV) and DNA virus mimics (VACV-70), RNA virus influenza virus (PR8), and RNA virus metabolism products dsRNA long poly (I: C) (LPIC) as stimulus. MS19 (1 μM) or MS19-C (1 μM) transfected with Lipofectamine 3000 (Lipo3000) into cells and then incubated with different stimulus for 16 h. The concentration of TNF-α and IL-6 in the supernatant was detected by ELISA. The results showed that MS19 could significantly inhibit IL-6 and TNF-α production from BMDM triggered Curdlan, DNA virus mimics VACV-70, and RNA virus mimics LPIC (Figures 1A–F). Similarly, the suppressive effects of MS19 were also observed on the expression of inflammatory cytokines IL-6 and TNF-α induced by bacterial LPS, DNA virus, and RNA virus in BMDM (Figures 1G–L). Those results showed that MS19 could significantly inhibit the expression of inflammatory cytokines induced by various PAMPs in macrophages. Interestingly, with the base substitution from G to C, MS19-C has been proved that it has lost the inhibitory effect against the different PAMPs-induced inflammation, which indicated that the inhibitory effect of MS19 was in a sequence-specific manner.

MS19 drove the suppression of NF-κB but not the mitogen-activated protein kinase signaling in pathogen-associated molecular patterns-induced inflammation

Based on the inhibition features of MS19 against various kinds of PAMPs, we deduced that MS19 should inhibit some common molecular pathways among all the inflammatory signaling. To further investigate the possible mechanisms of MS19 to inhibit the PAMPs-induced inflammation, we

focused on the NF-κB and MAPK signaling pathways of the TLR4 downstream pathway, which are the most extensively investigated inflammatory signaling pathways. Therefore, we first examined the effects of MS19 on the phosphorylation levels of p65 NF-κB in the presence of different stimuli including LPS, HSV-1, and PR8 in RAW264.7 cells. As reflected in **Figure 2**, stimulation with these PAMPs increased the phosphorylation level of p65 in RAW264.7 cells, whereas co-treatment with MS19 significantly reduced the upregulation.

To determine if LPS/TLR4 downstream MAPK signaling pathways were activated, we measured the levels of nuclear phosphorylated mitogen-activated protein (MAP) kinases in LPS-treated peritoneal macrophages by Western blot. The results showed that the phosphorylation of TAK-1, ERK, and p38, the activation of major constitutes of MAPKs family, had no obvious changes with MS19 treatment in LPS-stimulated cells (**Figure 3**). Comparatively, the total protein expression of TAK-1, ERK, and p38 in cells were not affected by the stimulation and treatments. These results indicated that MS19 exhibited potential anti-inflammatory effects *via* inhibiting the NF-κB but not the MAPK signaling pathways in macrophages.

MS19 suppressed the nucleocytoplasmic translocation and secretion of HMGB1 in lipopolysaccharide-stimulated macrophages

HMGB1 is important in the initiation and progression of proinflammatory processes. It could be released into the extracellular environment during exogenous stimulus, such as LPS. Some non-immunogenic nucleotides with high-affinity HMGB binding may function as suppressing agents for HMGB-mediated inflammation disease by blocking TLR4 activation and macrophage cytokine release (Yang et al., 2010; Yanai et al., 2011). Next, we evaluated the inhibitory effects of MS19 on the nucleocytoplasmic translocation and secretion of HMGB1 in LPS-stimulated RAW264.7 cells using immunofluorescence assay and ELISA. As shown in **Figures 4A,B**, HMGB1 was strictly located in nucleus of untreated macrophages, and the translocation of HMGB1 from the nucleus to cytoplasm was happened when the cells were exposed with LPS ($P < 0.001$). However, MS19 displayed a strong suppressive effect on HMGB1 translocation in LPS-stimulated cells ($P < 0.01$). Furthermore, LPS-induced high HMGB1 level in supernatant was also inhibited by treating with MS19 ($P < 0.01$) (**Figure 4C**). Similar to the expression of inflammatory cytokines, no obvious difference of HMGB1 nucleocytoplasmic translocation and secretion was observed in RAW264.7 cells between the group treated with LPS and LPS + MS19-C. The data demonstrated that MS19 inhibited the translocation of HMGB1 to the cytosol, thereby reducing its active secretion.

MS19 alleviated the lipopolysaccharide-induced acute lung injury and mortality in mice

Next, we evaluated the inhibitory effect of MS19 on the acute lung pathological inflammation caused by LPS in mice. These mice were treated with LPS or/and MS19 on day 1, then three mice of each group were euthanized, and BALF was collected from the lungs, and then, the lungs were removed for histopathological examination at day 2. The survival and weight of the rest eight mice were recorded daily for 8 days. As shown in **Figure 5A**, LPS administration could induce a dramatic loss of body weight in mice, nearly 20% weight loss in the LPS group at day 4. The weight of the mice in MS19 alone group was no change until the end of experiment. However, in the LPS + MS19 group, LPS stimulation induced an initial dramatic decrease 1–3 days after injection, followed by recovery at day 4 and a further increase at day 5. From day 8 post injection, the body weight of the mice treated with LPS + MS19 was gradually recovered toward the normal until at the end of experiment at day 15, whereas the body weight of the mice treated with LPS was not recovered resulted in only two mice were lived at day 8. Six of the eight mice in the LPS + MS19 group were still alive ($P < 0.05$) (**Figure 5B**). The mortality rates of the mice treated with PBS or MS19 alone or LPS alone or LPS + MS19 were 100, 100, 25, or 75%, respectively, indicating the more potential of MS19 on inhibiting lung inflammation responses.

Lung pathological results showed that the mice stimulated with LPS showed thickened and congested alveolar walls, intra-alveolar edema, and numerous infiltrated neutrophils and macrophages in their lung tissues. In contrast, mice treated with MS19 showed no or much less pathological changes in their lung tissues (**Figure 5C**). The pathological score of the lung tissues in MS19-treated mice was lower than that in mice inoculated with LPS only ($P < 0.05$) (**Figure 5D**). In addition, the secretion of HMGB1, TNF-a, and IL-6 in the BALF of mice treated with LPS was significantly higher than that of the PBS mice, while the levels of these inflammatory mediator levels in the mice treated with MS19 were obviously lower than that in LPS group (**Figure 5E**). The results indicated that MS19 has a potential protection against the lethal LPS-induced ALI by inhibiting the production of inflammatory cytokines.

Discussion

Excessive TLR signaling may lead to persistent inflammation and tissue destruction. For instance, severity of the coronavirus disease 2019 (COVID-19) is associated with cytokine storm in patients, which could be produced by over-activation of TLR pathways (Tang et al., 2020; Manik and Singh, 2021). Therefore, it is quite obvious that targeted manipulation of TLR signaling pathway may possess the decrease of excessive inflammatory

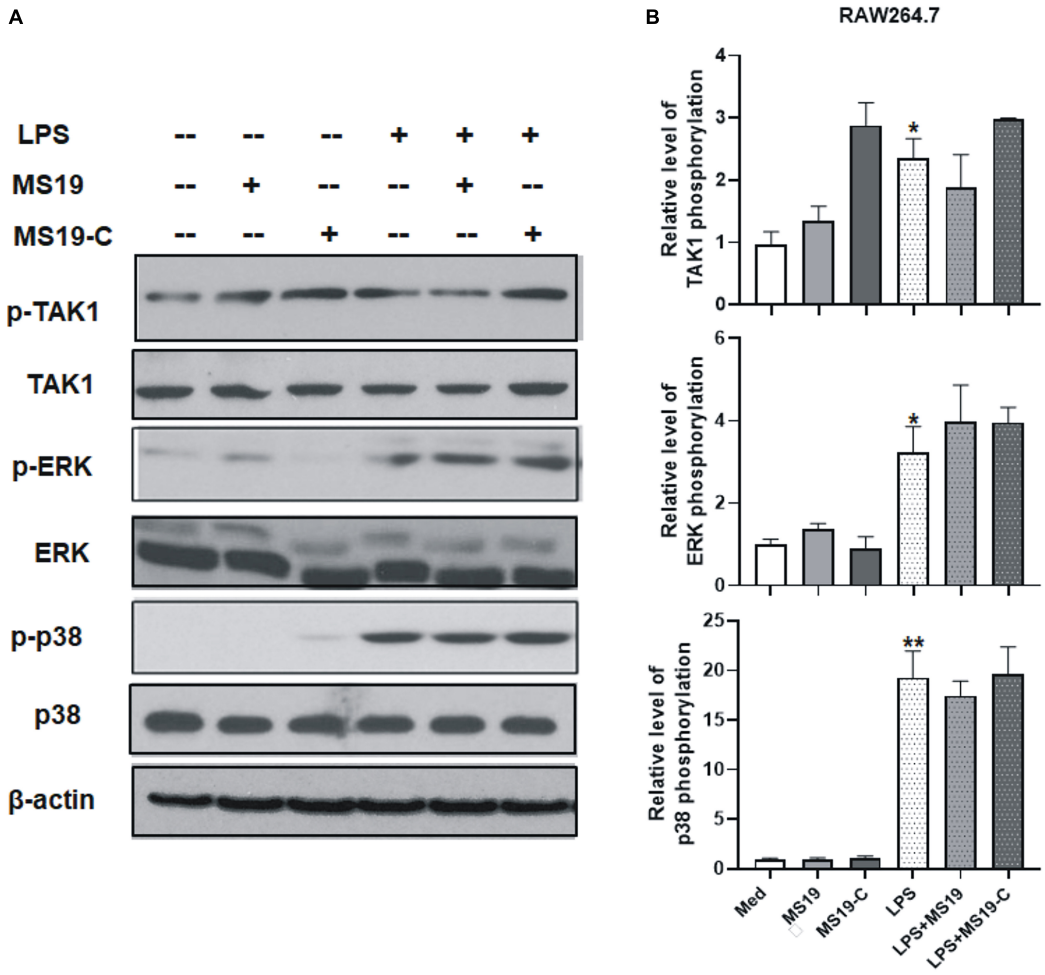

FIGURE 3
Effect of MS19 on the expression of MAPK signaling pathway in LPS-stimulated RAW264.7 cells. The protein expressions of p-TAK1, TAK, p-ERK, ERK, p-p38, p38, and β-actin in RAW264.7 cells were detected by Western blot **(A)**. Band intensity was measured for calculating the expression of the proteins relative to the intensity of β-actin protein **(B)**. Data represent the mean ± SEM. $*p < 0.05$, $**p < 0.01$, vs. medium group.

responses. In this study, we found that MS19 could inhibit the various PAMPs-induced inflammatory cytokines remarkably, and extensively, and the inhibition is associated with NF-κB signaling pathway.

Multiple pathogens and their PAMPs were used to stimulate macrophages in this study. Various PAMPs trigger inflammatory responses may interact with different innate immune receptors. For example, pathogen lipoprotein and polysaccharide sensed by TLR2, bacterial LPS recognized by TLR4, viral and bacterial DNA with unmethylated CpG-DNA motifs sensed by TLR9, viral ssRNA and dsRNA could be recognized by TLR7/8 and TLR3, respectively (Naqvi et al., 2022). Thus, one virus particle can activate a complex pattern of TLRs, for instance, influenza A virus could be recognized by a bunch of TLRs including TLR2, -3, -4, and -7/8 (Pulendran and Maddur, 2015; Dai et al., 2018). Our result reflected that MS19 extensively inhibited the production of IL-6 and TNF-α induced by various PAMPs, which including the LPS, curdlan, dsRNA, and dsDNA mimics, as well as DNA and RNA virus. Moreover, in our previous published articles, we demonstrated that MS19 could inhibit the IFN-α production in human PBMC and pDC stimulated with RNA virus and DNA virus (Sun et al., 2010). Those results hinted toward not a direct interference at the receptors; therefore, we deduced that the MS19 might target one or more molecules of co-existing in the downstream of TLRs signaling. Three major signaling pathways, namely, NF-κB, MAPKs, and IRFs, are responsible for mediating TLRs-induced proinflammatory responses (Yang et al., 2010). In our previous study, MS19 was thought to bind with IRF5 because of the consensus AAAG repeat—binding site and prevented the nuclear translocation of IRF5 with subsequent induction of inflammatory genes (Xiao et al., 2017). However, considering the complexity of inflammation, it was possible that there still have additional targets for MS19 to act its anti-inflammation effect. Just like

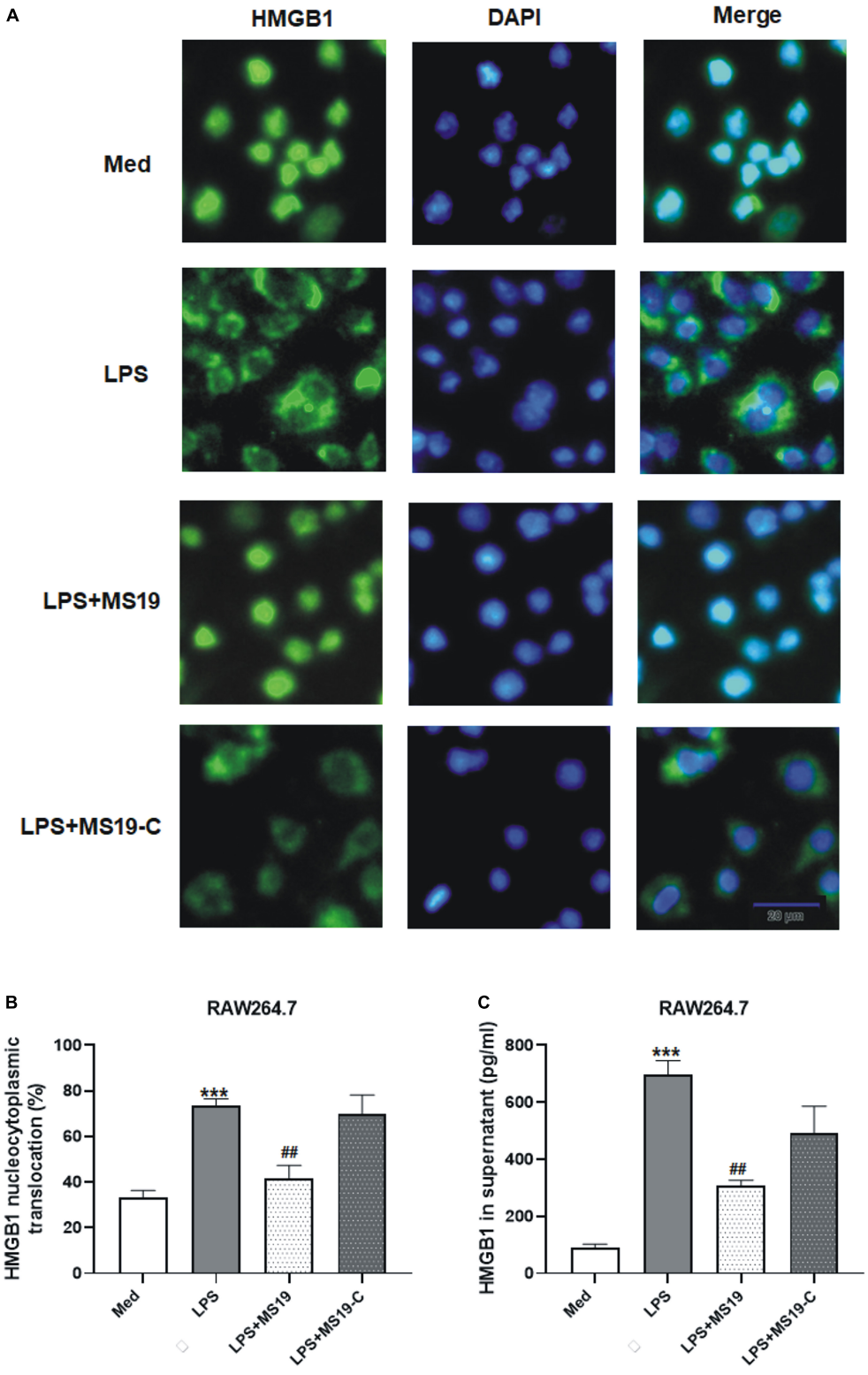

FIGURE 4
Suppression of HMGB1 translocation and secretion in RAW264.7 cells treated with MS19 after LPS exposure. Immunofluorescence images of nucleocytoplasmic translocation of HMGB1 **(A)**. RAW264.7 cells were incubated with LPS with or without MS19 for 2 h and examined by fluorescence microscopy. HMGB1 are stained in green with FITC, and cell nuclei are stained in blue with DAPI. The percentage of nucleocytoplasmic translocation of HMGB1 in RAW264.7 cells was calculated **(B)**. The HMGB1 level in supernatant after RAW264.7 cells received 16 h exposure of LPS in the presence or absence of MS19, as determined using ELISA **(C)**. Data are representatives of three independent experiments and are expressed as means ± SEM. $^{***}p < 0.001$, vs. medium group; $^{\#\#}p < 0.01$, vs. LPS group.

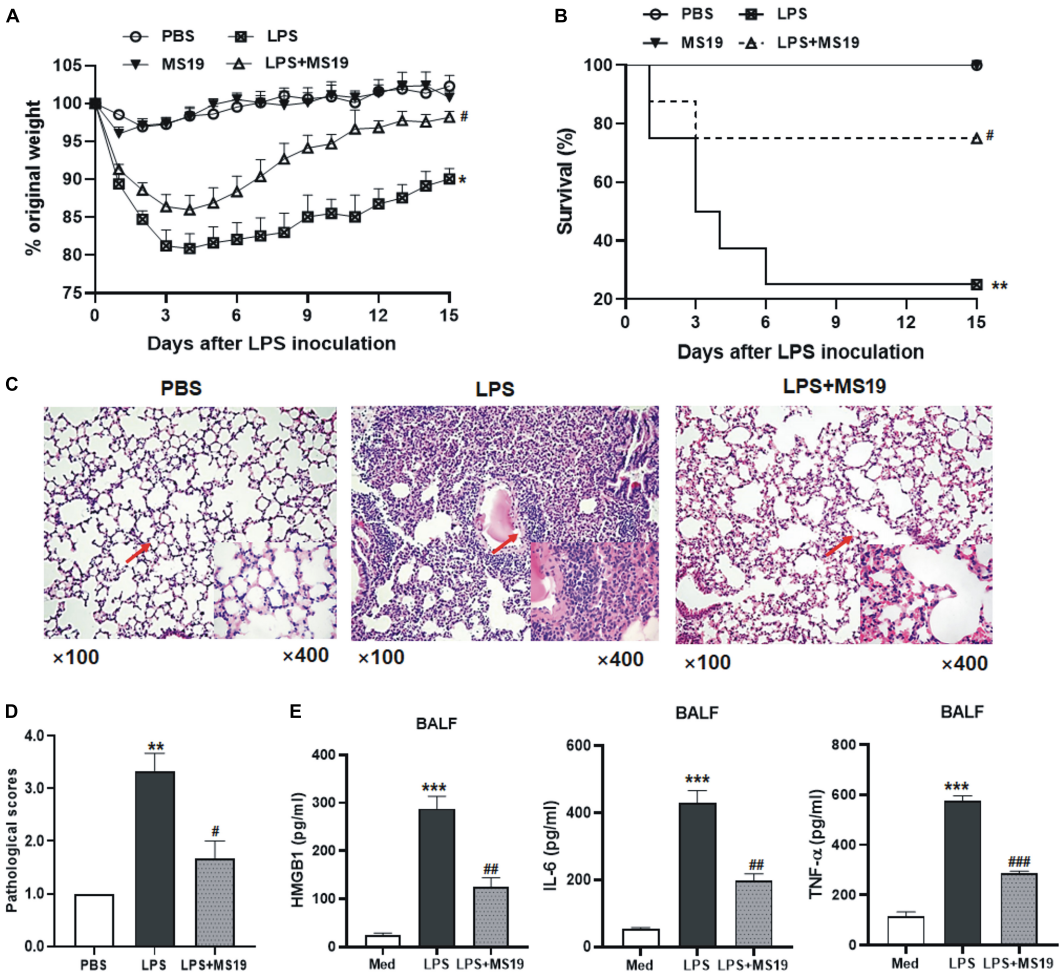

FIGURE 5
Protective effect of MS19 on LPS-induced acute lung injury in mice. Mice (n = 11) were challenged nasally with LPS or PBS at 6 h after intravenous injection with MS19 or PBS. The body weight change of mice **(A)**. The percent survival of mice in different groups at 8 days after LPS challenge **(B)**. Representative images of lung pathology after H&E staining **(C)**. Lung injury scores **(D)**. ELISA of HMGB1, IL-6, and TNF-α level in the BALF samples of mice in each group **(E)**. Data represent the mean ± SEM. $^{*}p < 0.05$, $^{**}p < 0.01$, and $^{***}p < 0.001$, vs. PBS group; $^{\#}p < 0.05$, $^{\#\#}p < 0.01$, and $^{\#\#\#}p < 0.001$, vs. LPS group.

A151, an ODN containing 4 repeats of the TTAGGG motif, which was initially identified as a TLR9 antagonist that inhibits immune activation by CpG ODNs (Steinhagen et al., 2018). However, subsequent studies have found A151 also can bind to the cytosolic DNA sensors AIM2 and compete with DNA to inhibit cyclic GMP-AMP synthase (cGAS) pathway, resulting in the inflammasome inhibition (Eichholz et al., 2016; Steinhagen et al., 2018).

In this study, we focused on the TLR4 signaling pathways in macrophage induced by LPS to investigate whether MS19 could inhibit the NF-κB or MAPK transduction. Excitingly, MS19 significantly inhibited the phosphorylation levels of p65 NF-κB in LPS-stimulated cells. This finding was a supplement for the inflammatory inhibition mechanism of MS19. By means of mechanism, MS19 inhibited the TNF-α production in macrophage stimulated with LPS by blocking the HMGB1 translocation and secretion. LPS activation of TLR4 and caspase-11 both generate extracellular HMGB1 release. TLR4 activates both the MyD88-dependent and TRIF-dependent pathways (Lu et al., 2008). HMGB1-induced TNF-α production is TRIF and MyD88-dependent pathway, consistent with what is known regarding LPS downstream signaling (Kim et al., 2013). qRT-PCR results showed that MS19 reduced the overexpression of TRAF6, MyD88, and IRF3 mRNA caused by LPS in RAW264.7 (**Supplementary Figure 1** and **Supplementary Table 1**). In our unpublished results, MS19 also could inhibit the IFN-α and IFN-β production in macrophage and pDC stimulated with DNA and RNA virus. TRIF-signaling downstream of LPS-bound TLR4 leads to the activation of the IFN-regulatory factors IRF3/7 (Fitzgerald et al., 2003) and produce the IFN-β and

IFN-α. The type I interferon expression was TRIF dependent and did not require MyD88. So, we speculated that MS19 may inhibit the TNF-α release both in TRIF- and MyD88-dependent pathway. Besides TLR4, caspase-11 is also drive inflammatory response by mediated the HMGB1 translocation from the nucleus to the cytoplasm. LPS induced activation of caspase-11 in macrophages, leading to reduced ASC speck formation, caspase-1 activation, matured IL-1β release. But, MS19 did not affect the proinflammatory cytokines IL-1 level in macrophage stimulated with LPS (data not shown). We speculated that the inhibition of MS19 on HMGB1 translocation in macrophage may be dependent on TLR4, independent of caspase-11. About the TLR4 downstream signaling pathway, treatment of RAW264.7 cell with MS19 did not affect the phosphorylation and expression of TAK1, ERK, and p38 MARK. Thus, MARKs pathway was not involved in the inflammatory regulation of MS19. Surely, besides the TLRs signaling, there still have more pathways are involved the inflammation, such as the cytosolic sensor signaling including the nucleotide-binding and oligomerization domain-like receptors (NLRs), the retinoic acid-inducible gene 1-like receptors (RLRs) and the cGAS (Decout et al., 2021; Kienes et al., 2021; Pu et al., 2022). Thus, more experiments are still needed to understand the full inhibition mechanisms of MS19 in the future.

The effect of all inhibitory ODNs is associated with high sequence specificity. For instance, the sequences of antisense oligodeoxynucleotides are limited to pair with the specific target RNA (Alharbi et al., 2020). Moreover, among the traditional suppressive ODNs, INH-ODN 2088, and A151, the inhibitory effect against TLRs signaling was based on the motif of CC(T)XXX 3–5 GGG or TTAGGG, respectively (Zhang et al., 2015; Steinhagen et al., 2018). To investigate the key base of MS19 in the inhibitory effect, we substituted all the guanine (G) to cytosine (C) to form the control ODN MS19-C. The results showed that the MS19-C had no more inhibitory activities in triggering the expression of IL-6 and TNF-α, as well as the activation of NF-κB signaling after different PAMPs stimulation. These data indicated that the G-rich ODN may exhibit a stronger inhibition ability than non-G ODN. This finding was consistent with a previous study, which identified a G-rich ODN with ploy G motif (G-ODN), could block the secretion of TNF-a and IL-12p40 and interfere with the upregulation of major histocompatibility complex (MHC) class II and costimulatory molecules (Peter et al., 2008). Interestingly, certain G-rich DNA sequences can fold into a variety of four-stranded structures, which are called G-quadruplexes (Zuffo et al., 2018). The sequence feature of MS19 has six G bases in it and with a specific interval, which may facilitate to form the G quadruplex-like structures. Compared with the non-G quadruplex ODN, G quadruplex ODN blocked more efficiently TLR7- and TLR9-mediated innate immune responses (Römmler et al., 2013). This phenomenon might be related with the regulatory role of G quadruplex in inflammatory-related gene promoters (Stein and Eckert, 2021). However, more is not always better; some new evidence suggested that inhibitory ODNs containing many G triplets, or quadruples were easy to form higher order structures, also called G4 stacks, which made their immunological and pharmacological behaviors unpredictable (Lenert, 2010; Römmler et al., 2013; Zuffo et al., 2018). Therefore, keep the appropriate number of G base or with the G modification allows the development of inhibitory ODNs with superior inhibitory potency for inflammatory diseases (Römmler et al., 2013).

HMGB1 is an evolutionarily conserved protein, presenting in the nucleus of eukaryotic cells under basal conditions. Generally, the secretion of extracellular HMGB1 by innate immune cells in response to PAMPs or released by injured cells has been identified to play a key role in the pathogenesis of sterile and infectious inflammation (Ueno et al., 2021). The release of HMGB1 was confirmed in our study. LPS induced the nucleocytoplasmic translocation, and secretion of HMGB1 was decreased by treating with MS19. The HMGB1 release is mediated by the nuclear export protein XPO1 and secretory lysosomes, which can be triggered by a variety of cytokines and signaling pathways. Some reports have showed that the inhibition of the NF-κB signaling pathway limits HMGB1 secretion in activated immune cells (Li et al., 2020; Chen et al., 2022). Although the target of NF-κB signaling directly responsible for this process is still unclear, a possible mechanism of that is the TNF-α production. The reason is that the release TNF-α and HMGB1 in a time-dependent manner with response to LPS stimulation in macrophages and monocytes. Furthermore, the direct TNF-α suppression *via* gene knockout or TNF-α neutralizing antibodies partially inhibited LPS-induced HMGB1 release in macrophages (Chen et al., 2004; Chen et al., 2022). Therefore, we speculated that the inhibition role of MS19 on HMGB1 secretion is partially mediated through NF-κB signaling and TNF-α-dependent mechanism, since that ODN exhibited a strong inhibition against the NF-κB activation and TNF-α production in this study. In addition, after its release, extracellular HMGB1 usually acts as a DAMP molecule and transmits signals to the cell interior *via* the activation of receptors including TLR4, resulting in the formation of a positive feedback loop that potentially amplifies local inflammatory responses (Su et al., 2021; Teo Hansen Selno et al., 2021). Thus, MS19 might also interact with the secreted HMGB1, leading to the functional inactivation by the induction of a conformational change. Three critical elements of ODNs, namely, phosphorothioate modification, base sequence, and length of ODN, were identified for their high-affinity binding to HMGB1 (Yanai et al., 2011). The MS19 used in this study has phosphorothioate modification and potential G-quadruple structure, thereby resulting in the possibility of HMGB1 inactivation through direct binding.

In animal experiments, a classic experimental model of ALI induced by LPS has been used in this study. LPS results in symptoms and inflammatory response in animal models, closely resembling ALI in human (Ehrentraut et al., 2019). Following the LPS challenge, we observed that MS19 suppressed the LPS-induced HMGB1, TNF-α, and IL-6 inflammatory cytokines in the BALF of mice, which is consistent with the results in cultured macrophages. Moreover, MS19 exhibited the anti-inflammatory effects on the pathological changes of ALI, for example, the thickened alveolar walls and numerous infiltrated inflammatory cells were markedly reduced. The decrease of pathological changes is tightly associated with the inhibition of inflammatory cytokines and HMGB1 release (Lai et al., 2016). More importantly, MS19 significantly improved the survival rate of mice in LPS-induced ALI model, which is similar with the previous animal results of MS19 in rescuing the mice from bacterial septic peritonitis, burn-induced systemic inflammation, and coxsackievirus B3 (CVB3)-induced myocarditis (Gao et al., 2017; Xiao et al., 2017; Nie et al., 2019). Those data provided a supplemental experimental basis for the therapeutic applications in the treatment of numerous inflammatory diseases. It is noteworthy that MS19 inhibited the inflammatory response through the NF-κB signaling but not the MAPK transduction; this inhibition would be specific. Sometimes, a specific inhibition should be favorable, the MAPK signaling is known to be involved in many regulatory pathways (Mathien et al., 2021); thereby, the lack of suppression of MAPKs by MS19 might avoid the potential danger of side effects such as increasing infection rates as a result of excess immunologic suppression.

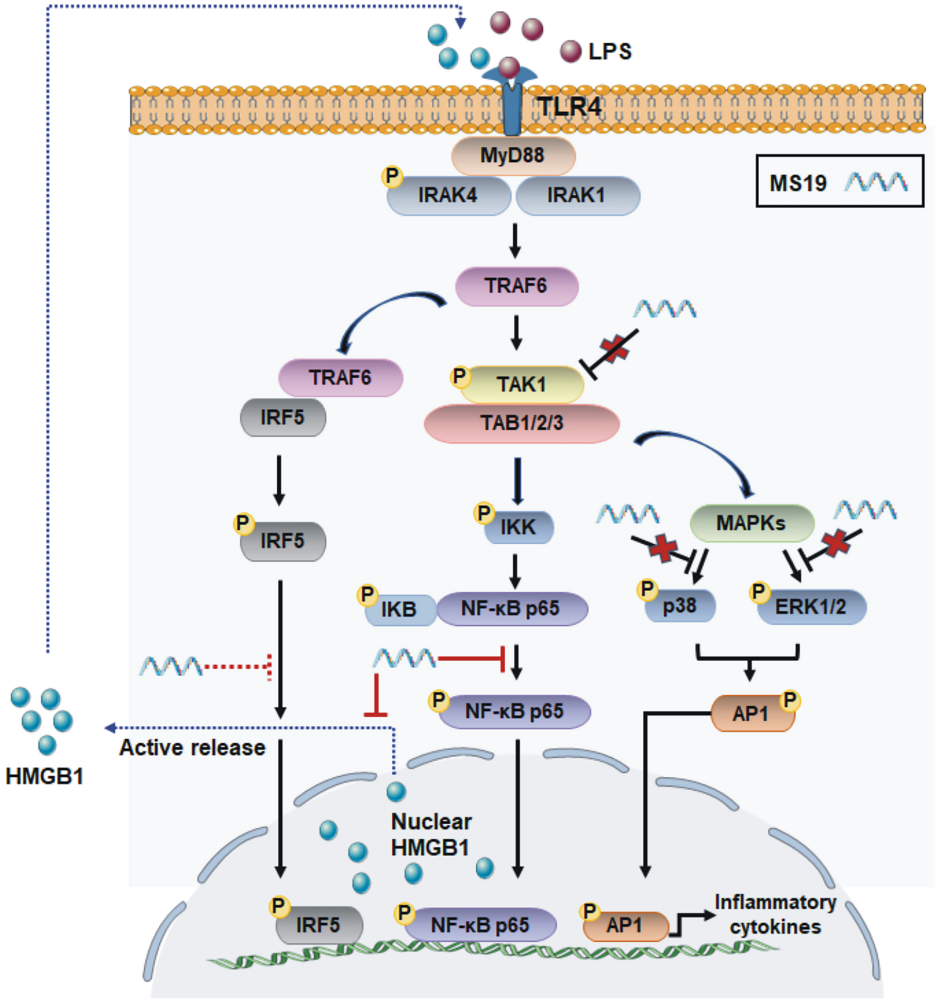

FIGURE 6
Scheme of the anti-inflammatory mechanisms of MS19 *via* the inhibition of NF-κB signaling and HMGB1 release in LPS/TLR4 pathway. MS19 inhibits the phosphorylation of p65 NF-κB and release of HMGB1 induced by LPS (red solid line); MS19 does not inhibit the phosphorylation of TAK-1, ERK, and p38 MAPK (red cross); our previous study reported that MS19 inhibits the expression and nuclear translocation of IRF5 (red dotted line).

Conclusion

We demonstrated that MS19 remarkably and extensively inhibited multiple PAMPs induced the expression of inflammatory cytokines IL-6 and TNF-α in BMDM and RAW264.7 cells. The inhibition role of TNF-α production of MS19 may be due to block nucleocytoplasmic translocation and secretion of HMGB1, and the inhibition is associated with NF-κB signaling but not the MAPK transduction (**Figure 6**). Those data may provide a new insight for understanding how MS19 reduces the excessive inflammatory responses in the ALI mouse model induced and excessive cytokine-mediated lethal shock syndrome model. We know that both cytokines TNF-α and HMGB1 were known to be the central mediator of cytokine storm in severe COVID-19 disease (Chen et al., 2020). Kridin et al. (2021) recently analyzed outcomes of COVID-19 in patients with psoriasis treated with anti-TNF biologics and found that TNF blockade significantly decreased the risk of COVID-19-associated hospitalization (Ablamunits and Lepsy, 2022). HMGB1 inhibitors are also promising drug candidates for the treatment of patients suffering from COVID-19. Clinical trials are urgently needed to test different TNF-α/NF-κB inhibitors or HMGB1 antibodies for treatment or prevention of severe COVID-19 cases. Thus, our findings on MS19 in controlling TNF-a production and HMGB1 secretion may provide potential therapeutic application involving targeting cytokines TNF-α- and HMGB1-mediated overactivated inflammation injury induced by SARS-CoV-2.

Data availability statement

The original contributions presented in the study are included in the article/**Supplementary material**, further inquiries can be directed to the corresponding authors.

Ethics statement

The animal study was reviewed and approved by the ethics committee of the College of Basic Medical Sciences of Jilin University.

Author contributions

CZ and HuiW conducted all the experiments. SS and HRW contributed to the writing of the manuscript. MY and MF provided the ideas and revised the draft manuscript. YS and HuaW approved the version to be published. All authors read and approved the final manuscript.

Funding

This project was supported by the National Natural Science Foundation of China (grant number 81902111); the Natural Science Foundation of Science and Technology Department of Jilin Province (grant number 20180101133JC); and the Foundation of Science and Technology Training Program of Health Committee in Jilin Province (grant numbers 2014Q017, 2018Q008 and 2020Q009).

Conflict of interest

The authors declare that the research was conducted in the absence of any commercial or financial relationships that could be construed as a potential conflict of interest.

Publisher's note

All claims expressed in this article are solely those of the authors and do not necessarily represent those of their affiliated organizations, or those of the publisher, the editors and the reviewers. Any product that may be evaluated in this article, or claim that may be made by its manufacturer, is not guaranteed or endorsed by the publisher.

Supplementary material

The Supplementary Material for this article can be found online at: https://www.frontiersin.org/articles/10.3389/fmicb.2022.964112/full#supplementary-material

References

Ablamunits, V., and Lepsy, C. (2022). Blocking TNF signaling may save lives in COVID-19 infection. *Mol. Biol. Rep.* 49, 2303–2309. doi: 10.1007/s11033-022-07166-x

Alharbi, A. S., Garcin, A. J., Lennox, K. A., Pradeloux, S., Wong, C., Straub, S., et al. (2020). Rational design of antisense oligonucleotides modulating the activity of TLR7/8 agonists. *Nucleic Acids Res.* 48, 7052–7065. doi: 10.1093/nar/gkaa523

Bailey, J. D., Shaw, A., McNeill, E., Nicol, T., Diotallevi, M., Chuaiphichai, S., et al. (2020). Isolation and culture of murine bone marrow-derived macrophages for nitric oxide and redox biology. *Nitric Oxide* 10, 17–29. doi: 10.1016/j.niox.2020.04.005

Bode, C., Wang, J., and Klinman, D. M. (2014). Suppressive oligodeoxynucleotides promote the generation of regulatory T cells by

inhibiting STAT1 phosphorylation. *Int. Immunopharmacol.* 23, 516–522. doi: 10.1016/j.intimp.2014.09.027

Chen, G., Li, J., Ochani, M., Rendon-Mitchell, B., Qiang, X., Susarla, S., et al. (2004). Bacterial endotoxin stimulates macrophages to release HMGB1 partly through CD14- and TNF-dependent mechanisms. *J. Leukoc. Biol.* 76, 994–1001. doi: 10.1189/jlb.0404242

Chen, R., Huang, Y., Quan, J., Liu, J., Wang, H., Billiar, T. R., et al. (2020). HMGB1 as a potential biomarker and therapeutic target for severe COVID-19. *Heliyon* 6:e05672. doi: 10.1016/j.heliyon.2020.e05672

Chen, R., Kang, R., and Tang, D. (2022). The mechanism of HMGB1 secretion and release. *Exp. Mol. Med.* 54, 91–102. doi: 10.1038/s12276-022-00736-w

Dai, J., Gu, L., Su, Y., Wang, Q., Zhao, Y., Chen, X., et al. (2018). Inhibition of curcumin on influenza A virus infection and influenzal pneumonia via oxidative stress, TLR2/4, p38/JNK MAPK and NF-κB pathways. *Int. Immunopharmacol.* 54, 177–187. doi: 10.1016/j.intimp.2017.11.009

Decout, A., Katz, J. D., Venkatraman, S., and Ablasser, A. (2021). The cGAS-STING pathway as a therapeutic target in inflammatory diseases. *Nat. Rev. Immunol.* 21, 548–569. doi: 10.1038/s41577-021-00524-z

Ding, X., Li, S., and Zhu, L. (2021). Potential effects of HMGB1 on viral replication and virus infection-induced inflammatory responses: a promising therapeutic target for virus infection-induced inflammatory diseases. *Cytokine Growth Factor Rev.* 62, 54–61. doi: 10.1016/j.cytogfr.2021.08.003

Ehrentraut, H., Weisheit, C. K., Frede, S., and Hilbert, T. (2019). Inducing Acute Lung Injury in Mice by Direct Intratracheal Lipopolysaccharide Instillation. *J. Vis. Exp.* 1–7. doi: 10.3791/59999

Eichholz, K., Bru, T., Tran, T. T., Fernandes, P., Welles, H., Mennechet, F. J., et al. (2016). Immune-Complexed Adenovirus Induce AIM2-Mediated Pyroptosis in Human Dendritic Cells. *PLoS Pathog.* 12:e1005871. doi: 10.1371/journal.ppat.1005871

Fang, M., Wan, M., Guo, S., Sun, R., Yang, M., Zhao, T., et al. (2011). An oligodeoxynucleotide capable of lessening acute lung inflammatory injury in mice infected by influenza virus. *Biochem. Biophys. Res. Commun.* 415, 342–347. doi: 10.1016/j.bbrc.2011.10.062

Fitzgerald, K. A., Rowe, D. C., Barnes, B. J., Caffrey, D. R., Visintin, A., Latz, E., et al. (2003). LPS-TLR4 signaling to IRF-3/7 and NF-κB involves the toll adapters TRAM and TRIF. *J. Exp. Med.* 198, 1043–1055. doi: 10.1084/jem.20031023

Gao, S., Li, X., Nie, S., Yang, L., Tu, L., Dong, B., et al. (2017). An AAAG-Rich Oligodeoxynucleotide Rescues Mice from Bacterial Septic Peritonitis by Interfering Interferon Regulatory Factor 5. *Int. J. Mol. Sci.* 18:1034. doi: 10.3390/ijms18051034

Ge, Y., Huang, M., and Yao, Y. M. (2021). The Effect and Regulatory Mechanism of High Mobility Group Box-1 Protein on Immune Cells in Inflammatory Diseases. *Cells* 10:1044. doi: 10.3390/cells10051044

Herzner, A. M., Wolter, S., Zillinger, T., Schmitz, S., Barchet, W., Hartmann, G., et al. (2016). G-rich DNA-induced stress response blocks type-I-IFN but not CXCL10 secretion in monocytes. *Sci. Rep.* 6:38405. doi: 10.1038/srep38405

Hu, D., Su, X., Sun, R., Yang, G., Wang, H., Ren, J., et al. (2009). Human microsatellite DNA mimicking oligodeoxynucleotides down-regulate TLR9-dependent and -independent activation of human immune cells. *Mol. Immunol.* 46, 1387–1396. doi: 10.1016/j.molimm.2008.12.008

Jiang, N., Li, Z., Luo, Y., Jiang, L., Zhang, G., Yang, Q., et al. (2021). Emodin ameliorates acute pancreatitis-induced lung injury by suppressing NLRP3 inflammasome-mediated neutrophil recruitment. *Exp. Ther. Med.* 22:857. doi: 10.3892/etm.2021.10289

Kienes, I., Weidl, T., Mirza, N., Chamaillard, M., and Kufer, T. A. (2021). Role of NLRs in the Regulation of Type I Interferon Signaling, Host Defense and Tolerance to Inflammation. *Int. J. Mol. Sci.* 22:1301. doi: 10.3390/ijms22031301

Kim, S., Kim, S. Y., Pribis, J. P., Lotze, M., Mollen, K. P., Shapiro, R., et al. (2013). Signaling of high mobility group box 1 (HMGB1) through toll-like receptor 4 in macrophages requires CD14. *Mol. Med.* 19, 88–98. doi: 10.2119/molmed.2012.00306

Kridin, K., Schonmann, Y., Tzur Bitan, D., Damiani, G., Peretz, A., Weinstein, O., et al. (2021). Coronavirus disease COVID-19-associated hospitalization and mortality in patients with psoriasis: a population-based study. *Am. J. Clin. Dermatol.* 22, 709–718. doi: 10.1007/s40257-021-00605-8

Lai, J.-l, Liu, Y.-h, Liu, C., Qi, M.-p, Liu, R.-n, Zhu, X.-f, et al. (2016). Indirubin Inhibits LPS-Induced Inflammation via TLR4 Abrogation Mediated by the NF-kB and MAPK Signaling Pathways. *Inflammation* 40, 1–12. doi: 10.1007/s10753-016-0447-7

Lenert, P. S. (2010). Classification, mechanisms of action, and therapeutic applications of inhibitory oligonucleotides for Toll-like receptors (TLR) 7 and 9. *Mediators Inflamm.* 2010:986596. doi: 10.1155/2010/986596

Li, P., and Chang, M. (2021). Roles of PRR-Mediated Signaling Pathways in the Regulation of Oxidative Stress and Inflammatory Diseases. *Int. J. Mol. Sci.* 22:7688. doi: 10.3390/ijms22147688

Li, W., Deng, M., Loughran, P. A., Yang, M., Lin, M., and Yang, C. (2020). LPS Induces Active HMGB1 Release From Hepatocytes Into Exosomes Through the Coordinated Activities of TLR4 and Caspase-11/GSDMD Signaling. *Front. Immunol.* 11:229. doi: 10.3389/fimmu.2020.00229

Lu, Y. C., Yeh, W. C., and Ohashi, P. S. (2008). LPS/TLR4 signal transduction pathway. *Cytokine* 42, 145–151. doi: 10.1016/j.cyto.2008.01.006

Manik, M., and Singh, R. K. (2021). Role of toll-like receptors in modulation of cytokine storm signaling in SARS-CoV-2-induced COVID-19. *J. Med. Virol.* 94, 869–877. doi: 10.1002/jmv.27405

Mathien, S., Tesnière, C., and Meloche, S. (2021). Regulation of Mitogen-Activated Protein Kinase Signaling Pathways by the Ubiquitin-Proteasome System and Its Pharmacological Potential. *Pharmacol. Rev.* 73, 263–296. doi: 10.1124/pharmrev.120.000170

Mu, X., and Hur, S. (2021). Immunogenicity of In Vitro-Transcribed RNA. *Acc. Chem. Res.* 54, 4012–4023. doi: 10.1021/acs.accounts.1c00521

Naqvi, I., Giroux, N., Olson, L., Morrison, S. A., Llanga, T., Akinade, T. O., et al. (2022). DAMPs/PAMPs induce monocytic TLR activation and tolerance in COVID-19 patients; nucleic acid binding scavengers can counteract such TLR agonists. *Biomaterials* 283:121393. doi: 10.1016/j.biomaterials.2022.121393

Nie, S., Dong, B., Gao, S., Zhou, Y., Lu, W., Fang, M., et al. (2019). The protective effect of interfering TLR9-IRF5 signaling pathway on the development of CVB3-induced myocarditis. *Clin. Immunol.* 207, 24–35. doi: 10.1016/j.clim.2019.07.002

Park, W. S., Lee, J., Na, G., Park, S., Seo, S. K., Choi, J. S., et al. (2022). Benzyl Isothiocyanate Attenuates Inflammasome Activation in *Pseudomonas aeruginosa* LPS-Stimulated THP-1 Cells and Exerts Regulation through the MAPKs/NF-kappaB Pathway. *Int. J. Mol. Sci.* 23:1228. doi: 10.3390/ijms23031228

Peter, M., Bode, K., Lipford, G. B., Eberle, F., Heeg, K., and Dalpke, A. H. (2008). Characterization of suppressive oligodeoxynucleotides that inhibit Toll-like receptor-9-mediated activation of innate immunity. *Immunology* 123, 118–128. doi: 10.1111/j.1365-2567.2007.02718.x

Pu, J., Chen, D., Tian, G., He, J., Huang, Z., Zheng, P., et al. (2022). All-Trans Retinoic Acid Attenuates Transmissible Gastroenteritis Virus-Induced Inflammation in IPEC-J2 Cells via Suppressing the RLRs/NF-kappaB Signaling Pathway. *Front Immunol* 13:734171. doi: 10.3389/fimmu.2022.734171

Pulendran, B., and Maddur, M. S. (2015). Innate immune sensing and response to influenza. *Curr. Top Microbiol. Immunol.* 386, 23–71. doi: 10.1007/82_2014_405

Römmler, F., Jurk, M., Uhlmann, E., Hammel, M., Waldhuber, A., Pfeiffer, L., et al. (2013). Guanine modification of inhibitory oligonucleotides potentiates their suppressive function. *J. Immunol.* 191, 3240–3253. doi: 10.4049/jimmunol.1300706

Stein, M., and Eckert, K. A. (2021). Impact of G-Quadruplexes and Chronic Inflammation on Genome Instability: additive Effects during Carcinogenesis. *Genes* 12:1779. doi: 10.3390/genes12111779

Steinhagen, F., Zillinger, T., Peukert, K., Fox, M., Thudium, M., Barchet, W., et al. (2018). Suppressive oligodeoxynucleotides containing TTAGGG motifs inhibit cGAS activation in human monocytes. *Eur. J. Immunol.* 48, 605–611. doi: 10.1002/eji.201747338

Su, W., Cui, H., Wu, D., Yu, J., Ma, L., Zhang, X., et al. (2021). Suppression of TLR4-MyD88 signaling pathway attenuated chronic mechanical pain in a rat model of endometriosis. *J. Neuroinflamm.* 18:65. doi: 10.1186/s12974-020-02066-y

Sun, L., Liu, Y., Liu, X., Wang, R., Gong, J., Saferali, A., et al. (2022). Nano-Enabled Reposition of Proton Pump Inhibitors for TLR Inhibition: toward A New Targeted Nanotherapy for Acute Lung Injury. *Adv. Sci.* 9:e2104051. doi: 10.1002/advs.202104051

Sun, R., Sun, L., Bao, M., Zhang, Y., Wang, L., Wu, X., et al. (2010). A human microsatellite DNA-mimicking oligodeoxynucleotide with CCT repeats negatively regulates TLR7/9-mediated innate immune responses via selected TLR pathways. *Clin. Immunol.* 134, 262–276. doi: 10.1016/j.clim.2009.11.009

Tang, J., Cheng, X., Yi, S., Zhang, Y., Tang, Z., Zhong, Y., et al. (2021). Euphorbia Factor L2 ameliorates the Progression of K/BxN Serum-Induced Arthritis by Blocking TLR7 Mediated IRAK4/IKKbeta/IRF5 and NF-kB Signaling Pathways. *Front. Pharmacol.* 12:773592. doi: 10.3389/fphar.2021.773592

Tang, Y., Liu, J., Zhang, D., Xu, Z., Ji, J., and Wen, C. (2020). Cytokine Storm in COVID-19: the Current Evidence and Treatment Strategies. *Front. Immunol.* 11:1708. doi: 10.3389/fimmu.2020.01708

Teo Hansen Selno, A., Schlichtner, S., Yasinska, I. M., Sakhnevych, S. S., Fiedler, W., et al. (2021). High Mobility Group Box 1 (HMGB1) Induces Toll-Like Receptor 4-Mediated Production of the Immunosuppressive Protein Galectin-9 in Human Cancer Cells. *Front. Immunol.* 12:675731. doi: 10.3389/fimmu.2021.675731

Ueno, K., Nomura, Y., Morita, Y., and Kawano, Y. (2021). Prednisolone Suppresses the Extracellular Release of HMGB-1 and Associated Inflammatory Pathways in Kawasaki Disease. *Front. Immunol.* 12:640315. doi: 10.3389/fimmu.2021.640315

Xiao, Y., Lu, W., Li, X., Zhao, P., Yao, Y., Wang, X., et al. (2017). An oligodeoxynucleotide with AAAG repeats significantly attenuates burn-induced systemic inflammatory responses via inhibiting interferon regulatory factor 5 pathway. *Mol. Med.* 23, 166–176. doi: 10.2119/molmed.2016.00243

Xue, J., Suarez, J. S., Minaai, M., Li, S., Gaudino, G., Pass, H. I., et al. (2021). HMGB1 as a therapeutic target in disease. *J. Cell Physiol.* 236, 3406–3419. doi: 10.1002/jcp.30125

Yanai, H., Chiba, S., Ban, T., Nakaima, Y., Onoe, T., Honda, K., et al. (2011). Suppression of immune responses by nonimmunogenic oligodeoxynucleotides with high affinity for high-mobility group box proteins (HMGBs). *Proc. Natl. Acad. Sci. U S A* 108, 11542–11547. doi: 10.1073/pnas.1108535108

Yang, H., Hreggvidsdottir, H. S., Palmblad, K., Wang, H., Ochani, M., Li, J., et al. (2010). A critical cysteine is required for HMGB1 binding to Toll-like receptor 4 and activation of macrophage cytokine release. *Proc. Natl. Acad. Sci. U S A* 107, 11942–11947. doi: 10.1073/pnas.1003893107

Yue, L., Qidian, L., Jiawei, W., Rou, X., and Miao, H. (2022). Acute iron oxide nanoparticles exposure induced murine eosinophilic airway inflammation via TLR2 and TLR4 signaling. *Environ. Toxicol.* 37, 925–935. doi: 10.1002/tox.23455

Zhang, L., Römmler, F., Hammel, M., Waldhuber, A., Müller, T., Jurk, M., et al. (2015). Guanine-Modified Inhibitory Oligonucleotides Efficiently Impair TLR7- and TLR9-Mediated Immune Responses of Human Immune Cells. *PLoS One* 10:e0116703. doi: 10.1371/journal.pone.0116703

Zheng, C., Chen, J., Chu, F., Zhu, J., and Jin, T. (2019). Inflammatory Role of TLR-MyD88 Signaling in Multiple Sclerosis. *Front. Mol. Neurosci.* 12:314. doi: 10.3389/fnmol.2019.00314

Zhou, M., Aziz, M., and Wang, P. (2021). Damage-Associated Molecular Patterns As Double-Edged Swords in Sepsis. *Antioxid. Redox Signal* 35, 1308–1323. doi: 10.1089/ars.2021.0008

Zuffo, M., Guedin, A., Leriche, E. D., Doria, F., Pirota, V., Gabelica, V., et al. (2018). More is not always better: finding the right trade-off between affinity and selectivity of a G-quadruplex ligand. *Nucleic Acids Res.* 46, e115. doi: 10.1093/nar/gky607

frontiers | Frontiers in Microbiology

TYPE Original Research
PUBLISHED 12 September 2022
DOI 10.3389/fmicb.2022.995567

OPEN ACCESS

EDITED BY
Na Li,
Hainan Medical University, China

REVIEWED BY
Zhoujin Tan,
Hunan University of Chinese Medicine, China
Shao Gang Huang,
Guangdong Provincial Hospital of Chinese Medicine, China

*CORRESPONDENCE
Jianye Yuan
yuanjianye@hotmail.com

†These authors have contributed equally to this work

SPECIALTY SECTION
This article was submitted to Microorganisms in Vertebrate Digestive Systems, a section of the journal Frontiers in Microbiology

RECEIVED 18 July 2022
ACCEPTED 15 August 2022
PUBLISHED 12 September 2022

CITATION
Meng Y, Feng Y, Hang L, Zhou Y, Wang E and Yuan J (2022) No synergistic effect of fecal microbiota transplantation and shugan decoction in water avoidance stress-induced IBS-D rat model. *Front. Microbiol.* 13:995567. doi: 10.3389/fmicb.2022.995567

No synergistic effect of fecal microbiota transplantation and shugan decoction in water avoidance stress-induced IBS-D rat model

Yangyang Meng†, Ya Feng†, Lu Hang, Yan Zhou, Enkang Wang and Jianye Yuan*

Institute of Digestive Diseases, Longhua Hospital, Shanghai University of Traditional Chinese Medicine, Shanghai, China

Background: It has been reported that 5-hydroxytryptamine (5-HT, serotonin) metabolism is involved in the pathogenesis of irritable bowel syndrome (IBS) and that either Shugan decoction (SGD) or fecal microbiota transplantation (FMT) can alleviate the symptoms of IBS in patients and animal models. But the synergistic effect of FMT and SGD on 5-HT metabolism and IBS symptoms has not been investigated.

Aim: The main purpose of this study is to observe the synergistic effect of FMT with SGD on symptoms and 5-HT metabolism in IBS-D rats induced by water avoidance stress (WAS). Moreover, the possible material basis of the FMT was investigated.

Methods: In experiment I, rats were randomly divided into seven groups. Control group: routine feeding; WAS→ Control group: routine feeding with fecal microbiota liquid (FML) 1 (derived from rats in WAS group) gavage since the fourth day; WAS group: 10 days WAS with routine feeding; SGD group: 10 days WAS with SGD gavage since the fourth day on the base of routine feeding; Control→ WAS group: 10 days WAS with FML2 (derived from rats in Control group) gavage since the fourth day with routine feeding; SGD→ WAS group: 10 days WAS with FML3 (derived from rats in SGD group) gavage since the fourth day with routine feeding; SGD + (Control→ WAS) group: 10 days WAS with SGD and FML2 (derived from rats in Control group) gavage since the fourth day with routine feeding. In experiment II, rats were randomly divided into three groups. Control group: routine feeding; Control→ WAS group: 10 days WAS with FML2 gavage since the fourth day with routine feeding; FControl→ WAS group: 10 days WAS with FML2 filtrate gavage since the fourth day. The number of fecal pellets output (FPT) and the pain pressure threshold (PPT) were recorded. The histological changes in colon mucosa were observed by hematoxylin-eosin (HE) stain. The number of enterochromaffin cells (ECs), the content of 5-HT, and the expression of serotonin reuptake transporter (SERT) protein in the colon were measured by immunofluorescence or western blotting.

Results: Compared with that in the control group, the PPT and the expression of SERT in the WAS group and that in the WAS→ Control group were decreased with the increased number of ECs and the level of 5-HT in colon. But the FPT was not increased in the WAS→ Control group although that was increased in the WAS group. Compared with that in the WAS group, the FPT, the PPT, the number of ECs, the level of 5-HT, and the expression of SERT protein in colon in the SGD group, control→ WAS group, SGD→ WAS group, and SGD+(Control→ WAS) group were all recovered. The recovery of these indicators in the Control→ WAS group and that in the FControl→ WAS group was not significantly different.

Conclusion: No synergistic effect of SGD with FMT on IBS symptoms induced by WAS was found. The metabolites of intestinal microbiota may be the main active substances of the FML derived from normal rats to alleviate WAS-induced IBS symptoms.

KEYWORDS

water avoidance stress, irritable bowel syndrome, visceral hypersensitivity, fecal microbiota transplantation, serotonin

Introduction

Irritable bowel syndrome (IBS) is a chronic and recurrent functional intestinal disease with abdominal pain, abdominal distension, or abdominal discomfort as the main symptoms, which is related to or accompanied by defecation habits changes without organic lesions (Lacy et al., 2021). According to the Rome IV standard, IBS can be divided into four subtypes: constipation-predominant IBS (IBS-C), diarrhea-predominant IBS (IBS-D), mixed IBS (IBS-M), and unclassified IBS (IBS-U). Among them, IBS-D is identified as the most common subtype of IBS. It has been found that the prevalence of IBS varies greatly from country to country. According to 53 studies that used the Roman III standard, the combined prevalence rate of IBS is 9.2% in 38 countries, and it is 3.8% in 34 countries shown by six studies that used the Rome IV standard (Oka et al., 2020). Although IBS is not a fatal disease, it actually reduces the quality of life of patients to a different extent.

The pathological mechanisms of IBS have not been discovered entirely, it may be related to gastrointestinal dysmotility, increased gut permeability, visceral hypersensitivity (VH), mucosal immune activation, intestinal dysbiosis, altered gut–brain interaction, and genetic and psychosocial factors (Gwee et al., 2019). Increasing evidence support that the dysfunction of microbiota–gut–brain axis is the important pathological basis of IBS (De Palma et al., 2014).

5-hydroxytryptamine (5-HT), also known as serotonin, is a key neurotransmitter and signal molecule in the brain–gut axis (Dy and Camilleri, 2000). About 90–95% of the 5-HT is produced in the gut, most of which is released by enterochromaffin cells (ECs). 5-HT exerts its biological effects by binding to various 5-HT receptors, among which 5-HT_3 and 5-HT_4 receptors are closely associated with the pathogenesis of IBS (Vahora et al., 2020). The reuptake of 5-HT is mainly performed by a serotonin transporter (SERT) to transport 5-HT into the cells, in which 5-HT is degraded and the metabolites are excreted from the body through the kidney (Bertrand and Bertrand, 2010). So, the number of ECs and the expression of SERT control the level of local 5-HT to a certain extent.

There is a complex bidirectional interaction between intestinal microbiota and 5-HT metabolism. Fung et al. (2019) found that increased 5-HT or fluoxetine (an inhibitor of SERT) in the intestinal tract can change the diversity of intestinal microorganisms and the colonization of some specific strains in mice. The studies of Jones et al. (2020) showed that intestinal microbiota and their metabolites affect the level of 5-HT in the gut and in the circulation by regulating the synthesis of 5-HT in ECs. Therefore, regulating intestinal microbiota is becoming an important way of treating IBS. And prebiotics, probiotics, antibiotics, dietary adjustment, and fecal microbiota transplantation (FMT) have been provided in clinical practice (Herndon et al., 2020).

FMT also known as "fecal transplantation" or "fecal bacteriotherapy," is to transplant the functional bacteria derived from the feces of healthy people into the gastrointestinal tract of patients to restore the balance of intestinal microecology (Bakken et al., 2011). Pinn et al. (2014) reported that the symptoms were alleviated after FMT in 70% of patients with IBS who were not cured by conventional treatment. Huang et al. (2019) found that FMT can effectively relieve the symptoms of refractory patients with IBS, and the curative effect can be maintained for 3–6 months. Johnsen et al. (2018) deemed that

the effect of frozen fecal microbiota is better than that of fresh fecal microbiota.

Shugan decoction (SGD) is a Chinese Herbal Prescription that can significantly ease IBS-D patients' abdominal pain, diarrhea, and emotional disorder by harmonizing liver–spleen according to the traditional Chinese medicine theory. Animal experiments showed that SGD can alleviate VH and defecation in water avoidance stress (WAS)-induced IBS model rats (Shang et al., 2013).

As mentioned above, the occurrence of IBS-D often accompanies disturbances of the intestinal microbiota. As a means of regulating the intestinal microbiota, FMT is an effective treatment for IBS-D. As a Chinese Herbal Prescription for treating IBS-D, SGD plays an important role in treating IBS-D. Both SGD and FMT have a therapeutic effect on IBS in human beings and animals, but the synergism between SGD and FMT has not been evaluated. Therefore, the aim of this study was to observe the effect of SGD combined with FMT on IBS-like symptoms induced by WAS in rats. In addition, we also explored whether FMT exerts its therapeutic effect on IBS rats *via* regulating the 5-HT signal in colon and evaluated the efficacy of filtered fecal microbiota liquid (FML).

Materials and methods

Agents and materials

SGD is composed of Bupleuri Radix (Chaihu) (Shanghai Hongqiao Traditional Chinese Medicine Co., Ltd. Lot number: 190806), Citri Reticulatae Pericarpium (Chenpi) (Shanghai Hongqiao Traditional Chinese Medicine Co., Ltd. Lot number: 190911), Paeoniae Radix Alba (Baishao) (Shanghai Hongqiao Traditional Chinese Medicine Co., Ltd. Lot number: 190213), Saposhnikoviae Radix (Fangfeng) (Shanghai Wanshicheng National Pharmaceutical products Co., Ltd. Lot number: 190921-1), Atractylodis Macrocephalae Rhizoma (Baizhu) (Shanghai Hongqiao Traditional Chinese Medicine Co., Ltd. Lot number: 190923), which were obtained from the pharmacy department of Longhua Hospital, Shanghai University of Traditional Chinese Medicine. Saikosaponin A (National Institute for Food and Drug Control, Lot number: 110777-201912), paeoniflorin (National Institute for Food and Drug Control, Lot number: 110736-201943), 5-O-methylvisammioside (National Institute for Food and Drug Control, Lot number: 111523-201811), hesperidin (National Institute for Food and Drug Control, Lot number: 110721-201818), and cimicifugoside (National Institute for Food and Drug Control; Lot number: 111522-201913) were purchased from Shanghai Chaorui Biological Technology Co., Ltd. (Shanghai, China). Antibodies used in this study include: Anti-Serotonin transporter antibody (Abcam: ab181034), GAPDH Mouse Monoclonal antibody (Proteintech, 6004-1-lg), Goat anti-Mouse IgG-HRP antibody (HUABIO, HA1006), Goat anti-Rabbit IgG-HRP antibody (HUABIO, HA1001), Donkey Anti-Rat IgG (Abcam, ab150155) and Goat Anti-Mouse IgG (Proteintech, SA00013-1).

Preparation of SGD

The quality ratios of Bupleuri Radix (Chaihu), Citri Reticulatae Pericarpium (Chenpi), Paeoniae Radix Alba (Baishao), Saposhnikoviae Radix (Fangfeng), and Atractylodis Macrocephalae Rhizoma (Baizhu) are 6:3:4:4:6. SGD extract was prepared in the Herbal Chemistry Lab in Shanghai University of TCM. The extraction process is as follows: herbal pieces were soaked in distilled water for 30 min and then were boiled in six times of water for 1 h. The decoction was filtered by four layers of gauze and the residues were boiled again with 6-time water as above. The filtrates were mixed together, concentrated, and freeze-dried to powder.

Analysis and identification of SGD by high-performance liquid chromatography

The ingredients of SGD were analyzed by HPLC as reported in our previous study (Wang et al., 2020). Briefly, Saikosaponin A, paeoniflorin, 5-O-methylvisammioside, hesperidin, or cimicifugoside was dissolved in methanol and obtained 1 mg/mL of standard solution separately. Five hundred milligrams of SGD extract power was weighed and dissolved in distilled water. After ultrasonic shock for 40 min, the SGD solution was fixed at a constant volume of 10 mL. One milliliter of solution was injected into the activated C_{18} column, and eluted with 10 mL water and 10 mL methanol in sequence. The methanol eluent was collected and was concentrated to dry, then dissolved in 1 mL of methanol, and a 50.89 mg/mL of SGD sample solution was obtained through filtrating by 0.45 μm microporous membrane. The standard solution and the SGD sample solution were analyzed using the Dionex UltiMate™ 3000 RSLC nano system (Thermo Scientific, MA, USA) equipped with a Corona®ultra™CAD detector, Luna®C18 Column (Phenomenex, 250×4.6 mm, 5 mm), and a data station with analytical software (CHROMELEON®). Mobile phases consisted of A-purified water and B-acetonitrile. Gradient was set as follows: 0 min, 5% B; 35 min 65.5% B; 35.001 min, 100% B; 40 min, 100% B. Column temperature was set at 25 °C, DAD detection wavelength: 203 nm, 254 nm, and 366 nm.

Animals

Eighty-nine male Sprague-Dawley (SD) rats, weighing 200 g ± 20 g, were provided by Shanghai Bikai Experimental Animal

Co., Ltd. (production license No.: SCXK [Shanghai] 2018-0006), and were raised in the Experimental Animal Center of Shanghai University of TCM under the standard temperature (21–24 °C), humidity (50% ± 5%), light and dark cycle (12 h/12 h), and they had free access to standard rat chow and tap water. All the experiments in this study are in accordance with the regulations of the Animal Ethics Committee of Shanghai University of TCM (No. PZSHUTCM190906001). All the experiments were carried out between 9:00 AM and 11:00 AM.

Preparation of FML

After a week of adaptive feeding, nine rats were randomly divided into three groups ($n = 3$ in each group): Control group: no treatment; WAS group: 10 days WAS; SGD group: 10 days WAS and dealing with SGD intragastric administration since the fourth day. Feces of rats in each group were collected. A certain quality of feces was weighed on a sterilized bending plate and was diluted with aseptic 0.9% NaCl solution at 37 °C with the ratio of 1: 10. FML was obtained after filtering by 2, 4, and 8 layers of aseptic gauze, respectively. FML filtration method: FML was centrifugated at 10,000 rpm and was filtrated with a 0.45 μm disposable needle filter. FMT was performed with 0.1 g feces per 100 g body weight.

Animals grouping and treatment

Experiment I: After a week of adaptive feeding, 56 rats were randomly divided into seven groups ($n = 8$ in each group): Control group: routine feeding; WAS→ Control group: routine feeding with FML1 (derived from rats in WAS group) gavage since the fourth day; WAS group: 10 days WAS on the base of routine feeding; SGD group: 10 days WAS with SGD gavage since the fourth day on the base of routine feeding; Control→ WAS group: 10 days WAS with FML2 (derived from rats in Control group) gavage since the fourth day on the base of routine feeding; SGD→ WAS group: 10 days WAS FML3 (derived from rats in SGD group) gavage since the fourth day on the base of routine feeding; SGD + (Control→ WAS) group: 10 days WAS with SGD and FML2 (derived from rats in Control group) gavage since the fourth day on the base of routine feeding.

Experiment II: After a week of adaptive feeding, 24 rats were randomly divided into three groups ($n = 8$ in each group). Control group: routine feeding; Control→ WAS group: 10 days WAS with FML2 (derived from rats in Control group) gavage since the fourth day on the base of routine feeding; FControl→ WAS group: 10 days WAS with FML2 (derived from rats in Control group) filtrate gavage since the fourth day.

Water avoidance stress

Refer to the method initiated by (Bradesi et al., 2005; Wang et al., 2020), the rats were placed on a platform (10 cm long, 8 cm wide, 8 cm high) which was fixed in the center of an organic glass pool (45 cm long, 25 cm wide, 25 cm high) filled with water (25 °C) to suffer from WAS for 1 h every day in 10 consecutive days.

Fecal pellets counting

The amount of FPT of rats during WAS was counted every day.

Colorectal distension

On the 10th day after WAS, the pressure threshold to induce abdominal withdrawal reflex (AWR) in rats was measured by colorectal distension (CRD) test. The methods were as follows: a balloon (5 mm diameter and 1 cm long) with a catheter (2 mm diameter) was inserted into the colorectum 1 cm above the anus. The catheter was fixed to the root of the rat tail with adhesive tape. Then the balloon was inflated gradually by one experimenter and the pressure values were monitored. Meanwhile, the abdominal wall reactions of the rats were observed by the other experimenter and a voice sign was made by him when the first AWR appeared and the immediate pressure value was recorded by the former experimenter. The average value, which was named the pain pressure threshold (PPT), was calculated after three repeated measurements which were performed with a 3-min interval between every two successive measurements.

HE stain and immunofluorescence

The colon tissue was fixed in 4% paraformaldehyde for 48 h after the content was washed off with ice normal saline. Then the paraffin sections were made by dehydration, transparency, wax soaking, embedding, and sectioning. Hematoxylin-eosin (HE) solution staining, neutral gum sealing, and observation under the ordinary optical microscope (Nikon Corporation, Japan) were done in sequence. The paraffin slice was put into buffering solution of citric acid to repair the antigen for 15 min in a microwave oven after dewaxing. Then it was washed with PBS three times (5 min each time) after cooling. The tissue was incubated with 3% H_2O_2 for 15 min and was washed before it was incubated with serotonin antibody (1:250) and Chromogranin A (1:100) antibody overnight at 4 °C. Then it was incubated with secondary antibodies (donkey anti-rat IgG 1:500 and Goat Anti-Mouse IgG 1:250) after it was washed with PBS three times (5 min each time). LSM800 laser

confocal microscope (Zeiss, Germany) was used to observe the immunofluorescence after adding anti-quenching DAPI and seal.

Protein extraction and western blotting

The shredded colonic tissue was put into the RIPA lysis buffer with a protease inhibitor for homogenate. And then the homogenate was centrifuged at 4 °C, 12,000 rpm for 15 min, and the supernatant was collected. BCA protein assay kit (CWBIO: CW0014s) was used to measure protein concentration. Samples were mixed with 5× loading buffer and were heated at 95 °C for 10 min to denature. Then, 100 mg of total proteins were loaded on 10% SDS polyacrylamide gels and electrophoresed. The proteins were then transferred to the PVDF membrane (Millipore, Darmstadt, Germany). The PVDF membrane was incubated with 5% BSA for 1 h and then was incubated with SERT antibody (1:1,000) overnight. Then it was incubated with a secondary antibody (goat anti-rabbit IgG-HRP1:20,000) for 1 h after it was washed with Tris-buffered saline and Tween 20 (TBST) three times (10 min each time). The membranes were washed again. Specific protein bands were visualized using the ECL kit (Millipore: WBKLS500) and imaged with SyngeneG (BOX ChemiXT4).

Statistical analysis

SPSS version 24.0 (SPSS, Chicago, IL, USA) and GraphPad Prism 5.0 (La Jolla, CA, USA) were used for data analysis. Each value was expressed as mean ± SE. If data were subject to normality and homogeneity of variance, an one-way analysis of variance (one-way ANOVA) and followed LSD *t*-test was used for analyzing the differences among the groups. If disobedient, the rank-sum test was used. $P < 0.05$ was considered statistically significant.

Results

Chemical composition of SGD

Referring to the components of SGD in Chinese Pharmacopeia, we confirmed the principal ingredients of SGD extract as follows: saikosaponin A, paeoniflorin, 5-O-methylvisammioside, hesperidin, and cimicifugoside (Figure 1).

Effect of FML1 on normal rats

HE staining showed that FML1-like WAS did not induce colonic pathological changes in normal rats (Figure 2).

Compared with that in the control group, the PPT in the WAS→ Control group, as well as that in the WAS group, decreased significantly ($P < 0.05$); but the number of FPT of rats in the WAS→ Control group was not increased ($P > 0.05$) although that in the WAS group increased significantly ($P < 0.05$) (Figure 3).

Effect of SGD combined with FML2 on WAS rats

HE staining showed that FML2-like SGD did not influence the colon mucosa obviously (Figure 2).

Compared with that in WAS group, the number of FPT of rats in the SGD group, Control→ WAS group, SGD→ WAS group, or SGD + (Control→ WAS) group was significantly reduced ($P < 0.05$, $P < 0.05$, $P < 0.05$, $P < 0.05$), accompanied with the significantly increased PPT ($P < 0.001$, $P < 0.001$, $P < 0.001$, $P < 0.001$), but there was no significant difference among that in these four groups ($P > 0.05$) (Figure 3).

Effect of FML2 filtrate on WAS rats

We compared the effects of filtered and unfiltered FML2 on the abnormal colonic motility and VH of WAS rats by transplantation to further confirm whether the microbiota or their metabolites in FML2 played the primary role. It was shown that the number of FPT of rats in either the Control→ WAS group or FControl→ WAS group was significantly reduced on the fourth and fifth day ($P < 0.05$, $P < 0.05$) with the increased PPT ($P < 0.001$, $P < 0.001$) compared to that in WAS group. But there were no significant differences between that in the Control→ WAS group and that in the FControl→ WAS group ($P > 0.05$) (Figure 4).

Effect of FML1 on 5-HT content, ECs number, and SERT expression in the colon of normal rats

Compared with that in Control group, the intensity of green (ECs) and red (5-HT) fluorescence in the colon of rats in WAS→ Control group was increased significantly ($P < 0.01$, $P < 0.001$) (Figure 5), while the expression of SERT protein was decreased significantly ($P < 0.05$) (Figure 6).

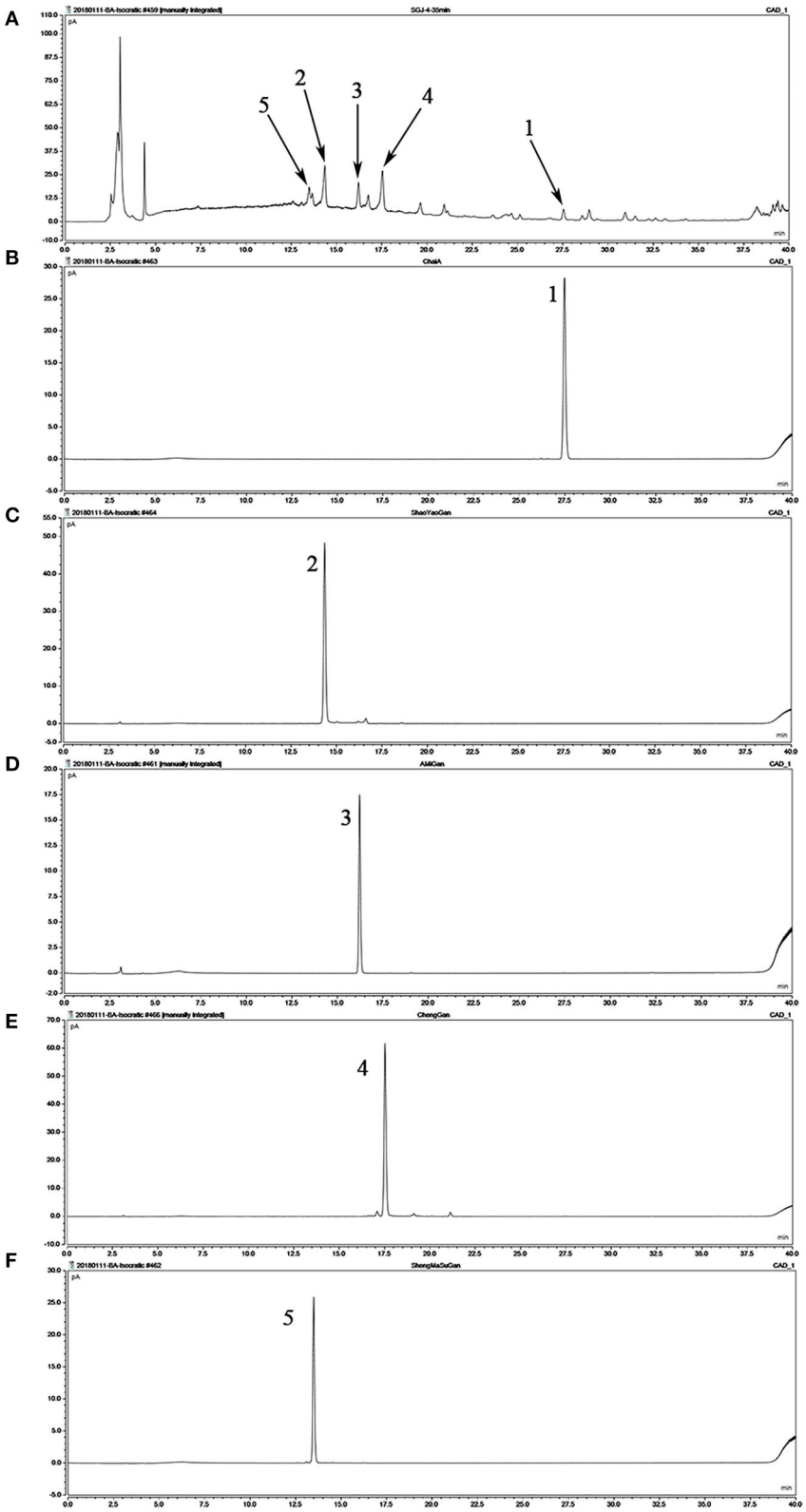

FIGURE 1
Analysis of the chemical composition of Shugan decoction (SGD) extract by HPLC. **(A)** HPLC chromatogram of SGD extract; **(B)** HPLC chromatogram of saikosaponin A; **(C)** HPLC chromatogram of paeoniflorin; **(D)** HPLC chromatogram of 5-O-methylvisammioside; **(E)** HPLC chromatogram of hesperidin; **(F)** HPLC chromatogram of cimicifugoside. Peak 1: saikosaponin A; Peak 2: paeoniflorin; Peak 3: 5-O-methylvisammioside; Peak 4: hesperidin; Peak 5: cimicifugoside.

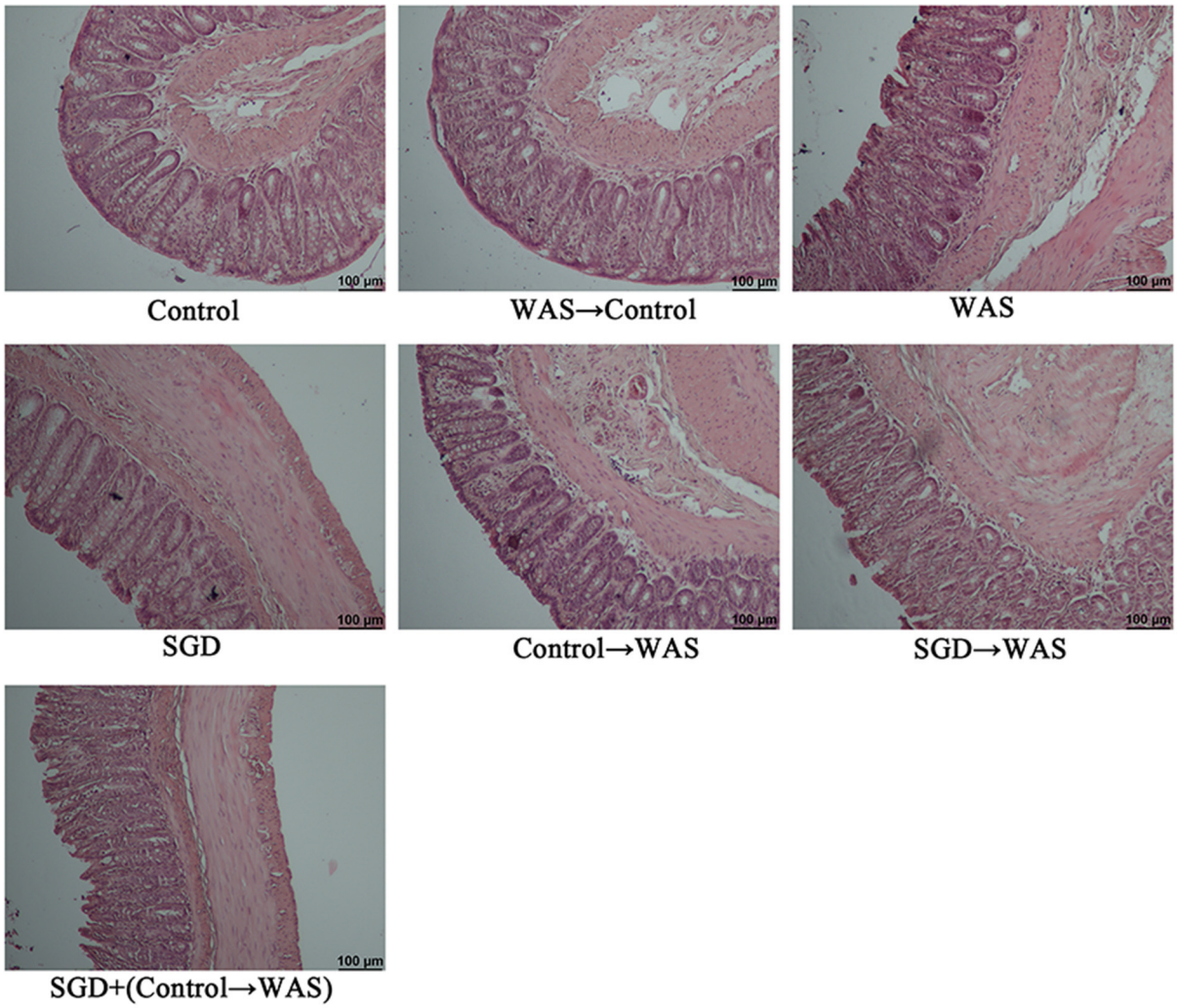

FIGURE 2
Histopathological examination of colon in rats.

Effect of FML2 on 5-HT content, ECs number, and SERT expression in the colon of WAS rats

Compared with that in the WAS group, the intensity of green (ECs) and red (5-HT) fluorescence in the colon of rats in the Control→ WAS group or in the SGD→ WAS group was decreased significantly ($P < 0.01$, $P < 0.001$) (Figure 5), and the expression of SERT protein was increased significantly ($P < 0.05$, $P < 0.01$) (Figure 6).

Effect of filtered FML on 5-HT content, ECs number, and SERT expression in the colon of WAS rats

Compared with that in WAS group, the intensity of green (ECs) and red (5-HT) fluorescence in the colon of rats in the FControl→ WAS group was significantly reduced ($P < 0.05$, $P < 0.01$) (Figure 7), and the expression of SERT protein was increased significantly ($P < 0.05$) (Figure 8).

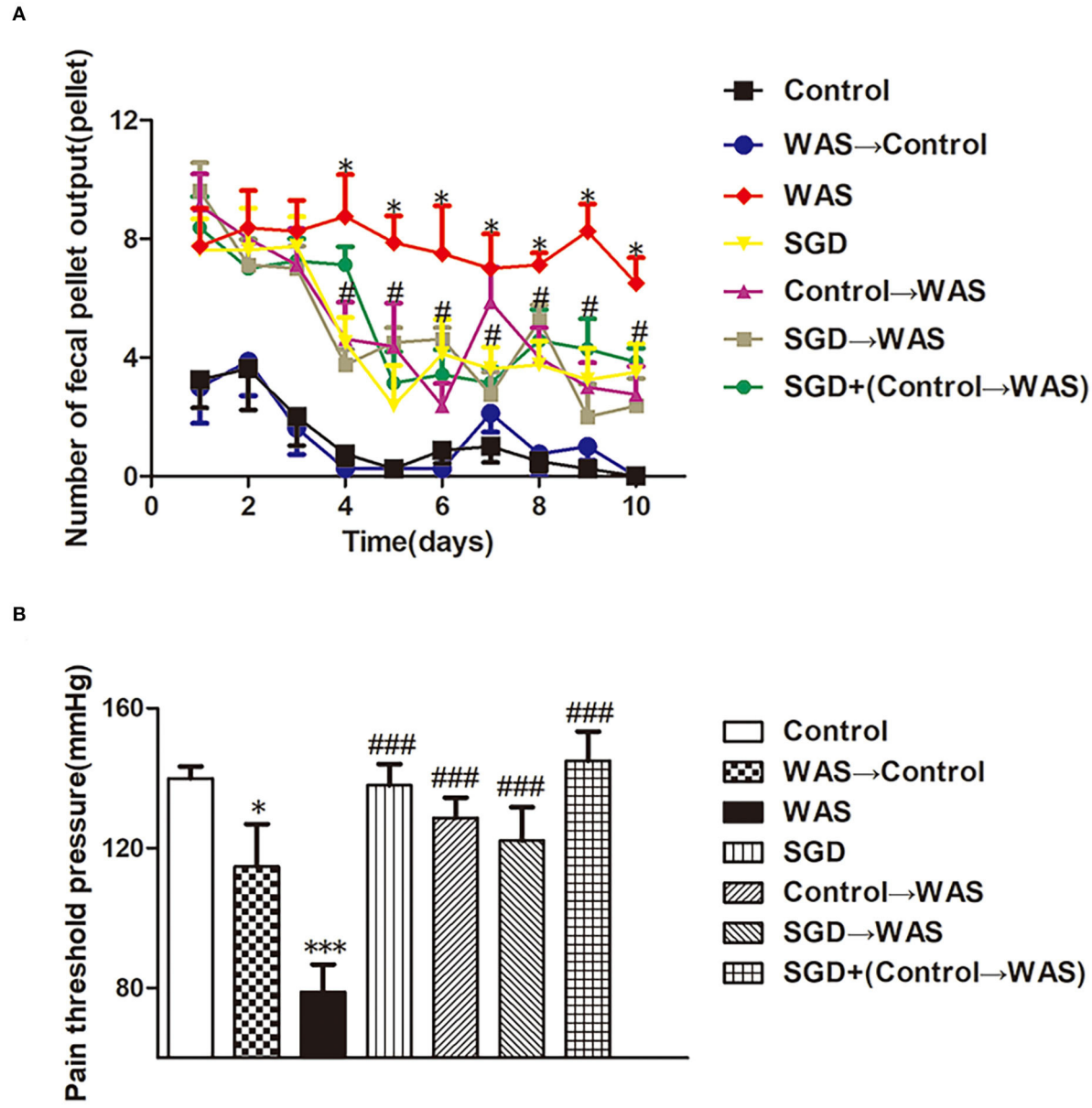

FIGURE 3
Effects of several FMT combined with or without SGD on IBS-like symptoms of WAS rats. **(A)** Fecal pellet numbers output of rats every day. **(B)** PPT in rats (All results are expressed as mean ± SE $n = 8$/group, $^{*}P < 0.05$ vs. Control, $^{***}P < 0.001$ vs. Control, $^{\#}P < 0.05$ vs. WAS, $^{\#\#\#}P < 0.001$ vs. WAS).

Discussion

Intestinal microecological imbalance plays an important role in the pathogenesis of IBS. It is suggested that neurotransmitters, compounds, metabolites, enzymes, and endocrine factors derived from intestinal microbiota may be involved in the pathogenesis of IBS (Mishima and Ishihara, 2020), namely, abnormal intestinal motility, VH, damaged intestinal mucosal barrier, and wrong neuro-immune signals, which are inextricably linked to the intestinal microbiota (Distrutti et al., 2016). In this study, we found that transplanting FML1 (derived from WAS rats) into control rats increased the visceral sensitivity of control rats, which maybe indirectly support WAS inducing VH by damaging gut microecological balance. However, FML1 transplantation did not influence the number of FPT of control rats, which suggested that

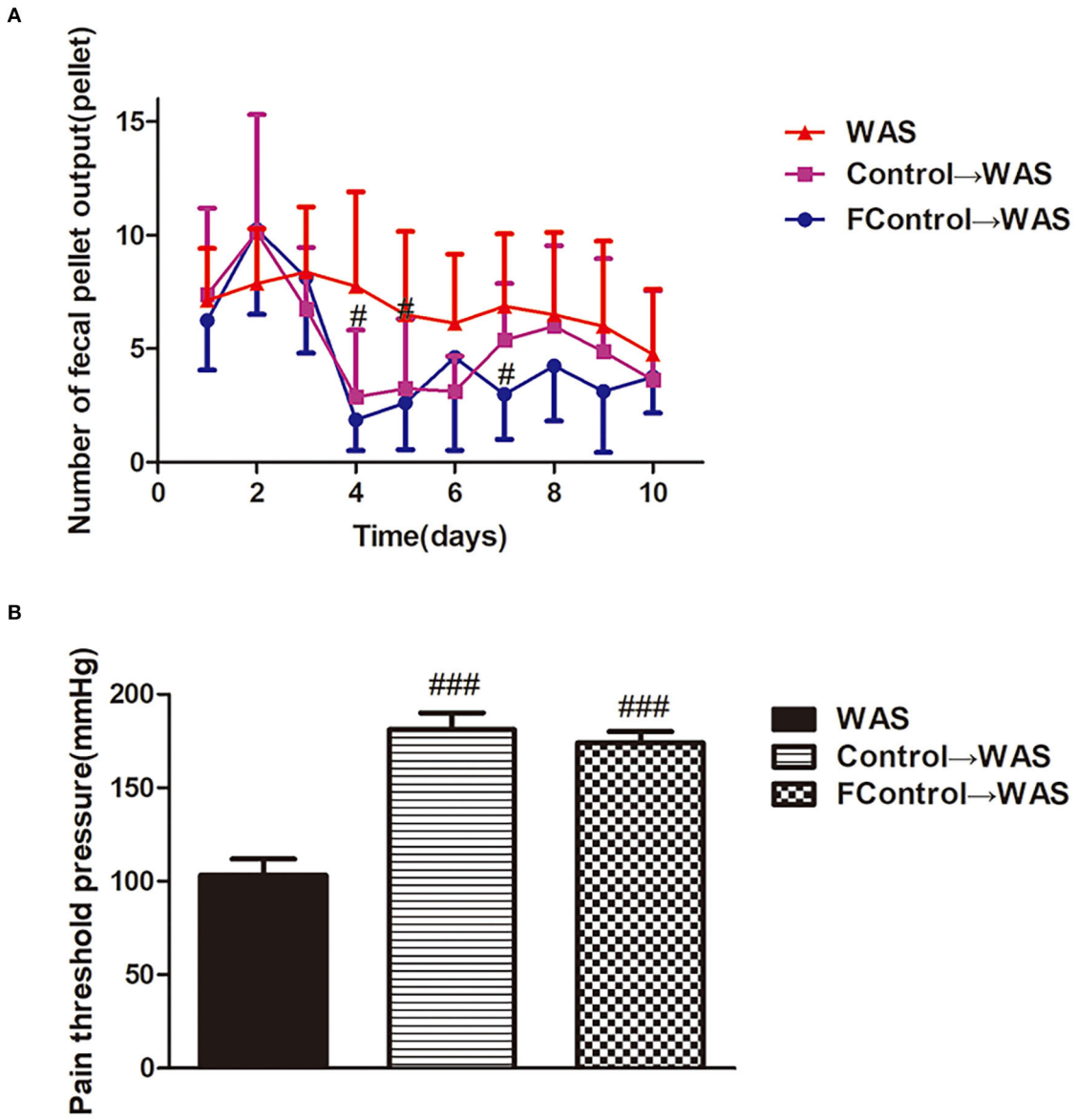

FIGURE 4
Effect of filtered FML on IBS-like symptoms of WAS rats. **(A)** Fecal pellet numbers output of rats every day. **(B)** PT in rats (All results are expressed as mean ± SE $n = 8$/group, $^{\#}P < 0.05$ vs. WAS, $^{\#\#\#}P < 0.001$ vs. WAS).

the mechanisms involved in WAS-induced rat IBS are complex and are not limited to intestinal dysbiosis. SGD gavage, transplanting FML2 (derived from control rats), or transplanting FML3 (derived from rats in the SGD group) could reduce the number of FPT and decrease the visceral sensitivity of WAS rats. But it failed to show the synergistic effect of SGD and FML2 transplantation, which may be due to SGD and FML2 sharing the same way-regulating intestinal microbiota to improve VH and abnormal defecation induced by WAS in rats. This finding indicates that although either SGD or FMT is effective, the combination therapy of them is unnecessary in the clinical practice of IBS treatment.

The intestinal microbiota is involved in the regulation of metabolism of 5-HT. The results of this study confirmed that transplanting FML1 to normal rats could increase the content of 5-HT in colon. The simultaneously increased number of ECs and decreased expression of SERT may contribute to the elevated 5-HT level. Interestingly, there are other studies that reported transplanting the intestinal microbiota from normal mice to

10.3389/fmicb.2022.995567

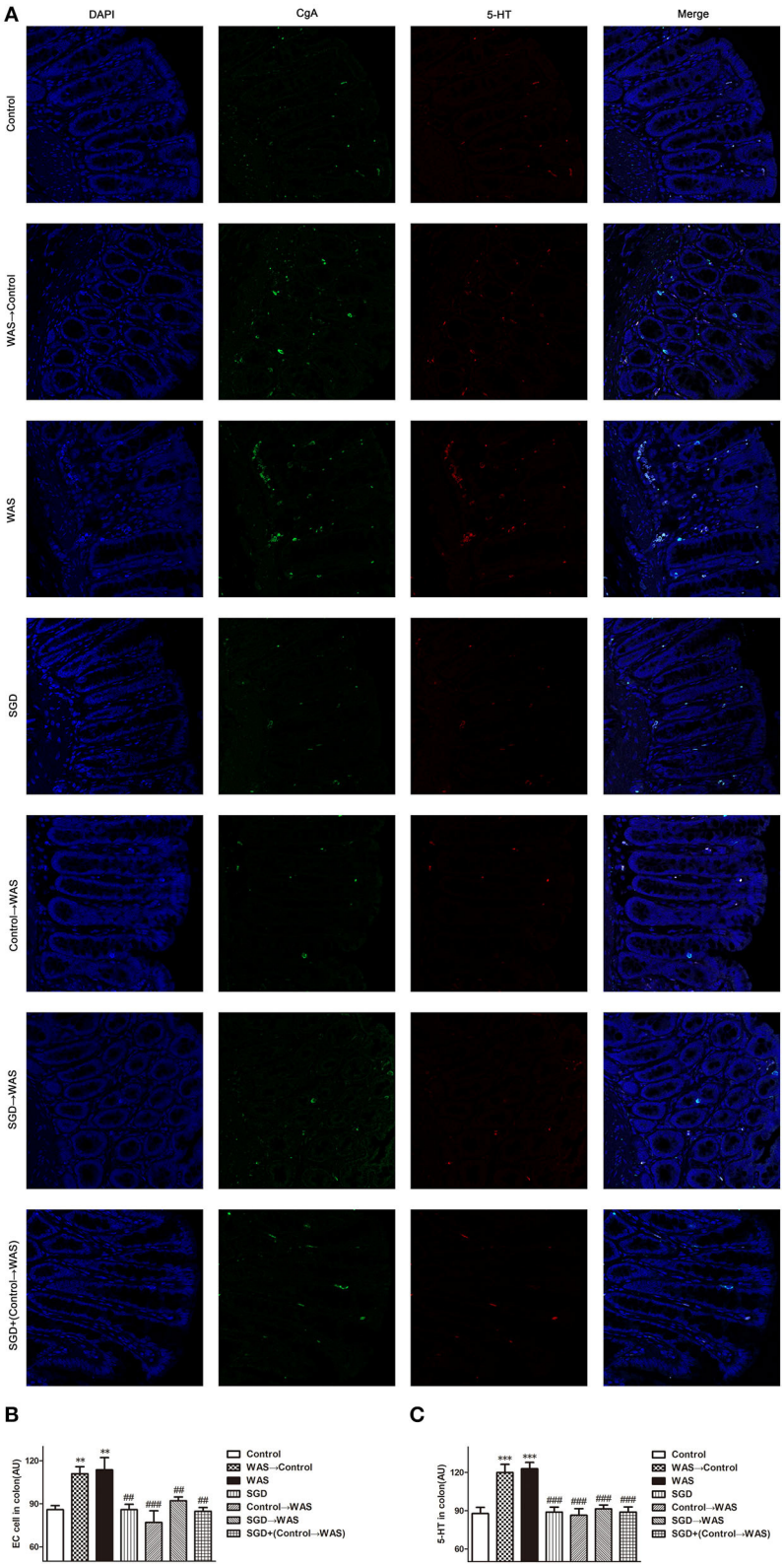

FIGURE 5
Effects of several FMT combined with or without SGD on ECs numbers and 5-HT content in the colon of rats. **(A)** Colon immunofluorescence staining in rats. **(B)** Statistical plot of ECs numbers in the colon. **(C)** Statistical plot of the 5-HT content in the colon (All results are expressed as mean ± SE $n = 5$/group, $^{**}P < 0.01$ vs. Control, $^{***}P < 0.001$ vs. Control, $^{\#\#}P < 0.01$ vs. WAS, $^{\#\#\#}P < 0.001$ vs. WAS).

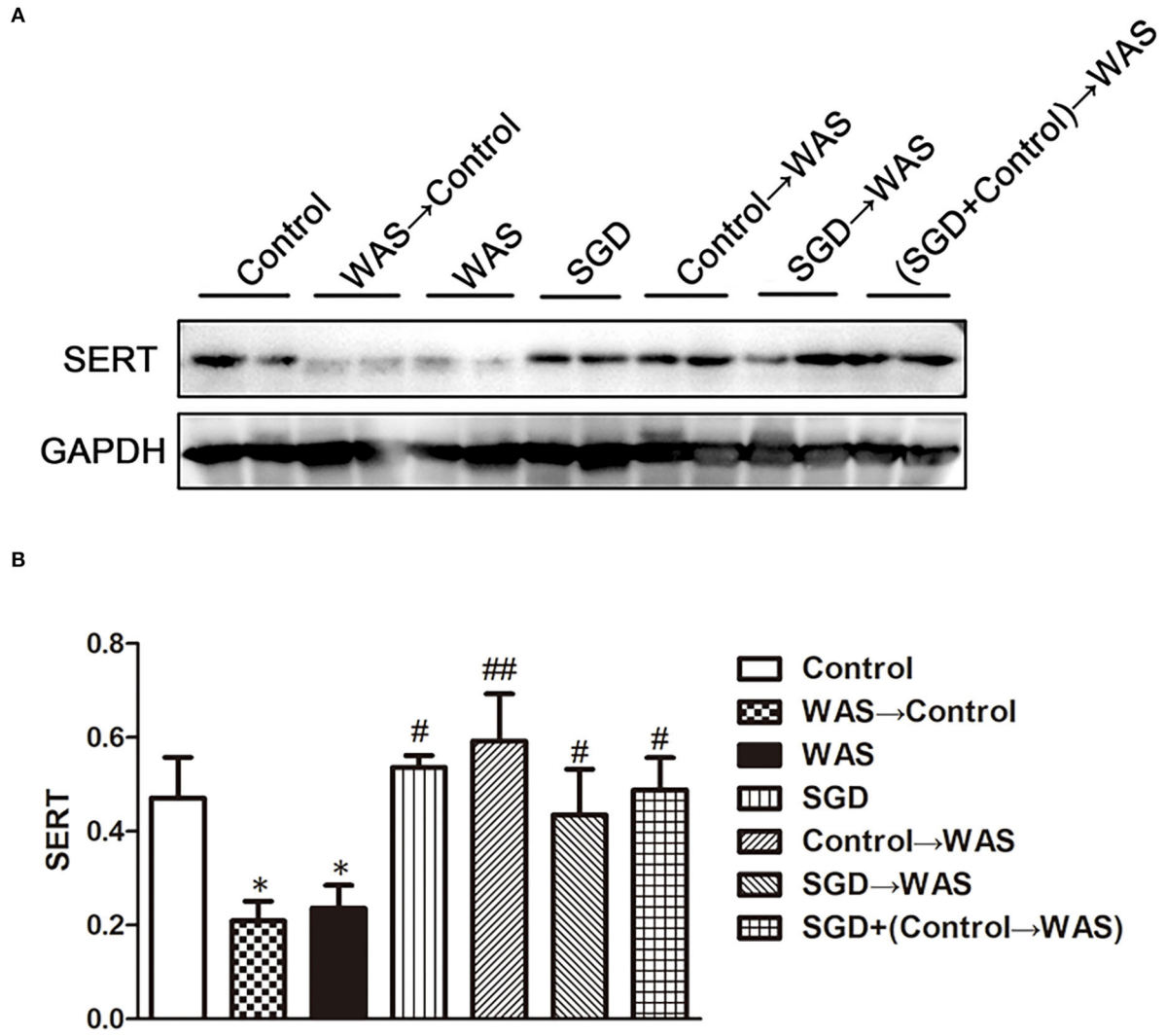

FIGURE 6
Effects of several FMT combined with or without SGD on SERT expression in the colon of rats. **(A)** SERT protein expression plot in the colon. **(B)** Statistical plot of SERT protein expression in the colon (All results are expressed as mean ± SE n = 3/group, $^{*}P < 0.05$ vs. Control, $^{\#}P < 0.05$ vs. WAS, $^{\#\#}P < 0.01$ vs. WAS).

germ-free mice could cause a significant increase of 5-HT levels in colon of the latter (Yano et al., 2015; Hata et al., 2017; Yang et al., 2017), which seems to be quite contrary to our result. After all, germ-free mice are different from normal mice. SGD gavage, transplanting FML2, or transplanting FML3 could decrease the high level of 5-HT in colon of WAS rats by normalizing the number of ECs and the expression of SERT in colon maybe via regulating gut microbiota. Cao et al. (2018) have shown that the supernatant of Lactobacillus acidophilus and *Bifidobacterium longum* could upregulate the mRNA and protein levels of SERT in intestinal epithelial cells. We did not know what component of FML derived from control rats, i.e., FML2, exerted their regulating effect on IBS symptoms, 5-HT level, ECs number, and SERT expression in colon of WAS rats yet.

To further identify microbiota or their metabolites in FML2 play the primary role in alleviating the IBS-like symptoms of WAS rats, we compared the effect of filtered FML2 (generally, it is regarded that bacteria can be eliminated by a 0.45 μm filter) and unfiltered FML2 on the IBS-like symptoms of WAS rats. It was found that filtered FML2 and unfiltered FML2 are equally effective. We speculated that the metabolites of the microbiota seem to play a major role in FMT. Certainly, this speculation needs to be confirmed further. In fact, a similar report has shown that filtered fecal solution FMT could treat *Clostridium*

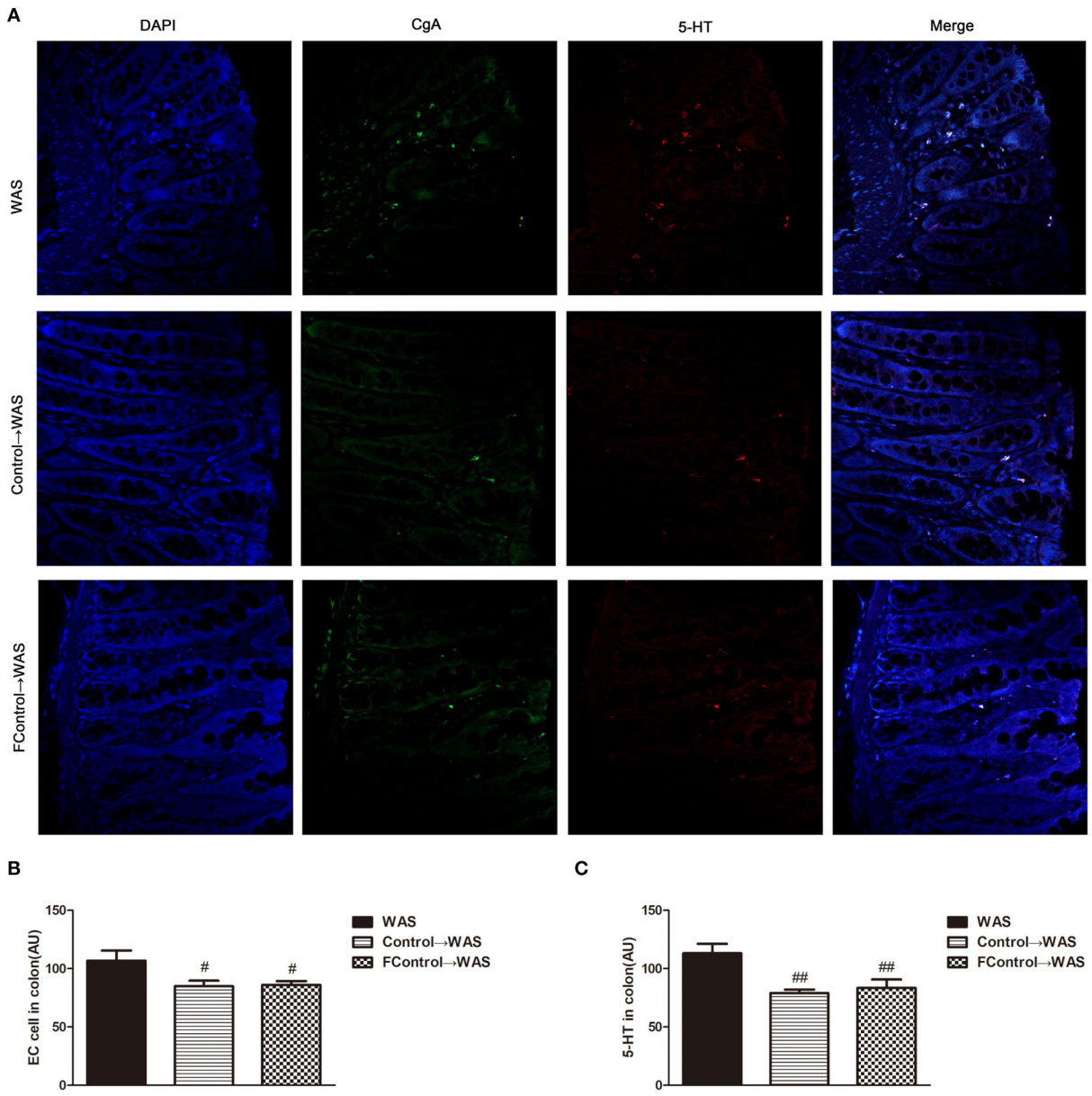

FIGURE 7
Effect of filtered FML on ECs numbers and 5-HT Content in the Colon of Rats. **(A)** Colon immunofluorescence staining in rats. **(B)** Statistical plot of ECs numbers in the colon. **(C)** Statistical plot of the 5-HT content in the colon (All results are expressed as mean ± SE n = 5/group, $^{\#}P < 0.05$ vs. WAS, $^{\#\#}P < 0.01$ vs. WAS).

difficile infections (Ott et al., 2017). Recent studies suggested that changes in metabolites of intestinal microbiota such as short-chain fatty acids (SCFAs) and bile acids may be involved in the pathogenesis of IBS. A meta-analysis on the levels of SCFAs in feces from healthy people and from patients with IBS suggested that butyrate in feces from patients with IBS-D is significantly increased and that propionate and butyrate in feces from patients with IBS-C are significantly decreased compared with that in feces from healthy people (Sun et al., 2019). The significantly increased concentration of SCFAs in feces of IBS-D model mice has also been reported (Shaidullov et al., 2021). It has been realized that changes in bile acid metabolism are associated with diarrhea and VH in patients with IBS (Wei et al., 2020). Li et al. (2019) have shown that bile acid induces VH through signal transduction of mucosal mast cells to pain receptors.

In summary, our data suggested that both SGD and FMT with healthy FML can effectively improve IBS-like symptoms

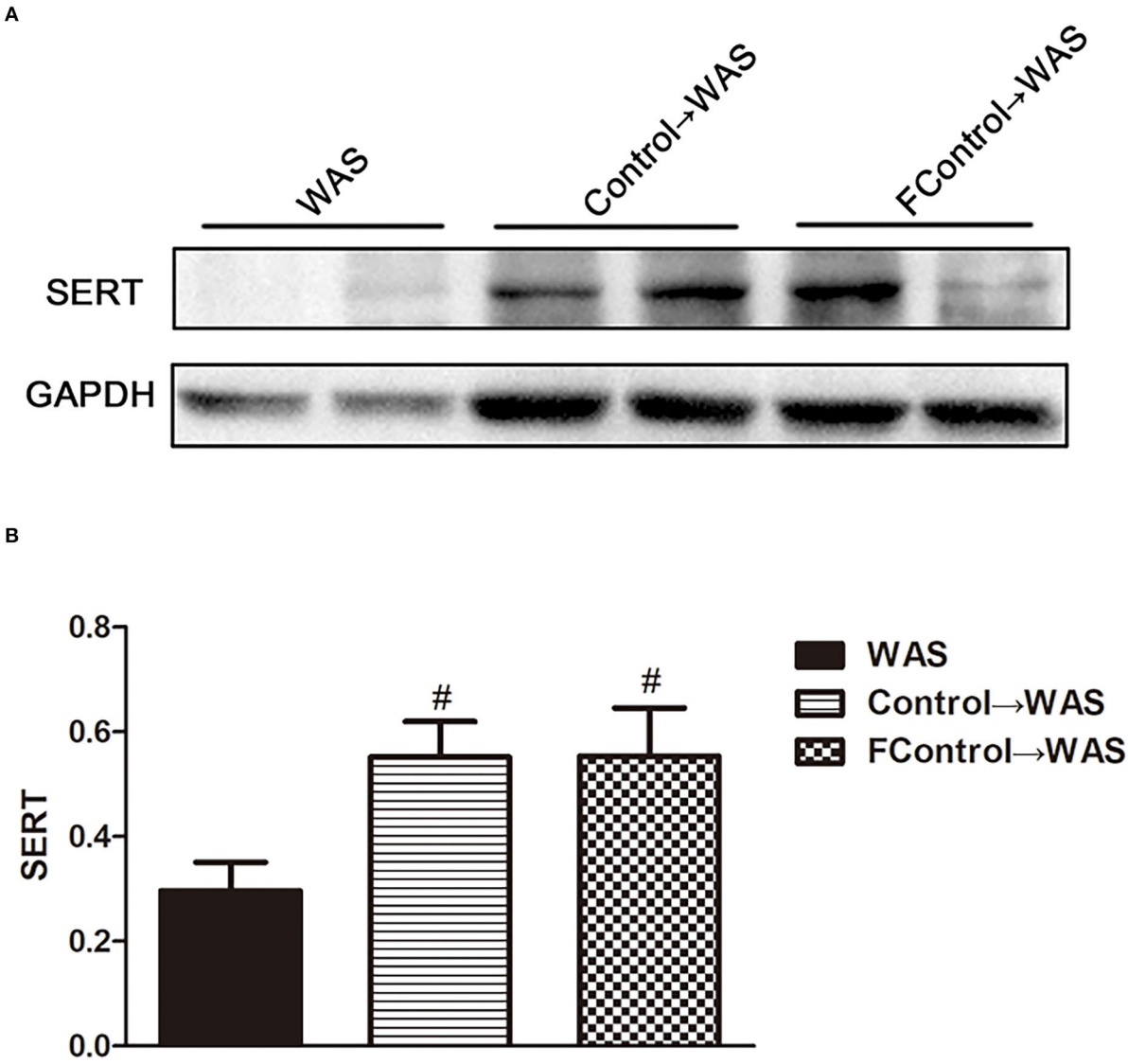

FIGURE 8
Effect of filtered FML on SERT expression in the colon of rats. **(A)** SERT protein expression plot in the colon. **(B)** Statistical plot of SERT protein expression in the colon (All results are expressed as mean ± SE n = 3/group, $^{\#}P < 0.05$ vs. WAS).

and regulate colon 5-HT levels in WAS rats, but they have no synergistic effect. Therefore, the combination of FMT and traditional Chinese medicine compounds like SGD is not clinically recommended for IBS. The metabolites of intestinal microbiota may play an important role as effective substances in the treatment of FMT on IBS. Therefore, when using FMT for IBS, we recommend filtered FMT, which can effectively reduce infection risk due to microbiota invasion (Ott et al., 2017). Nevertheless, the animal model could not fully reflect the pathophysiology of human disease, and the therapeutic effect of FMT combined with or without SGD on patients with IBS needs to be further verified.

Data availability statement

The original contributions presented in the study are included in the article/supplementary material, further inquiries can be directed to the corresponding author.

Ethics statement

The animal study was reviewed and approved by the Animal Ethics Committee of Shanghai University of TCM.

Author contributions

YM and YF wrote the draft of the paper. LH, YZ, EW, YM, and YF carried out the animal experiments. JY designed the experiments and revised the paper. All authors contributed to the article and approved the submitted version.

Funding

This work was supported by the National Natural Science Foundation of China (No. 81874391).

Conflict of interest

The authors declare that the research was conducted in the absence of any commercial or financial relationships that could be construed as a potential conflict of interest.

Publisher's note

All claims expressed in this article are solely those of the authors and do not necessarily represent those of their affiliated organizations, or those of the publisher, the editors and the reviewers. Any product that may be evaluated in this article, or claim that may be made by its manufacturer, is not guaranteed or endorsed by the publisher.

References

Bakken, J. S., Borody, T., Brandt, L. J., Brill, J. V., Demarco, D. C., Franzos, M. A., et al. (2011). Treating Clostridium difficile infection with fecal microbiota transplantation. *Clin. Gastroenterol. Hepatol.* 9, 12. doi: 10.1016/j.cgh.2011.08.014

Bertrand, P. P., and Bertrand, R. L. (2010). Serotonin release and uptake in the gastrointestinal tract. *Auton. Neurosci.* 153, 47–57. doi: 10.1016/j.autneu.2009.08.002

Bradesi, S., Schwetz, I., Ennes, H., Lamy, C., Ohning, G., Fanselow, M., et al. (2005). Repeated exposure to water avoidance stress in rats: a new model for sustained visceral hyperalgesia. *Am. J. Physiol. Gastrointest. Liver Physiol.* 289, 1. doi: 10.1152/ajpgi.00500.2004

Cao, Y., Feng, L., Wang, B., Jiang, K., Li, S., Xu, X., et al. (2018). *Lactobacillus acidophilus* and supernatants upregulate the serotonin transporter expression in intestinal epithelial cells. *Saudi J. Gastroenterol.* 24, 1. doi: 10.4103/sjg.SJG_333_17

De Palma, G., Collins, S. M., and Bercik P. (2014). The microbiota-gut-brain axis in functional gastrointestinal *disorders*. *Gut Microbes.* 5, 3. doi: 10.4161/gmic.29417

Distrutti, E., Monaldi, L., Ricci, P., and Fiorucci S. (2016). Gut microbiota role in irritable bowel syndrome: new therapeutic strategies. *World J. Gastroenterol.* 22, 7. doi: 10.3748/wjg.v22.i7.2219

Dy, K., and Camilleri, M. (2000). Serotonin: a mediator of the brain-gut connection. *Am. J. Gastroenterol.* 95, 10. doi: 10.1016/S0002-9270(00)01970-5

Fung, T., Vuong, H., Luna, C., Pronovost, G., Aleksandrova, A., Riley, N., et al. (2019). Intestinal serotonin and fluoxetine exposure modulate bacterial colonization in the *gut*. *Nat. Microbiol.* 4, 12. doi: 10.1038/s41564-019-0540-4

Gwee, K., Gonlachanvit, S., Ghoshal, U., Chua, A., Miwa, H., Wu, J., et al. (2019). Second Asian consensus on irritable bowel syndrome. *J Neurogastroenterol. Motil.* 25, 3. doi: 10.5056/jnm19041

Hata, T., Asano, Y., Yoshihara, K., Kimura-Todani, T., Miyata, N., Zhang, X. T., et al. (2017). Regulation of gut luminal serotonin by commensal microbiota in mice. *PLoS ONE.* 12, 7. doi: 10.1371/journal.pone.0180745

Herndon, C., Wang, Y., and Lu C. (2020). Targeting the gut microbiota for the treatment of irritable bowel syndrome. *Kaohsiung J. Med. Sci.* 36, 3. doi: 10.1002/kjm2.12154

Huang, H. L., Chen, H. T., Luo, Q. L., Xu, H. M., He, J., Li, Y. Q., et al. (2019). Relief of irritable bowel syndrome by fecal microbiota transplantation is associated with changes in diversity and composition of the gut microbiota. *J. Dig. Dis.* 20, 8. doi: 10.1111/1751-2980.12756

Johnsen, P. H., Hilpüsch, F., Cavanagh, J. P., Leikanger, I.S., Kolstad, C., Valle, P. C., et al. (2018). Faecal microbiota transplantation versus placebo for moderate-to-severe irritable bowel syndrome: a double-blind, randomised, placebo-controlled, parallel-group, single-centre trial. *Lancet Gastroenterol. Hepatol.* 3, 1. doi: 10.1016/S2468-1253(17)30338-2

Jones, A. L., Sun, W. E., Martin, A.M., and Keating, D. J. (2020). The ever-changing roles of serotonin. *Int. J. Biochem. Cell Biol.* 125, 105776. doi: 10.1016/j.biocel.2020.105776

Lacy, B., Pimentel, M., Brenner, D., Chey, W., Keefer, L., Long, M., et al. (2021). ACG clinical guideline: management of irritable bowel *syndrome*. *Am. J. Gastroenterol.* 116, 1. doi: 10.14309/ajg.0000000000001036

Li, W. T., Luo, Q. Q., Wang, B., Chen, X., Yan, X. J., Qiu, H. Y., et al. (2019). Bile acids induce visceral hypersensitivity via mucosal mast cell-to-nociceptor signaling that involves the farnesoid X receptor/nerve growth factor/transient receptor potential vanilloid 1 axis. *FASEB J.* 33, 2. doi: 10.1096/fj.201800935RR

Mishima, Y., and Ishihara, S. (2020). Molecular mechanisms of microbiota-mediated pathology in irritable bowel syndrome. *Int. J. Mol. Sci.* 21, 22. doi: 10.3390/ijms21228664

Oka, P., Parr, H., Barberio, B., Black, C., Savarino, E., and Ford A. (2020). Global prevalence of irritable bowel syndrome according to Rome III or IV criteria: a systematic review and meta-analysis. *Lancet Gastroenterol.* 5, 10. doi: 10.1016/S2468-1253(20)30217-X

Ott, S., Waetzig, G., Rehman, A., Moltzau-Anderson, J., Bharti, R., Grasis, J., et al. (2017). Efficacy of sterile fecal filtrate transfer for treating patients with *Clostridium difficile* infection. *Gastroenterology* 152, 4. doi: 10.1053/j.gastro.2016.11.010

Pinn, D. M., Aroniadis, O. C., and Brandt L J. (2014). Is fecal microbiota transplantation the answer for irritable bowel syndrome? A single-center experience. *Am. J. Gastroenterol.* 109, 11. doi: 10.1038/ajg.2014.295

Shaidullov, I. F., Sorokina, D. M., Sitdikov, F. G., Hermann, A., Abdulkhakov, S. R, and Sitdikova G F. (2021). Short chain fatty acids and colon motility in a mouse model of irritable bowel syndrome. *BMC Gastroenterol.* 21, 1. doi: 10.1186/s12876-021-01613-y

Shang, J. J., Yuan, J. Y., Xu, H., Tang, R. Z., Dong, Y. B., and Xie J. Q. (2013). Shugan-decoction relieves visceral hyperalgesia and reduces TRPV1 and SP colon expression. *World J. Gastroenterol.* 19, 44. doi: 10.3748/wjg.v19.i44.8071

Sun, Q., Jia, Q., Song, L., and Duan, L. (2019). Alterations in fecal short-chain fatty acids in patients with irritable bowel syndrome: a systematic review and meta-analysis. *Medicine* 98, 7. doi: 10.1097/MD.0000000000014513

Vahora, I. S., Tsouklidis, N., Kumar, R., Soni, R., and Khan, S. (2020). How serotonin level fluctuation affects the effectiveness of treatment in irritable bowel *syndrome*. *Cureus* 12, 8. doi: 10.7759/cureus.9871

Wang, Y., Dong, Y., Wang, E., Meng, Y., Bi, Z., Sun, S., et al. (2020). Shugan decoction alleviates colonic dysmotility in female SERT-knockout rats by decreasing, M_3 receptor expression. *Front. Pharmacol.* 11, 01082. doi: 10.3389/fphar.2020.01082

Wei, W., Wang, H. F., Zhang, Y., Zhang, Y. L., Niu, B. Y., and Yao, S. K. (2020). Altered metabolism of bile acids correlates with clinical parameters and the gut microbiota in patients with diarrhea-predominant irritable bowel syndrome. *World J. Gastroenterol.* 26, 45. doi: 10.3748/wjg.v26.i45.7153

Yang, M., Fukui, H., Eda, H., Kitayama, Y., Hara, K., Kodani, M., et al. (2017). Involvement of gut microbiota in the association between gastrointestinal motility and 5HT expression/M2 macrophage abundance in the gastrointestinal tract. *Mol. Med. Rep.* 16, 3. doi: 10.3892/mmr.2017.6955

Yano, J. M., Yu, K., Donaldson, G. P., Shastri, G. G., Ann, P., Ma, L., et al. (2015). Indigenous bacteria from the gut microbiota regulate host serotonin biosynthesis. *Cell* 161, 2. doi: 10.1016/j.cell.2015.02.047

frontiers | Frontiers in Microbiology

TYPE Original Research
PUBLISHED 17 November 2022
DOI 10.3389/fmicb.2022.1051653

OPEN ACCESS

EDITED BY
Na Li,
Hainan Medical University,
China

REVIEWED BY
Weida Liu,
Chinese Academy of Medical Sciences and Peking Union Medical College, China
Jian Han,
Lanzhou University,
China
Huaiqiu Huang,
Third Affiliated Hospital of Sun Yat-sen University, China

*CORRESPONDENCE
Zhiqi Song
songzhiqi@dmu.edu.cn
Li Wang
wli99@jlu.edu.cn

SPECIALTY SECTION
This article was submitted to Infectious Agents and Disease, a section of the journal Frontiers in Microbiology

RECEIVED 23 September 2022
ACCEPTED 18 October 2022
PUBLISHED 17 November 2022

CITATION
Liu C, He D, Yu A, Deng Y, Wang L and Song Z (2022) Correlation analysis between gut microbiota characteristics and melasma.
Front. Microbiol. 13:1051653.
doi: 10.3389/fmicb.2022.1051653

Correlation analysis between gut microbiota characteristics and melasma

Cong Liu[1], Dan He[2], Anye Yu[1], Yaru Deng[1], Li Wang[2]* and Zhiqi Song[1]*

[1]Department of Dermatology, First Affiliated Hospital of Dalian Medical University, Dalian, China, [2]Department of Pathogenobiology, Jilin University Mycology Research Center, Key Laboratory of Zoonosis Research, Ministry of Education, College of Basic Medical Sciences, Jilin University, Changchun, China

In recent years, many studies have shown that the gut microbiota can affect the occurrence and development of a variety of human diseases. A variety of skin diseases are related to the regulation of the gut–skin axis, such as psoriasis, atopic dermatitis, and acne. Gut microbial dysbiosis can promote the development of these diseases. The gut microbiota can affect estrogen metabolism, β-glucuronidase secreted by the gut microbiota can promote the reabsorption of estrogen by the gut, and estrogen is transported to other parts of the body through the circulatory system. The occurrence and development of melasma are closely related to abnormal metabolism of estrogen. The relationship between the structure of the gut microbiota and melasma remains unclear. Epidemiological surveys were conducted in patients with melasma and healthy subjects (control group) in this study. The feces were collected for 16S rRNA sequencing analysis of the gut microbiota. To compare the similarities and differences in species diversity of the gut microbiota between these two groups, we calculated the α-diversity and β-diversity indices and analyzed the differences between them. We found that the abundance of *Collinsella* spp., *Actinomyces* spp. (belonging to Actinobacteria), *Parabacteroides* spp., *Bacteroides* spp., *Paraprevotella* spp. (belonging to Bacteroidetes), *Blautia* spp., and *Roseburia* spp. (belonging to Firmicutes) in the melasma group were significantly different compared with that in the healthy group. The largest difference was found in Actinobacteria ($p<0.05$), and there were also significant differences in the abundance of Coriobacteriia, Actinobacteria, Coriobacteriales, Coriobacteriaceae, and *Collinsella* spp. between the two groups (all $p<0.05$). Many of these differences in the microbiota were closely related to the production of β-glucuronidase and the regulation of estrogen synthesis or metabolism. Changes in the gut microbiota structure and the biological effects of *Collinsella* spp. in the microbiota in patients with melasma can play an important role in the occurrence and development of melasma by affecting the body's estrogen metabolism. This study provides a theoretical basis and experimental data reference for future studies on the relationship between the gut microbiota and melasma, and may be helpful for the prevention and treatment of melasma.

KEYWORDS

melasma, gut microbiota, *Collinsella* spp., estrogen metabolism, β-glucuronidase

Introduction

The gut microbiota is the largest and most complex micro-ecosystem in the human body, and it has metabolic functions that the rest of the body does not possess. In recent years, investigation of the effect of the gut microbiota on human health has received widespread attention. Numerous studies have shown that the gut microbiota is closely related to multiple systems in the human body (Adak and Khan, 2019; Qi et al., 2021). With regard to the gut microbiota and skin diseases, previous studies mainly focused on inflammatory skin diseases, such as psoriasis, atopic dermatitis, and acne (De Pessemier et al., 2021). At present, only the relationship between gut microbial dysbiosis and vitiligo has been preliminarily discussed (Ni et al., 2020). There have been few studies on non-inflammatory skin diseases, especially pigmented dermatosis.

At present, an increasing number of studies are actively examining the relationship between the gut microbiota and skin diseases, which has led to the concept of the gut–skin axis. The gut–skin axis links the gut microbiota to skin diseases through the gut barrier, inflammatory mediators, and metabolites (De Pessemier et al., 2021). How the gut microbiota affects skin diseases by regulating the gut–skin axis has become a hot topic of research. Previous studies have shown a bidirectional connection between the gut microbiota and skin homeostasis, gut microbial dysbiosis plays a special role in the pathophysiological process of the occurrence and development of a variety of inflammatory diseases. These diseases can promote the development of psoriasis, atopic dermatitis, acne, and others (Shah et al., 2013; Thrash et al., 2013; Salem et al., 2018). Additionally, the consumption of probiotics or live bacteria that benefit the gastrointestinal system may also prevent and control the occurrence of these skin diseases (Salem et al., 2018; De Pessemier et al., 2021).

Melasma is a stubborn pigmented dermatosis that is difficult to treat and easy to relapse after treatment, and it is a non-inflammatory skin disease. Melasma is more common in women than in men and can occur from puberty to menopause. The occurrence and development of melasma are closely related to estrogen concentrations (Lee, 2015; Filoni et al., 2019). Studies suggested the gut microbiota can affect estrogen metabolism (Plottel and Blaser, 2011; Flores et al., 2012a; Qi et al., 2021). The β-glucuronidase secreted by certain gut microbiota can deconjugate metabolized estrogen and phytoestrogen and promote their reabsorption by the gut. Estrogen is transported to distal parts of the body through the circulatory system, such as the skin and vagina (Baker et al., 2017). Previous studies demonstrated that the expression of estrogen receptors in skin lesions in patients with melasma is upregulated, estrogen then binds to the relevant estrogen receptors and affects the formation of melasma (Lieberman and Moy, 2008; Lee, 2015; Baker et al., 2017).

At present, the relationship between the gut microbiota and melasma is unclear. This study aimed to investigate the characteristics of the gut microbiota in patients with melasma and to examine the relationship between the gut microbiota and melasma to provide an experimental basis and theoretical support for the prevention and treatment of melasma.

Materials and methods

Subjects

In this study, we recruited 30 patients with melasma and 30 healthy people as controls in the First Affiliated Hospital of Dalian Medical University. All participants were from Dalian (Liaoning Province, China). We used questionnaires to collect information of the participants, such as age, sex, body mass index, marital and fertility status, menstrual status, bowel habits, sunscreen habits, dietary habits and disease conditions. The non-pregnant, non-menstruating women were retained as study participants. None of them had a history of taking special medications such as birth control pills. The clinical type of skin lesions in the patients was zygomatic. Then excluding those who had received systemic antibiotic treatment within 3 months before fecal samples were collected, and people with diseases which related to estrogen or gut microbial dysbiosis (e.g., gynecological, digestive and immune diseases). Finally, 7 patients with melasma and 10 healthy people as controls were retained. All patients with melasma were assessed by the modified Melasma Area and Severity Index (mMASI; Pandya et al., 2011) and examined by dermatologists. This study was approved by the Ethics Committee of the First Affiliated Hospital of Dalian Medical University, and all participants signed informed consent forms.

Collection of fecal samples and DNA extraction

In all participants, fresh fecal samples were collected by fecal microbial DNA collection and preservation kits (TinyGene, Shanghai, China). All consumables were aseptic, and fecal samples were frozen and stored at −80°C after collection. Subsequently, the genomic DNA of samples was extracted by the QIAamp DNA Stool Mini Kit (Qiagen, Hilden, Germany).

16S rRNA amplification and sequencing

The sequences in the V4-V5 region of 16S rRNA were selected, and pair-end sequencing was performed in accordance with the requirements of Illumina Miseq high-throughput sequencing. After the target region and fusion primers were designed, two-step polymerase chain reaction (PCR) amplification was performed. The PCR product was recovered by using the AxyPrepDNA gel recovery kit (Axygen Scientific Inc., Silicon Valley, United States). Real-time fluorescence quantification was performed using an

FTC-3000TM real-time PCR system (Funglyn, Shanghai, China). The PCR products from different samples were indexed and mixed at equal ratios, to complete the construction of an Miseq library. Then used for high-throughput sequencing and bioinformatics analysis.

Microbiome analysis and statistical analysis

We distributed the sample reads from the raw data obtained by sequencing through a barcode to obtain the effective sequence of samples. After low-quality sequences at the ends were removed by Trimmomatic,[1] Flash software[2] was used to merge the paired reads into a sequence according to the overlap relationship between PE (Pair-end) reads. Additionally, Mothur software[3] was used for quality control and filtering to obtain an optimized sequence. Subsequently, operational taxonomic unit (OTU) clustering was performed by UPARSE software[4] under a similarity of 97%. Additionally, the chimera generated by PCR amplification was removed by UCHIME software, and the singleton OTUs were removed. The OTU representative sequence was compared using Mothur and the Silva 128 database, and species information was annotated. A statistical analysis of community structure was conducted at different classification levels.

We then conducted α-diversity and β-diversity analysis using Mothur. For α-diversity analysis, Chao, ACE, Shannon, and Simpson index values under different random sampling were calculated, and the non-parametric Wilcox test was used to analyze differences. For β-diversity analysis, Bray–Curtis analysis based on OTUs and species information was used, and ANOSIM was used to analyze differences. We plotted curve charts, box plots, sample clustering tree and histogram combination analysis diagram, and histograms of species distribution by using R language.

To identify differences in abundance in the gut microbiota between patients with melasma and controls, we used the t-test, the Wilcoxon non-parametric test, matastats (differentially abundant features analysis), and the linear discriminant analysis (LDA) effect size method. According to the obtained OUT or community abundance data, rigorous statistical methods were used for comparative analysis. The t-test and the Wilcoxon non-parametric test were adopted in the ggpubr package in R language. Matastats analysis used the metastas command in Mothur. In LEfSe analysis, a $p < 0.05$ (Kruskal–Wallis test) and log10[LDA] ≥ 2.0 were considered to indicate a significant difference in microorganisms.

1 http://www.usadellab.org/cms/index.php?page=trimmomatic
2 http://ccb.jhu.edu/software/FLASH/index.shtml
3 http://mothur.org/
4 https://drive5.com/usearch/manual8.1/uparse_pipeline.html

Results

General information and epidemiological survey statistics

We collected fecal samples from patients in the melasma group (Group M, age: 39.57 ± 7.76 years) and healthy subjects in the control group (Group B, age: 36.4 ± 6.29 years). The mean mMASI score was 3.32 ± 1.15. There were significant differences in dietary habits between the two groups ($p < 0.05$). Different from the healthy people, the patients with melasma had a harmful habit of a high-fat diet. Details of the participants are shown in Table 1.

Characteristics of the gut microbiota in patients with melasma

To compare the similarities and differences in species diversity of the gut microbiota between the two groups, we calculated the α-diversity index and analyzed the differences between them. We found that there was no significant difference in α-diversity between the two groups ($p = 0.41$). This lack of finding suggested that there was no significant difference in species diversity of the gut bacteria between the two groups (Figures 1, 2).

To compare differences in species diversity between Group M and Group B (comparison of the similarity between samples), we conducted β-diversity analysis. A sample clustering tree and histogram combination analysis diagram (Figure 3) showed obvious convergence of samples in Group M and Group B, and samples that had similar β-diversity were clustered together. This finding suggested that there was a difference in the gut microbiota between the two groups, and the gut microbiota in Group M showed obvious similarities.

A sample community structure histogram (Figure 3) and species distribution histogram (Figures 4, 5) show the relative abundance of different bacteria. We found that, at the phylum level, the highest abundance was Bacteroidetes, followed by Firmicutes, Proteobacteria, Tenericutes, Actinobacteria in the two groups. At the species level, the overall abundance of *Bacteroides* spp., such as *B. vulgatus*, *B. plebeius*, *B. coprocola* (belonging to

TABLE 1 Characteristics of patients with melasma and controls.

	Group M	Group B	*p* value
Age (years)	39.57 ± 7.76	36.4 ± 6.29	0.391
BMI	22.31 ± 2.69	21.57 ± 1.60	0.539
Dietary Habits*			
Greasy	3.29 ± 0.76	2.2 ± 1.03	0.024
Light	2.14 ± 0.38	3.1 ± 0.99	0.017
Yogurt/Probiotics	2.14 ± 0.69	2.9 ± 0.88	0.065
Meat	3.57 ± 0.98	2.4 ± 0.97	0.029
Vegetables	2.14 ± 0.69	3.1 ± 0.88	0.024
mMASI	3.32 ± 1.15		

*Dietary Habits: Preference of food, rated 1 to 5.

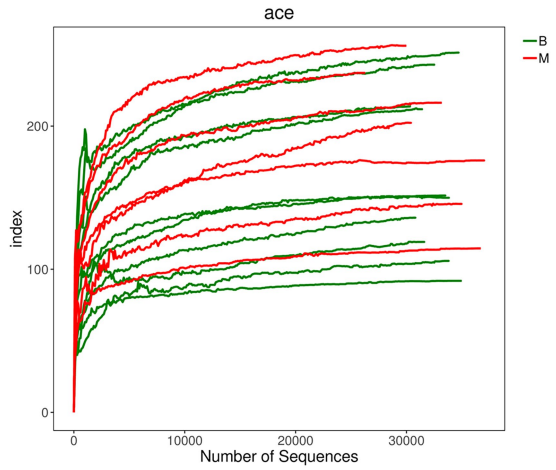

FIGURE 1
Comparison of α-diversity between Group M and Group B. ACE index dilution curve chart. There was no significant difference in α-diversity between the two groups.

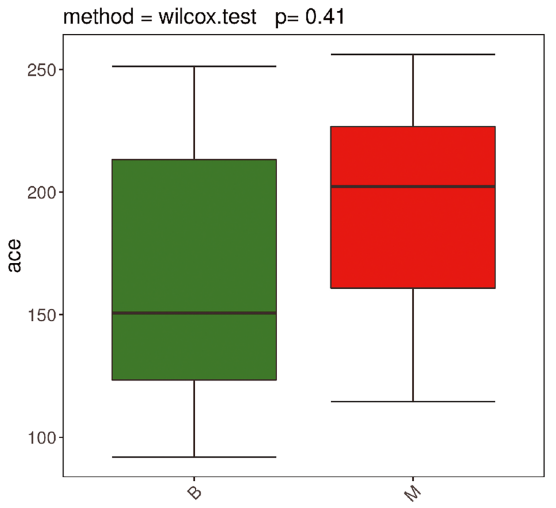

FIGURE 2
Comparison of α-diversity between Group M and Group B. ACE index non-parametric Wilcox test box plot (p=0.41). There was no significant difference in α-diversity between the two groups.

Bacteroidetes) in the gut bacteria in Group M was different from that in Group B. The results of α-diversity and β-diversity analyses suggested that although the gut microbiota in Group M was not significantly different from that in Group B, the abundance of part of the microbiota was different. Additionally, these microbial strains and their biological function would be a priority for investigation.

We further investigated the differences in abundance in the gut microbiota between the groups. Significant differences ($p < 0.05$) that were found under each classification level (phyla, class, order, family, genus, species, and OTU). LDA effect size analysis showed that some microbiota showed a significant difference in abundance between the two groups. The significant differences and biological relevance of microbial strains between the two groups are displayed in a clustering tree (Figure 6). Some microbial strains in the gut microbiota in Group M that showed significant differences from those in the gut microbiota in Group B are shown in Tables 2, 3.

Notably, at the phylum level, the abundance of Actinobacteria in Group M was significantly lower than that in Group B ($p < 0.05$). There were also significant differences in the abundance of Coriobacteriia, Actinobacteria, Coriobacteriales, Coriobacteriaceae, and *Collinsella* spp. between the two groups (all $p < 0.05$). These findings suggested that the differential microbiota between patients with melasma and healthy subjects, and may play an important role in the occurrence of melasma. Additionally, the abundance of Bacteroidetes, Firmicutes, and Proteobacteria was different in some microbial strains between the two groups. There were also significant differences in the abundance of Tenericutes, Mollicutes, Deltaproteobacteria, Desulfovibrionales, Desulfovibrionaceae, *Terrisporobacter* spp., *Holdemanella* spp., *Parasutterella* spp. between the two groups. This finding suggested that these genera may play a co-regulatory role in the occurrence and development of melasma (Table 3; Figure 6).

Discussion

The gut microbiota, which has recently received a lot of attention, is related to inflammatory skin diseases (De Pessemier et al., 2021). However, there have been limited studies on the gut microbiota and pigmented dermatosis (Ni et al., 2020), and no studies on melasma have been reported.

The gut microbiota secretes β-glucuronidase to dissociate estrogen in the early stage, promotes its reabsorption of estrogen into the blood through the intestines, and transports estrogen to distal parts of the body to bind with the estrogen receptor to take effect. Therefore, the gut microbiota affects the metabolism of human estrogen. In this process, the gut microbiota and estrogen act on the distal effector sites through circulatory metabolism (Baker et al., 2017; De Pessemier et al., 2021). Studies have shown that estrogen concentrations in patients with melasma are abnormal compared with those in the healthy population (Pérez et al., 1983; Lee, 2015). Additionally, the expression of estrogen receptors in skin lesions in patients with melasma is upregulated (Lieberman and Moy, 2008; Lee, 2015), which further confirms the role of estrogen in this disease. Whether the gut microbiota in patients with melasma is different from that in the healthy population, whether there are some characteristic components of the microbiota, and whether these will affect the occurrence and development of melasma, are important issues that need to be examined.

In the healthy human intestines, the relative abundance of Bacteroidetes and Firmicutes accounts for more than 90% of the gut microbiota, and they play a major role in maintaining gut

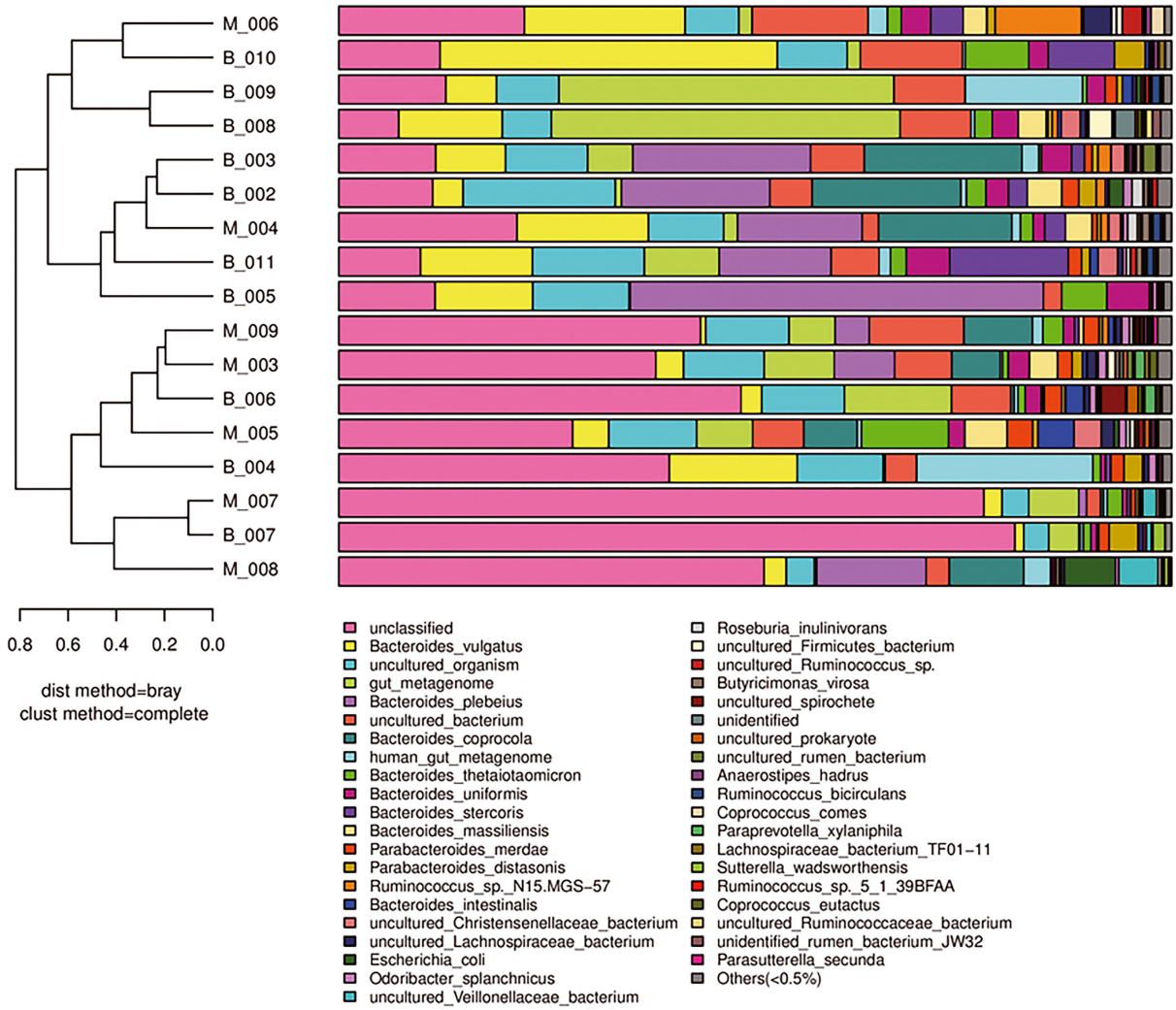

FIGURE 3
β-Diversity analysis of Group M and Group B. A sample clustering tree and histogram combination analysis diagram at the species level is shown. The left side shows a hierarchical clustering analysis between samples based on community composition. The two groups of samples show the phenomenon of convergence in the same group. The right side shows a histogram of a community structure of the corresponding samples.

homeostasis, while Proteobacteria and Actinobacteria only account for nearly 10% (Arumugam et al., 2011; Segata et al., 2012). Bacteroidetes, Firmicutes, Proteobacteria, and Actinobacteria constitute the four main phyla in the human gut microbiota (Arumugam et al., 2011; Segata et al., 2012). The abundance of Bacteroidetes, Firmicutes, Proteobacteria, and Actinobacteria in the intestines in patients with melasma was different from that in the healthy population, especially for Actinobacteria. Many of the differential microbiota are related to the metabolic regulation of estrogen in the body, indicating that they may play an important role in the occurrence of melasma.

Although Actinobacteria accounts for a small proportion of the gut microbiota, it showed the most significant difference in abundance between patients with melasma and healthy people. Actinobacteria also plays an important role in maintaining homeostasis of the gut environment (Binda et al., 2018). Moreover, its secondary metabolites are abundant, has important biological value, and it can produce naturally derived antibiotics, antifungals, anthelmintics, and anticancer compounds, which can be applied clinically (Barka et al., 2016). The most common Bifidobacteria in the Actinobacteria family is also a widely used probiotic (Binda et al., 2018). Our study showed that the abundance of Actinobacteria in patients with melasma was significantly lower than that in healthy people. There were also significant differences in the Coriobacteriia, Actinobacteria, Coriobacteriales, Coriobacteriaceae, and *Collinsella* spp. between the two groups. Actinobacteria can participate in the aerobic degradation of estrogen (Yu et al., 2013; Wu et al., 2019). Coriobacteriaceae has also been reported to be involved in the synthesis of the phytoestrogen S-equol. S-equol reduces the incidence of menopausal symptoms, osteoporosis, skin aging, hair loss, prostate cancer, and ovarian

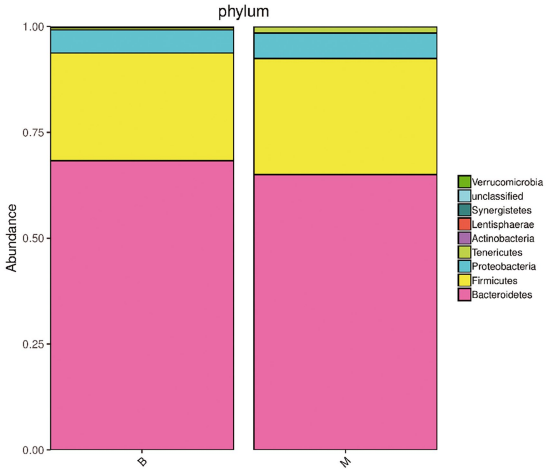

FIGURE 4
Histogram of species distribution of bacterial microbiota in Group M and Group B. Phylum level. The dominant bacteria in the gut microbiota of the two groups of samples were Bacteroidetes, Firmicutes, Proteobacteria, Tenericutes, and Actinobacteria, and their abundance was different between the two groups.

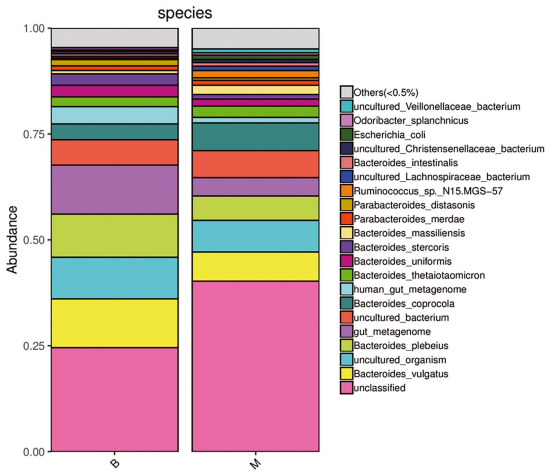

FIGURE 5
Histogram of species distribution of bacterial microbiota in Group M and Group B. Species level. Under the existing detection and identification methods, the microbial strain (pink) that could not be annotated in the gut microbiota in Group M was significantly higher than that in Group B. The overall abundance of the dominant bacterial microbiota such as *Bacteroides vulgatus* (yellow), *B. plebeius* (light green), *B. coprocola* (dark green) belonging to Bacteroidetes in Group M was also different from that in Group B.

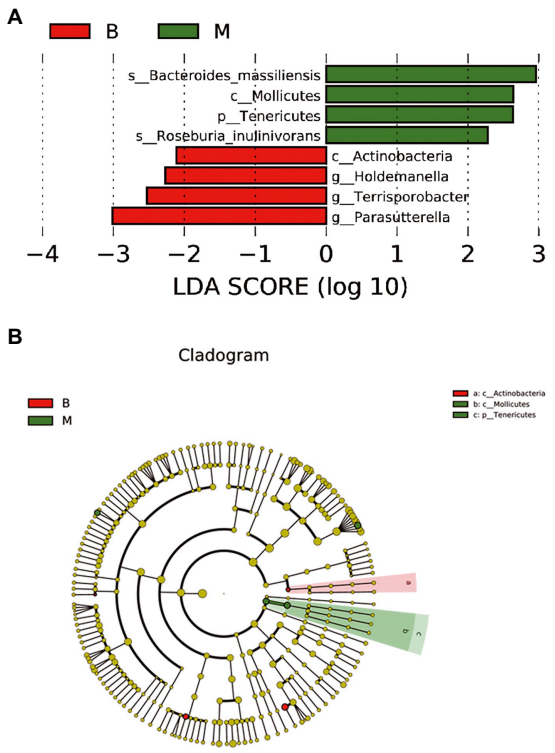

FIGURE 6
LDA effect size analysis between Group M and Group B. **(A)** Microbial species with a significant difference in abundance and a significant effect between the two groups. **(B)** A clustering tree. The concentric circles from the inside to the outside represent the classification levels of phylum, class, order, family, and genus (or species). The green and red nodes indicate microbial species that played an important role in groups M and B. The diameter of the node circle is proportional to the relative abundance of the taxonomic microbiota, which reflects a significant difference in microbial strains between the two groups and their biological correlation.

cancer by selectively activating estrogen receptors, and has a variety of biological and clinical uses (Lee et al., 2018).The findings suggest that the differential microbiota may play an important role in the occurrence of melasma as a characteristic part of the microbiota in these patients. A decrease in the abundance of Actinobacteria in the microbiota may affect estrogen concentrations of the body, and then affect the occurrence and development of melasma. This possibility could provide a new target for the prevention and treatment of melasma.

As dominant members of the microbiota with the highest proportion in the human gut, Bacteroidetes and Firmicutes are important for biological function. Studies have shown that Bacteroidetes degrades polysaccharides, and may promote inflammation and stimulate angiogenesis (Johnson et al., 2017). Firmicutes member Lactobacillus is also a common probiotic that helps the body absorb energy and fat (Jeong et al., 2017). Disorder of Bacteroidetes and Firmicutes are also been related to skin diseases such as psoriasis (Sikora et al., 2020). There have been reports that Clostridia (belonging to Firmicutes) affects estrogen concentrations in the body through β-glucuronidase. Moreover, estrogen can reverse changes in the microbiota, forming a two-way regulation (Flores et al., 2012a,b). In our study, we found that the abundance of Bacteroidetes and Firmicutes and *Bacteroides* spp. (belonging

TABLE 2 Summary of the abundance of microbial strains at different species levels between Group M and Group B.

OTU ID	Phylum	Class	Order	Family	Genus
97	Actinobacteria	Coriobacteriia	Coriobacteriales	Coriobacteriaceae	*Collinsella*
275	Actinobacteria	Coriobacteriia	Coriobacteriales	Coriobacteriaceae	
303	Actinobacteria	Actinobacteria	Actinomycetales	Actinomycetaceae	*Actinomyces*
39	Bacteroidetes	Bacteroidia	Bacteroidales	Porphyromonadaceae	*Parabacteroides*
388	Bacteroidetes	Bacteroidia	Bacteroidales	Bacteroidaceae	*Bacteroides*
11	Bacteroidetes	Bacteroidia	Bacteroidales	Bacteroidaceae	*Bacteroides*
170	Bacteroidetes	Bacteroidia	Bacteroidales	Bacteroidaceae	*Bacteroides*
120	Bacteroidetes	Bacteroidia	Bacteroidales	Prevotellaceae	*Paraprevotella*
47	Firmicutes	Clostridia	Clostridiales	Lachnospiraceae	
130	Firmicutes	Clostridia	Clostridiales	Lachnospiraceae	
179	Firmicutes	Clostridia	Clostridiales	Lachnospiraceae	*Blautia*
228	Firmicutes	Clostridia	Clostridiales	Lachnospiraceae	
79	Firmicutes	Clostridia	Clostridiales	Lachnospiraceae	
36	Firmicutes	Clostridia	Clostridiales	Lachnospiraceae	
60	Firmicutes	Clostridia	Clostridiales	Lachnospiraceae	*Roseburia*
410	Firmicutes	Clostridia	Clostridiales	Ruminococcaceae	
127	Firmicutes	Clostridia	Clostridiales	Ruminococcaceae	*Ruminiclostridium*
334	Firmicutes	Clostridia	Clostridiales	Ruminococcaceae	
381	Firmicutes	Clostridia	Clostridiales	Ruminococcaceae	
391	Firmicutes	Clostridia	Clostridiales	Ruminococcaceae	
139	Firmicutes	Clostridia	Clostridiales	Ruminococcaceae	
224	Firmicutes	Clostridia	Clostridiales	Peptostreptococcaceae	*Intestinibacter*
336	Firmicutes	Clostridia	Clostridiales	Peptostreptococcaceae	*Terrisporobacter*
403	Firmicutes	Clostridia	Clostridiales	Peptococcaceae	
370	Firmicutes	Clostridia	Clostridiales		
375	Firmicutes	Erysipelotrichia	Erysipelotrichales	Erysipelotrichaceae	
62	Firmicutes	Erysipelotrichia	Erysipelotrichales	Erysipelotrichaceae	*Holdemanella*
16	Proteobacteria	Betaproteobacteria	Burkholderiales	Alcaligenaceae	*Parasutterella*
117	Tenericutes	Mollicutes			

to Bacteroidetes), Clostridia and *Blautia* spp. (belonging to Firmicutes) were different between patients with melasma and healthy people. They can regulate the secretion and activity of β-glucuronidase, thereby affecting the body's estrogen concentrations (Gloux et al., 2011; Flores et al., 2012a; Pellock et al., 2018; Creekmore et al., 2019; Dai et al., 2019; Ibrahim et al., 2019; Zhang et al., 2019). These results indicate that the differential microbiota may play a co-regulatory role in the occurrence and development of melasma.

In addition, we conducted an epidemiological study on patients with melasma, and found that these patients, unlike healthy people, had a bad habit of a high-fat diet. Studies have shown that different dietary patterns can affect the growth and reproduction of Actinobacteria, Bacteroidetes and Firmicutes (Brahe et al., 2015; Guo et al., 2017). In this study, we found gut microbial dysbiosis in patients with melasma, with a decrease in Actinobacteria and Bacteroidetes and an increase in Firmicutes, which may have been related to the patients' high-fat diet. This finding suggested that patients should improve their dietary habits or consume probiotics (e.g., Bifidobacterium, Lactobacillus) to regulate the gut microbiota (Gibson and Roberfroid, 1995; Menon et al., 2013). Adjustment of the ratios of Actinobacteria, Bacteroidetes, and Firmicutes in the human gut and improving the structure of the gut microbiota may be an auxiliary means to improve the patient's condition or prevent the occurrence of diseases.

In conclusion, the gut microbiota structure in patients with melasma is different to that of healthy people. The abundance of *Collinsella* spp., *Actinomyces* spp. (belonging to Actinobacteria), *Parabacteroides* spp., *Bacteroides* spp., *Paraprevotella* spp. (belonging to Bacteroidetes), *Blautia* spp., *Roseburia* spp. (belonging to Firmicutes), and that of other members of the microbiota are different from those of healthy people. In particular, *Collinsella* spp. is a characteristic member of the microbiota in patients with melasma. The biological effects of these differential microbiota play an important role in the occurrence and development of melasma by affecting estrogen metabolism. This study provides a theoretical basis and experimental data reference for future studies on the relationship between melasma and the gut microbiota. Add the gut–skin axis in the understanding of

TABLE 3 Microbial strains with significant differences at each classification level between Group M and Group B.

	Mean relative abudance (%)		Variance		*p* value
	Group M	Group B	Group M	Group B	
Phylum					
Actinobacteria	0.0552	0.1992	0	0.000004	0.0358
Class					
Deltaproteobacteria	0.0133	0.0379	0	0	0.027611
Coriobacteriia	0.0489	0.1711	0	0.000003	0.034333
Actinobacteria	0.00630	0.02810	0.000047	0.000345	0.036
Order					
Desulfovibrionales	0.0133	0.0379	0	0	0.02696
Coriobacteriales	0.0489	0.1711	0	0.000003	0.03124
Family					
Desulfovibrionaceae	0.0133	0.0379	0	0	0.029737
Coriobacteriaceae	0.0489	0.1711	0	0.000003	0.035368
Genus					
Parasutterella spp.	0.4602	2.3846	0.000054	0.000596	0.015688
Collinsella spp.	0.0237	0.1371	0	0.000003	0.03815
Terrisporobacter spp.	0	0.0021	0	0	0.046446
Holdemanella spp.	0.11706	0.33713	0.003371	0.000353	0.012

Species with a significant difference of $p < 0.05$ were selected.

melasma pathogenesis, may be helpful for the prevention and treatment of melasma.

Data availability statement

The data presented in the study are deposited in the NCBI's Gene Expression Omnibus repository, accession number GSE214430.

Ethics statement

The studies involving human participants were reviewed and approved by the Ethics Committee of the First Affiliated Hospital of Dalian Medical University. The patients/participants provided their written informed consent to participate in this study.

Author contributions

LW and ZS: conceptualization, design, and review and editing. CL, AY, and YD: collect the fecal samples and epidemiological survey. DH: data analysis. CL and DH: original manuscript. All authors contributed to the article and approved the submitted version.

Funding

This study was supported by grants from the National Natural Science Foundation of China (82073416).

Acknowledgments

We thank all members of our department for helpful discussions. We also thank Ellen Knapp, from LiwenBianji (Edanz; www.liwenbianji.cn/), for editing the English text of a draft of this manuscript.

Conflict of interest

The authors declare that the research was conducted in the absence of any commercial or financial relationships that could be construed as a potential conflict of interest.

Publisher's note

All claims expressed in this article are solely those of the authors and do not necessarily represent those of their affiliated organizations, or those of the publisher, the editors and the reviewers. Any product that may be evaluated in this article, or claim that may be made by its manufacturer, is not guaranteed or endorsed by the publisher.

References

Adak, A., and Khan, M. R. (2019). An insight into gut microbiota and its functionalities. *Cell. Mol. Life Sci.* 76, 473–493. doi: 10.1007/s00018-018-2943-4

Arumugam, M., Raes, J., Pelletier, E., Le Paslier, D., Yamada, T., Mende, D. R., et al. (2011). Enterotypes of the human gut microbiome. *Nature* 473, 174–180. doi: 10.1038/nature09944

Baker, J. M., Al-Nakkash, L., and Herbst-Kralovetz, M. M. (2017). Estrogen-gut microbiome axis: physiological and clinical implications. *Maturitas* 103, 45–53. doi: 10.1016/j.maturitas.2017.06.025

Barka, E. A., Vatsa, P., Sanchez, L., Gaveau-Vaillant, N., Jacquard, C., Meier-Kolthoff, J. P., et al. (2016). Taxonomy, physiology, and natural products of Actinobacteria. *Microbiol. Mol. Biol. Rev.* 80, 1–43. doi: 10.1128/MMBR.00019-15

Binda, C., Lopetuso, L. R., Rizzatti, G., Gibiino, G., Cennamo, V., and Gasbarrini, A. (2018). Actinobacteria: a relevant minority for the maintenance of gut homeostasis. *Dig. Liver Dis.* 50, 421–428. doi: 10.1016/j.dld.2018.02.012

Brahe, L. K., Le Chatelier, E., Prifti, E., Pons, N., Kennedy, S., Blædel, T., et al. (2015). Dietary modulation of the gut microbiota--a randomised controlled trial in obese postmenopausal women. *Br. J. Nutr.* 114, 406–417. doi: 10.1017/S0007114515001786

Creekmore, B. C., Gray, J. H., Walton, W. G., Biernat, K. A., Little, M. S., Xu, Y., et al. (2019). Mouse gut microbiome-encoded β-Glucuronidases identified using metagenome analysis guided by protein. *Structure* 4, e00452–e00419. doi: 10.1128/mSystems.00452-19

Dai, S., Pan, M., El-Nezami, H. S., Wan, J., Wang, M. F., Habimana, O., et al. (2019). Effects of lactic acid bacteria-fermented soymilk on Isoflavone metabolites and short-chain fatty acids excretion and their modulating effects on gut microbiota. *J. Food Sci.* 84, 1854–1863. doi: 10.1111/1750-3841.14661

De Pessemier, B., Grine, L., Debaere, M., Maes, A., Paetzold, B., and Callewaert, C. (2021). Gut-skin axis: current knowledge of the interrelationship between microbial dysbiosis and skin conditions. *Microorganisms* 9, 9:353. doi: 10.3390/microorganisms9020353

Filoni, A., Mariano, M., and Cameli, N. (2019). Melasma: how hormones can modulate skin pigmentation. *J. Cosmet. Dermatol.* 18, 458–463. doi: 10.1111/jocd.12877

Flores, R., Shi, J., Fuhrman, B., Xu, X., Veenstra, T. D., Gail, M. H., et al. (2012a). Fecal microbial determinants of fecal and systemic estrogens and estrogen metabolites: a cross-sectional study. *J. Transl. Med.* 10:253. doi: 10.1186/1479-5876-10-253

Flores, R., Shi, J., Gail, M. H., Gajer, P., Ravel, J., and Goedert, J. J. (2012b). Association of fecal microbial diversity and taxonomy with selected enzymatic functions. *PLoS One* 7:e39745. doi: 10.1371/journal.pone.0039745

Gibson, G. R., and Roberfroid, M. B. (1995). Dietary modulation of the human colonic microbiota: introducing the concept of prebiotics. *J. Nutr.* 125, 1401–1412. doi: 10.1093/jn/125.6.1401

Gloux, K., Berteau, O., El Oumami, H., Béguet, F., Leclerc, M., and Doré, J. (2011). A metagenomic β-glucuronidase uncovers a core adaptive function of the human intestinal microbiome. *Proc. Natl. Acad. Sci. U. S. A.* 108, 4539–4546. doi: 10.1073/pnas.1000066107

Guo, X., Li, J., Tang, R., Zhang, G., Zeng, H., Wood, R. J., et al. (2017). High fat diet alters gut microbiota and the expression of Paneth cell-antimicrobial peptides preceding changes of circulating inflammatory cytokines. *Mediat. Inflamm.* 2017, 9474896–9474899. doi: 10.1155/2017/9474896

Ibrahim, A., Hugerth, L. W., Hases, L., Saxena, A., Seifert, M., Thomas, Q., et al. (2019). Colitis-induced colorectal cancer and intestinal epithelial estrogen receptor beta impact gut microbiota diversity. *Int. J. Cancer* 144, 3086–3098. doi: 10.1002/ijc.32037

Jeong, S. Y., Kang, S., Hua, C. S., Ting, Z., and Park, S. (2017). Synbiotic effects of β-glucans from cauliflower mushroom and *lactobacillus fermentum* on metabolic changes and gut microbiome in estrogen-deficient rats. *Genes Nutr.* 12:31. doi: 10.1186/s12263-017-0585-z

Johnson, E. L., Heaver, S. L., Walters, W. A., and Ley, R. E. (2017). Microbiome and metabolic disease: revisiting the bacterial phylum Bacteroidetes. *J. Mol. Med.* 95, 1–8. doi: 10.1007/s00109-016-1492-2

Lee, A. Y. (2015). Recent progress in melasma pathogenesis. *Pigment Cell Melanoma Res.* 28, 648–660. doi: 10.1111/pcmr.12404

Lee, P. G., Lee, S. H., Kim, J., Kim, E. J., Choi, K. Y., and Kim, B. G. (2018). Polymeric solvent engineering for gram/liter scale production of a water-insoluble isoflavone derivative, (S)-equol. *Appl. Microbiol. Biotechnol.* 102, 6915–6921. doi: 10.1007/s00253-018-9137-8

Lieberman, R., and Moy, L. (2008). Estrogen receptor expression in melasma: results from facial skin of affected patients. *J. Drugs Dermatol.* 7, 463–465. PMID: 18505139

Menon, R., Watson, S. E., Thomas, L. N., Allred, C. D., Dabney, A., Azcarate-Peril, M. A., et al. (2013). Diet complexity and estrogen receptor β status affect the composition of the murine intestinal microbiota. *Appl. Environ. Microbiol.* 79, 5763–5773. doi: 10.1128/AEM.01182-13

Ni, Q., Ye, Z., Wang, Y., Chen, J., Zhang, W., Ma, C., et al. (2020). Gut microbial dysbiosis and plasma metabolic profile in individuals with vitiligo. *Front. Microbiol.* 11:592248. doi: 10.3389/fmicb.2020.592248

Pandya, A. G., Hynan, L. S., Bhore, R., Riley, F. C., Guevara, I. L., Grimes, P., et al. (2011). Reliability assessment and validation of the Melasma area and severity index (MASI) and a new modified MASI scoring method. *J. Am. Acad. Dermatol.* 64, 78–72. doi: 10.1016/j.jaad.2009.10.051

Pellock, S. J., Walton, W. G., Biernat, K. A., Torres-Rivera, D., Creekmore, B. C., Xu, Y., et al. (2018). Three structurally and functionally distinct β-glucuronidases from the human gut microbe Bacteroides uniformis. *J. Biol. Chem.* 293, 18559–18573. doi: 10.1074/jbc.RA118.005414

Pérez, M., Sánchez, J. L., and Aguiló, F. (1983). Endocrinologic profile of patients with idiopathic melasma. *J. Invest. Dermatol.* 81, 543–545. doi: 10.1111/1523-1747.ep12522896

Plottel, C. S., and Blaser, M. J. (2011). Microbiome and malignancy. *Cell Host Microbe* 10, 324–335. doi: 10.1016/j.chom.2011.10.003

Qi, X., Yun, C., Pang, Y., and Qiao, J. (2021). The impact of the gut microbiota on the reproductive and metabolic endocrine system. *Gut Microbes* 13, 1–21. doi: 10.1080/19490976.2021.1894070

Salem, I., Ramser, A., Isham, N., and Ghannoum, M. A. (2018). The gut microbiome as a major regulator of the gut-skin Axis. *Front. Microbiol.* 9:1459. doi: 10.3389/fmicb.2018.01459

Segata, N., Haake, S. K., Mannon, P., Lemon, K. P., Waldron, L., Gevers, D., et al. (2012). Composition of the adult digestive tract bacterial microbiome based on seven mouth surfaces, tonsils, throat and stool samples. *Genome Biol.* 13:R42. doi: 10.1186/gb-2012-13-6-r42

Shah, K. R., Boland, C. R., Patel, M., Thrash, B., and Menter, A. (2013). Cutaneous manifestations of gastrointestinal disease: part I. *J. Am. Acad. Dermatol.* 68, e1–e21. doi: 10.1016/j.jaad.2012.10.037

Sikora, M., Stec, A., Chrabaszcz, M., Knot, A., Waskiel-Burnat, A., Rakowska, A., et al. (2020). Gut microbiome in psoriasis: an updated review. *Pathogens* 9:463. doi: 10.3390/pathogens9060463

Thrash, B., Patel, M., Shah, K. R., Boland, C. R., and Menter, A. (2013). Cutaneous manifestations of gastrointestinal disease: part II. *J. Am. Acad. Dermatol.* 68:211.e1-33; quiz 244-246. doi: 10.1016/j.jaad.2012.10.036

Wu, K., Lee, T. H., Chen, Y. L., Wang, Y. S., Wang, P. H., Yu, C. P., et al. (2019). Metabolites involved in aerobic degradation of the a and B rings of estrogen. *Appl. Environ. Microbiol.* 85, e02223–e02218. doi: 10.1128/AEM.02223-18

Yu, C. P., Deeb, R. A., and Chu, K. H. (2013). Microbial degradation of steroidal estrogens. *Chemosphere* 91, 1225–1235. doi: 10.1016/j.chemosphere.2013.01.112

Zhang, J., Lacroix, C., Wortmann, E., Ruscheweyh, H. J., Sunagawa, S., Sturla, S. J., et al. (2019). Gut microbial beta-glucuronidase and glycerol/diol dehydratase activity contribute to dietary heterocyclic amine biotransformation. *BMC Microbiol.* 19:99. doi: 10.1186/s12866-019-1483-x

frontiers | Frontiers in Microbiology

TYPE Original Research
PUBLISHED 28 November 2022
DOI 10.3389/fmicb.2022.1050637

OPEN ACCESS

EDITED BY
Na Li,
Hainan Medical University,
China

REVIEWED BY
Duc-Cuong Bui,
University of Texas Medical Branch at Galveston, United States
Yong Zhang,
University of Massachusetts Amherst, United States

*CORRESPONDENCE
Li Wang
wli99@jlu.edu.cn

SPECIALTY SECTION
This article was submitted to Infectious Agents and Disease, a section of the journal Frontiers in Microbiology

RECEIVED 22 September 2022
ACCEPTED 04 November 2022
PUBLISHED 28 November 2022

CITATION
Zhao B, He D, Gao S, Zhang Y and Wang L (2022) Hypothetical protein FoDbp40 influences the growth and virulence of *Fusarium oxysporum* by regulating the expression of isocitrate lyase. *Front. Microbiol.* 13:1050637. doi: 10.3389/fmicb.2022.1050637

Hypothetical protein FoDbp40 influences the growth and virulence of *Fusarium oxysporum* by regulating the expression of isocitrate lyase

Busi Zhao[1], Dan He[1], Song Gao[2], Yan Zhang[1] and Li Wang[1]*

[1]Department of Pathogenobiology, Jilin University Mycology Research Center, Key Laboratory of Zoonosis Research, Ministry of Education, College of Basic Medical Sciences, Jilin University, Changchun, China, [2]Beijing ZhongKaiTianCheng Bio-technology Co. Ltd., Beijing, China

Fungal growth is closely related to virulence. Finding the key genes and pathways that regulate growth can help elucidate the regulatory mechanisms of fungal growth and virulence in efforts to locate new drug targets. *Fusarium oxysporum* is an important plant pathogen and human opportunistic pathogen that has research value in agricultural and medicinal fields. A mutant of *F. oxysporum* with reduced growth was obtained by *Agrobacterium tumefaciens*-mediated transformation, the transferred DNA (T-DNA) interrupted gene in this mutant coded a hypothetical protein that we named FoDbp40. FoDbp40 has an unknown function, but we chose to explore its possible functions as it may play a role in fungal growth regulatory mechanisms. Results showed that *F. oxysporum* growth and virulence decreased after FoDbp40 deletion. FOXG_05529 (NCBI Gene ID, isocitrate lyase, ICL) was identified as a key gene that involved in the reduced growth of this mutant. Deletion of FoDbp40 results in a decrease of more than 80% in ICL expression and activity, succinate level, and energy level, plus a decrease in phosphorylated mammalian target of rapamycin level and an increase in phosphorylated 5′-adenosine monophosphate activated protein kinase level. In summary, our study found that the FoDbp40 regulates the expression of ICL at a transcriptional level and affects energy levels and downstream related pathways, thereby regulating the growth and virulence of *F. oxysporum*.

KEYWORDS

***Fusarium oxysporum*, CCCH-type zinc finger, ICL, growth, AMPK/mTOR**

Introduction

Fusarium species belong to a large genus of filamentous fungi which can infect plants and humans. In 2022, *Fusarium* species were incorporated in High Priority Group of the WHO fungal priority pathogens list (WHO, 2022). *Fusarium oxysporum* can infect cotton, rice, wheat, and other crops, causing diseases including cotton wilt, crown rot in cereal

crops, and head blight in wheat. The fungus seriously affects food safety and causes huge economic loss (Kazan and Gardiner, 2018; Melotto et al., 2020; Zhu et al., 2021). *Fusarium* species are also important opportunistic pathogens in humans, mainly causing corneal infection (keratitis; Alkatan and Al-Essa, 2019), but it can also cause invasive and disseminated infection in immunocompromised people, posing threats to human health (Nucci and Anaissie, 2007; Muraosa et al., 2017).

Fungi virulence is closely related to growth. The cell wall is an essential structure for fungal growth, and some components of cell wall, such as β-1,3-glucans, can participate in activating host immune response and affect virulence in *Aspergillus fumigatus* (Chotirmall et al., 2014). In *Cryptococcus neoformans*, a microtubule-associated CAP-glycine protein (Cgp1) can promote the production of capsules, thereby enhancing virulence (Wang et al., 2018). In *Aspergillus fumigatus*, *Beauveria bassiana*, and *Fusarium graminearum*, strains with slowed growth and sporulation were found to have lower virulence (Paisley et al., 2005; Safavi et al., 2007; Wang et al., 2021). Therefore, studying and finding key regulatory factors, mechanisms, and pathways that regulate fungal growth is crucial to understanding the fungal growth profile, finding new drug targets, and fungal prevention and control methodologies.

Hypothetical proteins are proteins predicted to be expressed from an open reading frame, but with unknown function. Presently, scores of hypothetical proteins exist in the genomes of various animals, plants, fungi, and microorganisms, potentially involving diverse biological processes, including gene expression and protein folding, as well as various life functions, such as host-pathogen interactions and drug tolerance (Wang et al., 2012; Uddin et al., 2019; Pranavathiyani et al., 2020). Hypothetical proteins that regulate growth and virulence have been found in the bacteria *Chlamydia trachomatis* and fungi *Magnaporthe grisea*, among many others (Chen et al., 2006; Lin et al., 2021).

The glyoxylate metabolism pathway is an anabolic variation of the TCA cycle that occurs in most other organisms and converts isocitrate to glyoxylate and succinate. It plays an important role in the growth, pathogenesis, and stress tolerance of fungi such as yeast and *Fusarium* species (Park et al., 2016; Vico et al., 2021). ICL is a key enzyme in the glyoxylate metabolism pathway, responsible for catalyzing the synthesis of succinate, thereby regulating carbon metabolism and ATP synthesis (Gengenbacher et al., 2010; Selinski and Scheibe, 2014). ICL is not present in human and is, therefore, a potential therapeutic target against fungal infection (Bhusal et al., 2017).

Nucleic acid-binding proteins can bind to specific sequences of DNA or RNA and are involved in the transcriptional regulation of cellular processes, such as DNA damage repair and gene expression (Andres et al., 2019; Bartas et al., 2021). Zinc finger proteins are the most abundant class of transcription factors in eukaryotic genomes. These proteins can bind to DNA or RNA, even protein to regulate transcription and play an important role in many life processes (Corkins et al., 2013; Zou et al., 2018). According to protein sequence, fold, and function, zinc finger proteins can be divided into over 20 primary types, such as C_2H_2, CCHC, CCCH and so on. Current research mainly focuses on C_2H_2 type zinc finger proteins (Interpro IPR036236), which have the zinc ion coordinated by two cysteine and two histidine residues. CCCH-type zinc finger proteins have a zinc ion coordinated by three cysteines and a single histidine (C-x8-C-x5-C-x3-H; Interpro IPR036855) and account for about 0.8% of zinc finger proteins (Berg and Shi, 1996), but have seldom been reported in fungi. CCCH zinc finger proteins are known as RNA-binding proteins and associated with post-transcriptional regulation of mRNA (Fu and Blackshear, 2017). In addition to its role in RNA metabolism, recent studies demonstrated that CCCH zinc finger proteins also modulate transcription (Zou et al., 2018; Wang et al., 2022). A RNA-binding CCCH zinc finger protein Zc3h10 was also proved to activate UCP1 promoter by binding to a distal upstream region (Yi et al., 2019).

In this study, a mutant of *F. oxysporum* with reduced growth was obtained by *Agrobacterium tumefaciens*-mediated transformation (ATMT), in which the expression of main genes involved in glyoxylate metabolism pathway were down-regulated. The T-DNA interrupted gene FOXG_12762 encodes a hypothetical protein containing CCCH-type zinc finger--FoDbp40 [Fo for *F. oxysporum*, Dbp for DNA binding protein, 40 (kDa) for the calculated molecular mass]. The regulation of the expression of ICL by FoDbp40 was elucidated, and the influence of FoDbp40 on the growth and virulence of *F. oxysporum* was discussed.

Materials and methods

Construction of random insertion *Fusarium oxysporum* mutants

Wild type *F. oxysporum* JLCC31768 and *Agrobacterium tumefaciens* AgrN (containing plasmid pXEN carrying neomycin and kanamycin resistance tags[*neo*]) were used to generate *F. oxysporum* mutants (He et al., 2021). Wild type and AgrN (Table 1) were preserved at and obtained from the Jilin University Mycology Research Center (Jilin, China).

ATMT of *F. oxysporum* was performed as described previously to obtain mutants with single-strand transferred DNA (T-DNA) inserts (He et al., 2021). The DNA of randomly selected mutants containing the *neo* gene was isolated and amplified using DNA extraction kits (Beyotim, Shanghai, China) and specific neoF and neoR primers (He et al., 2021). The products were then sequenced by Comate Bioscience Co., Ltd. (Jilin, China) to confirm whether T-DNA was inserted into the *F. oxysporum* genome.

Analysis of T-DNA interrupted gene

Sequences flanking the inserted T-DNA were amplified by touchdown thermal asymmetric interlaced polymerase chain

TABLE 1 Strains used in this study.

Strain name	Information
WT	Wild type of *Fusarium oxysporum* JLCC31768, which was obtained from the Jilin University Mycology Research Center (He et al., 2021)
FOM312	T-DNA inserted mutant with reduced growth and virulence (obtained in this study)
Δ12762	Deleted FOXG_12762 from wild type (obtained in this study)
C12762	Complemented FOXG_12762 to Δ12762 (obtained in this study, EGFP contained)
AgrN	*Agrobacterium tumefaciens* containing pXEN, which was obtained from the Jilin University Mycology Research Center (He et al., 2021)

reaction (TAIL-PCR) using previously described primers (Gao et al., 2016). The products were sequenced (Comate Bioscience Co., Ltd. Jilin, China) and aligned against the *F. oxysporum* f. sp. *lycopersici* genome (GCF_000149955.1) using the Basic Local Alignment Search Tool (BLAST[1]) to determine the insertion sites (Lorenzini and Zapparoli, 2019). Bioinformatic analysis for nuclear localization signals was performed by NLStradamus program (Cheng et al., 2019; http://www.moseslab.csb.utoronto.ca/software/).

Construction of the FoDbp40 deletion and complementation strain

We based the method for constructing the targeted knockout of FoDbp40 on homologous genetic recombination by ATMT, with the *neo* marker gene replacing the target gene (He et al., 2021). Primers used are listed in Supplementary Table S2.

Our complementation strain was constructed according to methods described earlier (Roth and Chilvers, 2019). The FoDbp40 open reading frame and its own terminator region were amplified separately. To visualize the localization of FoDbp40 in *F. oxysporum*, the enhanced green fluorescent protein (EGFP) open reading frame was amplified from pEGFP-N3 by PCR. The resulting three DNA fragments were ligated using a One Step Cloning kit (Vazyme, Nanjing, China) and the resulting construct was transformed into protoplasts to create the deletion mutant we named Δ12762. The verification of the deletion and complementation were completed by PCR and observed phenotype. Primers used for all reactions are listed in Table 2. Graphs showing mechanism of the methods were also provided in Supplementary Figures S1, S2.

1 https://blast.ncbi.nlm.nih.gov/Blast.cgi

Growth analysis and microscopic examination

Fusarium oxysporum was grown on potato dextrose agar (PDA) for 5 days at 25°C for growth analysis. The conidia were washed down with sterile 0.85% saline containing approximately 1%—Tween® 20 and diluted to 1×10^5 CFU/ml. Then 2 μl of the suspension was dripped onto PDA plates and grown for 5 days at 25°C. Conidia were collected from 5-day-old cultures on PDA. The quantification for each strain was performed in triplicate. Each plate was washed three times with sterile 0.85% saline containing approximately 1%—Tween® 20 and the conidia suspension were adjusted to appropriate volume.

Slide cultures were prepared and then examined with microscope after lactophenol cotton blue staining. To visualize the localization of FoDbp40, the slide cultures were stained with 10 μg/ml 4′,6-diamidino-2-phenylindole (DAPI; Beyotime, Jiangsu, China) for nuclei staining, and then examined with a BX53 microscope (Evident Olympus, Tokyo, Japan).

Virulence assay

Human corneal epithelial cells (HCEC) were purchased from BeNa culture collection (Jiangsu, China), maintained in Minimum Essential Medium (MEM; XP Biomed Ltd., Shanghai, China) supplemented with 10% heat-inactivated fetal bovine serum (FBS; Gibco, New York, NY, USA) and cultured in 60 ml flasks kept at 37°C in a humidified incubator containing 5% CO_2.

For *in vitro* cytotoxicity assay, the cultured HCEC were co-cultured with *F. oxysporum* conidia for 24 h (Kolar et al., 2017) in 96-well plates (1×10^4 cells/well), then the lactate dehydrogenase (LDH) released from the cultured HCEC was measured using a lactate dehydrogenase cytotoxicity assay kit (Beyotime, Jiangsu, China; Jin et al., 2007).

An *in vivo* virulence assay was performed with AB strain zebrafish (ZFIN ID: ZDB-GENO-960809–7) as previously described (Laanto et al., 2012). Briefly, zebrafish (three-day post-fertilization) were infected with the *F. oxysporum* conidia by bathing. The fish were individually challenged with 1×10^4 CFU/ml conidia, and survival was recorded every 12 h. All the experiments in this study were approved by the animal ethics committee of Jilin University.

Analysis of gene expression by RT-qPCR

The RNA extraction and construction of cDNA libraries was performed as described previously (He et al., 2021; Wei et al., 2022). Conidia of *F. oxysporum* (1×10^6 CFU) were added to PDB medium and incubated for 24 h. The mycelia were collected and ground to a powder in liquid nitrogen. Total RNA was extracted from the ground material using RNAiso Plus

TABLE 2 Primers used for the vector construction.

Name	Sequence	
12762LF	GATCTTCACTAGTGGGAATTCAGGGCCGCAACGGAAAC	PCR primers for the construction of the gene deletion
12762LR	AGCTCGAATTGCAAGGAGGGAGCGTCAAAGAA	
12762RF	CAGAATAAAGTTTGAGGTCCTGGTGGTGGT	
12762RR	CAGGTCGACTCTAGAGGATCCACCCGTTGCAGTCAAAGCC	
12762NF	CCCTCCTTGCAATTCGAGCTCGGTACCCAG	
12762NR	GGACCTCAAACTTTATTCTGTCTTTTTATTGCCGTCCC	
12762p-F	gaccatgattacgccaagcttGCTGAGAAGGACAGGCCG	PCR primers for the construction of the complementation vector
12762p-R	ttacccttcttgggaggcatGATGGGCAGTTGGTGGCG	
12762+e-F	ATGCCTCCCAAGAAGGGTAAG	
12762+e-R	cTTACTTGTACAGCTCGTCCATGC	
12F	CCGCTAGCGCTACCGGACTCAGATCTATGCCTCCCAAGAAGGGTAAGGAGG	PCR primers for construction of the vector for Luciferase reporter assay
12R	GCGATGGATCCCGGGCCCGCGGCCGCTGCCGCCGCCGCCGCTGCCGCCGCCGCCAGATCCGGTTGCTGTCTCAGCTA	
05529proF	ctggcctaactggccggtaccCACAGAGGAAGCAGAGCGAATT	
05529proR	cagtaccggattgccaagcttTCTAGCTCGGCTTTCCACCG	
XF	CGAGTGGTGATTTTGTGCCG	PCR primers for identification
XR	AAACTGAAGGCGGGAAACGA	
TRF	GCCTATGGAAAAACGCCAGC	
TRR	CAACTGTTGGGAAGGGCGA	

According to the instruction, some primers for vector construction was design with a cohesive end which was wrote as normal letter.

TABLE 3 Primers used for qPCR.

Name	Sequence
Fu18SF	CGCCAGAGGACCCCTAAAC
Fu18SR	ATCGATGCCAGAACCAAGAGA
05529F	GAAGGAGGTTGAGGCTGTCAAG
05529R	CGTAGGTGTAGCTGGCATCTC
10116F	AGCTCTGATGGTCCCTGGAT
10116R	TGCGTTTACAACCAGAAAGCAG
01304F	ACCTAAGCGAAACGGGTCTG
01304R	ATTGAATGCCGTGGTCTCGT
10419F	CGCACTCGACTACATTCCCA
10419R	GTGCAGAGATGCCCTTGACT
12762F	GTCAAAGAAGGGCAACCAGC
12762R	TGGTCTTCAGGACGAATCCAG

The number in the primer name is the same as the gene ID. For example, 12762F is used for amplification of FOXG_12762. All primers in this table were designed with a Tm of 60°C.

(TaKaRa, Japan). Real-time, quantitative PCR (RT-qPCR) analysis was performed with a SYBR Green master mix (Monad, Shanghai, China) and the ABI QuantStudio 3 PCR system (Applied Biosystems, Waltham, MA, USA). Relative expression levels of the genes were calculated using the threshold cycle ($2^{-\Delta\Delta CT}$ also known as 22DDCT) method (Livak and Schmittgen, 2001). Gene expression levels were normalized against the expression of the 18S rRNA housekeeping gene (Table 3). Details regarding the relevant primers are provided in Supplementary Table S3.

ICL activity assay and measurement of succinic acid

Isocitrate lyase (ICL) activity was measured with an ICL activity assay kit of (Comin Corporation, Suzhou, China). After 24 h cultured in PDB, mycelia were collected and ground to a powder in liquid nitrogen. The mycelium powder was homogenized in 200 µl distilled water, and then centrifuged at 12,000 *g* at 4°C for 15 min. The supernatant was treated according to manufacturer's protocol, and the absorbance of the samples at 340 nm was detected using a spectrophotometer (Agilent Biotek, Santa Clara, CA, USA). The ICL activity was expressed as nmol/min/g.

Succinic acid was detected by high performance liquid chromatography (HPLC). A RIGOL (Suzhou, China) L3000 chromatograph and RIGOL C18 reversed-phase column (250 mm × 4.6 mm, 5 µm) were employed. The mobile phase was prepared as follows: 1.56 g of sodium dihydrogen phosphate was dissolved in 800 ml of water, then 16 ml of methanol was added and the pH was adjusted to 4–5 with a phosphoric acid solution; 10 µl of samples were loaded; the flow rate was 0.8 ml/min; the column temperature was 30°C; the sampling time was 30 min at 214 nm UV.

Luciferase reporter assay

The FOXG_12762 (NCBI Gene ID, mRNA accession XM_018392621) CDS region was inserted into the pEGFP-N3 (Takara Clontech, Kyoto, Japan) multiple cloning site (MCS) to

construct our FoDbp40-EGFP fusion protein expression vector (vector 1). The FOXG_05529 (NCBI Gene ID, isocitrate lyase) promoter region (regarded as −2,000 to +200) was inserted upstream of *luc2* in pGL4.10 (Promega, Madison, WI, USA) to construct our 05529pro-luc2 expression vector (vector 2).

Human embryonic kidney 293 (HEK-293) cells were maintained in high-glucose, GlutaMAX™ Dulbecco's Modified Eagle Medium (DMEM; Thermo Fischer Scientific, Waltham, MA, USA) supplemented with 10% heat-inactivated FBS (Gibco Thermo Fischer Scientific, Waltham, MA, USA) and cultured in 60 ml flasks kept at 37°C in a humidified incubator containing 5% CO_2. For transfections, HEK-293 cells were grown in FBS-containing medium in six-well plates until they reached 70% confluency. The transfection solution was prepared by mixing vector 1, pGL4.10 (Promega, Madison, WI, USA) basic vector or vector 2, pGL4.74 (Promega, Madison, WI, USA) containing the luciferase reporter gene *hRluc* for internal reference, Lipofectamine® 3,000 (Invitrogen Thermo Fischer Scientific, Waltham, MA, USA). Twenty-four hours later fluorescence from the enhanced green fluorescent protein (EGFP) was examined under an Olympus Model IX71 fluorescent microscope (Evident Olympus, Tokyo, Japan) to judge whether the FoDbp40-EGFP fusion protein was successfully expressed. Firefly and *Renilla* luminescence were tested using a Dual-Glo® Luciferase Assay System (Promega, Madison, WI, USA)[2] with a spectrophotometer (Agilent Biotek, Santa Clara, CA, USA). The relative expression of *luc2* was expressed as the ratio of firefly to *Renilla* luminescence signal. HEK-293 cells and pEGFP-N3 were obtained from Jilin University Mycology Research Center (Jilin, China). Primers used are provided in Supplementary Table S2.

ATP level assay

Mycelia ATP levels were determined using an ATP assay kit (Beyotime, Jiangsu, China) according to the manufacturer's instructions. After 24 h cultured in PDB, 100 mg of mycelia were collected and ground into powder in liquid nitrogen, the powder was homogenized in a lysis buffer and then centrifuged at 12,000 *g* for 5 min at 4°C. The supernatant was mixed with the working solution. The mixture was put into microwell plates and fluorescence intensity was measured with a spectrophotometer (Agilent Biotek, Santa Clara, CA, USA). The ATP levels were expressed as nmol/g.

Western blot analysis

The western blot method was performed as previously described (Li et al., 2010). 1×10^6 conidia were inoculated in 50 ml of potato dextrose broth (PDB) and cultured with shaking at 28°C for 24 h. Mycelia were harvested and ground into powder in liquid nitrogen, then suspended in radioimmunoprecipitation assay (RIPA) buffer containing 1 mM phenylmethylsulfonyl fluoride (PMSF). 20 μg of sample was loaded in each lane of a 10% SDS-PAGE gel. After electrophoresis, the samples were transferred to a polyvinylidene fluoride (PVDF) membrane. The membrane was then blocked with Tris-buffered saline with 0.1% Tween® 20 detergent (TBST) buffer containing 5% milk. After incubation with primary and secondary antibodies, blots were developed using enhanced chemiluminescence (ECL) western blot detection reagent (Bio-Rad, Hercules, California, USA) and images were acquired using a Tanon 4,200 Chemiluminescence Imaging System (Tanon, Shanghai, China). Antibodies used (anti-Actin, anti-AMPK alpha-1, anti-Phospho-AMPK alpha-1, mTOR, and anti-Phospho-mTOR) were purchased from Invitrogen (Thermo Fischer Scientific, Waltham, MA, USA).

Statistical analysis

All statistical analyses were performed using GraphPad Prism software version 6 (Dotmatics, San Diego, CA, USA). One-way analysis of variance followed by *t*-test was used for comparisons between the groups. $p < 0.05$ was considered to indicate a statistically significant difference.

The flow chart of present study was provided in supplementary materials (Supplementary Figure S3).

Results

Screening of *Fusarium oxysporum* mutants with reduced growth

Mutants of *F. oxysporum* were obtained by random insertion of T-DNA into the *F. oxysporum* genome using ATMT. A single specific amplicon can be amplified from all mutants (Supplementary Figure S4). The sequenced fragment was 100% identical to the *neo* gene, which proved that the T-DNA was successfully inserted into the *F. oxysporum* genome.

Mutant strains growth was compared to wild type *F. oxysporum* and FOM312 was identified with significantly reduced radial growth (Figure 1A). There were also other mutants were screened out with changed phenotype including slowed down growth, mycelial morphology changed, pigment decreased, etc., which were not discussed here.

Detection of the expression of genes involved in glyoxylate metabolism pathway in FOM312

The expression of four genes related to the glyoxylate metabolism pathway in FOM312 was detected by qPCR (Figure 2). The results showed that the expression of the four genes was down-regulated, and the expression of ICL was the most down-regulated. ICL is the rate limiting enzyme of the

2 https://www.promega.com.cn/products/luciferase-assays/

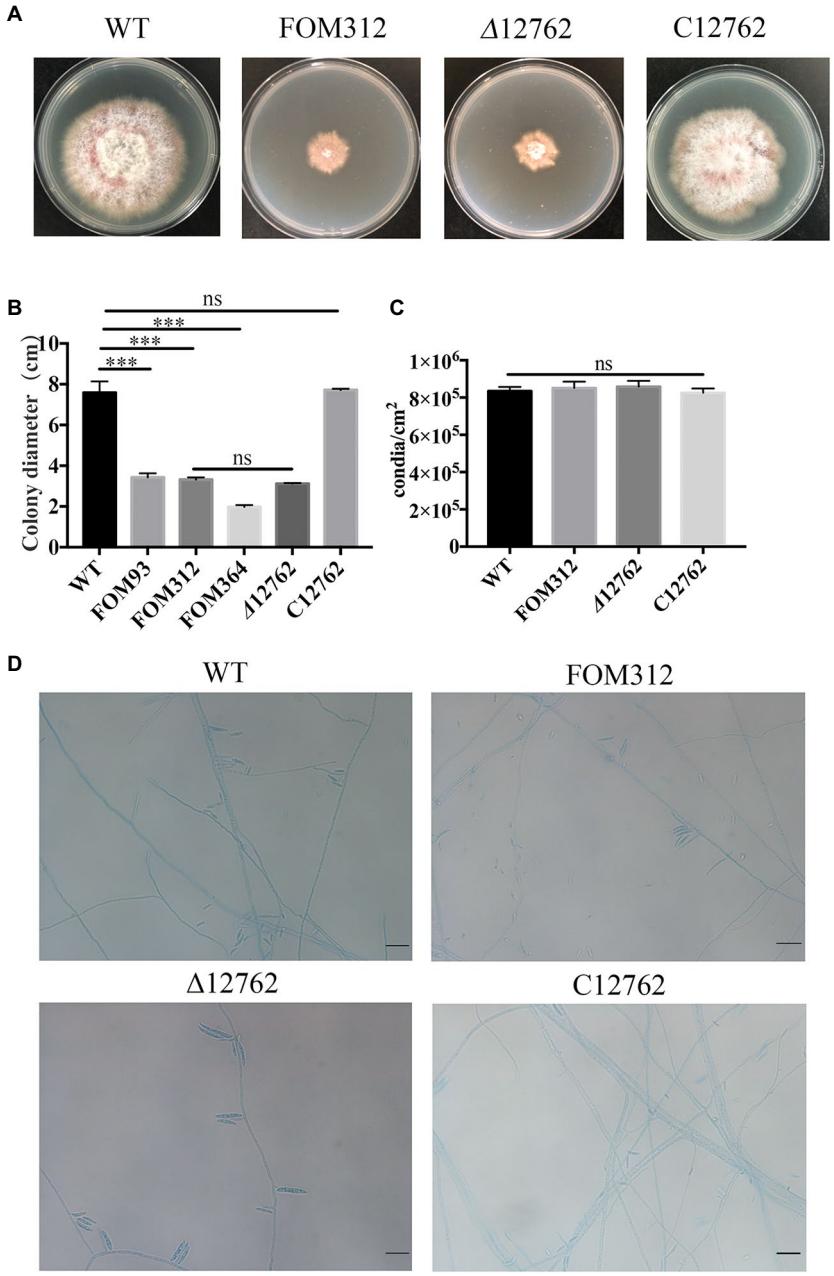

FIGURE 1
(A) Radial growth of wild type (WT), FOM312, Δ12762, and C12762. Strains were cultured on PDA medium and incubated at 25°C for 5days. **(B)** The quantitative data for A (***$p < 0.001$). **(C)** Conidial production rate of wild type, FOM312, Δ12762, and C12762. **(D)** The slide culture of wild type, FOM312, Δ12762, and C12762 (bar=25μm). The experiment was repeated three times.

glyoxylate metabolism pathway. Therefore, we speculate that FoDbp40 may affect energy metabolism and the growth of *F. oxysporum* by regulating ICL expression.

Analysis of T-DNA interrupted gene in the FOM312

T-DNA interrupted genes in FOM312 was verified by sequencing the TAIL-PCR products. The T-DNA in FOM312 inserted into FOXG_12762, which is located on chromosome 9 and encodes a hypothetical protein.

An amino acid sequence analysis performed with MEGA indicated that similar proteins are produced by other fungal species (Figure 3). FOXG_12762 encodes a hypothetical protein containing a CCCH zinc finger domain. This hypothetical protein has a high sequence identity (more than 70%) with homologs in common *Fusarium* species such as *F. graminearum* and *F. solani* and filamentous fungi such as *Aspergillus fumigatus* and *Torrubiella hemipterigena*. Sequence identity with other homologs,

such as *Aspergillus nidulans* and *Aspergillus flavus*, is lower (60–70%). The homologs in *Aspergillus fumigatus* (79%), *Colletotrichum incanum* (80%), and *Torrubiella hemipterigena* (81%) are annotated as CCCH finger DNA binding proteins. According to the bioinformatic analysis for nuclear localization signals, there are three sections of the sequence predicted to be nuclear localization signals (Figure 3; Supplementary Figure S5).

Constructs for gene deletion and mutant complementation of FOXG_12762

A knockout strain (Δ12762) and complementation strain (C12762) of FOXG_12762 were constructed. The deletion and complementation were verified by PCR (Supplementary Figures S1, S2). After 5 days of culture at 25°C, the Δ12762 colony was similarly sized to FOM312. The C12762 colony was similar in size to the wild type (Figures 1A,B). The expression of FOXG_12762 was significantly decreased after interrupted by T-DNA in FOM312, and was similar with wild type in C12762, while no signal was detected in Δ12762, which proved the successful deletion and complementation (Figure 4A). Based on the microscopic phenotype, the hyphae in the FOM312 and Δ12762 reduced compared with wild-type and C12762 (Figure 1D). Nevertheless, there was no much difference in conidial production between them (Figure 1C).

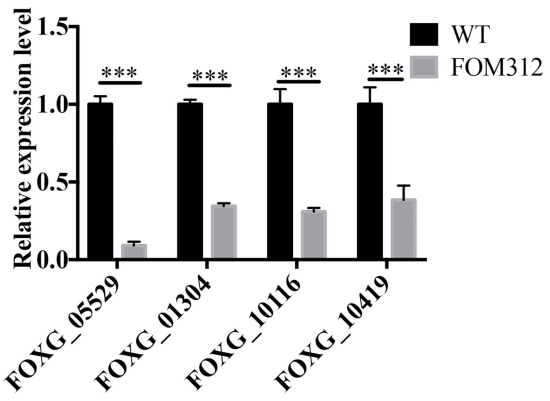

FIGURE 2
The relative expression level of four genes involved in glyoxylate metabolic pathway in FOM312. FOXG_05529 codes isocitrate lyase; FOXG_01304 codes 2-methylcitrate synthase; FOXG_10116 codes a formate/nitrite transporter domain; FOXG_10419 codes malate dehydrogenase. 18S rRNA was used as normalizing (***$p < 0.001$). The experiment was repeated three times.

Analysis of ICL expression regulation by FOXG_12762

The expression level of FOXG_05529 and ICL activity were detected and results show that the mRNA level of FOXG_05529 and ICL activity in Δ12762 and FOM312 decreased compared with wild type and C12762 (Figures 4B,C). HPLC results show that the level of succinic acid in FOM312 and Δ12762 also decreased, and the level of succinic acid in C12762 was close to that of wild type (Figure 4D). These results indicate that FoDbp40 can regulate the expression level and activity of ICL and affect the growth of *F. oxysporum*.

FoDbp40 has high sequence identity to various CCCH zinc finger DNA-binding proteins in other fungi. This implies that it may has functions of binding to DNA and regulating transcription. To confirm whether FoDbp40 can regulate the transcription of the ICL-encoding gene FOXG_05529, the action of FoDbp40 on the promoter region of FOXG_05529 was investigated using dual luciferase reporter technology. The HEK-293 cells co-transfected with the FoDbp40-EGFP fusion protein expression vector (vector 1) and the 05529pro-luc2 expression vector (vector 2) can produce green fluorescence under 488 nm wavelength excitation, which indicates that the FoDbp40-EGFP fusion protein was successfully expressed in the HEK-293 cells (Figures 5A–C). Compared with the vector 2 transfection group, the *luc2* fluorescence signal of the vector 1 and vector 2 co-transfected group was significantly enhanced (Figure 5D). These results indicate that FoDbp40 can act on the FOXG_05529 promoter region to promote the transcription and expression of downstream genes.

The cellular localization of the FoDbp40-EGFP fusion protein was observed using fluorescence microscopy. Results show that FoDbp40-EGFP is primarily located in the nucleus, as demonstrated by DAPI staining (Figure 6).

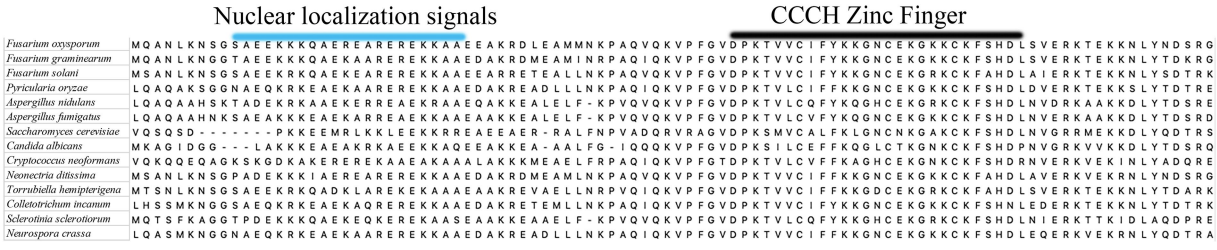

FIGURE 3
A part of the alignment result of amino acid sequences of FOXG_12762 and its most similar homologs from other fungi.

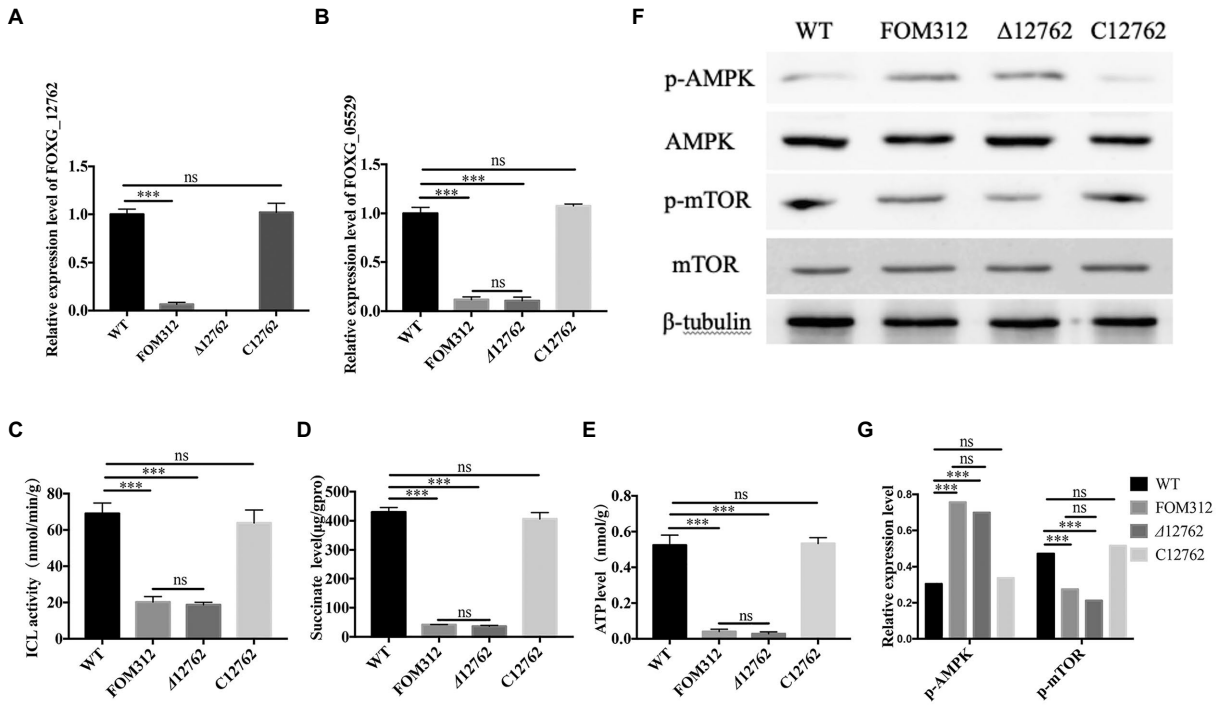

FIGURE 4
The detection of ICL-AMPK-mTOR axis. **(A)** Relative expression levels of FOXG_12762 in WT, FOM312, Δ12762 and C12762. **(B)** Relative expression levels of FOXG_05529 in WT, FOM312, Δ12762 and C12762. **(C)** ICL activity of WT, FOM312, Δ12762 and C12762. **(D)** Succinate level of WT, FOM312, Δ12762 and C12762. **(E)** ATP level in WT, FOM312, Δ12762 and C12762. **(F)** The expression level of AMPK, p-AMPK, mTOR, p-mTOR. **(G)** The quantization diagram of **E**, the expression of p-AMPK and p-mTOR was expressed as the ratio to β-tubullin (***$p<0.001$). The experiment was repeated three times.

FoDbp40 regulates the AMPK/mTOR signaling pathway and energy levels

Considering the activity of ICL in regulating energy metabolism, we detected the ATP levels in wild type, FOM312, Δ12762, and C12762. ATP levels are decreased in the FOM312 and Δ12762 strains compared with the wild type and C12762 strain (Figure 4E). The 5′-adenosine monophosphate activated protein kinase (AMPK) and mammalian target of rapamycin (mTOR) phosphorylation levels were detected by western blot. The results show that the level of phosphorylated-AMPK (p-AMPK) increased and the level of phosphorylated-mTOR (p-mTOR) decreased in Δ12762 and FOM312 compared with wild type and C12762 (Figures 4F,G). These results indicate that the loss of FoDbp40 causes a decrease in ATP levels, which affects the regulation of AMPK/mTOR pathways, thereby causing reduced growth and virulence of *F. oxysporum*.

Deletion of FOXG_12762 reduced the virulence of *Fusarium oxysporum*

Different concentrations of conidia were co-cultured with HCEC for 24 h, and HCEC cell viability was detected by an LDH detection kit (Beyotime, Shanghai, China). Results show that FOM312 and Δ12762 (1.8×10^6 CFU/ml for half maximal inhibitory concentration [IC_{50}]) have a lower cytotoxicity compared with wild type (2.4×10^6 CFU/ml for IC_{50}). This indicates that the deletion of FOXG_12762 results in decreased *F. oxysporum* virulence in HCEC (Figure 7A).

The IC_{50} of wild type with HCEC was 1.8×10^6 CFU/ml; therefore, this concentration was selected to stimulate HCEC cells to observe inflammation levels. Results show that the expression levels of IL-1β, IL-6, and TNF-α in HCEC increase after 6 h of stimulation (Figures 7B–D). Compared with the wild type treated group, the levels of inflammatory factors in the FOM312 and Δ12762 treated groups were lower, and the level of inflammatory factors in the C12762 treated group were close to those of the wild type treated group. This indicates that the deletion of FOXG_12762 can reduce the level of inflammatory response caused by *F. oxysporum*.

Zebrafish were inoculated with 1×10^4 CFU/ml conidia to observe survival rates. Results show that the lethality of FOM312 and Δ12762 groups was lower than wild type and C12762, which suggest that the virulence of *F. oxysporum* decreased due to a deficiency of FOXG_12762 (Figure 7E).

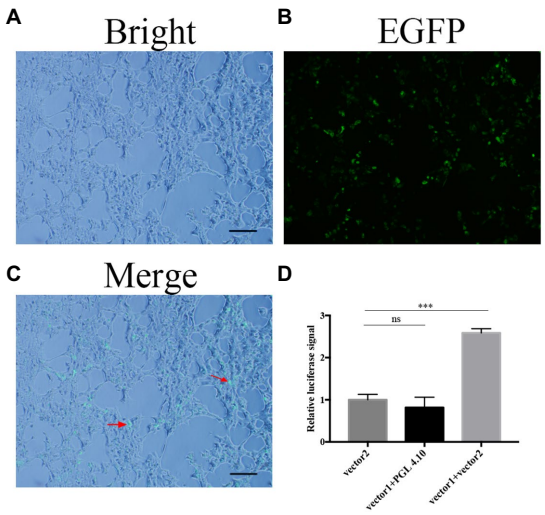

FIGURE 5
Transcription of FOXG_05529 is regulated by Fodbp40. **(A–C)** The FoDbp40-EGFP fusion protein was successfully expressed in HEK-293 (bar=100μm). **(D)** The expression level of 05529pro-luc2 in HEK-293 with and without FoDbp40 (***p<0.001). The experiment was repeated three times.

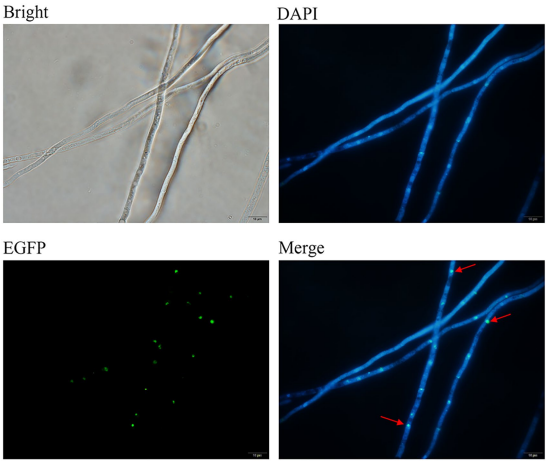

FIGURE 6
Subcellular localization of FoDbp40 in *F. oxysporum*. FoDbp40-EGFP is mainly localized in the nucleus, as demonstrated by 4′6-diamidino-2-phenylindole (DAPI) staining (bar=10μm).

Discussion

Fusarium species are important plant pathogens and human opportunistic pathogens that seriously affect the yield of crops and human health. Fungi growth is closely related to virulence. Exploring the regulatory mechanism of *Fusarium* growth is helpful for the development of new drugs, as well as the prevention and control of *Fusarium* infection. Constructing random mutants of fungi by ATMT is convenient due to high efficiency, which has been extensively used in numerous fungi to clarify the function of unknown genes (Schmidpeter et al., 2017; de Vallée et al., 2019). We used the ATMT method combined with phenotypic screening to search for key genes in growth and regulatory mechanisms in *F. oxysporum*.

The glyoxylate metabolism pathway plays an important role in the growth, pathogenesis, and stress tolerance of fungi (Park et al., 2016; Vico et al., 2021). Therefore, the expression of four genes related to glyoxylate metabolic pathways were detected. The results showed that the four genes were down-regulated in FOM312 compared with wild type. Among the four genes, the rate limiting enzyme ICL was most down-regulated, so we speculated that the interruption of T-DNA in FOM312 may disturbed the expression of ICL.

In order to investigate the mechanism of regulation of ICL, the function of T-DNA interrupted gene FOXG_12762 in FOM312 was analyzed. FOXG_12762 encodes a hypothetical protein that we name FoDbp40. Presently the annotation of hypothetical proteins is primarily through homology search and the identification of conserved domains by sequence alignment algorithms (Ijaq et al., 2015). Our amino acid sequence alignment shows the FoDbp40 protein sequence to contain a CCCH zinc finger domain conserved in several pathogenic fungi (Figure 3). Homologs in other fungi such as *Aspergillus fumigatus* and *Torrubiella hemipterigena* are annotated as CCCH zinc finger DNA binding proteins. Although CCCH zinc finger proteins were known as RNA-binding proteins (Fu and Blackshear, 2017), Recent studies showed that CCCH zinc finger proteins also bind to DNA and modulate transcription (Zou et al., 2018; Wang et al., 2022). Therefore, we speculate that FoDbp40 may have the ability to bind target DNA and function in transcriptional regulation.

In this study, we observed the regulatory effect of FoDbp40 on ICL expression (Figure 4) and demonstrated that this regulatory effect is achieved at the transcriptional level by acting on the promoter region of ICL (Figure 5). Additionally, we observed the FoDbp40 protein to localize in the nucleus (Figure 6) in line with the bioinformatic analysis (Supplementary Figure S5), which is similar to other known CCCH zinc finger protein transcription factors, including C3H12 and SAW1 (Wang et al., 2020; Seok et al., 2022). Our results indicate that FoDbp40 is a novel transcriptional regulator that can affect the expression and activity of ICL.

The glyoxylate metabolic pathway saves carbon sources by skipping the step of generating CO_2 in the tricarboxylic acid cycle (TCA) while generating required intermediates. This plays an important role in the regulation of ATP synthesis (Park et al., 2016). The expression and activity of ICL and corresponding succinate levels are decreased after the deletion of FOXG_12762 (Figure 4). These results demonstrated the regulatory effect of FoDbp40 on ICL and glyoxylate metabolic pathway.

As mentioned above, ICL is a key enzyme in the glyoxylate metabolism pathway, thereby regulating carbon metabolism and

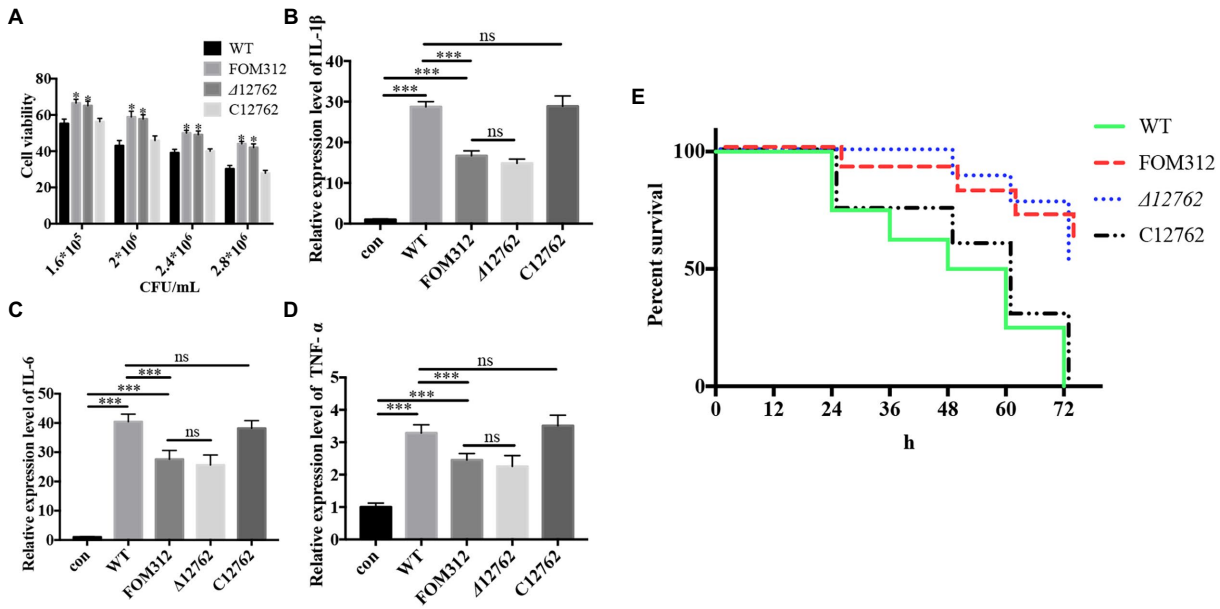

FIGURE 7
Virulence of *F. oxysporum*. **(A)** Cytotoxicity of *F. oxysporum* in HCEC (*p<0.05 vs. wild type). **(B–D)** Expression of cytokines in HCEC co-cultured with *F. oxysporum* (***p<0.001). **(E)** Virulence of *F. oxysporum* in zebrafish (n=8). The experiment was repeated three times.

ATP synthesis (Gengenbacher et al., 2010; Selinski and Scheibe, 2014). AMPK, an AMP-dependent protein kinase, is a key molecule in the regulation of biological energy metabolism. Intracellular energy level can regulate the phosphorylation of AMPK, which in turn regulates the Ras, ERK, mTOR, and other related pathways that crosstalk with AMPK, thus affecting cell growth (Hardie, 2014; Grahl et al., 2015). The regulation of growth by the AMPK/mTOR pathways has been reported in yeast (Forte et al., 2019), but has not been reported in *Fusarium* species.

The affect of FoDbp40 on the level of ATP and AMPK/mTOR pathway which involed in the growth regulation was analyzed at next. The results showed that the deletion of FoDbp40 results in a severe decrease of ATP levels in *F. oxysporum* (by more than 80%), while promoting phosphorylation of AMPK and dephosphorylation of mTOR (Figure 4). These results demonstrated the regulatory effects of FoDbp40 on energy metabolism and AMPK/mTOR pathways through the ICL.

Fusarium species often cause corneal infection in clinic. Some studies have used HCEC cells to establish *in vitro* model of cornea infection by pathogens such as *Fusarium solani* (Kolar et al., 2017). *F. solani* and *F. oxysporum* both belong to the genus *Fusarium*, which were the most predominant pathogenic *Fusarium* in clinic with similar infection and pathogenic patterns. Therefore, HCEC cells were used in this study to evaluate the virulence of *F. oxysporum*.

The pathogenesis of keratitis is often accompanied by an inflammatory response related to its prognosis (Matsumoto et al., 2005). Pattern recognition receptors on cell surfaces can regulate the expression of inflammatory cytokines after recognizing pathogens. These include IL-1 β, IL-6, and TNF-α; all cause inflammatory response (Yu et al., 2017). After the deletion of FOXG_12762, the cytotoxicity of *F. oxysporum* conidia in HCEC was attenuated, and the expression levels of pro-inflammatory cytokines in infectious keratitis decreased (Figure 7).

Dananjaya et al. (2017) have used zebrafish to evaluate the virulence of *F. oxysporum*. Considering that *F. oxysporum* often cause superficial infection in clinic, we established a model of *F. oxysporum* infection in zebrafish with the method of bathing referring to the virulence assay of Laanto et al. (2012) proceeded with *Flavobacterium columnare*. The results showed that there was a stable killing effect on zebrafish infected with *F. oxysporum*. Therefore, we believe that this model is suitable for evaluating the virulence of pathogenic fungi in superficial infection. In this study, the deletion of FOXG_12762 results in attenuated virulence of *F. oxysporum* in zebrafish (Figure 7). These results indicate that FOXG_12762 plays an important role in regulating *F. oxysporum* virulence.

In summary, our findings demonstrate that the gene encoding ICL is a key component affecting the growth of *F. oxysporum*. Furthermore, the putative protein FoDbp40 can regulate the expression of ICL at the transcriptional level, thereby affecting the level of ATP and the AMPK/mTOR pathways, and consequently regulate *F. oxysporum* growth and virulence. ICL and FoDbp40 have potential as new targets in the development of antifungal drugs.

Data availability statement

The original contributions presented in the study are included in the article/Supplementary material, further inquiries can be directed to the corresponding author.

Ethics statement

The animal study was reviewed and approved by the animal ethics committee of Jilin University (Jilin University, Changchun, China).

Author contributions

DH and LW: conceptualization and design. BZ and YZ: methodology and experiments. SG: data analysis. BZ and DH: original manuscript. LW: review and editing. All authors contributed to the article and approved the submitted version.

Funding

This study was supported by grants from the National Natural Science Foundation of China (81772162 and U1704283) and the Foundation of Jilin Education Committee (JJKH20211150KJ).

Acknowledgments

We thank all staff of our research center for helpful discussions. We also thank Steven M. Thompson from Liwen Bianji (Edanz; www.liwenbianji.cn/), for editing the English text of a draft of this manuscript.

Conflict of interest

SG was employed by Beijing ZhongKaiTianCheng Bio-technonogy Co. Ltd., Beijing, China.

The remaining authors declare that the research was conducted in the absence of any commercial or financial relationships that could be construed as a potential conflict of interest.

Publisher's note

All claims expressed in this article are solely those of the authors and do not necessarily represent those of their affiliated organizations, or those of the publisher, the editors and the reviewers. Any product that may be evaluated in this article, or claim that may be made by its manufacturer, is not guaranteed or endorsed by the publisher.

Supplementary material

The Supplementary material for this article can be found online at: https://www.frontiersin.org/articles/10.3389/fmicb.2022.1050637/full#supplementary-material

SUPPLEMENTARY FIGURE S1
(A) Mechanism of the deletion of FOXG_12762. **(B)** Amplification of neo fragment from the candidate strains. M, maker; lane 1, wild type; lane 2, pXEN plasmid, 3-5, different candidate strains. **(C)** Amplification of part of FOXG_12762 sequence from the candidate strains. M, maker; lane 1, water as blank; lane 2, wild type; lane 3-5, different candidate strains.

SUPPLEMENTARY FIGURE S2
(A) Mechanism of the complementation of FOXG_12762.
(B) Amplification of FOXG_12762-EGFP sequence from the candidate strains. M, maker; lane 1, Δ12762; lane 2-4, different candidate strains. A fragment (~4500bp) could be obtainded from the candidates.

SUPPLEMENTARY FIGURE S3
The flow chart of analyzing the function of FoDbp40 on the growth and virulence of F. oxysporum.

SUPPLEMENTARY FIGURE S4
Amplification of neo fragment (~700bp) in some randomly selected mutants. M: Trans 2 K marker; lane1: water as blank; lane2: pXEN plasmid; lane3: wild-type F. oxysporum; lane4-16: different mutants.

SUPPLEMENTARY FIGURE S5
The prediction of nuclear localization signals in FOXG_12762. Three nuclear localization signals were predicted.

References

Alkatan, H. M., and Al-Essa, R. S. (2019). Challenges in the diagnosis of microbial. Keratitis: a detailed review with update and general guidelines. *Saudi J. Ophthalmol.* 33, 268–276. doi: 10.1016/j.sjopt.2019.09.002

Andres, S. N., Li, Z. M., Erie, D. A., and Scott Williams, R. (2019). Ctp 1 protein-DNA filaments promote DNA bridging and DNA double-strand break repair. *J. Biol. Chem.* 294, 3312–3320. doi: 10.1074/jbc.RA118.006759

Bartas, M., Červeň, J., Guziurová, S., Slychko, K., and Pečinka, P. (2021). Amino acid composition in various types of nucleic acid-binding proteins. *Int. J. Mol. Sci.* 22:922. doi: 10.3390/ijms22020922

Berg, J. M., and Shi, Y. (1996). The galvanization of biology: a growing appreciation for the roles of zinc. *Science* 271, 1081–1085. doi: 10.1126/science.271.5252.1081

Bhusal, R. P., Bashiri, G., Kwai, B. X. C., Sperry, J., and Leung, I. K. H. (2017). Targeting isocitrate lyase for the treatment of latent tuberculosis. *Drug Discov. Today* 22, 1008–1016. doi: 10.1016/j.drudis.2017.04.012

Chen, C., Chen, D., Sharma, J., Cheng, W., Zhong, Y., Liu, K., et al. (2006). The hypothetical protein CT813 is localized in the chlamydia trachomatis inclusion membrane and is immunogenic in women urogenitally infected with *C. trachomatis*. *Infect. Immun.* 74, 4826–4840. doi: 10.1128/IAI.00081-06

Cheng, J. H., Lai, G. H., Lien, Y. Y., Sun, F. C., Hsu, S. L., Chuang, P. C., et al. (2019). Identification of nuclear localization signal and nuclear export signal of VP1 from the chicken anemia virus and effects on VP2 shuttling in cells. *Virol. J.* 16:45. doi: 10.1186/s12985-019-1153-5

Chotirmall, S. H., Mirkovic, B., Lavelle, G. M., and McElvaney, N. G. (2014). Immunoevasive Aspergillus virulence factors. *Mycopathologia* 178:363070, 363–370. doi: 10.1007/s11046-014-9768-y

Corkins, M. E., May, M., Ehrensberger, K. M., Hu, Y. M., Liu, Y. H., Bloor, S. D., et al. (2013). Zinc finger protein Loz1 is required for zinc-responsive regulation of gene expression in fission yeast. *Proc. Natl. Acad. Sci. U. S. A.* 110, 15371–15376. doi: 10.1073/pnas.1300853110

Dananjaya, S. H. S., Udayangani, R. M. C., Shin, S. Y., Edussuriya, M., Nikapitiya, C., Lee, J., et al. (2017). In vitro and in vivo antifungal efficacy of plant based lawsone against *Fusarium oxysporum* species complex. *Microbiol. Res.* 201, 21–29. doi: 10.1016/j.micres.2017.04.011

de Vallée, A., Bally, P., Bruel, C., Chandat, L., Choquer, M., Dieryckx, C., et al. (2019). A similar Secretome disturbance as a Hallmark of non-pathogenic Botrytis cinerea ATMT-mutants? *Front. Microbiol.* 10:2829. doi: 10.3389/fmicb.2019.02829

Forte, G. M., Davie, E., Lie, S., Franz-Wachtel, M., Ovens, A. J., Wang, T., et al. (2019). Import of extracellular ATP in yeast and man modulates AMPK and TORC1 signalling. *J. Cell Sci.* 132:jcs223925. doi: 10.1242/jcs.223925

Fu, M., and Blackshear, P. J. (2017). RNA-binding proteins in immune regulation: a focus on CCCH zinc finger proteins. *Nat. Rev. Immunol.* 17, 130–143. doi: 10.1038/nri.2016.129

Gao, S., He, D., Li, G., Zhang, Y., Lv, H., and Wang, L. (2016). A method for amplification of unknown flanking sequences based on touchdown PCR and suppression-PCR. *Anal. Biochem.* 509, 79–81. doi: 10.1016/j.ab.2016.07.001

Gengenbacher, M., Rao, S. P. S., Pethe, K., and Dick, T. (2010). Nutrient-starved, non-replicating mycobacterium tuberculosis requires respiration, ATP synthase and isocitrate lyase for maintenance of ATP homeostasis and viability. *Microbiology* 156, 81–87. doi: 10.1099/mic.0.033084-0

Grahl, N., Demers, E. G., Lindsay, A. K., Harty, C. E., Willger, S. D., Piispanen, A. E., et al. (2015). Mitochondrial activity and Cyr1 are key regulators of Ras1 activation of *C. albicans* virulence pathways. *PLoS Pathog.* 11:e1005133. doi: 10.1371/journal.ppat.1005133

Hardie, D. G. (2014). AMPK--sensing energy while talking to other signaling pathways. *Cell Metab.* 20, 939–952. doi: 10.1016/j.cmet.2014.09.013

He, D., Feng, Z., Gao, S., Wei, Y., Han, S., and Wang, L. (2021). Contribution of NADPH-cytochrome P450 reductase to azole resistance in *Fusarium oxysporum*. *Front. Microbiol.* 12:709942. doi: 10.3389/fmicb.2021.709942.

Ijaq, J., Chandrasekharan, M., Poddar, R., Bethi, N., and Sundararajan, V. S. (2015). Annotation and curation of uncharacterized proteins-challenges. *Front. Genet.* 6:119. doi: 10.3389/fgene.2015.00119

Jin, X., Qin, Q., Tu, L., Zhou, X., Lin, Y., and Qu, J. (2007). Toll-like receptors (TLRs) expression and function in response to inactivate hyphae of fusarium solani in immortalized human corneal epithelial cells. *Mol. Vis.* 13, 1953–1961. PMID: 17982419. http://www.molvis.org/molvis/v13/a220/.

Kazan, K., and Gardiner, D. M. (2018). Fusarium crown rot caused by *Fusarium pseudograminearum* in cereal crops: recent progress and future prospects. *Mol. Plant Pathol.* 19, 1547–1562. doi: 10.1111/mpp.12639

Kolar, S. S., Baidouri, H., and McDermott, A. M. (2017). Role of pattern recognition receptors in the modulation of antimicrobial peptide expression in the corneal epithelial innate response to F. solani. *Invest. Ophthalmol. Vis. Sci.* 58, 2463–2472. doi: 10.1167/iovs.16-20658

Laanto, E., Bamford, J. K., and Laakso, J. (2012). Phage-driven loss of virulence in a fish pathogenic bacterium. *PLoS One* 7:e53157. doi: 10.1371/journal.pone.0053157

Li, L., Murdock, G., and Bagley, D. (2010). Genetic dissection of a mitochondria-vacuole signaling pathway in yeast reveals a link between chronic oxidative stress and vacuolar iron transport. *J. Biol. Chem.* 285, 10232–10242. doi: 10.1074/jbc.M109.096859

Lin, L., Cao, J., Du, A., An, Q., Chen, X., Yuan, S., et al. (2021). eIF3k domain-containing protein regulates Conidiogenesis, Appressorium turgor, virulence, stress tolerance, and physiological and pathogenic development of Magnaporthe oryzae Oryzae. *Front. Plant Sci.* 12:748120. doi: 10.3389/fpls.2021.748120

Livak, K. J., and Schmittgen, T. D. (2001). Analysis of relative gene expression data using real-time quantitative PCR and the 2(-Delta Delta C(T)) method. *Methods* 25, 402–408. doi: 10.1006/meth.2001.1262

Lorenzini, M., and Zapparoli, G. (2019). Yeast-like fungi and yeasts in withered grape carposphere: characterization of Aureobasidium pullulans population and species diversity. *Int. J. Food Microbiol.* 289, 223–230. doi: 10.1016/j.ijfoodmicro.2018.10.023

Matsumoto, K., Ikema, K., and Tanihara, H. (2005). Role of cytokines and chemokines in pseudomonal keratitis. *Cornea* 24, S43–S49. doi: 10.1097/01.ico.0000178737.35297.d4

Melotto, M., Brandl, M. T., Jacob, C., Jay-Russell, M. T., Micallef, S. A., Warburton, M. L., et al. (2020). Breeding crops for enhanced food safety. *Front. Plant Sci.* 11:428. doi: 10.3389/fpls.2020.00428

Muraosa, Y., Oguchi, M., Yahiro, M., Watanabe, A., Yaguchi, T., and Kamei, K. (2017). Epidemiological study of fusarium species causing invasive and superficial Fusariosis in Japan. *Med. Mycol.* 58, E5–E13. doi: 10.3314/mmj.16-00024

Nucci, M., and Anaissie, E. (2007). Fusarium infections in immunocompromised patients. *Clin. Microbiol. Rev.* 20, 695–704. doi: 10.1128/cmr.00014-07

Paisley, D., Robson, G. D., and Denning, D. W. (2005). Correlation between in vitro growth rate and in vivo virulence in *Aspergillus fumigatus*. *Med. Mycol.* 43, 397–401. doi: 10.1080/13693780400005866

Park, Y., Cho, Y., Lee, Y. H., Lee, Y. W., and Rhee, S. (2016). Crystal structure and functional analysis of isocitrate lyases from *Magnaporthe oryzae* and *Fusarium graminearum*. *J. Struct. Biol.* 194, 395–403. doi: 10.1016/j.jsb.2016.03.019

Pranavathiyani, G., Prava, J., Rajeev, A. C., and Pan, A. (2020). Novel target exploration from hypothetical proteins of *Klebsiella pneumoniae* MGH 78578 reveals a protein involved in host-pathogen interaction. *Front. Cell. Infect. Microbiol.* 10:109. doi: 10.3389/fcimb.2020.00109

Roth, M. G., and Chilvers, M. I. (2019). A protoplast generation and transformation method for soybean sudden death syndrome causal agents fusarium virguliforme and F. brasiliense. *Fungal Biol. Biotechnol.* 6:7. doi: 10.1186/s40694-019-0070-0

Safavi, S. A., Shah, F. A., Pakdel, A. K., Reza Rasoulian, G., Bandani, A. R., and Butt, T. M. (2007). Effect of nutrition on growth and virulence of the entomopathogenic fungus *Beauveria bassiana*. *FEMS Microbiol. Lett.* 270, 116–123. doi: 10.1111/j.1574-6968.2007.00666.x

Schmidpeter, J., Dahl, M., Hofmann, J., and Koch, C. (2017). ChMob2 binds to ChCbk1 and promotes virulence and conidiation of the fungal pathogen *Colletotrichum higginsianum*. *BMC Microbiol.* 17:22. doi: 10.1186/s12866-017-0932-7

Selinski, J., and Scheibe, R. (2014). Pollen tube growth: where does the energy come from? *Plant Signal. Behav.* 9:e977200. doi: 10.4161/15592324.2014.977200

Seok, H. Y., Kim, T., Lee, S. Y., and Moon, Y. H. (2022). Non-TZF transcriptional activator AtC3H12 negatively affects seed germination and seedling development in Arabidopsis. *Int. J. Mol. Sci.* 23:1572. doi: 10.3390/ijms23031572

Uddin, R., Siddiqui, Q. N., Sufian, M., Azam, S. S., and Wadood, A. (2019). Proteome-wide subtractive approach to prioritize a hypothetical protein of XDR-mycobacterium tuberculosis as potential drug target. *Genes Genomics* 41, 1281–1292. doi: 10.1007/s13258-019-00857-z

Vico, S. H., Prieto, D., Monge, R. A., Román, E., and Pla, J. (2021). The Glyoxylate cycle is involved in white-opaque switching in *Candida albicans*. *J. Fungi* 7:502. doi: 10.3390/jof7070502

Wang, L., Chen, J., Zhao, Y., Wang, S., and Yuan, M. (2022). OsMAPK6 phosphorylates a zinc finger protein OsLIC to promote downstream OsWRKY30 for rice resistance to bacterial blight and leaf streak. *J. Integr. Plant Biol.* 64, 1116–1130. doi: 10.1111/jipb.13249

Wang, B., Fang, R., Chen, F., Han, J., Liu, Y. G., Chen, L., et al. (2020). A novel CCCH-type zinc finger protein SAW1 activates OsGA20ox3 to regulate gibberellin homeostasis and anther development in rice. *J. Integr. Plant Biol.* 62, 1594–1606. doi: 10.1111/jipb.12924

Wang, H. C., Ko, T. P., Wu, M. L., Ku, S. C., Wu, H. J., and Wang, A. H. (2012). Neisseria conserved protein DMP19 is a DNA mimic protein that prevents DNA binding to a hypothetical nitrogen-response transcription factor. *Nucleic Acids Res.* 40, 5718–5730. doi: 10.1093/nar/gks177

Wang, L. L., Lee, K. T., Jung, K. W., Lee, D. G., and Bahn, Y. S. (2018). The novel microtubule-associated CAP-glycine protein Cgp1 governs growth, differentiation, and virulence of *Cryptococcus neoformans*. *Virulence* 9, 566–584. doi: 10.1080/21505594.2017.1423189

Wang, C., Wang, Y., Zhang, L., Yin, Z., Liang, Y., Chen, L., et al. (2021). The Golgin protein RUD3 regulates *Fusarium graminearum* growth and virulence. *Appl. Environ. Microbiol.* 87, e02522–e02520. doi: 10.1128/AEM.02522-20

Wei, Y., He, D., Zhao, B., Liu, Y., Gao, S., Zhang, X., et al. (2022). The sat1 gene is required for the growth and virulence of the human pathogenic fungus aspergillus fumigatus. *Microbiol. Spectr* 10:e0155821. doi: 10.1128/spectrum.01558-21

WHO (2022). WHO fungal priority pathogens list to guide research, development and public health action. Available at: https://www.who.int/news/item/25-10-2022-who-releases-first-ever-list-of-health-threatening-fungi

Yi, D., Dempersmier, J. M., Nguyen, H. P., Viscarra, J. A., Dinh, J., Tabuchi, C., et al. (2019). Zc3h10 acts as a transcription factor and is phosphorylated to activate the thermogenic program. *Cell Rep.* 29, 2621–2633.e4. doi: 10.1016/j.celrep.2019.10.099

Yu, Y., Zhong, J., Peng, L., Wang, B., Li, S., Huang, H., et al. (2017). Tacrolimus downregulates inflammation by regulating pro−/anti-inflammatory responses in LPS-induced keratitis. *Mol. Med. Rep.* 16, 5855–5862. doi: 10.3892/mmr.2017.7353

Zhu, Y., Abdelraheem, A., Lujan, P., Idowu, J., Sullivan, P., Nichols, R., et al. (2021). Detection and characterization of fusarium wilt (*Fusarium oxysporum* f. sp. vasinfectum) race 4 causing fusarium wilt of cotton seedlings in New Mexico. *Plant Dis.* 105, 3353–3367. doi: 10.1094/PDIS-10-20-2174-RE

Zou, Q., Gang, K., Yang, Q., Liu, X., Tang, X., Lu, H., et al. (2018). The CCCH-type zinc finger transcription factor Zc3h8 represses NF-κB-mediated inflammation in digestive organs in zebrafish. *J. Biol. Chem.* 293, 11971–11983. doi: 10.1074/jbc.M117.802975

frontiers | Frontiers in Microbiology

TYPE Original Research
PUBLISHED 01 February 2023
DOI 10.3389/fmicb.2023.1121863

OPEN ACCESS

EDITED BY
Ruixin Zhu,
Tongji University,
China

REVIEWED BY
Esteban C. Gabazza,
Mie University,
Japan
Nelson da Cruz Soares,
University of Sharjah,
United Arab Emirates

*CORRESPONDENCE
Yan Geng
✉ gengyan@jiangnan.edu.cn
Qingjun You
✉ youqingjun@jiangnan.edu.cn

†These authors have contributed equally to this work

SPECIALTY SECTION
This article was submitted to Infectious Agents and Disease, a section of the journal Frontiers in Microbiology

RECEIVED 13 December 2022
ACCEPTED 13 January 2023
PUBLISHED 01 February 2023

CITATION
Shen J, Ni Y, Guan Q, Li R, Cao H, Geng Y and You Q (2023) *Stenotrophomonas maltophilia* promotes lung adenocarcinoma progression by upregulating histone deacetylase 5. *Front. Microbiol.* 14:1121863. doi: 10.3389/fmicb.2023.1121863

Stenotrophomonas maltophilia promotes lung adenocarcinoma progression by upregulating histone deacetylase 5

Jiyu Shen[1†], Yalan Ni[1,2†], Qijie Guan[3], Rui Li[2], Hong Cao[4], Yan Geng[5*] and Qingjun You[1,2*]

[1]Department of Oncology, Affiliated Hospital of Jiangnan University, Wuxi, China, [2]Key Laboratory of Carbohydrate Chemistry and Biotechnology, Ministry of Education; School of Biotechnology, Jiangnan University, Wuxi, Jiangsu, China, [3]National Engineering Research Center of Cereal Fermentation and Food Biomanufacturing, Jiangnan University, Wuxi, China, [4]Department of Nutrition, Affiliated Hospital of Jiangnan University, Wuxi, China, [5]School of Life Science and Health Engineering, Jiangnan University, Wuxi, China

Introduction: Lung cancer is the leading cause of cancer death worldwide, and lung adenocarcinoma (LADC) is the most common lung cancer. Lung cancer has a distinct microbiome composition correlated with patients' smoking status. However, the causal evidence of microbial impacts on LADC is largely unknown.

Methods: We investigated microbial communities' differences in Formalin-Fixed Paraffin-Embedded tissues of ever-smoke (n=22) and never-smoke (n=31) patients with LADC through bacterial 16S rRNA gene high-throughput sequencing. Then nitrosamines 4-(methylnitrosamino)-1-(3-pyridyl)-1-butanone (NNK)-induced lung cancer mouse model and A549 cells were used to study the effect of *Stenotrophomonas maltophilia* (*S. maltophilia*) in LADC.

Results and Discussion: We found a significant increase of genus *Stenotrophomonas* in LADC tissues of patients with primary tumor size greater than 3 cm and never-smoker patients. We further found that intratracheal infection with *S. maltophilia* promoted tumor progression in the NNK-induced lung cancer mouse model. We performed RNA-seq analysis on lung tissues and found that *S. maltophilia* treatment drove inflammation and upregulated tumor associated cell signaling, including Apelin signaling pathway. Mechanistically, histone deacetylase 5 (HDAC5) gene expression was significantly upregulated in *S. maltophilia* treated groups, and was required for *S. maltophilia* induced cell proliferation and migration in LADC cell line A549. Therefore, we provide in vivo and in vitro evidence to demonstrate that *S. maltophilia* promotes LADC progression, in part, through HDAC5.

KEYWORDS

non–small-cell lung cancer, tumor microbiota, *Stenotrophomonas maltophilia*, cell signaling pathway, inflammation, high-throughput sequencing

Introduction

Lung adenocarcinoma (LADC) accounts for about 40% of all lung cancer, which is the predominant cause of cancer death worldwide (Sung et al., 2020). Adenocarcinoma of the lung belongs to non-small cell lung cancer (NSCLC), which usually occurs in the lung periphery and evolves from the mucosal glands. Although smoking tobacco is the leading driver of any lung cancer, including LADC (Schuller, 2002; Kenfield et al., 2008), only 15% of smokers will develop lung cancer

(Samet et al., 2009), and the non-smoking-related etiology and carcinogenesis remain poorly understood (Jemal et al., 2018). As is well-known, primary tumor size is a significant prognostic factor in lung adenocarcinoma patients. Tumor size arises as a more important prognostic factor, from ≤1 cm to 7 cm, each centimeter separates tumors with a significantly different prognosis, and the 3-cutoff point separates T1 from T2 tumors (Detterbeck et al., 2016; Rami-Porta et al., 2017; Kim et al., 2019).

Mounting evidence suggests lung cancer is associated with many infectious diseases, such as COPD, tuberculosis, HIV, and *Chlamydia* infections (Chaturvedi et al., 2010; Yu et al., 2011; Dima et al., 2019; Cribbs et al., 2020). Meanwhile, lung infections destroy bronchial epithelial cells, creating a vicious circle (Huang and Shi, 2019). Studies have proved that the bacterial composition of bronchoalveolar fluid in lung cancer patients is different from that in benign disease patients. The microbiome composition of lung cancer in the lower airway sample is more similar to that of the buccal sample, which enriched with *Veillonella*, *Streptococcus*, *Prevotella*, and *Rothia* is related to lung cancer stage and prognosis (Lee et al., 2016; Tsay et al., 2020). Inhalation of antibiotics can reduce the lung colonization of melanoma (Le Noci et al., 2018).

In recent years, studies have proved that every tumor type has a distinct microbiome composition, and these intratumor bacteria are mostly intracellular and are present in both cancer and immune cells, suggesting an association with tumor development and clinical features (Nejman et al., 2020). The intratumor microbiota is a crucial mediator in tumor progression and migration. Studies have found that the tumor-resident microbiota can promote lung metastatic colonization in breast cancer through the upregulation of fluid shear stress pathway (Fu et al., 2022). Administration of bacteria through tail vein impairs tumor chemosensitivity (Yu et al., 2017) and promotes tumor progression (Le Noci et al., 2018; Parhi et al., 2020). However, the composition of the human LADC microbiome and the role of distinct altered bacterial species in lung cancer are still unknown.

In this study, we analyzed the differences in microbial compositions in ever-and never-smokers with LADC. Then we focused on the *Stenotrophomonas* genus, whose abundance correlated with the smoking status and primary tumor size. *Stenotrophomonas maltophilia* is the only species that infect humans, so we investigated the role of its type strain *S. maltophilia* (ATCC#13637) on the progression of lung cancer induced by nitrosamines 4-(methylnitrosamino)-1-(3-pyridyl)-1-butanone (NNK) in carcinogen-sensitive mouse strains A/Jmice. Further, we explored the potential mechanism of action of *S. maltophilia*. These findings suggest that a higher abundance of *S. maltophilia* is a risk factor in LADC and provide novel insights to evaluate cellular and molecular targets from the perspective of intratumor bacteria.

Results

Clinical characterization of lung adenocarcinoma patients

A total of 53 LADC samples were included in this study. These patients were admitted to the hospital and underwent surgery between January 2014 and December 2015. None of the patients in this study received antibiotics or chemotherapy before surgery. We collected information on gender, age, Primary tumor dimension, Lymphatic metastasis, clinical stage and followed the patient's survival as of January 17, 2021. The mean age of the total cohort was 62.2 years, with 50.6% men and 41.5% smokers. The proportion of men in the ever-smokers group was higher than in the never-smokers group (94.1 vs. 31.9) because women rarely smoke. For primary tumor size, 35 patient tumor size is less than 3 cm, 18 patient tumor size is higher than 3 cm. In total, 16 samples belonged to the I–II stages and 6 samples to the III–IV stages in ever-smokers, while 24 samples belonged to the I–II stages and 7 samples to the III–IV stages in never-smokers (Table 1). According to the survival curve of the patients, we found that smoke might be a negative prognostic factor in LADC patients, but this was not statistically significant (Supplementary Figure S1A).

Different clinical feature lung adenocarcinoma patients have distinct lung tumor microbial compositions

To analyze the composition of the tissue microbial profile, we successfully sequenced the 16S rRNA gene in Formalin-Fixed Paraffin-Embedded (FFPE) tissue samples from ever-smokers ($n = 22$) or never-smokers ($n = 31$) LADC. Firstly, we found alpha diversity metrics including Shannon, Chao1, ACE, and Simpson indexes according to amplicon sequence variants (ASVs) were comparable between two groups (Supplementary Figure S1B). We also visualized the Bray-Curtis distance of beta diversity by principal coordinate analysis (PCoA) between ever-smokers and never-smokers ($p > 0.05$, Supplementary Figure S1C). But we found that Chao1 and ACE index between primary tumor size ≤3 cm and > 3 cm group is significant (Figure 1A).

Then, we conducted the taxonomic assignment to build the microbial abundance profile. The two groups were both enriched by Proteobacteria, as the dominant phylum, followed by Actinobacteriota, Firmicutes and Bacteroidetes (Supplementary Figure S2), which was in consistent with the previous report (Nejman et al., 2020). We observed a significant increase of Acidobacteriota ($p = 0.046912$) in LADC tissues of never-smokers than ever-smokers. We identified in total 60 bacterial classes, 25 orders, 30 families, and 35 genera with a relative abundance higher than 0.1%. We also performed the analysis at class, order, family, and genera levels (Supplementary Figures S3, S4). At the genus level, the tumor microbiota of LADC in the ever-smokers was enriched with *Escherichia_Shigella* and *Sphingomonas*, but did not reach statistical significance (Supplementary Figure S5). While *Stenotrophomonas*,

TABLE 1 Clinical characteristics of the lung adenocarcinoma patients.

Characteristic	Ever-smokers (n=22)	Never-smokers (n=31)	P value
Age, mean ± SD	66.77 (±6.597)	62.64 (±9.138)	ns
Overall survival, mean ± SD	62.86 (±27.692)	67.77 (±18.599)	ns
Sex, male	19	9	$p < 0.001$
Stage, n (%)			
I	14 (64%)	18 (58%)	ns
II	4 (18%)	6 (19%)	ns
III	4 (18%)	7 (23%)	ns
IV	0	0	

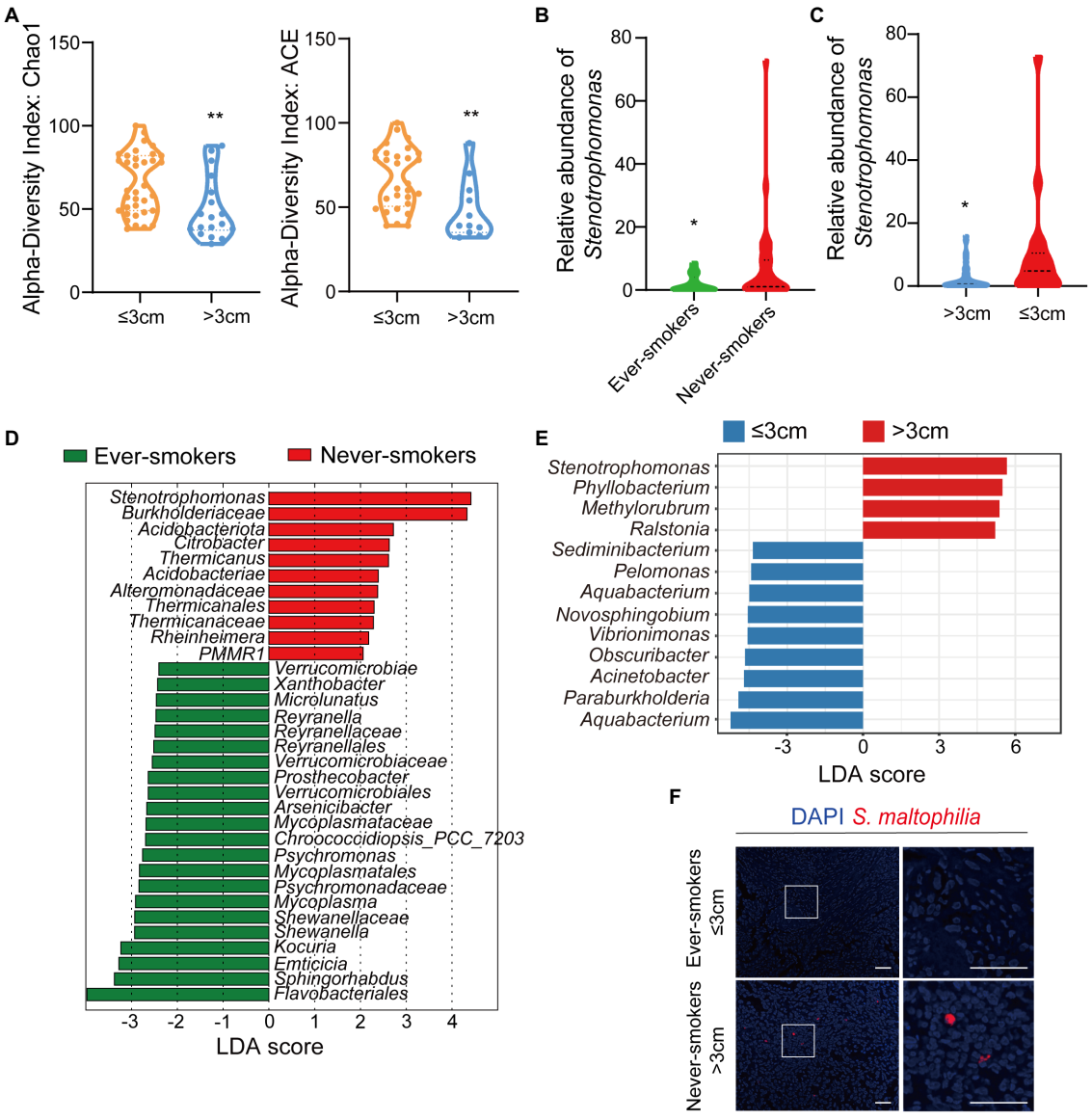

FIGURE 1
The microbiota was changed in lung tissues between the ever-smoker and never-smoker lung adenocarcinoma patients. **(A)** Taxonomic alpha-diversity calculated with the Chao index (p =0.0057) and Ace index (p =0.0058) between primary tumor size ≤3cm and>3cm groups. **(B)** Relative abundances of *Stenotrophomonas* in the microbiota of ever-smoke and never-smoke groups. **(C)** Relative abundances of *Stenotrophomonas* in the microbiota of ≤3cm and>3cm groups. **(D)** Linear discriminant analysis. Differential abundance of taxa was ranked according to their effect size between the Ever-smokers and Never-smoker groups. **(E)** Linear discriminant analysis. Differential abundance of taxa was ranked according to their effect size between primary tumor size ≤3cm and>3cm group. The selection of discriminative taxa between groups was based on an LDA score cutoff of 3.0 and differences in the relative abundances of taxa (converted to log base 10) were statistically determined based on a Kruskal-Wallis and pairwise Wilcoxon tests. A value of $p < 0.05$ and a score≥2.0 were considered significant. The length of the histogram represents the LDA score; i.e., the degree of influence of species with significant differences between different groups. **(F)** Representative FISH images of LADC tissue sections using a fluorescent probe specific to *Stenotrophomonas*. *$p < 0.05$, **$p < 0.01$ by Student's t-test.

Ralstonia, and *Corynebacterium* were identified to be enriched in the never-smokers. Among them, *Stenotrophomonas* was more than 3.9 fold higher in lung tumors of never-smokers ($p < 0.05$, Figure 1B). We also found a significant increase of *Stenotrophomonas* in LADC tissues of primary tumor size >3 cm than ≤3 cm groups (Figure 1C).

Next, we used the LEfSe algorithm to identify the critical bacterial taxa that account for the differences between smoking status or primary tumor size. LEfSe estimates the effect size of significantly different abundant of taxa and ranks them represented by the length of each bar (Segata et al., 2011). We found family Verrucomicrobiaceae and its higher taxonomies, including class Verrucomicrobiae and order Verrucomicrobiales, were significantly enriched in ever-smokers (Figure 1D). There was an increase in the family Burkholderiaceae in never-smokers compared with ever-smokers. Moreover, LADC microbiota of never-smokers was enriched in Acidobacteriota and *Stenotrophomonas*, in line with phylum and genus level observations (Figure 1D). We also found that the genus *Stenotrophomonas* was enriched in the group of primary tumor size higher than 3 cm patients through LEfSe analysis (Figure 1E). There was a linear correlation between the relative abundance of *Stenotrophomonas* and primary tumor size (Supplementary Figure S6). To validate the presence of *Stenotrophomonas* in LADC tissues,

we used FISH with a specific probe against its 16S rRNA. We found the presence of *Stenotrophomonas* DNA within LADC tissues in never-smokers, but not in that of ever-smokers (Figure 1F). These results indicates that *Stenotrophomonas* could be identified as biomarker in LADC.

Intratracheal inoculation of *Stenotrophomonas maltophilia* promotes lung cancer progression

Although various studies have revealed that microbiome contributes to tumor induction and progression (Dapito et al., 2012; Li et al., 2016, 2019; Le Noci et al., 2018; Jin et al., 2019; Tsay et al., 2020; Fu et al., 2022), the causal relationship between *Stenotrophomonas* and lung cancer remains largely unknown. *S. maltophilia*, the only species of *Stenotrophomonas* that infects humans, is considered a "newly emerging pathogen of concern" (An and Berg, 2018). To investigate whether *S. maltophilia* could colonize in the lung, we harvested lung lobes and cultured the lung homogenate in the nutrient broth after 48 h of bronchial injection of *S. maltophilia* in mice. We visualized and validated the colonizing ability of *S. maltophilia* in lung lobes by 16S rRNA gene sequencing (Supplementary Figure S7).

To explore whether *S. maltophilia* contributes to lung cancer progression, we compared tumor development between mice intratracheal inoculated with *S. maltophilia* and their control A/J mice in lung cancer model induced by NNK (Akopyan and Bonavida, 2006; Figure 2A). We found that NNK treatment affected the weight gain in mice, but not *S. maltophilia* treatment (Supplementary Figure S8). Compared with the NNK model group, NNK_ *S. maltophilia* group displayed heavy tumor burden, with the increased number of lung nodules and area of tumor (Figures 2B,C). At the cellular level, although NNK_ *S. maltophilia* group did not affect P53 expression, it exhibited increased tumor cell proliferation as demonstrated by immunohistochemical (IHC) analysis of Ki-67 staining (Figure 2C). Together, these results indicate that *S. maltophilia* plays a profound role in promoting tumor development in NNK induced lung cancer model.

Intratracheal inoculation of *Stenotrophomonas maltophilia* leads to a distinct transcriptional profile in lung tissues

To investigate the underlying mechanisms of *S. maltophilia* on lung cancer progression, we characterized the transcriptional profile of lung tissue using RNA sequencing (RNA-Seq). Constrained Principal Co-ordinates Analysis (CPCoA) clustering analysis showed that the CTL and NNK groups were clearly separate, while two *S. maltophilia* treatment groups were relatively close to each other (Figure 3A). These results indicate that the NNK and *S. maltophilia* treatment groups had distant gene expression signatures.

Gene set enrichment analysis (GSEA) revealed 34 overrepresented gene sets in *S. maltophilia* group compared to CTL group based on normalized gene set enrichment scores (NES; Supplementary Figure S9). Among them, various inflammatory pathways, including B cell receptor signaling pathway, Th17 cell differentiation, NF-kappa B signaling pathway, as well as regulation of actin cytoskeleton were significantly enriched in *S. maltophilia* group (Figures 3B–F). Sixteen gene sets were enriched in NNK_ *S. maltophilia* group compared with NNK group (Supplementary Figure S10). Interestingly, metabolism associated with tumor reprogramming, including propanoate metabolism, citrate cycle (TCA cycle), carbon metabolism, and fatty acid metabolism, were significantly enriched in NNK_ *S. maltophilia* group (Figures 3G–I). These data suggest that *S. maltophilia* may trigger inflammatory response, regulate cytoskeleton, and promote cancer metabolism.

Next, differentially expressed genes (DEGs) were identified through pairwise comparisons of groups. Compared with the CTL group, the number of DEGs in the *S. maltophilia*, NNK, and NNK_*S. maltophilia* groups was 3,786 (1832/1954; upregulated and downregulated DEGs, respectively), 3,373 (1,335/2038), and 2,283 (1,163/1120) respectively (Figures 3J–L; Supplementary Figure S11; Supplementary Table S1). A total of 1,034 DEGs were identified between NNK and NNK_S. *maltophilia* groups, among them 564 genes were upregulated in the lung tissues of NNK_*S. maltophilia* group and 470 genes were downregulated (Figure 3K). NNK_S. *maltophilia* group and *S. maltophilia* groups displayed similar gene expression profiles, and only 286 DEGs (the lowest number among all comparisons) were identified between these two groups (Supplementary Table S1). Additionally, we were able to identify 322 common DEGs between the CTL-*vs*-*S. maltophilia*, and NNK-*vs*-NNK_*S. maltophilia* (Supplementary Figure S12; Supplementary Table S2).

We next calculated the specific KEGG pathway enrichment of upregulated DEGs in *S. maltophilia* treated groups. Non-small cell lung cancer, Pathways in cancer and Ras signaling pathway enrichment confirmed that NNK induced lung cancer in A/J mice (Supplementary Figure S13). Although *S. maltophilia* treatment did not trigger lung cancer development in A/J mice, we found that pathway in cancer, MicroRNAs in cancer, Central carbon metabolism in cancer, and Non-small cell lung cancer was enriched in *S. maltophilia* group compared with CTL group (Figure 4A). KEGG pathway analysis also revealed that mice treated by *S. maltophilia* turned on many immunity-related signals, including the B cell receptor signaling pathway, Th1 and Th2 cell differentiation, Chemokine signaling pathway, Th17 cell differentiation, T cell receptor signaling pathway, NF-kappa B signaling pathway, and Toll-like Receptor signaling pathway (Figure 4A). Several Toll-like Receptor (TLR) genes were highly upregulated in *S. maltophilia* groups compared to CTL or NNK group (Figure 4B). Consistent with GSEA, we found propanoate metabolism and fatty acid metabolism was enriched in NNK_ *S. maltophilia* group compared with NNK group (Figure 4C).

The Apelin signaling pathway was enriched in the *S. maltophilia* group compared with the CTL group and in NNK_ *S. maltophilia* group compared with NNK group (Figures 4A,C). We found that 11 genes that belonged to the Apelin signaling pathway were upregulated in NNK_*S. maltophilia* group (Supplementary Table S3). Interestingly, five of them (*Hdac5*, *Ccn2*, *Mef2c*, *Plcb4*, *Prkag3*) were overexpressed in both *S. maltophilia* and NNK_*S. maltophilia* group (Figure 4D). Among them, HDAC5 (histone deacetylase 5), as a member of the class IIa family of HDACs, is a well-known oncogene in numerous cancer types, including lung cancer (Zhong et al., 2018; Yang et al., 2021). These results suggest that *S. maltophilia* may promote lung cancer progression by driving inflammation, regulating tumor cell signaling and metabolism at the transcriptional level.

Stenotrophomonas maltophilia promoted cell proliferation and cell migration of lung epithelial cells

To explore the possible mechanism of *S. maltophilia* in promoting LADC in mice, we performed *in vitro* experiments using cultured A549

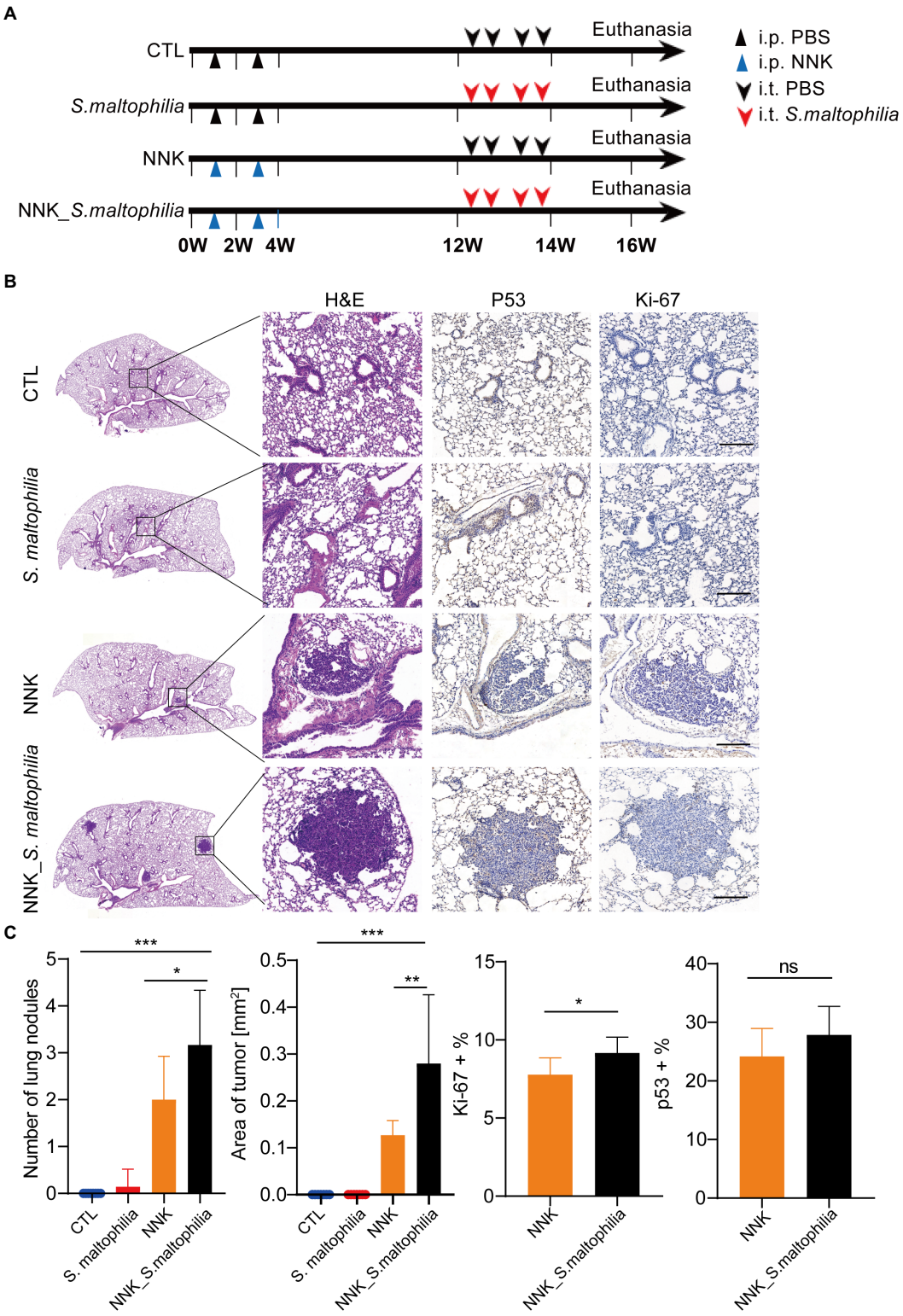

FIGURE 2
Stenotrophomonas maltophilia promotes lung cancer progression in mice. **(A)** Study design and diagram. **(B)** H&E staining, IHC staining of p53 and Ki-67 in lung tissues. Scale bar = 100μM. **(C)** The quantification of nodules on the lung surface, primary tumor area (mm^2), and percentage of p53 and Ki-67 positive area. Results are expressed as the mean±SEM. **p* <0.05, ***p* <0.01, ****p* <0.001 by Student's *t*-test. For each experiment, *n* =5–8 mice/group. ns, no significance.

cells exposed to the microbial products (Figure 5A). At first, we used three concentrations of bacteria for the *in vitro* experiment: multiplicity of infection (MOI) of 1, 10, and 100. We found that compared with CTL, 4 h pre-incubation with *S. maltophilia*_1 and *S. maltophilia*_2 significantly promoted A549 cell proliferation (Figure 5B). Then to explore the potential factors of *S. maltophilia* that contribute to tumor cell proliferation, we exposed A549 cells to heat killed or the supernatants from viable bacteria. The result showed that both of them

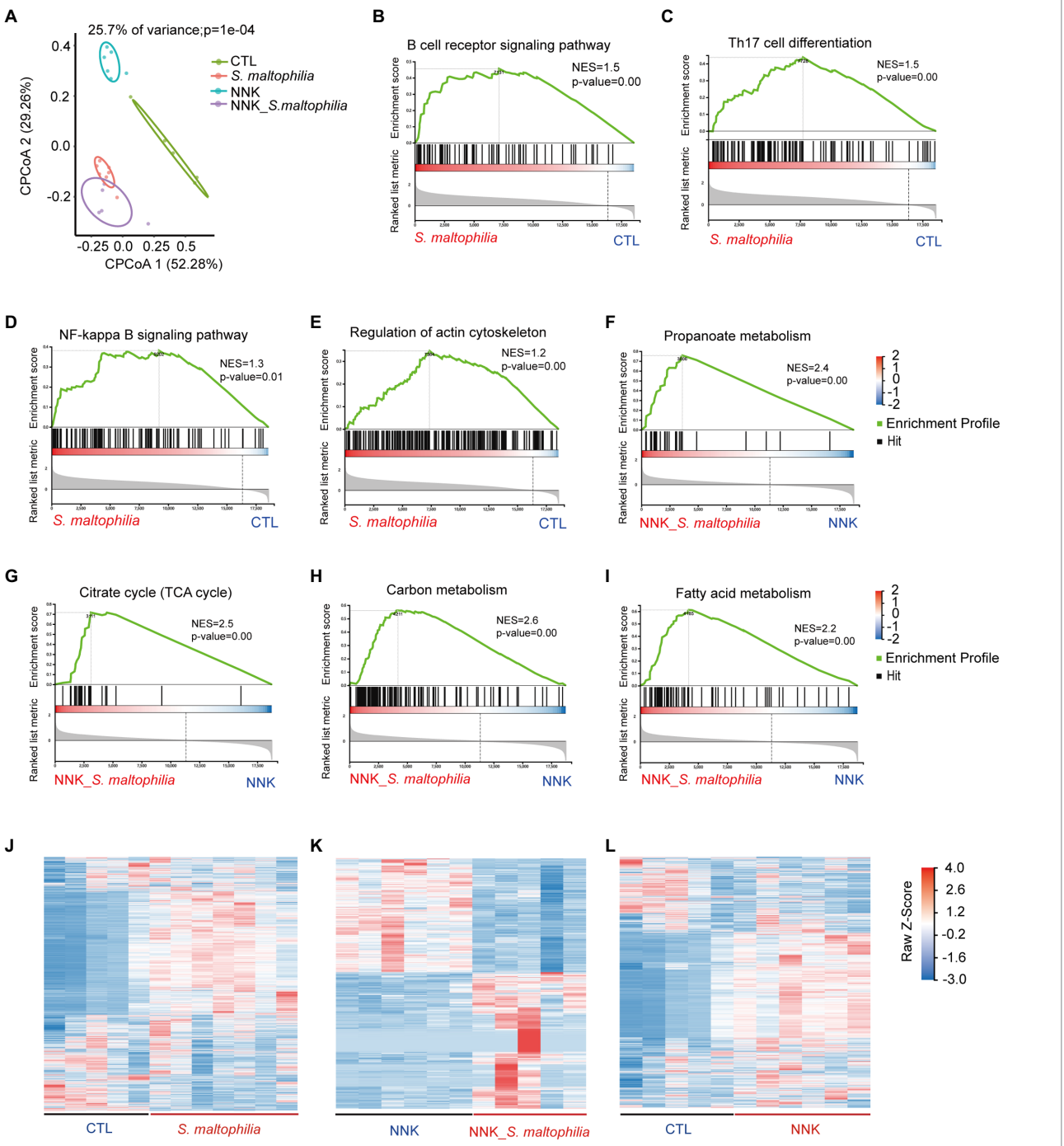

FIGURE 3
Stenotrophomonas maltophilia modulates gene expression in lung tissues by RNA-seq analysis. **(A)** Constrained PCoA clustering analysis of RNA-seq data. **(B–I)** GSEA Plot for the B cell receptor signaling pathway, Th17 cell differentiation, NF-kappa B signaling pathway, regulation of actin cytoskeleton, Propanoate metabolism, Citrate cycle (TCA cycle), Carbon metabolism, and Fatty acid metabolism, respectively. **(J)** Heatmap of different genes in lung tissues of *S. maltophilia* group compared with CTL group. **(K)** Heatmap of different genes in lung tissues of NNK_*S. maltophilia* group compared with NNK group. **(L)** Heatmap of different genes in lung tissues of NNK group compared with CTL group.

did not promote cell proliferation (Figure 5C). These data suggest that viable *S. maltophilia* may need to communicate with the cell to stimulate its proliferation.

Stenotrophomonas maltophilia treatment also promoted cell migration in A549 cell lines (Figure 5D). To verify the transcriptome results in mouse lungs, we performed qPCR assays. We found that pre-exposure to *S. maltophilia* significantly increased the mRNA expression of HDAC5 in A549 cells (Figure 5E). We further confirmed the up-regulated expression of HDAC5 in A549 cells treated with *S. maltophilia* by western blot (Figure 5F). Considering the tumor-promoting role of HDAC5, we further reasoned if HDAC5 silencing would abrogate the *S. maltophilia* induced cell proliferation and migration in lung cancer cells. We verified that HDAC5-specific siRNA markedly downregulated its gene expression, as well as inhibited cell proliferation and migration in A549 cells (Figures 6A–C). Further, we found that the cell proliferation and migration stimulated by *S. maltophilia* were also attenuated by HDAC5 interference

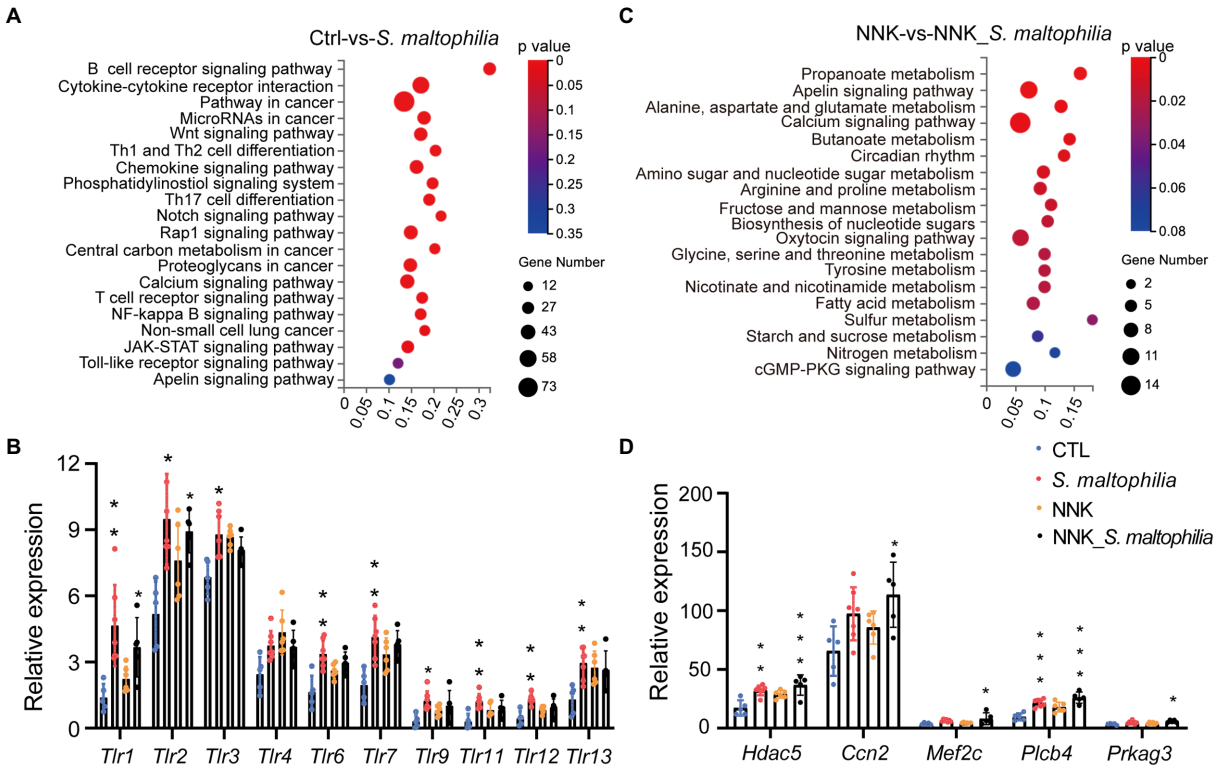

FIGURE 4
Stenotrophomonas maltophilia modulates gene expression in lung tissues by RNA-seq analysis. **(A)** KEGG pathway enrichment analysis of upregulated genes of RNA-seq data between CTL and *S. maltophilia* groups. **(B)** Relative expression of Toll-like receptors. **(C)** KEGG pathway enrichment analysis of upregulated genes of RNA-seq data between NNK and NNK_S. maltophilia groups. **(D)** Relative expression of Apelin signaling pathway genes. **p* <0.05, ***p* <0.01, ****p* <0.001, compared with CTL.

(Figures 6A–C). These findings demonstrate that *S. maltophilia* promotes lung cancer cell proliferation and migration partially through HDAC5.

Discussion

Recently, there has been increasing awareness that human tumors contain a significant amount of viable commensal microbiota (Banerjee et al., 2018; Riquelme et al., 2019; Nejman et al., 2020; Dumont-Leblond et al., 2021). Whether these microbes are passengers or drivers of tumor progression is an intriguing question that emerges. But a detailed and comprehensive analysis of the microbial ecosystem of the pathologic and lung cancer tissues remains incompletely studied. In this study, firstly, we represent for the report to characterize the microbiota composition of 53 samples from human LADC tissue. We performed 16S rRNA sequencing of the LADC and took measures to control for contamination. We explored the distinct microbiome composition inside the LADC, and uncovered significant associations between the bacteria and transcriptional changes in lung cancer cells that may be relevant for lung cancer pathogenesis. Overall, we observed significant intratumor microbiome dysbiosis in LADC patients with a different clinical feature. We found although there was no significant difference in tumor microbial alpha and beta diversity between ever-smokers and never-smokers LADC, representatives of the phyla Acidobacteriota and genus *Stenotrophomonas* were predominant in never-smokers. And we also found genus *Stenotrophomonas* was significantly enriched in the group of patients with primary tumor size higher than 3 cm patients. However, due to the limited number of cases, there is still no systematic evaluation of risk factors or clinic features associated to a different microbiome microenvironment.

Most recently, a higher abundance of *S. maltophilia* was found in hepatocellular carcinoma microbiota of the patients with cirrhosis, which induced the senescence of hepatic stellate cells and promoted the process of hepatocarcinogenesis (Liu et al., 2022). Notably, we demonstrated for the first time that the upregulation of HDAC5 caused by *S.maltophilia* infection is associated with tumor progression, supporting a causal role in the process of lung tumor growth.

Study have suggested that chronic colonization *C. difficile* is a potential driver of colorectal cancer in patients (Drewes et al., 2022). Coincidentally, *S. maltophilia* is an opportunistic pathogen that is multidrug resistant and causes a variety of human infections and forms biofilms in infected patients (Brooke, 2021), the most common *S. maltophilia*-associated human infections are bacteremia and respiratory infections (Batra et al., 2017). *S. maltophilia* is intrinsically resistant to a wide range of antibiotics, including β-lactams, carbapenems, fluoroquinolones, tetracyclines, chloramphenicol, aminoglycosides, polymyxins, macrolides, and TMP-SMX (Brooke, 2012), Once infected, it will colonize for a long time and is challenging to eliminate with antibiotics. In a previous study, variation in replication and persistence of *S. maltophilia* can be seen with clinical strains in A/J mice (Rouf et al., 2011), which demonstrated that our model is suitable for studying the function of *S. maltophilia*. In our study, we found that lung cancer mice treated with *S. maltophilia* have increased tumor burden compared with those treated with PBS. Future work identifying the effect of *S. maltophilia* colonization, duration, and toxin production on cancer cell interactions in humans will be needed to determine the tumorigenic risk to patients.

10.3389/fmicb.2023.1121863

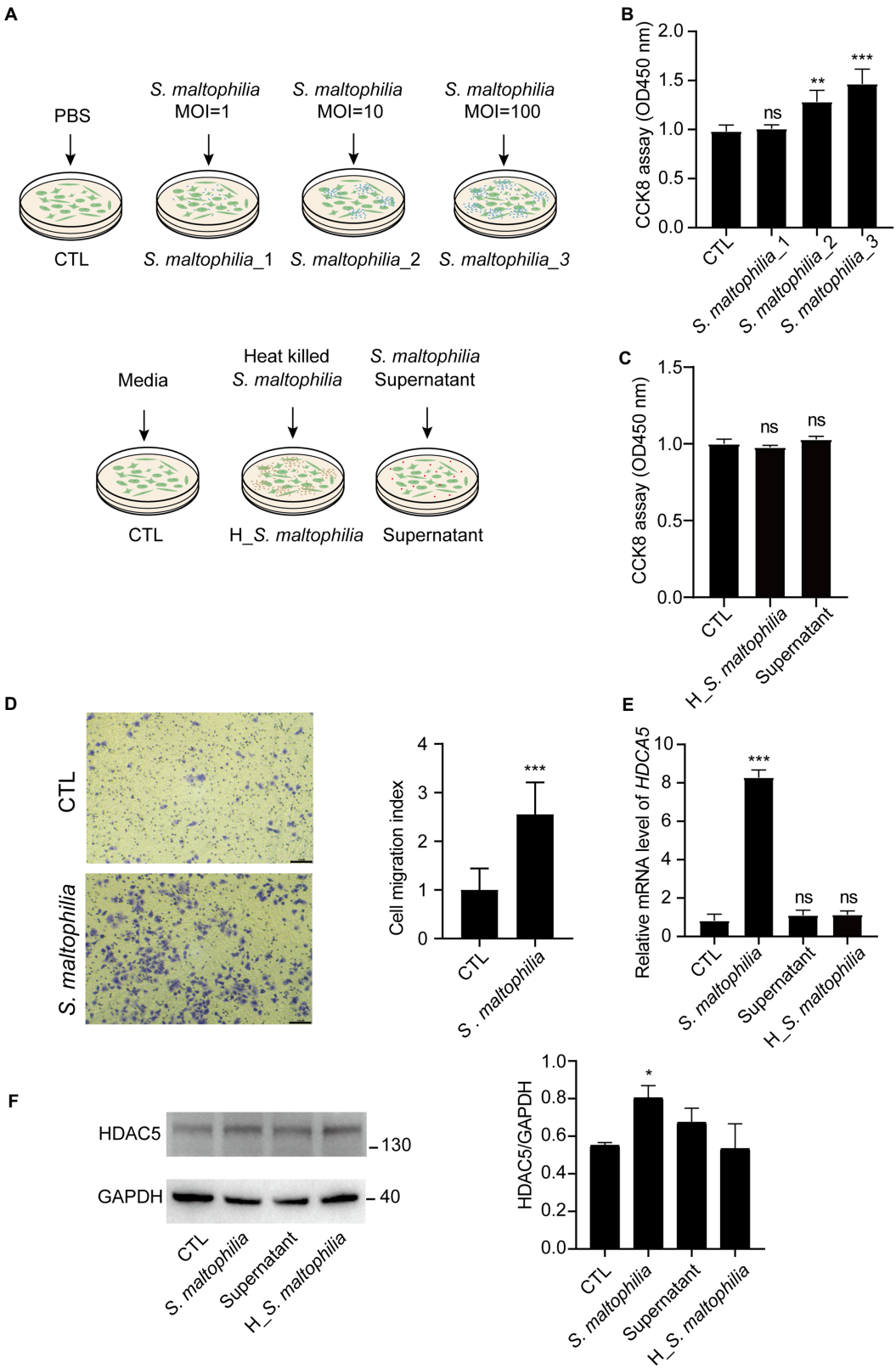

FIGURE 5
Stenotrophomonas maltophilia promoted cell and migration in lung epithelial cells. **(A)** Schematic experimental design for two *in vitro* experiments. For all conditions, A549 cells were exposed for 4h and then harvested for RNA isolation. Experiment 1: Cells were infected with *S. maltophilia* (ATCC #13637) at three different multiplicity of infection (MOI) of 1, 10, and 100 for 4h. Experiment 2: exposure to media alone, *S. maltophilia* (heat-killed), and supernatant. **(B)** Effect of *S. maltophilia* on A549 cell viability. **(C)** Effect of heat-killed *S. maltophilia* and supernatant on A549 cell viability, ns: no significance. **(D)** Effects of *S. maltophilia* on A549 cell line migration. **(E)** Effects of *S. maltophilia* on HDAC5 gene expression in A549 cells. ***p* <0.01 compared with CTL, ****p* <0.001 compared with CTL. **(F)** Western blot and statistical analysis of HDAC5 expression in A549 cells. **p* <0.05. ns, no significance.

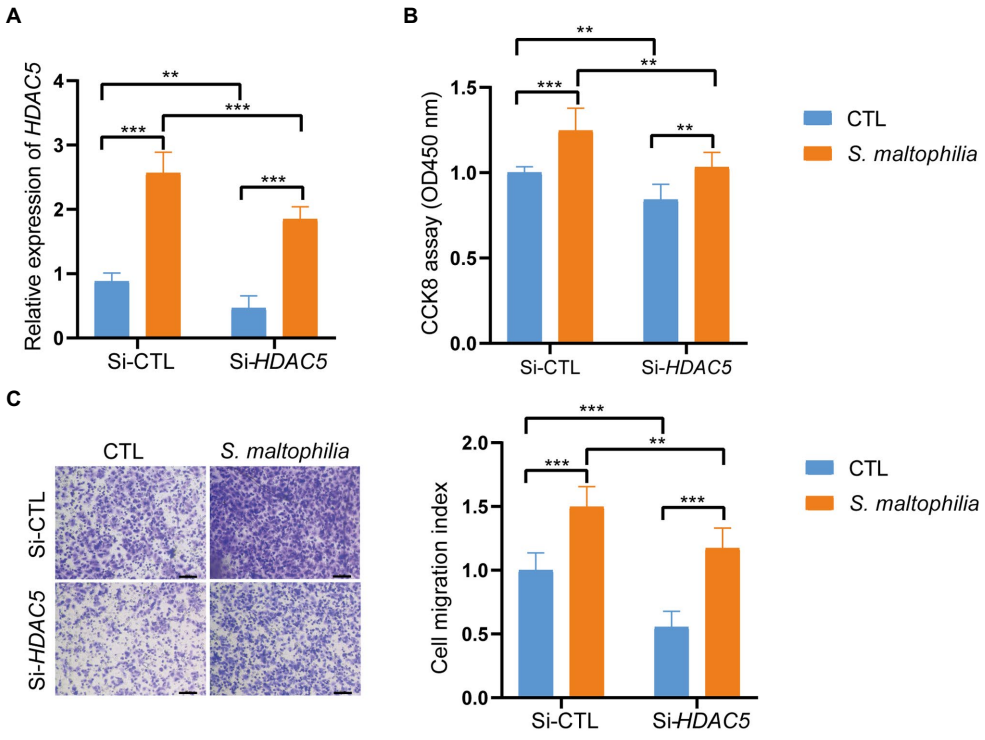

FIGURE 6
Inhibition of HDAC5 suppressed lung cancer cellular functions. Lung cancer cells A549 were transfected with si-HDAC5 or negative control (si-NC). **(A)** The HDAC5 expression levels were detected by qRT-PCR. **(B)** CCK-8 assay was used to test the cell proliferation. **(C)** Transwell migration assay was used to test the cell migration ability. *$p < 0.05$, ***$p < 0.001$ by Student's t-test.

Histone deacetylase 5 is a class II HDAC (de Ruijter et al., 2003), which is expressed in lung, brain, myocardium, skeletal muscle, and placenta, and accumulating evidence indicates that it has variable expression and functions in different types of tumors (Stypula-Cyrus et al., 2013; Zhong et al., 2018; Oltra et al., 2020). The functions of HDAC5 in tumorigenesis have been investigated in a variety of cancers, and HDAC5 was also shown to promote cell proliferation, invasion and metastasis in cancer (Chen et al., 2014; Liu et al., 2014; Cao et al., 2016, 2017; Zhong et al., 2018). PCR and immunohistochemical analyses have shown that HDAC5 was highly expressed in the cytoplasm of malignant epithelial cells, and HDAC5 expression was positively associated with distant metastasis and lymph node metastasis (Li et al., 2016). HDAC5 was also shown to promote cell invasion and metastasis in lung cancer (Gong et al., 2020). Our data point to mechanisms of *S. maltophilia* induced tumorigenesis, including increased Apelin signaling pathway, which HDAC5 gene is the most important. Consistent with our data from the mouse model, we also found *S. maltophilia* induced HDAC5 expression in lung cancer cells. These bacteria may affect the host by shedding different microbial bioactive molecules, because heat-killed *S. maltophilia* and supernatants did not cause proliferation and migration and did not upregulate the HDAC5 gene expression of cancer cells *in vitro*.

We acknowledge several limitations. Our sample size is not large enough, and we only detected the bacterial species with the widely used V4 amplification from formalin-fixed paraffin embedded lung tumors. The coverage and resolution of the detection of *S. maltophilia* species may not be fully achieved. Our experiment did not uncover which specific components of the bacteria are responsible for tumor progression. We only verified the functions of HDAC5 in *S. maltophilia* stimulated cell proliferation and migration. There might be other mechanisms responsible for the tumor promoting effect of *S. maltophilia*.

In conclusion, we profiled the differences of the composition of microbiota in LADC using 16S rRNA gene high-throughput sequencing and found *Stenotrophomonas* increased in LADC tissues of patient with primary tumor size greater than 3 cm and never-smoker patients. Further *in vivo* and *in vitro* evidence demonstrate that *S. maltophilia* promotes cell proliferation and migration, as well as LADC progression, in part, through HDAC5.

Materials and methods

Patients and sample collection

Formalin-Fixed Paraffin-Embedded (FFPE) tissue samples of 53 patients diagnosed with LADC in the period from Jan 2014 to Dec 2015 were included. All procedures conformed to the Code of Ethics of the World Medical Association (Declaration of Helsinki) and complied with the guidelines of the Institutional Review Board of the Affiliated Hospital of Jiangnan University (IRB: LS2021072).

Isolation and identification of microbiota in lung adenocarcinoma

DNA was extracted from each FFPE sample using the TIANquick FFPE DNA kit (Tiangen, #DP330-02, Beijing, China) according to the manufacturer's instruction. In addition, we introduced 3 negative controls which are empty tubes that were processed together with the

samples for sequencing. All negative controls were processed according to the same protocols.

The DNA was amplified by polymerase chain reaction (PCR) with a bacterial 16S rRNA gene V4 region universe primer pair (341F: 5'-ACT CCT ACG GGA GGC AGC AG-3′ and 806R: 5′-GGA CTA CHV GGG TWT CTA AT-3′; Zhong et al., 2018). Barcoded libraries were generated and the products were sequenced on the HiSeq2500 platform (BGI, Wuhan, China) using the PE300 module. Clean tags were assigned to ASVs using DADA2 (Divisive Amplicon Denoising Algorithm) software in the Quantitative Insights Into Microbial Ecology (QIIME) 2 package, and tags with ≥100% similarity were clustered to the same ASV. Representative ASVs were annotated using Silva_species_assignment_v138 reference database. The ASVs without annotation or annotated to polluted species were removed. Picrust2 (v2.2.0) was used for function predictions.

Common and specific ASVs among groups were compared and displayed in R 3.6.2 with "venn" package (v3.1.1) and Bray-Curtis similarities were calculated in R with "vegan" package (v3.5.1). Alpha diversity was applied to analyze the complexity of species diversity of a sample using Chao 1, ACE, Shannon, and Simpson indices. All indices of our samples were calculated with Mother (v1.31.2). Observed species and Chao 1 were selected to identify community richness, whereas Shannon was used to identify the community diversity. Beta diversity was calculated on both weighted and unweighted UniFrac using QIIME (v1.80). Partial least squares discrimination analysis (PLS-DA) was built using the mixOmics package (v3.2.1) in R. The differential abundance at the phylum, class, order, family, genus, and species levels between groups were performed using LEfSe, with $p \leq 0.01$ and LDA ≥ 2.

Bacteria

Stenotrophomonas maltophilia (ATCC #13637 = CGMCC# 1.1788 = BCRC#10737 = DSM#50170 = LMG#958 = NBRC#14161 = NCTC#10257) were purchased from the China General Microbiological Culture Collection Center. *S. maltophilia* were cultured in nutrient broth (Solarbio #n8300, China) at 30°C in an aerobic chamber for 24 to 48 h.

Animals and treatments

Female A/J mice aged 5 weeks were purchased from GemPharmatech Co., Ltd (Nanjing, China). All mice were housed in a specific-pathogen-free (SPF) environment with access to a standard chow diet and drinking water *ad libitum*. After a week of acclimation, mice were randomly divided into control group (CTL), bacteria solution (*S. maltophilia*) group, NNK treatment group (NNK, 100 mg/kg, biweekly for 4 weeks), and NNK + bacteria solution group (NNK_ *S. maltophilia*; $n = 8$ per group). The mice were injected intraperitoneally (i.p) or intratracheal inoculation (i.t) at the indicated doses and timepoints (Figure 2A). The intratracheal inoculation of *S. maltophilia* (1.5×10^6 cfu/mL) were performed as described (DuPage et al., 2009). All mice were treated in accordance to the guidelines of the European Community (Directive 2010/63/EU) and the procedures were approved by the Committee of Ethics in Jiangnan University (#JN. No 20211130a0320401[504]).

Histology and immunohistochemistry

The left lobe of the lung from the sacrificed mice was harvested and fixed by 4% paraformaldehyde. After embedding, sections were prepared and stained with hematoxylin–eosin. IHC staining was performed on unstained sections after antigens retrieval with citrate buffer (10 mM Sodium Citrate, 0.05%Tween 20, pH6.0; Jin et al., 2019). The following antibodies were used, including Ki-67 (1: 200 Abcam #ab16667, Cambridge, United Kingdom) and P53 (1: 2000 proteintech #60283-2-Ig, Chicago, United States), secondary antibody (MXB Biotechnologies #KIT-9922, Fuzhou, China). Digitally scanned images of stained slides were created with the Panorama MIDI (3DHISTECH Ltd., Budapest, Hungary).

Cell culture, treatment, and viability assay

The A549 cell lines were kindly provided by Stem Cell Bank (Chinese Academy of Sciences). Cell were maintained in RPMI1640 (Gibco #11875093, Waltham, MA, United States) containing 10% FBS (Gibco #10099141C, Waltham, MA, United States), 1% Penicillin–Streptomycin-Amphotericin B Solution (Beyotime #C0224-100 ml, Shanghai, China), cultured in an incubator at 37°C under 95% air and 5%CO_2. Cells were grown and 1×10^6 cells plated in each well (6-well plates with 2 ml of media) and exposed them to different microbial challenges under *in vitro* experiments. Cells were infected with *S. maltophilia* (ATCC #13637) at three different multiplicy of infection (MOI) of 1, 10, and 100 for 4 h. Then the cells were washed twice, and incubated with fresh culture medium for 12 h. For heat inactivation, the bacteria were incubated at 60°C for 15 min. Cell viability was detected by a cell counting Kit-8 (Teyebio #TY0312, Shanghai, China) according to the manufacturer's instruction.

A549 cells were chosen to perform further experiments. A549 cells (2×10^5) were seeded in a 6-well tissue culture plate with 2 mL antibiotic-free RPMI-1640 medium supplemented with 10% FBS. When cells reached 60–80% confluence, the cells were transfected with HDAC5 siRNA, and control vector (Guangzhou RiboBio Co., Ltd., Guangzhou, China) using LipoRNAi™ Transfection Reagent (Beyotime, #C0535, Shanghai, China) according to the manufacturer's specification. Then, A549 cells were incubated with the compound at 37°C in a CO_2 incubator for 6 h. Following, the transfection mixture was replaced with fresh medium to culture for 48 h. Finally, the A549 cells were assayed using the appropriate protocol.

Transwell migration assay

For Boyden chamber assays, cell suspension (1×10^5cells) was placed into the upper compartment of a 8 μM pore size Transwell chamber (Merck #PTEP24H48, Billerica, MA, United States) in 24-well plate. In each well, serum-free medium was used in the top chamber, while medium containing 10%FBS were used in the bottom chamber. After 24 h culture, cells migrated to the bottom side of the membrane were fixed and stained with the 0.1% crystal violet solution. The migrated cells was counted in five randomly chosen fields per filter from triplicate filters per sample at ×400 magnification. The cell migration index was calculated as the number of cells able to migrate normalized to controls (mean ± SEM).

Fluorescence *in situ* hybridization

FISH was conducted with the paraffin-embedded lung tissue according to the protocol described previously (Geller et al., 2017). Briefly, after deparaffinization and rehydration, the slides were incubated

with 0.2 M HCl for 12 min at 37°C, and then were incubated with Triton at 37°C for 17 min. Slides were washed twice with PBS and incubated with lysozyme for 15 min at 37°C, and then they were hybridized with the probe specific to ASV4. Before visualization, DAPI was added to the slides. The *S. maltophilia* probe used for FISH was: GTC GTC CAG TAT CCA CTG C, 5′ modification: Cy3 (Liu et al., 2022). Then the images were captured using Confocal Laser Scanning microscopy (Carl Zeiss Microscopy, United States).

RNA isolation and qRT-PCR analysis

RNAs were extracted from lung tissues and cells using Trizol reagent (Invitrogen, Waltham, United States) and were reversely transcripted into cDNAs. MultiScribe Reverse Transcriptase (Abm #G492, Canada) was used for cDNA synthesis, and then qRT-PCR was performed by using SYBR™ Select Master Mix (Thermo Fisher Scientific, Waltham, United States) according to the manufacturer's protocols. Gene expression was measured relative to the endogenous reference gene β-actin using the comparative ΔCT method.

Sequences of the specific primer sets are as follows: HDAC5 (NM_001015053.2), forward, 5′-GTG ACA CCG TGT GGA ATG AG-3′; reverse, 5′- AGT CCA CGA TGA GGA CCT TG; β-actin (NM_001101.5), forward, 5'-CTC TTC CAG CCT TCC TTC CT-3′; reverse, 5'-AGC ACT GTG TTG GCG TAC AG-3′.

Immunoblotting

Cells were lysed in RIPA buffer (Yeasen, Shanghai, China) and followed by 12% SDS-PAGE separation. Separated proteins were transferred onto polyvinylidene difluoride (PVDF) membranes (Merck Millipore, Billerica, MA, United States). The membranes were blocked by 5% bovine albumin in tris-buffered saline plus 0.1% Tween 20 for 1 h at room temperature. The membranes were probed with HDAC5 Antibody (Abcam, #ab55403, Cambridge, United Kingdom) and then probed with anti-rabbit IgG Antibody (Cell Signaling, #7074P2, Danvers, MA, United States). After washing with TBS-T, the membranes were visualized with SuperSignal West Pico PLUS substrate (Thermo Fisher Scientific Inc., Waltham, MA, United States). GAPDH Antibody (Cell Signaling, #5174S, Danvers, MA, United States) was used as a loading control.

Library construction, RNA-seq, and data analysis

The total RNA isolated from each lung tissue sample was applied to RNA-Seq library preparation, by following the protocol described before (Zhu et al., 2018). Briefly, the mRNA was purified by oligo dT-attached magnetic beads and fragmented into small pieces, followed by first-strand and second-strand cDNA synthesis. After PCR amplification, purification, heat denaturation and cyclization, the final cDNA library was sequenced on the BGISEQ-500 platform (BGI-Shenzhen, China) using 50-bp single reads.

The sequencing data was filtered with SOAPnuke (v1.5.2; Li et al., 2008) by (1) Removing reads containing sequencing adapter; (2) Removing reads whose low-quality base ratio (base quality less than or equal to 5) is more than 20%; (3) Removing reads whose unknown base ("N" base) ratio is more than 5%, afterwards clean reads were obtained and stored in FASTQ format. The clean reads were mapped to the reference genome using HISAT2 (v2.0.4; Kim et al., 2015). Bowtie2 (v2.2.5; Langmead and Salzberg, 2012) was applied to align the clean reads to the reference coding gene set, then expression level of gene was calculated by RSEM (v1.2.12; Li and Dewey, 2011). Essentially, differential expression analysis was performed using the DESeq2 (v1.4.5; Love et al., 2014). with $|\log2 \text{ (Fold change)}| > 0.4$ and Q value ≤ 0.05. The heatmap was drawn by pheatmap (v1.0.8) according to the gene expression level calculated by RSEM (v1.2.12). GO (Gene Ontology) and KEGG (Kyoto Encyclopedia of Genes and Genome) enrichment analysis of annotated different expressed gene was performed by Phyper based on Hypergeomertric test. The significant levels of terms and pathways were corrected by Q value with a rigorous threshold (Q value ≤ 0.05) by Bonferroni.

Statistical analysis

Data are expressed as the mean ± SEM (standard error of the mean). All experiments were repeated at least three times. Student's two-tailed *t*-test was used for comparing differences between two groups. One-way or two-way ANOVA followed by Tukey–Kramer's multiple-comparison test was used for multiple comparisons. Significance was set at $p < 0.05$. GraphPad Prism software (version 8.0, San Diego, United States) was used for statistical analysis.

Data availability statement

The datasets presented in this study can be found in online repositories. The names of the repository/repositories and accession number (s) can be found at: https://nmdc.cn/, NMDC40015167. https://ngdc.cncb.ac.cn/gsa, GSA: CRA008629.

Ethics statement

The studies involving human participants were reviewed and approved by the Institutional Review Board of the Affiliated Hospital of Jiangnan University. The patients/participants provided their written informed consent to participate in this study. The animal study was reviewed and approved by the Committee of Ethics in Jiangnan University.

Author contributions

JS, YN, YG, and QY conceived and designed the study. JS, YN, QG, RL, and HC performed the experiments. JS, YN, QG, and RL performed the data analysis and bioinformatics analysis. JS wrote the manuscript. HC commented on the study. YG revised the manuscript. YG and QY approved submission of the manuscript. All authors contributed to the article and approved the submitted version.

Funding

This work was supported by the grant from the Innovation Team of Wuxi Health and Family Planning Commission (CXTD2021005), Project of Taihu Talent Plan, and Qing Lan Project in Jiangsu Province.

Conflict of interest

The authors declare that the research was conducted in the absence of any commercial or financial relationships that could be construed as a potential conflict of interest.

Publisher's note

All claims expressed in this article are solely those of the authors and do not necessarily represent those of their affiliated organizations, or those of the publisher, the editors and the reviewers. Any product that may be evaluated in this article, or claim that may be made by its manufacturer, is not guaranteed or endorsed by the publisher.

Supplementary material

The Supplementary material for this article can be found online at: https://www.frontiersin.org/articles/10.3389/fmicb.2023.1121863/full#supplementary-material

References

Akopyan, G., and Bonavida, B. (2006). Understanding tobacco smoke carcinogen NNK and lung tumorigenesis. *Int. J. Oncol.* 29, 745–752. doi: 10.3892/ijo.29.4.745

An, S. Q., and Berg, G. (2018). Stenotrophomonas maltophilia. *Trends Microbiol.* 26, 637–638. doi: 10.1016/j.tim.2018.04.006, [published Online First: 2018/05/15]

Banerjee, S., Tian, T., Wei, Z., Shih, N., Feldman, M. D., Peck, K. N., et al. (2018). Distinct microbial signatures associated with different breast cancer types. *Front. Microbiol.* 9:951. doi: 10.3389/fmicb.2018.00951

Batra, P., Mathur, P., and Misra, M. C. (2017). Clinical characteristics and prognostic factors of patients with *Stenotrophomonas maltophilia* infections. *J. Lab. Phys.* 9, 132–135. doi: 10.4103/0974-2727.199639 [published Online First: 2017/04/04

Brooke, J. S. (2012). *Stenotrophomonas maltophilia*: an emerging global opportunistic pathogen. *Clin. Microbiol. Rev.* 25, 2–41. doi: 10.1128/CMR.00019-11 [published Online First: 2012/01/11]

Brooke, J. S. (2021). Advances in the microbiology of *Stenotrophomonas maltophilia*. *Clin. Microbiol. Rev.* 34:e0003019. doi: 10.1128/CMR.00030-19

Cao, X., Liu, D. H., Zhou, Y., Yan, X. M., Yuan, L. Q., and Pan, J. (2016). Histone deacetylase 5 promotes Wilms' tumor cell proliferation through the upregulation of c-met. *Mol. Med. Rep.* 13, 2745–2750. doi: 10.3892/mmr.2016.4828

Cao, C., Vasilatos, S. N., Bhargava, R., Fine, J. L., Oesterreich, S., Davidson, N. E., et al. (2017). Functional interaction of histone deacetylase 5 (HDAC5) and lysine-specific demethylase 1 (LSD1) promotes breast cancer progression. *Oncogene* 36, 133–145. doi:10.1038/onc.2016.186.

Chaturvedi, A. K., Gaydos, C. A., Agreda, P., Holden, J. P., Chatterjee, N., and Goedert, J. J. (2010). Chlamydia pneumoniae infection and risk for lung cancer. *Cancer Epidemiol. Biomark. Prev.* 19, 1498–1505. doi: 10.1158/1055-9965.EPI-09-1261

Chen, J., Xia, J., Yu, Y. L., Wang, S. Q., Wei, Y. B., Chen, F. Y., et al. (2014). HDAC5 promotes osteosarcoma progression by upregulation of twist 1 expression. *Tum. Biol.* 35, 1383–1387. doi: 10.1007/s13277-013-1189-x

Cribbs, S. K., Crothers, K., and Morris, A. (2020). Pathogenesis of HIV-related lung disease: immunity, infection, and inflammation. *Physiol. Rev.* 100, 603–632. doi: 10.1152/physrev.00039.2018

Dapito, D. H., Mencin, A., Gwak, G. Y., Pradere, J. P., Jang, M. K., Mederacke, I., et al. (2012). Promotion of hepatocellular carcinoma by the intestinal microbiota and TLR4. *Cancer Cell* 21, 504–516. doi: 10.1016/j.ccr.2012.02.007

de Ruijter, A. J., van Gennip, A. H., Caron, H. N., Kemp, S., and van Kuilenburg, A. B. (2003). Histone deacetylases (HDACs): characterization of the classical HDAC family. *Biochem. J.* 370, 737–749. doi: 10.1042/BJ20021321

Detterbeck, F. C., Chansky, K., Groome, P., Bolejack, V., Crowley, J., Shemanski, L., et al. (2016). The IASLC lung cancer staging project: methodology and validation used in the development of proposals for revision of the stage classification of NSCLC in the forthcoming (eighth) edition of the TNM classification of lung cancer. *J. Thoracic Oncol.* 11, 1433–1446. doi: 10.1016/j.jtho.2016.06.028

Dima, E., Kyriakoudi, A., Kaponi, M., Vasileiadis, I., Stamou, P., Koutsoukou, A., et al. (2019). The lung microbiome dynamics between stability and exacerbation in chronic obstructive pulmonary disease (COPD): current perspectives. *Respir. Med.* 157, 1–6. doi: 10.1016/j.rmed.2019.08.012

Drewes, J. L., Chen, J., Markham, N. O., Knippel, R. J., Domingue, J. C., Tam, A. J., et al. (2022). Human colon cancer-derived Clostridioides difficile strains drive colonic tumorigenesis in mice. *Cancer Discov.* 12, 1873–1885. doi: 10.1158/2159-8290.CD-21-1273

Dumont-Leblond, N., Veillette, M., Racine, C., Joubert, P., and Duchaine, C. (2021). Non-small cell lung cancer microbiota characterization: prevalence of enteric and potentially pathogenic bacteria in cancer tissues. *PLoS One* 16:e0249832. doi: 10.1371/journal.pone.0249832

DuPage, M., Dooley, A. L., and Jacks, T. (2009). Conditional mouse lung cancer models using adenoviral or lentiviral delivery of Cre recombinase. *Nat. Protoc.* 4, 1064–1072. doi: 10.1038/nprot.2009.95

Fu, A., Yao, B., Dong, T., Chen, Y., Yao, J., Liu, Y., et al. (2022). Tumor-resident intracellular microbiota promotes metastatic colonization in breast cancer. *Cells* 185, 1356–1372.e26. doi: 10.1016/j.cell.2022.02.027

Geller, L. T., Barzily-Rokni, M., Danino, T., Jonas, O. H., Shental, N., Nejman, D., et al. (2017). Potential role of intratumor bacteria in mediating tumor resistance to the chemotherapeutic drug gemcitabine. *Science* 357, 1156–1160. doi: 10.1126/science.aah5043

Gong, S., Ying, L., Fan, Y., and Sun, Z. (2020). Fentanyl inhibits lung cancer viability and invasion via upregulation of miR-331-3p and repression of HDAC5. *Onco. Targets. Ther.* 13, 13131–13141. doi: 10.2147/OTT.S281095

Huang, C., and Shi, G. (2019). Smoking and microbiome in oral, airway, gut and some systemic diseases. *J. Transl. Med.* 17:225. doi: 10.1186/s12967-019-1971-7

Jemal, A., Miller, K. D., Ma, J., Siegel, R. L., Fedewa, S. A., Islami, F., et al. (2018). Higher lung cancer incidence in young women than young men in the United States. *N. Engl. J. Med.* 378, 1999–2009. doi: 10.1056/NEJMoa1715907

Jin, C., Lagoudas, G. K., Zhao, C., Bullman, S., Bhutkar, A., Hu, B., et al. (2019). Commensal microbiota promote lung cancer development via gammadelta T cells. *Cells* 176, 998–1013.e16. doi: 10.1016/j.cell.2018.12.040

Kenfield, S. A., Wei, E. K., Stampfer, M. J., Rosner, B. A., and Colditz, G. A. (2008). Comparison of aspects of smoking among the four histological types of lung cancer. *Tob. Control.* 17, 198–204. doi: 10.1136/tc.2007.022582

Kim, H., Goo, J. M., Suh, Y. J., Park, C. M., and Kim, Y. T. (2019). Implication of total tumor size on the prognosis of patients with clinical stage IA lung adenocarcinomas appearing as part-solid nodules: does only the solid portion size matter? *Eur. Radiol.* 29, 1586–1594. doi: 10.1007/s00330-018-5685-7

Kim, D., Langmead, B., and Salzberg, S. L. (2015). HISAT: a fast spliced aligner with low memory requirements. *Nat. Methods* 12, 357–360. doi: 10.1038/nmeth.3317

Langmead, B., and Salzberg, S. L. (2012). Fast gapped-read alignment with bowtie 2. *Nat. Methods* 9, 357–359. doi: 10.1038/nmeth.1923

Le Noci, V., Guglielmetti, S., Arioli, S., Camisaschi, C., Bianchi, F., and Sommariva, M. (2018). Modulation of pulmonary microbiota by antibiotic or probiotic aerosol therapy: a strategy to promote Immunosurveillance against lung metastases. *Cell Rep.* 24, 3528–3538. doi: 10.1016/j.celrep.2018.08.090

Lee, S. H., Sung, J. Y., Yong, D., Chun, J., Kim, S. Y., Song, J. H., et al. (2016). Characterization of microbiome in bronchoalveolar lavage fluid of patients with lung cancer comparing with benign mass like lesions. *Lung Cancer* 102, 89–95. doi: 10.1016/j.lungcan.2016.10.016

Li, B., and Dewey, C. N. (2011). RSEM: accurate transcript quantification from RNA-Seq data with or without a reference genome. *BMC Bioinformatics* 12:323. doi: 10.1186/1471-2105-12-323

Li, R., Li, Y., Kristiansen, K., and Wang, J. (2008). SOAP: short oligonucleotide alignment program. *Bioinformatics* 24, 713–714. doi: 10.1093/bioinformatics/btn025

Li, A., Liu, Z., Li, M., Zhou, S., Xu, Y., Xiao, Y., et al. (2016). HDAC5, a potential therapeutic target and prognostic biomarker, promotes proliferation, invasion and migration in human breast cancer. *Oncotarget* 7, 37966–37978. doi: 10.18632/oncotarget.9274

Li, J., Sung, C. Y., Lee, N., Ni, Y., Pihlajamäki, J., Panagiotou, G., et al. (2016). Probiotics modulated gut microbiota suppresses hepatocellular carcinoma growth in mice. *Proc. Natl. Acad. Sci. U. S. A.* 113, E1306–E1315. doi: 10.1073/pnas.1518189113, 26884164

Li, Y., Tinoco, R., Elmen, L., Segota, I., Xian, Y., and Fujita, Y. (2019). Gut microbiota dependent anti-tumor immunity restricts melanoma growth in Rnf5 (−/−) mice. *Nat. Commun.* 10:1492. doi: 10.1038/s41467-019-09525-y

Liu, Q., Zheng, J. M., Chen, J. K., Yan, X. L., Chen, H. M., and Nong, W. X. (2014). Histone deacetylase 5 promotes the proliferation of glioma cells by upregulation of notch 1. *Mol. Med. Rep.* 10, 2045–2050. doi: 10.3892/mmr.2014.2395

Liu, B., Zhou, Z., Jin, Y., Lu, J., Feng, D., Peng, R., et al. (2022). Hepatic stellate cell activation and senescence induced by intrahepatic microbiota disturbances drive progression of liver cirrhosis toward hepatocellular carcinoma. *J. Immunother. Cancer* 10:e003069. doi: 10.1136/jitc-2021-003069

Love, M. I., Huber, W., and Anders, S. (2014). Moderated estimation of fold change and dispersion for RNA-seq data with DESeq2. *Genome Biol.* 15:550. doi: 10.1186/s13059-014-0550-8

Nejman, D., Livyatan, I., Fuks, G., Gavert, N., Zwang, Y., Geller, L. T., et al. (2020). The human tumor microbiome is composed of tumor type-specific intracellular bacteria. *Science* 368, 973–980. doi: 10.1126/science.aay9189

Oltra, S. S., Cejalvo, J. M., Tormo, E., Albanell, M., Ferrer, A., Nacher, M., et al. (2020). HDAC5 inhibitors as a potential treatment in breast cancer affecting very young women. *Cancers* 12:412. doi: 10.3390/cancers12020412

Parhi, L., Alon-Maimon, T., Sol, A., Nejman, D., Shhadeh, A., Fainsod-Levi, T., et al. (2020). Breast cancer colonization by *Fusobacterium nucleatum* accelerates tumor growth and metastatic progression. *Nat. Commun.* 11:3259. doi: 10.1038/s41467-020-16967-2

Rami-Porta, R., Asamura, H., Travis, W. D., and Rusch, V. W. (2017). Lung cancer - major changes in the American joint committee on cancer eighth edition cancer staging manual. *CA Cancer J. Clin.* 67, 138–155. doi: 10.3322/caac.21390

Riquelme, E., Zhang, Y., Zhang, L., Montiel, M., Zoltan, M., Dong, W., et al. (2019). Tumor microbiome diversity and composition influence pancreatic cancer outcomes. *Cells* 178, 795–806.e12. doi: 10.1016/j.cell.2019.07.008

Rouf, R., Karaba, S. M., Dao, J., and Cianciotto, N. P. (2011). *Stenotrophomonas maltophilia* strains replicate and persist in the murine lung, but to significantly different degrees. *Microbiology* 157, 2133–2142. doi: 10.1099/mic.0.048157-0

Samet, J. M., Avila-Tang, E., Boffetta, P., Hannan, L. M., Olivo-Marston, S., Thun, M. J., et al. (2009). Lung cancer in never smokers: clinical epidemiology and environmental risk factors. *Clin. Cancer Res.* 15, 5626–5645. doi: 10.1158/1078-0432.CCR-09-0376

Schuller, H. M. (2002). Mechanisms of smoking-related lung and pancreatic adenocarcinoma development. *Nat. Rev. Cancer* 2, 455–463. doi: 10.1038/nrc824

Segata, N., Izard, J., Waldron, L., Gevers, D., Miropolsky, L., Garrett, W. S., et al. (2011). Metagenomic biomarker discovery and explanation. *Genome Biol.* 12:R60. doi: 10.1186/gb-2011-12-6-r60

Stypula-Cyrus, Y., Damania, D., Kunte, D. P., Cruz, M. D., Subramanian, H., Roy, H. K., et al. (2013). HDAC up-regulation in early colon field carcinogenesis is involved in cell tumorigenicity through regulation of chromatin structure. *PLoS One* 8:e64600. doi: 10.1371/journal.pone.0064600

Sung, H., Ferlay, J., Siegel, R. L., Laversanne, M., Soerjomataram, I., Jemal, A., et al. (2020). GLOBOCAN estimates of incidence and mortality worldwide for 36 cancers in 185 countries. *CA Cancer J. Clin.* 71, 209–249. doi: 10.3322/caac.21660

Tsay, J. J., Wu, B. G., Sulaiman, I., Gershner, K., Schluger, R., and Li, Y. (2020). Lower airway dysbiosis affects lung cancer progression. *Cancer Discov.* 11, 293–307. doi: 10.1158/2159-8290.Cd-20-0263 [published Online First: 2020/11/13]

Yang, J., Gong, C., Ke, Q., Fang, Z., Chen, X., Ye, M., et al. (2021). Insights into the function and clinical application of HDAC5 in cancer management. *Front. Oncol.* 11:661620. doi: 10.3389/fonc.2021.661620 [published Online First: 2021/06/29]

Yu, T., Guo, F., Yu, Y., Sun, T., Ma, D., Han, J., et al. (2017). *Fusobacterium nucleatum* promotes Chemoresistance to colorectal cancer by modulating autophagy. *Cells* 170, 548–563.e16. doi: 10.1016/j.cell.2017.07.008

Yu, Y. H., Liao, C. C., Hsu, W. H., Chen, H. J., Liao, W. C., Muo, C. H., et al. (2011). Increased lung cancer risk among patients with pulmonary tuberculosis: a population cohort study. *J. Thoracic Oncol.* 6, 32–37. doi: 10.1097/JTO.0b013e3181fb4fcc

Zhong, L., Sun, S., Yao, S., Han, X., Gu, M., and Shi, J. (2018). Histone deacetylase 5 promotes the proliferation and invasion of lung cancer cells. *Oncol. Rep.* 40, 2224–2232. doi: 10.3892/or.2018.6591

Zhu, F. Y., Chen, M. X., Ye, N. H., Qiao, W. M., Gao, B., Law, W. K., et al. (2018). Comparative performance of the BGISEQ-500 and Illumina HiSeq4000 sequencing platforms for transcriptome analysis in plants. *Plant Methods* 14:69. doi: 10.1186/s13007-018-0337-0

frontiers | Frontiers in Microbiology

TYPE Review
PUBLISHED 07 February 2023
DOI 10.3389/fmicb.2023.1115556

OPEN ACCESS

EDITED BY
Yuan Xiao,
Shanghai Jiao Tong University,
China

REVIEWED BY
Armando Rojas,
Catholic University of the Maule, Chile
Sunil Banskar,
University of Arizona,
United States

*CORRESPONDENCE
Xiaoyuan Lin
✉ lxy2019@cqu.edu.cn
Haibo Wu
✉ hbwu023@cqu.edu.cn

†These authors have contributed equally to this work and share first authorship

SPECIALTY SECTION
This article was submitted to Infectious Agents and Disease, a section of the journal Frontiers in Microbiology

RECEIVED 04 December 2022
ACCEPTED 12 January 2023
PUBLISHED 07 February 2023

CITATION
Xu S, Xiong Y, Fu B, Guo D, Sha Z, Lin X and Wu H (2023) Bacteria and macrophages in the tumor microenvironment.
Front. Microbiol. 14:1115556.
doi: 10.3389/fmicb.2023.1115556

Bacteria and macrophages in the tumor microenvironment

Shiyao Xu†, Yan Xiong†, Beibei Fu, Dong Guo, Zhou Sha, Xiaoyuan Lin* and Haibo Wu*

School of Life Sciences, Chongqing University, Chongqing, China

Cancer and microbial infections are significant worldwide health challenges. Numerous studies have demonstrated that bacteria may contribute to the emergence of cancer. In this review, we assemble bacterial species discovered in various cancers to describe their variety and specificity. The relationship between bacteria and macrophages in cancer is also highlighted, and we look for ample proof to establish a biological basis for bacterial-induced macrophage polarization. Finally, we quickly go over the potential roles of metabolites, cytokines, and microRNAs in the regulation of the tumor microenvironment by bacterially activated macrophages. The complexity of bacteria and macrophages in cancer will be revealed as we gain a better understanding of their pathogenic mechanisms, which will lead to new therapeutic approaches for both inflammatory illnesses and cancer.

KEYWORDS

bacteria, cancer, tumor-associated macrophages, M1/M2 macrophage polarization, tumor microenvironment

1. Bacterial diversity in different cancers

The immune system was traditionally thought to render tumors sterile. Thanks to technological advancements, numerous investigations in recent years have discovered that bacteria are prevalent in cancer. Many tumors' early stages are challenging to recognize, and most malignancies have metastasized by the time of initial diagnosis. The classification of these bacteria may be able to provide us with some information. Testing of bacterial DNA has shown that each cancer type, including those not directly related to the external environment, has a different bacterial composition (Nejman et al., 2020). The goal of this section is to give a summary of the bacteria found in cancer tissue. To gather and compile the microorganisms, we specialize in nine common cancer types: colorectal, gastric, esophageal, pancreatic, gallbladder, lung, breast, cervical, and prostate (Table 1). Pathogenic bacteria and human commensal microorganisms frequently coexist in the enormous and complex microbial community that makes up the human gastrointestinal tract. The gastrointestinal microbiome has a significant impact on metabolic health and general health, and it is also the microbiome that has been studied the most in-depth and is used as a model to study host-microbiota interactions and disorders. In addition to being infrequently researched, the quantity of microbiota living in the other organs is substantially lower than that of the gut and stomach (Sepich-Poore et al., 2021). It's uncertain how many and how diverse the bacteria are in cancer samples as compared to samples taken from healthy people. The quantity and diversity of bacteria are greater in breast tumor samples than in healthy, normal breast samples (Nejman et al., 2020). Breast cancer tissues of various grades and histological classifications and normal breast tissue differ greatly in terms of their bacterial composition (Nejman et al., 2020). Instead, the lung cancer tissue microbiome is less varied than the corresponding normal tissue microbiome (Peters et al., 2019). In reality, only one specific bacterial species, *Helicobacter pylori*, which is linked to gastric cancer designated by the World Health Organization as a class I carcinogen (Lunn et al., 2022), and research into other bacterial species' potential roles as biomarkers in the majority of cancer types

TABLE 1 Summary of the cancer microbiome.

Cancer	Phylum	Genus	References
Colorectal cancer	*Bacteroidetes*	*Bacteroides*	Nejman et al. (2020), Wu et al. (2013), Bullman et al. (2017), Dejea et al. (2018), Kwong et al. (2018), Yachida et al. (2019)
Colorectal cancer	*Bacteroidetes*	*Prevotella*	Bullman et al. (2017), Dejea et al. (2018), Kwong et al. (2018), Wirbel et al. (2019)
Colorectal cancer	*Bacteroidetes*	*Porphyromonas*	Yachida et al. (2019), Wirbel et al. (2019), Thomas et al. (2019)
Colorectal cancer	*Firmicutes*	*Peptostreptococcus; Solobacterium*	Kwong et al. (2018), Wirbel et al. (2019), Thomas et al. (2019)
Colorectal cancer	*Firmicutes*	*Streptococcus*	Kwong et al. (2018), Yachida et al. (2019)
Colorectal cancer	*Firmicutes*	*Clostridium; Gemella*	Kwong et al. (2018), Wirbel et al. (2019))
Colorectal cancer	*Firmicutes*	*Lachnospiraceae*	Dejea et al. (2018), Yachida et al. (2019)
Colorectal cancer	*Firmicutes*	*Roseburia*	Coutzac et al. (2020)
Colorectal cancer	*Proteobacteria*	*Escherichia*	Arthur et al. (2012), Dejea et al. (2018), Thomas et al. (2019), Wilson et al. (2019), Pleguezuelos-Manzano et al. (2020)
Colorectal cancer	*Proteobacteria*	*Campylobacter*	He et al. (2019)
Colorectal cancer	*Actinobacteria*	*Bifidobacterium*	Shi et al. (2020)
Colorectal cancer	*Actinobacteria*	*Parvimonas*	Kwong et al. (2018), Yachida et al. (2019), Wirbel et al. (2019), Thomas et al. (2019)
Colorectal cancer	*Fusobacteria*	*Fusobacterium*	Wu et al. (2013), Bullman et al. (2017), Dejea et al. (2018), Kwong et al. (2018), Yachida et al. (2019), Wirbel et al. (2019), Thomas et al. (2019), Mima et al. (2016), Mima et al. (2015), Castellarin et al. (2012), Kostic et al. (2012), Kostic et al. (2013), Rubinstein et al. (2013), Eklof et al. (2017), Yu et al. (2017), Garrett (2019), Abed et al. (2020)
Stomach cancer	*Bacteroidetes*	*Alloprevotella*	Aviles-Jimenez et al. (2014), Roberts et al. (2002)
Stomach cancer	*Firmicutes*	*Parvimonas*	Aviles-Jimenez et al. (2014), Roberts et al. (2002), Coker et al. (2018), Nagano et al. (2019), Baghban and Gupta (2016), Kim et al. (2010)
Stomach cancer	*Firmicutes*	*Dialister*	Aviles-Jimenez et al. (2014), Roberts et al. (2002), Coker et al. (2018), Nagano et al. (2019), Wang L. L. et al. (2014)
Stomach cancer	*Firmicutes*	*Streptococcus*	Coker et al. (2018), Nagano et al. (2019), Hsieh et al. (2018), Li et al. (2016), Zhao et al. (2015)
Stomach cancer	*Firmicutes*	*Slackia*	Aviles-Jimenez et al. (2014), Roberts et al. (2002), Coker et al. (2018), Nagano et al. (2019), Schulz et al. (2019), Contreras et al. (2000)
Stomach cancer	*Firmicutes*	*Lactobacillus*	Aviles-Jimenez et al. (2014), Hsieh et al. (2018)
Stomach cancer	*Firmicutes*	*Clostridium*	Hsieh et al. (2018), Salazar et al. (2013)
Stomach cancer	*Firmicutes*	*Staphylococcus*	Roberts et al. (2002), Weng et al. (2019)
Stomach cancer	*Firmicutes*	*Veillonella*	Dias-Jacome et al. (2016)
Stomach cancer	*Proteobacteria*	*Helicobacter*	Hsieh et al. (2018), Suzuki et al. (2009)
Stomach cancer	*Proteobacteria*	*Neisseria*	Aviles-Jimenez et al. (2014), Li et al. (2016)
Stomach cancer	*Proteobacteria*	*Sphingobium*	Dias-Jacome et al. (2016)
Stomach cancer	*Proteobacteria*	*Escherichia; Burkholderia*	Li et al. (2016)
Stomach cancer	*Fusobacteria*	*Fusobacterium*	Hsieh et al. (2018)
Esophageal cancer	*Firmicutes*	*Lactobacillus; Streptococcus*	Elliott et al. (2017)
Esophageal cancer	*Fusobacteria*	*Fusobacterium*	Yamamura et al. (2016)
Pancreatic cancer	*Bacteroidetes*	*Porphyromonas*	Poore et al. (2020), Riquelme et al. (2019), Pushalkar et al. (2018), Geller et al. (2017)
Pancreatic cancer	*Firmicutes*	*Streptococcus; Granulicatella*	Farrell et al. (2012)
Pancreatic cancer	*Proteobacteria*	*Pseudoxanthomonas*	Riquelme et al. (2019)
Pancreatic cancer	*Proteobacteria*	*Neisseria*	Farrell et al. (2012)
Pancreatic cancer	*Actinobacteria*	*Saccharopolyspora; Streptomyces*	Riquelme et al. (2019), Geller et al. (2017)
Gallbladder cancer	*Bacteroidetes*	*Bacteroidaceae; Prevotellaceae; Porphyromonadaceae*	Molinero et al. (2019)
Gallbladder cancer	*Firmicutes*	*Veillonellaceae*	Molinero et al. (2019)
Gallbladder cancer	*Proteobacteria*	*Salmonella*	Dutta et al. (2000), Nagaraja and Eslick (2014), Nath et al. (2008), Nath et al. (2010)
Gallbladder cancer	*Proteobacteria*	*Helicobacter*	de Martel et al. (2009), Pradhan and Dali (2004), Murata et al. (2004)

(Continued)

TABLE 1 (Continued)

Cancer	Phylum	Genus	References
Gallbladder cancer	*Proteobacteria*	*Escherichia*	Tsuchiya et al. (2018)
Gallbladder cancer	*Proteobacteria*	*Enterobacteriaceae*	Tsuchiya et al. (2018)
Gallbladder cancer	*Fusobacteria*	*Fusobacterium*	Tsuchiya et al. (2018)
Lung cancer	*Bacteroidetes*	*Prevotella*	Tsay et al. (2018), Dickson et al. (2016), Tsay et al. (2021)
Lung cancer	*Bacteroidetes*	*Capnocytophaga*	Liu et al. (2018), Yan et al. (2015)
Lung cancer	*Firmicutes*	*Streptococcus*	Tsay et al. (2018), Dickson et al. (2016), Tsay et al. (2021), Liu et al. (2018), Apostolou et al. (2011), Laroumagne et al. (2013), Hosgood et al. (2014), Cameron et al. (2017)
Lung cancer	*Firmicutes*	*Veillonella*	Tsay et al. (2018), Dickson et al. (2016), Tsay et al. (2021), Yan et al. (2015), Lee et al. (2016)
Lung cancer	*Firmicutes*	*Staphylococcus*	Dickson et al. (2016), Laroumagne et al. (2013)
Lung cancer	*Firmicutes*	*Lactobacillus*	Tsay et al. (2021), Jin et al. (2019)
Lung cancer	*Firmicutes*	*Gemella*	Tsay et al. (2021)
Lung cancer	*Firmicutes*	*Selenomonas*	Yan et al. (2015)
Lung cancer	*Firmicutes*	*Enterococcus*	Cameron et al. (2017)
Lung cancer	*Firmicutes*	*Megasphaera*	Lee et al. (2016)
Lung cancer	*Proteobacteria*	*Enterobacter*	Dickson and Huffnagle (2015), Gomes et al. (2019), Laroumagne et al. (2013), Cameron et al. (2017)
Lung cancer	*Proteobacteria*	*Acinetobacter*	Gomes et al. (2019), Cameron et al. (2017)
Lung cancer	*Proteobacteria*	*Haemophilus*	Tsay et al. (2021), Laroumagne et al. (2013)
Lung cancer	*Proteobacteria*	*Burkholderia*	Dickson et al. (2016), Tsay et al. (2021)
Lung cancer	*Proteobacteria*	*Moraxella*	Tsay et al. (2021)
Lung cancer	*Proteobacteria*	*Neisseria*	Yan et al. (2015)
Lung cancer	*Proteobacteria*	*Noviherbaspirillum; Aggregatibacter*	Jin et al. (2019)
Lung cancer	*Proteobacteria*	*Brevundimonas*	Dickson and Huffnagle (2015), Gomes et al. (2019)
Lung cancer	*Proteobacteria*	*Acidovorax*	Greathouse et al. (2018)
Lung cancer	*Proteobacteria*	*Morganella; Escherichia*	Le Noci et al. (2018)
Lung cancer	*Proteobacteria*	*Legionella*	Yu et al. (2016)
Lung cancer	*Actinobacteria*	*Rothia*	Tsay et al. (2018), Tsay et al. (2021)
Lung cancer	*Actinobacteria*	*Propionibacterium*	Dickson and Huffnagle (2015), Gomes et al. (2019)
Lung cancer	*Fusobacteria*	*Fusobacterium*	Tsay et al. (2021)
Lung cancer	*Deinococcus-Thermus*	*Thermus*	Yu et al. (2016)
Lung cancer	*Verrucomicrobia*	*Akkermansia*	Derosa et al. (2018), Routy et al. (2018)
Breast cancer	*Firmicutes*	*Bacillus; Staphylococcus*	Urbaniak et al. (2016)
Breast cancer	*Proteobacteria*	*Enterococcus*	Urbaniak et al. (2016)
Breast cancer	*Fusobacteria*	*Fusobacterium*	Parhi et al. (2020)
Cervical cancer	*Bacteroidetes*	*Prevotella*	So et al. (2020), Onderdonk et al. (2016)
Cervical cancer	*Firmicutes*	*Lactobacillus*	Poore et al. (2020), Pearce et al. (2014)
Cervical cancer	*Firmicutes*	*Dialister; Finegoldia Magna; Peptoniphilus*	So et al. (2020)
Cervical cancer	*Firmicutes*	*Parvimonas; Peptostreptococcus; Anaerococcus*	Onderdonk et al. (2016)
Cervical cancer	*Firmicutes*	*Clostridium*	Donders et al. (2017)
Cervical cancer	*Firmicutes*	*Streptococcus*	Donders et al. (2017), Liu et al. (2020)
Cervical cancer	*Firmicutes*	*Megasphaera*	Onderdonk et al. (2016), Fredricks et al. (2005)
Cervical cancer	*Proteobacteria*	*Hydrogenophilus; Burkholderia*	Zhou Y. et al. (2019)
Cervical cancer	*Actinobacteria*	*Atopobium*	So et al. (2020), Onderdonk et al. (2016), Fredricks et al. (2005), Gondwe et al. (2020)

(Continued)

TABLE 1 (Continued)

Cancer	Phylum	Genus	References
Cervical cancer	*Actinobacteria*	*Gardnerella*	So et al. (2020), Onderdonk et al. (2016), Pearce et al. (2014), Zhou Y. et al. (2019)
Cervical cancer	*Actinobacteria*	*Eggerthella*	Fredricks et al. (2005)
Cervical cancer	*Actinobacteria*	*Bifidobacterium*	Zhou Y. et al. (2019)
Cervical cancer	*Fusobacteria*	*Sneathia*	Onderdonk et al. (2016), Zhou Y. et al. (2019), Gondwe et al. (2020), Lee et al. (2013), Mitra et al. (2015), Audirac-Chalifour et al. (2016), Di Paola et al. (2017), Laniewski et al. (2018)
Cervical cancer	*Fusobacteria*	*leptotrichia*	Fredricks et al. (2005)
Cervical cancer	*Fusobacteria*	*Fusobacterium*	Zhou Y. et al. (2019)
Prostate cancer	*Bacteroidetes*	*Bacteroides*	Keay et al. (1999), Golombos et al. (2018), Liss et al. (2018), Alanee et al. (2019)
Prostate cancer	*Firmicutes*	*Staphylococcus*	Shrestha et al. (2018), Cavarretta et al. (2017)
Prostate cancer	*Firmicutes*	*Streptococcus*	Shrestha et al. (2018), Liss et al. (2018)
Prostate cancer	*Firmicutes*	*Faecalibacterium*	Miquel et al. (2013), Sokol et al. (2008)
Prostate cancer	*Firmicutes*	*Clostridium*	Ridlon et al. (2013)
Prostate cancer	*Proteobacteria*	*Escherichia*	Keay et al. (1999), Leskinen et al. (2003)
Prostate Cancer	*Proteobacteria*	*Proteus; Aeromonas*	Leskinen et al. (2003)
Prostate cancer	*Proteobacteria*	*Campylobacter*	Lara-Tejero and Galan (2000)
Prostate cancer	*Actinobacteria*	*Propionibacterium*	Sfanos et al. (2008), Cavarretta et al. (2017), Cohen et al. (2005)
Prostate cancer	*Actinobacteria*	*Corynebacterium*	Shrestha et al. (2018), Daisley et al. (2020)
Prostate cancer	*Verrucomicrobia*	*Akkermansiaceae*	Daisley et al. (2020)

The species of bacteria have been reported in studies that present in cancer.

has not yet produced any conclusive findings (Scott et al., 2019). There is a large variety of microbial taxa with variable abundance but little overlap in studies of males with prostate cancer (Shrestha et al., 2018). Not only is there a microbiota within cancer, but crosstalk occurs in all organs of the body. The proliferation and composition of bacteria where not in direct contact with the outside world, to some extent, represent the bacteria that can be transferred from one organ to another. The microbiological makeup of the lungs is more similar to that of the oropharynx, and enteric organisms are the primary source of bacterial DNA in cancer patients' pancreas tissue (Dickson and Huffnagle, 2015). Thanks to developments in polymerase chain reaction and metagenomics, we can now identify microbes more precisely. The researchers distinguish the microbiota of lung cancer tissue using different biological materials, such as bronchial or bronchoalveolar lavage fluid or sputum (Gomes et al., 2019), and the microbiota of prostate cancer using feces or urine microbiomes (Sfanos et al., 2008). But in every experiment, skin-associated germs could contaminate the reagents by transferring them from the personnel's skin. Cancer-associated microbes in general are sometimes difficult to distinguish, and the study of particular bacteria in malignancies is still in its early stages.

2. Macrophages in the tumor microenvironment

Macrophages are multipurpose immune cells that perform a variety of tasks, such as regulating tissue homeostasis, protecting against infections, and accelerating wound healing (Wynn and Vannella, 2016). Macrophages are found in peripheral organs because these immunological sentinel cells are crucial in keeping an eye out for invasive infections in the surrounding tissue (Sfanos et al., 2008). When a host is infected by a pathogen, monocytes are drawn to the invasion sites and cytokines are released, which prompt additional immune responses from other immune cells. Indeed, bacteria and their metabolites have recently been shown to affect macrophages and tumor microenvironments. Numerous disorders, including cancer and infections for which there is yet no clear direct link, are affected by macrophage activation. Here, we discuss macrophages from three angles: their origin, their activation indicators, and the bacterial collection that causes them to become polarized. We just briefly touch on the preceding two aspects, because they have recently been discussed (Murray et al., 2014; Wynn and Vannella, 2016; Shapouri-Moghaddam et al., 2018; Christofides et al., 2022). Instead, we focus on the results of macrophage polarization caused by certain bacteria.

2.1. The source of macrophages

All tissues have macrophages, a kind of leukocyte that is divided into various subpopulations according to where it is found and how it functions. Macrophages come from two different origins. On the other hand, tissue-resident macrophages derived from erythro-myeloid progenitors in the yolk sac and fetal liver, or monocyte–macrophage DC progenitors in the bone marrow (Cassetta and Pollard, 2020). Peripheral blood monocytes, which are drawn to tissues by chemokines, can also develop into tissue-resident macrophages (Long et al., 2019). One of the numerous and varied cell groups that make up the tumor microenvironment and can affect tumor formation is the tumor-associated macrophages that populate the tumor tissue (Vitale et al., 2019). It is firmly established that TAMs influence tumor development, immunological control, tumor angiogenesis, and metastasis in the tumor microenvironment (Lin et al., 2019). Although the precise timing and process of this remain unknown, the bulk of TAMs are typically

produced from blood monocytes, and tumor monocytes recruited *via* chemokines like CCL2 enter the tumor to develop into TAMs (Mantovani et al., 2008). Additionally, macrophages in metastatic tumors often referred to as metastasis-associated macrophages (MAMs), have different phenotypes and roles from those in primary tumors. TAMs states in patients have predictive relevance, according to some research, as their abundance correlates with various clinical outcomes (Pittet et al., 2022).

2.2. The polarization and markers of macrophages

Macrophage polarization is a biological process that eventually displays a certain phenotype after functionally responding to microenvironmental signals found in particular tissues. M1/M2 is acknowledged as the most straightforward word to describe macrophage phenotypes, based on the types of activation signals, such as immunological signals, tumor metabolism signals, and cell death signals. The M1 macrophage, a type of classical activation macrophage, plays a crucial role in anti-tumor immunity as well as mediating the host's defense against a variety of bacteria, protozoa, and viruses. It is also involved in several chronic inflammatory and autoimmune illnesses (Murray and Wynn, 2011). Conversely, the M2 macrophage is an alternatively activated macrophage that devours fragmented and apoptotic cells and has anti-inflammatory and pro-angiogenic activity to control wound healing (Murray and Wynn, 2011). Depending on the activating stimuli received, M2 macrophages have been further divided into M2a, M2b, M2c, and M2d (Shapouri-Moghaddam et al., 2018). TAMs are a polarized novel subset of the M2 macrophage population, which was named M2d in recent studies (Mantovani et al., 2002; Duluc et al., 2007). M1-polarized cells produce ROS and NO more effectively, as well as pro-inflammatory cytokines like TNF-α, IL-1, and IL-6, as well as chemokines like CXCL8, CCL2, CXCL9, and CXCL10. M2-polarized cells express the mannose receptor, which triggers the production of chemokines including CCL17, CCL18, CCL22, and CCL24. They also produce anti-inflammatory cytokines like IL-10 and TGF-β. The expression of macrophage activation indicators, as well as cytokines, chemokines, and other secreted mediators, have all been thoroughly discussed in these papers (Mantovani et al., 2004; Murray et al., 2014; Shapouri-Moghaddam et al., 2018). TAM subpopulations are also first categorized as M1 and M2 macrophages based on the expression of certain markers, with functions assumed to be anti-tumor/anti-inflammation and pro-tumor/pro-inflammation development, respectively. It is usually determined that the majority of TAMs isolated from primary and metastatic cancers exhibit a suppressive M2-like phenotype (Murray and Wynn, 2011). However, because numerous subsets of TAMs display the indicators of both M1-and M2-polarization signatures, this simple nomenclature is unable to discriminate between the varied phenotypes of TAMs (Laviron and Boissonnas, 2019). TAMs are not precisely divided into the M1 and M2 phenotypes *in vivo*. How to select reliable biomarkers to classify TAMs in the marker database remains the main issue of research nowadays.

2.3. Macrophage polarization by bacteria

In response to cues from the immediate milieu, macrophages can change from one functional phenotype to another. Particular signaling sources like pathogenic sources might cause phenotypic flipping in macrophage populations and promote the development of tumors. Although most microorganisms are phagocytosed and killed by macrophages, some bacteria live in macrophages as opportunistic residents and utilize them for replication (Geller et al., 2017). M1 macrophages are mediated by microbial stimuli, including intracellular bacteria, to support cytotoxic activity and infection resistance. To thrive in the microenvironment, some bacteria can increase M2 polarization or interfere with M1 polarization. To avoid cytotoxic effects and circumvent the cellular immune response, microbes like Mycobacterium tuberculosis may mediate M2-polarized macrophages (Kaufmann, 2016). Table 2 lists the phenotypes of macrophages in response to bacterial pathogens in the context of oncology. Our understanding of functional markers may be too simplistic, while the use of complex markers may be confusing for researchers outside of immunology. All things considered, we continue to define pro-tumor/pro-inflammatory macrophages as M1 and anti-tumor/anti-inflammation macrophages as M2. However, it should not be forgotten that a particular live scene is unlikely to fall exactly into the combinations in Table 2, and a deeper study is needed to obtain further information and standardization (Figure 1).

3. Molecular mechanisms involved in bacterial-driven macrophage polarization

Since the microbiota has existed in the gut since human birth, the immune system and bacteria may have always been connected. Different bacterial species use both common and distinctive intrinsic mechanisms to either support or kill cancer. When it comes to host-pathogen interactions, living bacteria or bacterial components typically trigger innate immune cell reactions and cause immune cells, such as monocytes and macrophages, to migrate to tumors. Several bacteria are known to be connected to cancer, such as *Helicobacter pylori* and *Salmonella typhi* that have been shown to affect tumor growth (Lax and Thomas, 2002). However, the method by which bacteria in tumors interact with macrophages to select for the M1/M2 activation pathway is rarely discussed. In this part, we examine the molecular processes by which typical bacteria influence the polarization of macrophages in tumors, focusing on some of the well-known strains, such as *Fusobacterium nucleatum*, *Helicobacter pylori*, and *Propionibacterium acnes*.

3.1. Bacteria significantly linked to cancer

3.1.1. Fusobacterium nucleatum

A member of the bacterial genus that may cause cancer is called *Fusobacterium nucleatum*, a Gram-negative anaerobic bacterium. *Fusobacterium nucleatum* has been discovered as a periodontal pathogen and has been preferentially isolated from the oral cavity. Additionally, it has been extensively addressed how *F. nucleatum* and colorectal cancer are related (Hashemi Goradel et al., 2019). The Toll-like receptors recognize the molecular characteristics of pathogens, and each TLR elicits a different cellular response to the pathogen. In the microenvironment of colorectal tumors, *F. nucleatum* has been shown to enhance macrophage M2

TABLE 2 An aggregate list of bacterial-driven macrophage polarization that has been studied is currently available.

Porphyromonas	*Porphyromonas gingivalis*	M1	Li et al. (2022)
Coxiella	*Coxiella burnetii*	M1	Abnave et al. (2017), Zarza et al. (2021)
Escherichia	*Escherichia coli*	M1	Liang et al. (2005), Pinheiro da Silva et al. (2007), Christoffersen et al. (2014)
Yersinia	*Yersinia pestis*	M1	Bi et al. (2012)
Legionella	*Legionella pneumophila*	M1	Kusaka et al. (2018)
Vibrio	*Vibrio cholerae*	M1	Khan et al. (2015)
Shigella	*Shigella dysenteriae*	M1	Biswas et al. (2007), Pore et al. (2010)
Streptococcus	*Streptococcus pyogenes*	M1	Kadioglu and Andrew (2004), Goldmann et al. (2007)
Streptococcus	*Streptococcus Gordonii*	M1	Croft et al. (2018)
Lacticaseibacillus	*Lactobacillus rhamnosus GG*	M1	Wang et al. (2020), Duan et al. (2021)
Bacillus	*Bacillus amyloliquefaciens*	M1	Fu et al. (2019)
Mycobacterium	*Mycobacterium ulcerans*	M1	Kiszewski et al. (2006)
Mycobacterium	*Mycobacterium avium*	M1	Murphy et al. (2006)
Mycobacterium	*Mycobacterium tuberculosis*	M1/M2	Ehrt et al. (2001), Chacon-Salinas et al. (2005), Huang et al. (2015), Sha et al. (2021), Lopes et al. (2016), Zhang et al. (2020a)
Mycobacterium	*Mycobacterium leprae*	M1/M2	Fallows et al. (2016)
Salmonella	*Salmonella typhimurium*	M1/M2	Luo et al. (2016), Monack et al. (1996), Bost and Clements (1997), Stapels et al. (2018)
Fusobacterium	*Fusobacterium nucleatum*	M1/M2	Wu et al. (2019), Xu et al. (2021), Chen et al. (2018)
Streptococcus	*Streptococcus pneumonia*	M2/M1	Yerneni et al. (2021), Smith et al. (2007)
Staphylococcus	*Staphylococcus aureus*	M2/M1	Peng et al. (2017), Pidwill et al. (2020), Tuohy et al. (2020)
Listeria	*Listeria monocytogenes*	M2/M1	Lizotte et al. (2014), Shaughnessy and Swanson (2007)
Tropheryma	*Tropheryma whipplei*	M2	Desnues et al. (2005)
Cutibacterium	*Propionibacterium acnes*	M2	Li et al. (2021)
Bifidobacterium	*Bifidobacterium pseudocatenulatum*	M2	Sohn et al. (2015)
Bacillus	*Bacillus subtilis*	M2	Paynich et al. (2017)
Lacticaseibacillus	*Lactobacillus paracasei KW3110*	M2	Yoshikawa et al. (2021), Moratalla et al. (2016)
Enterococcus	*Enterococcus faecalis*	M2	Polak et al. (2021)
Brucella	*Brucella abortus*	M2	Fernandes et al. (1996), Wang et al. (2022), Dornand et al. (2002), Glowacka et al. (2018), Ma et al. (2020)
Brucella	*Brucella melitensis*	M2	Wang et al. (2022)
Helicobacter	*Helicobacter pylori*	M2	Wang et al. (2017)

polarization through a TLR4-dependent mechanism. Infection with *F. nucleatum* may also activate the IL-6/p-STAT3/c-MYC signaling pathway in macrophages in a TLR4-dependent manner (Chen et al., 2018). The study further illustrates that *F. nucleatum* promotes M2 macrophage polarization through activation of the TLR4/NF-κB/S100A9 cascade (Hu et al., 2021). The transcriptional stimulation of downstream NF-κB and STAT3, which can activate the survival pathway of tumor cells, is one of the main functions of TLR signaling. *Fusobacterium nucleatum* has been demonstrated to promote the growth of colorectal cancer *via* stimulating TLR4 signaling to MyD88, which then triggers the nuclear factor NF-κB and miR21 production (Yang et al., 2017). *Fusobacterium nucleatum* regulates miR-1,322/CCL20 through the NF-κB signaling pathway in colorectal cancer cells ultimately inducing macrophage M2 polarization (Xu et al., 2021). By releasing bioactive chemicals, bacteria can impact the host or nearby cells. A potential new marker for colorectal cancer is AI-2 in the gut microbiota (Li et al., 2019). Interestingly, AI-2 of *F. nucleatum* can promote macrophage M1 polarization *via* TNFSF9/IL-1β signaling (Wu et al., 2019).

3.1.2. Helicobacter pylori

Helicobacter pylori is a Gram-negative bacterium that when infected can cause chronic gastritis and subsequently increase the risk of developing gastric tumors in infected patients. M2-polarized macrophages identified by the CD163 molecule were substantially expressed in gastric cancer and lowly expressed in marginal tissues, implying that macrophage polarization is intimately related to gastric cancer (Zhu et al., 2020). Macrophages detect the presence of pathogen-associated molecular patterns from *H. pylori* using PRRs such as TLRs and NLRs. Inflammation caused by *H. pylori* infection is associated with the expression of TLR4 and TLR9. TLR9 is found in the intracellular compartment and can recognize nucleic acids from bacteria. TLR4 plays a major role in the inflammation of the superficial gastric lining, whereas TLR9 plays a major role in the inflammation of

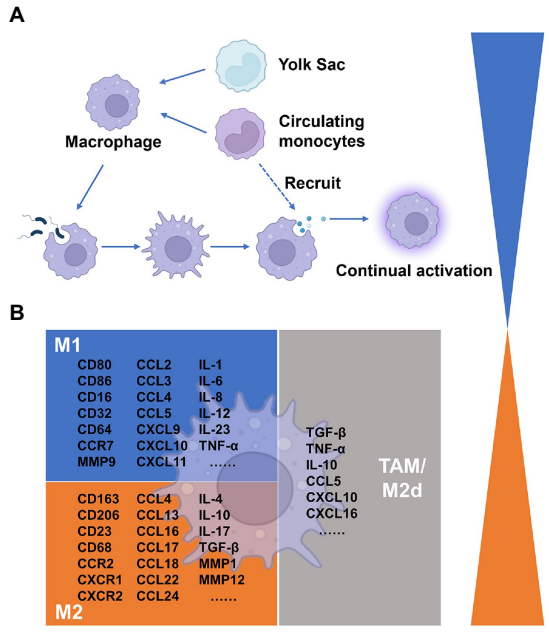

FIGURE 1
Summary of macrophages in the tumor microenvironment. **(A)** Origins of Macrophages. **(B)** Cytokines associated with macrophage differentiation to the classically and alternatively activated subsets.

gastric cancer (Wang T. R. et al., 2014). Bacterial peptidoglycan particles are detectable by NOD1. NOD1 collaborates with TLRs to detect bacteria and mediate the production of inflammatory factors. Loss of NOD1 accelerates stomach carcinogenesis in a mouse model. The wild-type phenotype of macrophages rapidly changed from M2 to M1 after the *H. pylori* infection. While wild-type macrophages convert to a mixed M1-M2 phenotype after infection with *H. pylori*, NOD1-deficient macrophages exhibit a more pronounced M2 phenotype (Suarez et al., 2019). Another study found that the deletion of MMP7 boosted M1 macrophage polarization and raised the risk of gastric cancer brought on by *H. pylori* (Krakowiak et al., 2015). Certain miRNAs may play a role in the bacterial infection's ability to persist. *Helicobacter pylori* can upregulate miRNAs targeting CIITA, thereby suppressing HLAII expression on macrophages which plays a key role in the presentation of antigens to T lymphocytes (Codolo et al., 2019; Coletta et al., 2021). After an *H. pylori* infection, macrophages regulate the release of proinflammatory cytokines *via* the increased expression of miR-155 (Yao et al., 2015).

3.2. Bacteria significantly linked to infection

3.2.1. Propionibacterium acnes

Propionibacterium acnes is a Gram-positive bacterium known as a cutaneous commensal. However, it can also manifest as an opportunistic pathogen, which gives the impression of intrusion. Through TLR4/PI3K/Akt signaling, *P. acnes* encourages M2 macrophage polarization in gastric cancer (Li et al., 2021). Regardless of the existence of malignancy, *P. acnes* infection can be found in the macrophages and epithelial cells of the prostate gland. However, persistent inflammation is linked to *P. acnes*-positive macrophage populations and is most likely a factor in the development of cancer. Both TLR4 and TLR2 are capable of identifying lipids and the LPS that Gram-negative bacteria generate. Interestingly, Kim et al. showed that *P. acnes* triggered an inflammatory response in macrophages by the activation of TLR2 while the TLR ligand may be the peptidoglycan (Kim et al., 2002). Due to the late discovery of the pathogenicity of *P. acnes*, little is known about this bacterium.

3.2.2. Staphylococcus aureus

Staphylococcus aureus is the leading causative agent in pneumonia and is initially cleared from the bloodstream by liver macrophages also called Kupffer cells. These infected cells will spread intracellular *S. aureus* throughout the body if they are unable to kill it, leading to disseminated infection. The virulence regulation of *S. aureus* is more sophisticated than that of many other bacterial pathogens. When combined with a strong Arg-1 induction, *S. aureus* biofilms can reduce iNOS expression and drive M2 macrophage polarization (Thurlow et al., 2011). In extramammary Paget S disease, *S. aureus* may be exacerbated by IL-17 and M2 macrophage polarization (Tuohy et al., 2020; Sakamoto et al., 2021). TGF-β levels were lower and inflammatory cytokines were more prominent in macrophages exposed to *S. aureus* in co-culture with osteosarcoma (Tuohy et al., 2020). The majority of the time, significant expression of conventional HDAC enzymes are linked to cancer, and it frequently indicates advanced disease and a poor prognosis for the patient. Interestingly, *S. aureus*-derived lactate inhibits the negative regulator HDAC11 to augment leukocyte IL-10 production in an HDAC6-dependent manner in the mouse prosthetic joint infection model (Heim et al., 2020). IL-10 expression correlated with the expression of HDAC6 and HDAC11 was also reported in *M. tuberculosis* infection (Wang et al., 2018).

3.3. Engineered bacteria

3.3.1. Bacillus Calmette-Guérin

Natural bacteria have been modified to acquire therapeutic functions as a result of the development of bioengineering technology. Bacillus Calmette-Guérin, a vaccine against tuberculosis, contains live-attenuated and non-toxic *M. tuberculosis*. The most advanced immunotherapy now available for non-muscle-invasive bladder cancer is BCG (Seow et al., 2010). To prevent the growth of malignancies, BCG instructs monocyte precursor cells to differentiate into functioning mature macrophages (Italiani and Boraschi, 2014). The pathogen BCG activates the MyD88 signaling pathway downstream of the cell surface TLRs, which in turn activates NF-κB and encourages cytokine transcription (de Queiroz et al., 2021). Through the TLR2/TLR4/IRF5 pathway, TRIM59 expression is elevated in BCG-activated macrophages (Jin et al., 2017). TRIM59 is a membrane protein expressed on macrophages that can increase the M1-polarized macrophages inside the tumor (Tian et al., 2019). In addition, BCG inhibits cervical carcinoma progression by promoting M1 macrophage polarization and inhibiting the pro-tumor activation of M2 macrophages *via* the Rb/E2F1 signaling pathway in Hela cells (Liu et al., 2021).

3.3.2. Salmonella

Salmonella species are facultative intracellular pathogenic bacteria that can invade and proliferate in macrophages and dendritic cells. In *Salmonella*-infected macrophages, the fatty acid regulator PPARδ is increased and may be linked to M2-polarized macrophages

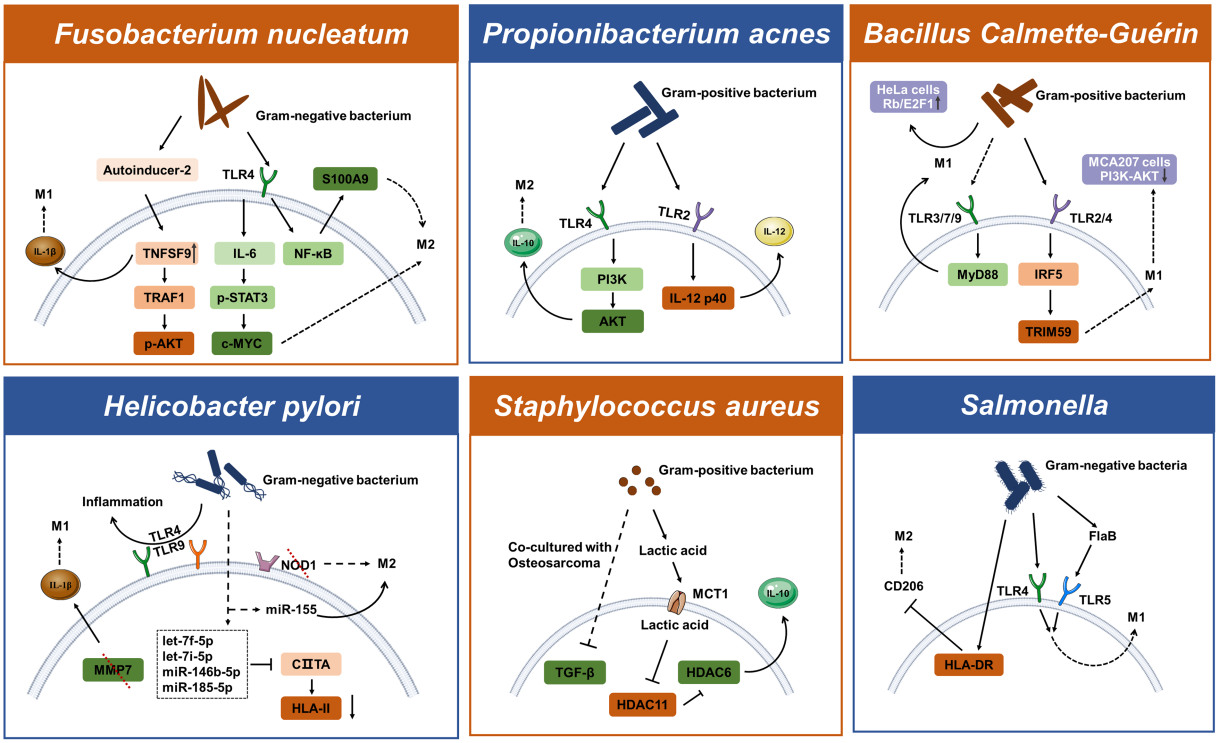

FIGURE 2
Schematic representation of mechanisms of bacteria-induced macrophage polarization.

(Eisele et al., 2013) and the PI3K/Akt pathway in gallbladder cancer can facilitate migration and invasion due to CCL18 produced by M2 macrophages (Zhou Z. et al., 2019). While some studies suggest that engineered *Salmonella* bacteria help tumor-associated macrophage polarization (see Figure 2) to achieve enhanced antitumor immune response *in vivo*. The anti-tumor effect of engineered *Salmonella* also appears to induce infiltration of abundant immune cells through TLR4 signaling. Molecular mechanisms suggest that this may be due to the presence of LPS in the outer membrane of Gram-negative bacteria thereby activating the TLR4/MyD88 pathway that mediated CCL2 production (Akhter et al., 2018). Some of the attenuated *Salmonella* strains and their derivatives used as drug carriers have also been tested in early clinical trials. A newly engineered *Salmonella typhimurium* strain called YB1 was reported to induce enhanced HLA-DR expression and reduced CD206 expression, and to remodel macrophages from the M2-to M1-polarized (Yang et al., 2018). Additionally, heterologous flagellin from the bacterial pathogen *Salmonella* activates the TLR5 pathway and changes tumor-infiltrating macrophages into M1-polarized macrophages (Chen et al., 2021). Another engineered bacteria that secrete FlaB *via* dual pathways, TLR4 and TLR5, also leads to M1-polarized macrophages (Zheng J. H. et al., 2017).

4. Effect of activated macrophages on the tumor microenvironment

While studies targeting the direct relationship between cancer and microbiome are quite limited at present, there have been some interesting studies demonstrating that certain pathogenic processes, such as altered metabolic states and chronic inflammation, display commonality across cancers (Trinchieri, 2012; Andrejeva and Rathmell, 2017). Microbiota participates in shaping an immune-tolerant environment through the recruitment and activation of macrophages and is characterized by the accumulation of pro-inflammatory factors including metabolic intermediates and effectors. These pro-inflammatory factors aid in the development of cancer by promoting angiogenesis, chemoresistance, immune cell suppression, tumor invasion, and metastasis (Coussens and Werb, 2002).

4.1. Dynamic changes in macrophage metabolism

The components of pathogenic organisms, such as LPS are commonly used tools to activate macrophages. LPS stimulation and TLR activation induce a series of biochemical metabolic alterations in macrophages. Metabolomic analysis of LPS-activated macrophages shows downregulation of TCA cycle intermediates and upregulation of aerobic glycolysis, which correlates directly with the expression profiles of altered metabolites (Tannahill et al., 2013; Lauterbach et al., 2019). The TCA cycle is a fragmented process resulting in the secretion of large volumes of metabolites such as lactate and succinate. The production of lactate in LPS-activated macrophages is enhanced and it inhibits the motility of activated T cells *in vitro* (Haas et al., 2015) and the cytotoxic activity of CD8 + CTLs (Fischer et al., 2007). By activating HIF-1α and MAPK, abundant lactate causes macrophages to produce VEGF and ARG1. Both VEGF and ARG1 promote tumor progressions by inducing angiogenesis and arginase depletion. Succinate is a pro-inflammatory

metabolite that inhibits prolyl hydroxylase activity and increases the production of ROS, which stabilizes HIF-1α (Liu et al., 2017). Several genes that promote tumor growth, including MMP9, are also activated by HIF (Zhang et al., 2015). Furthermore, considering that the HIF protein amount is under the control of iron-dependent prolyl hydroxylases (Bruick and McKnight, 2001) and Lcn-2 promotes downstream target gene activation (Bolignano et al., 2010), iron uptake is another mechanism behind the pro-tumorigenic activity of polarized macrophages. Iron is known to regulate the expression of several genes at the transcriptional level, most prominently *via* the generation of reactive oxygen species and their effects on the activity of NF-κB and other transcription factors (Templeton and Liu, 2003). Iron stimulates cell production of hydroxyl radicals through the overexpression of SOX9, which regulate tumor aggressiveness (Chanvorachote and Luanpitpong, 2016). Under infectious or inflammatory conditions, macrophages increase iron absorption while promoting inflammation (Jung et al., 2015). While macrophages infected with extracellular *E. coli* K88 reserve iron by elevating hepcidin transcription and increasing iron storage in cells, macrophages infected with intracellular *S. typhimurium* decrease free iron ions for intracellular bacterial proliferation and utilization (Gan et al., 2019). Reduced intracellular iron levels in macrophages prevent inflammatory cytokines like IL-6 and TNF-α from being translated (Wang et al., 2008). A key mechanism for pathogens to perturb the biochemical metabolism to promote their survival in macrophages is lipid metabolism. Lipid metabolism is a crucial way by which infections disrupt metabolic metabolism to aid in their survival in macrophages. Lipid droplets, which are now acknowledged as a well-established characteristic of many tumors, accumulate excessive amounts of lipids and cholesterol (Beloribi-Djefaflia et al., 2016). By changing the metabolism of host cells, *M. tuberculosis* encourages the production of macrophages with lipid bodies (Russell et al., 2009). *Helicobacter pylori* engagement of the intracellular NOD1 leads to the activation of NF-κB, which results in the up-regulation of COX-2 (Chang et al., 2004), and COX-2 plays a key role in the synthesis of lipid inflammatory mediators such as prostaglandins from arachidonic acid. In addition, microbial stimulation triggers the expression of SREBP-1a (Im et al., 2011) and the synthesis of phosphatidylcholine (Sanchez-Lopez et al., 2019), which is linked to the production of IL-1β and IL-18 (Oishi et al., 2017). Increases in dephosphorylation of SHP1 caused by higher levels of oxidative stress from fatty acid oxidation are correlated with tumor progression and involve a variety of immune cell types (Myers et al., 2020; Su et al., 2020).

4.2. Populations and expression of regulatory inflammatory factors in macrophage

In the context of immunity, activated macrophages undergo metabolic adjustments and modify the production of cytokines at the epigenetic, transcriptional, and post-translational levels in response to bacterial sensing. Furthermore, the release of increased concentrations of intermediates and effectors frequently controls the tumor immune microenvironment and aids in the development of tumors. TAMs attract naïve and Th2 lymphocytes and cause inefficient immunological reactions by secreting CCL17, CCL18, and CCL22 (Erreni et al., 2011). Additionally, through producing CCL18, which binds to PITPNM3 on the cancer cell membrane, TAMs in breast cancer increase the invasiveness of cancer cells (Chen et al., 2011). TAMs secrete PD-L1 to inhibit cytotoxic T cells and IL-10 to activate Treg (Zhu et al., 2016; Fang et al., 2021). Additionally, when PD-L1 is inhibited, TAMs may retain tumor immunosuppressive potential by boosting PD-L2 secretion (Umezu et al., 2019). TAMs can directly attract Treg cells to the site of the immunosuppressive milieu by generating CCL20 and CCL22, and they can also activate them by secreting IL-10 and TGF-β (Curiel et al., 2004; Biswas and Mantovani, 2010; Umezu et al., 2019). IL-6 and IL-10 are a group of cytokines, which are inducing tumor invasion and angiogenesis (Tamura et al., 2018). Recent studies showed that TAMs decrease E-cadherin by activating the TLR4/IL-10 signaling pathway promoting epithelial-to-mesenchymal transition in pancreatic cancer (Liu et al., 2013; Yao et al., 2018). Additionally, in transgenic mice models, IL-10 produced by TAMs is the key mediator in tumor resistance to paclitaxel and carboplatin (Ruffell et al., 2014). The IL-6 produced by TAMs promotes chemotherapy resistance in cancer cells by inhibiting the expression of miR-204-5p and activating the STAT3 pathway (Zhu et al., 2017).

4.3. MicroRNA in macrophage exosomes as critical regulators of the tumor microenvironment

Several proteins, including SHIP1, TAB2, and SOCS1, in the innate immune signaling pathways, are targeted by the miR-155 gene, which is increased in macrophages after LPS infection and alters affects the expression of inflammatory mediators (Androulidaki et al., 2009; Ceppi et al., 2009; Cremer et al., 2009). Through a post-transcriptional break, *Salmonella* can cause the let-7 family to suppress the expression of IL-6 and IL-10 (Schulte et al., 2011). In THP-1 cells infected with *M. tuberculosis*, miR-206 expression is noticeably elevated, and this raised miR-206 favorably regulates inflammatory cytokines and MMP9 *via* targeting TIMP3 (Fu et al., 2016). These are shown miRNA could regulate the modulation of innate immunity signaling pathways. The primary mechanism for extracellular miRNA synthesis uses exosomes with energy-dependent active secretion. Exosomes are extremely small extracellular vesicles that contain proteins, lipids and nucleic acids, among other active components (Tan et al., 2020). In pancreatic ductal adenocarcinoma, it has been discovered that TAM-EVs transport miR-501-3p to suppress TGFBR3 expression, activate the TGF-β pathway, and encourage tumor migration and invasion (Yin et al., 2019). The advancement of gastric cancer is aided by M2 macrophage-derived extracellular vesicles through a miR-130b-3p/MLL3/GRHL2 signaling cascade (Zhang et al., 2020b). Exosomal miRNAs may have an impact on the biology of different cell types in TME. The STAT3 pathway is inhibited and Treg/Th17 cell imbalance is produced by TAM-EVs enriched in miR-21-5p and miR-29a-3p (Zhou et al., 2018). MiR-29a-3p controlled the FOXO3/AKT/GSK3 axis to suppress the expression of PD-L1, and PD-L1 expression can impair CD8 + T cell activity, causing immunological escape (Lu et al., 2021). TAM-EVs also contribute significantly to the pathophysiology of tumor chemoresistance (Figure 3). MiR-21 from tumor-associated macrophages that is transferred exosomal provides cisplatin resistance on gastric cancer cells by enhanced activation of PI3K/AKT signaling pathway by down-regulation of PTEN (Zheng P. et al., 2017).

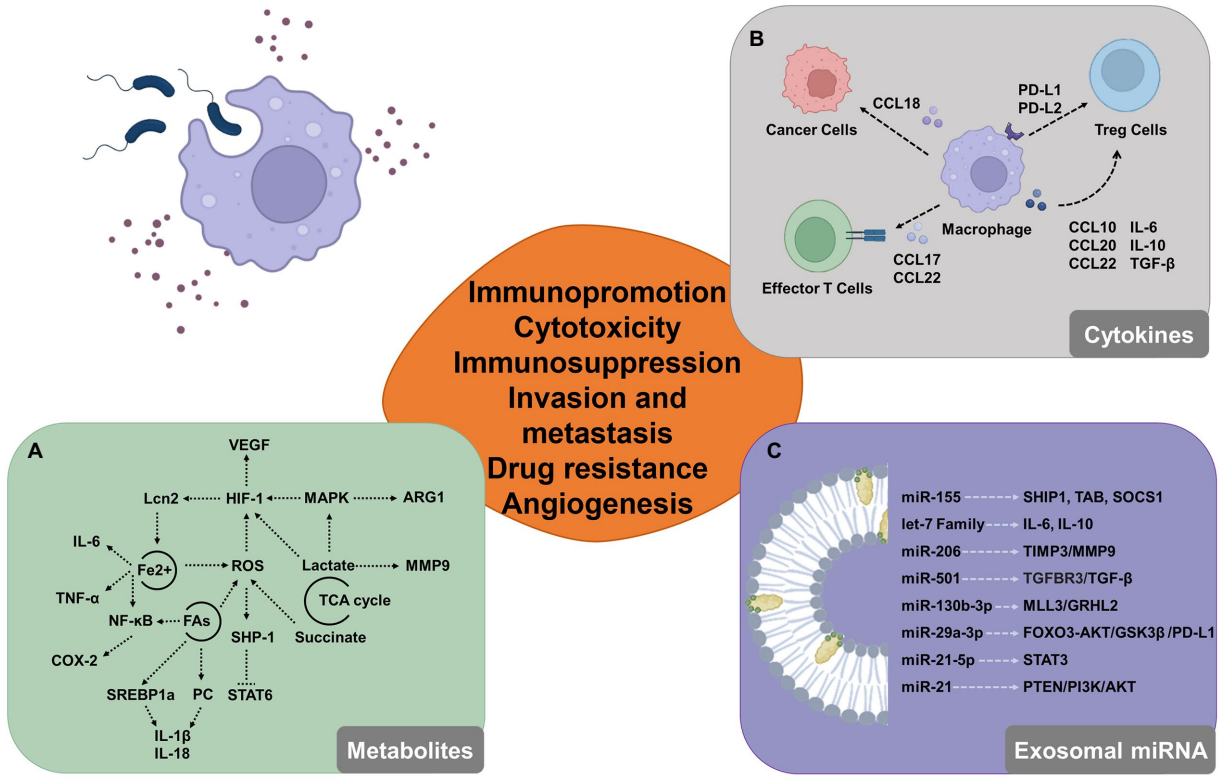

FIGURE 3
Potential involvement for macrophages that have been triggered by the microbiome in the tumor microenvironment. **(A)** By modifying the expression of intermediate metabolites, activated macrophages can modify glucose metabolism, iron cycling, and lipid metabolism and control the tumor microenvironment. **(B)** Activated macrophages release a variety of cytokines, chemokines, and growth factors that influence tumor formation by boosting cell proliferation and decreasing the activity of immune cells that can destroy tumors, like cytotoxic T cells. **(C)** Macrophage-derived exosomal miRNAs alter the immunological milieu by targeting proteins and activating molecules.

5. Discussion

Studies on the microbiome have progressed from focusing on the cultivation of oral and intestinal bacteria to mechanistically understanding the link between host and microbiome, and more recently, to microbial profiles of all ecological niches in the body. The use of specific microbial signatures of cancer types may improve early and minimally invasive diagnostic approaches, and in this review, we discuss the bacteria in different cancer. However, the part of cancer most clearly associated with bacterial species remains ill-defined. The speculation of the presence of microbiota within tumors was finally confirmed by sequencing-based diagnosis, but there are many challenges in discriminating tumor-specific bacteria. The most frequent issues are biased results brought on by the use of various tissue sample processing techniques and the confounding of chemicals or environmental pollutants. Exogenous bacteria can now be used as potential immunotherapeutic agents or as a neoadjuvant in the treatment of cancer (St Jean et al., 2008). We will be able to identify distinct pathways that can be exploited for diagnostic, preventative, and therapeutic purposes if we can more precisely identify a particular strain in the tumor.

The host's metabolism and immunity can be altered by the microbiota and its secreted components, which in turn can affect antitumor immunity. Numerous pathways suggest that bacteria acting as foreign microorganisms may indirectly contribute to the beginning or development of cancer. Unexpectedly, bacteria may multiply in macrophages and control them *via* a variety of interference tactics (Rosenberger and Finlay, 2003). During tumorigenesis and regression, macrophage polarization appears to act as an intermediate process that is activated by certain signals. Macrophages exhibit different phenotypes after receiving multiple stimulations which act on different receptors and thus exert regulatory effects by acting on multiple signaling pathways. It is a complicated story about how bacteria and macrophages interact. It should be emphasized that host cells are frequently cultivated *in vitro* for the majority of research against pathogens, including bacteria. Macrophage polarization is a result, and the molecular pathways of bacteria-driven macrophage polarization ought to connect to a particular environment concurrently, as the tumor microenvironment is a special environment that has the potential to preferentially generate macrophage polarization. In this article, we went over the molecular mechanisms of bacterial-induced macrophage polarization as well as the impact of activated macrophages on the tumor microenvironment.

A causal link between microbial enrichment in cancer and cancer itself cannot be shown, but understanding the relationships between microbes, macrophages, and cancer cells requires in-depth functional analysis per microbial scale is necessary. On one hand, one way to increase the efficiency and safety of tumor-targeted medicines is to modify bacteria using research on such pathogen-macrophage interactions. On the other hand, molecular mechanisms of cell polarization provide information and guidance for switching macrophage polarity in cancer.

Author contributions

SX, YX, BF, DG, ZS, XL, and HW contributed to the study's conception and design and commented on previous versions of the manuscript. Material preparation, data collection, and analysis were performed by BF, DG, and ZS. The first draft of the manuscript was written by SX and YX. All authors contributed to the article and approved the submitted version.

Funding

This work was supported by National Natural Science Foundation of China (No. 81970008 and 82000020), Fundamental Research Funds for the Central Universities (2019CDYGZD009 and 2020CDJYGRH-1005), Natural Science Foundation of Chongqing, China (cstc2020jcyj-bshX0105 and cstc2020jcyj-msxmX0460) and Chongqing Talents: Exceptional Young Talents Project (No. cstc2021ycjh-bgzxm0099). The funders had no role in study design, data collection and analysis, decision to publish, or preparation of the manuscript.

Conflict of interest

The authors declare that the research was conducted in the absence of any commercial or financial relationships that could be construed as a potential conflict of interest.

Publisher's note

All claims expressed in this article are solely those of the authors and do not necessarily represent those of their affiliated organizations, or those of the publisher, the editors and the reviewers. Any product that may be evaluated in this article, or claim that may be made by its manufacturer, is not guaranteed or endorsed by the publisher.

Supplementary material

The Supplementary material for this article can be found online at: https://www.frontiersin.org/articles/10.3389/fmicb.2023.1115556/full#supplementary-material

References

Abed, J., Maalouf, N., Manson, A. L., Earl, A. M., Parhi, L., Emgard, J. E. M., et al. (2020). Colon cancer-associated fusobacterium nucleatum may originate from the Oral cavity and reach colon tumors *via* the circulatory system. *Front. Cell. Infect. Microbiol.* 10:400. doi: 10.3389/fcimb.2020.00400

Abnave, P., Muracciole, X., and Ghigo, E. (2017). Coxiella burnetii lipopolysaccharide: what do we know? *Int. J. Mol. Sci.* 18:2509. doi: 10.3390/ijms18122509

Akhter, N., Hasan, A., Shenouda, S., Wilson, A., Kochumon, S., Ali, S., et al. (2018). TLR4/MyD88 -mediated CCL2 production by lipopolysaccharide (endotoxin): implications for metabolic inflammation. *J. Diabetes Metab. Disord.* 17, 77–84. doi: 10.1007/s40200-018-0341-y

Alanee, S., El-Zawahry, A., Dynda, D., Dabaja, A., McVary, K., Karr, M., et al. (2019). A prospective study to examine the association of the urinary and fecal microbiota with prostate cancer diagnosis after transrectal biopsy of the prostate using 16sRNA gene analysis. *Prostate* 79, 81–87. doi: 10.1002/pros.23713

Andrejeva, G., and Rathmell, J. C. (2017). Similarities and distinctions of cancer and immune metabolism in inflammation and tumors. *Cell Metab.* 26, 49–70. doi: 10.1016/j.cmet.2017.06.004

Androulidaki, A., Iliopoulos, D., Arranz, A., Doxaki, C., Schworer, S., Zacharioudaki, V., et al. (2009). The kinase Akt1 controls macrophage response to lipopolysaccharide by regulating microRNAs. *Immunity* 31, 220–231. doi: 10.1016/j.immuni.2009.06.024

Apostolou, P., Tsantsaridou, A., Papasotiriou, I., Toloudi, M., Chatziioannou, M., and Giamouzis, G. (2011). Bacterial and fungal microflora in surgically removed lung cancer samples. *J. Cardiothorac. Surg.* 6:137. doi: 10.1186/1749-8090-6-137

Arthur, J. C., Perez-Chanona, E., Muhlbauer, M., Tomkovich, S., Uronis, J. M., Fan, T. J., et al. (2012). Intestinal inflammation targets cancer-inducing activity of the microbiota. *Science* 338, 120–123. doi: 10.1126/science.1224820

Audirac-Chalifour, A., Torres-Poveda, K., Bahena-Roman, M., Tellez-Sosa, J., Martinez-Barnetche, J., Cortina-Ceballos, B., et al. (2016). Cervical microbiome and cytokine profile at various stages of cervical cancer: a pilot study. *PLoS One* 11:e0153274. doi: 10.1371/journal.pone.0153274

Aviles-Jimenez, F., Vazquez-Jimenez, F., Medrano-Guzman, R., Mantilla, A., and Torres, J. (2014). Stomach microbiota composition varies between patients with non-atrophic gastritis and patients with intestinal type of gastric cancer. *Sci. Rep.* 4:4202. doi: 10.1038/srep04202

Baghban, A., and Gupta, S. (2016). Parvimonas micra: a rare cause of native joint septic arthritis. *Anaerobe* 39, 26–27. doi: 10.1016/j.anaerobe.2016.02.004

Beloribi-Djefaflia, S., Vasseur, S., and Guillaumond, F. (2016). Lipid metabolic reprogramming in cancer cells. *Oncogenesis.* 5:e189. doi: 10.1038/oncsis.2015.49

Bi, Y., Wang, X., Han, Y., Guo, Z., and Yang, R. (2012). Yersinia pestis versus Yersinia pseudotuberculosis: effects on host macrophages. *Scand. J. Immunol.* 76, 541–551. doi: 10.1111/j.1365-3083.2012.02767.x

Biswas, A., Banerjee, P., Mukherjee, G., and Biswas, T. (2007). Porin of Shigella dysenteriae activates mouse peritoneal macrophage through toll-like receptors 2 and 6 to induce polarized type I response. *Mol. Immunol.* 44, 812–820. doi: 10.1016/j.molimm.2006.04.007

Biswas, S. K., and Mantovani, A. (2010). Macrophage plasticity and interaction with lymphocyte subsets: cancer as a paradigm. *Nat. Immunol.* 11, 889–896. doi: 10.1038/ni.1937

Bolignano, D., Donato, V., Lacquaniti, A., Fazio, M. R., Bono, C., Coppolino, G., et al. (2010). Neutrophil gelatinase-associated lipocalin (NGAL) in human neoplasias: a new protein enters the scene. *Cancer Lett.* 288, 10–16. doi: 10.1016/j.canlet.2009.05.027

Bost, K. L., and Clements, J. D. (1997). Intracellular salmonella Dublin induces substantial secretion of the 40-kilodalton subunit of interleukin-12 (IL-12) but minimal secretion of IL-12 as a 70-kilodalton protein in murine macrophages. *Infect. Immun.* 65, 3186–3192. doi: 10.1128/iai.65.8.3186-3192.1997

Bruick, R. K., and McKnight, S. L. (2001). A conserved family of prolyl-4-hydroxylases that modify HIF. *Science* 294, 1337–1340. doi: 10.1126/science.1066373

Bullman, S., Pedamallu, C. S., Sicinska, E., Clancy, T. E., Zhang, X., Cai, D., et al. (2017). Analysis of fusobacterium persistence and antibiotic response in colorectal cancer. *Science* 358, 1443–1448. doi: 10.1126/science.aal5240

Cameron, S. J. S., Lewis, K. E., Huws, S. A., Hegarty, M. J., Lewis, P. D., Pachebat, J. A., et al. (2017). A pilot study using metagenomic sequencing of the sputum microbiome suggests potential bacterial biomarkers for lung cancer. *PLoS One* 12:e0177062. doi: 10.1371/journal.pone.0177062

Cassetta, L., and Pollard, J. W. (2020). Tumor-associated macrophages. *Curr. Biol.* 30, R246–R248. doi: 10.1016/j.cub.2020.01.031

Castellarin, M., Warren, R. L., Freeman, J. D., Dreolini, L., Krzywinski, M., Strauss, J., et al. (2012). Fusobacterium nucleatum infection is prevalent in human colorectal carcinoma. *Genome Res.* 22, 299–306. doi: 10.1101/gr.126516.111

Cavarretta, I., Ferrarese, R., Cazzaniga, W., Saita, D., Luciano, R., Ceresola, E. R., et al. (2017). The microbiome of the prostate tumor microenvironment. *Eur. Urol.* 72, 625–631. doi: 10.1016/j.eururo.2017.03.029

Ceppi, M., Pereira, P. M., Dunand-Sauthier, I., Barras, E., Reith, W., Santos, M. A., et al. (2009). MicroRNA-155 modulates the interleukin-1 signaling pathway in activated human monocyte-derived dendritic cells. *Proc. Natl. Acad. Sci. U. S. A.* 106, 2735–2740. doi: 10.1073/pnas.0811073106

Chacon-Salinas, R., Serafin-Lopez, J., Ramos-Payan, R., Mendez-Aragon, P., Hernandez-Pando, R., Van Soolingen, D., et al. (2005). Differential pattern of cytokine expression by macrophages infected *in vitro* with different mycobacterium tuberculosis genotypes. *Clin. Exp. Immunol.* 140, 443–449. doi: 10.1111/j.1365-2249.2005.02797.x

Chang, Y. J., Wu, M. S., Lin, J. T., Sheu, B. S., Muta, T., Inoue, H., et al. (2004). Induction of cyclooxygenase-2 overexpression in human gastric epithelial cells by helicobacter pylori involves TLR2/TLR9 and c-Src-dependent nuclear factor-kappaB activation. *Mol. Pharmacol.* 66, 1465–1477. doi: 10.1124/mol.104.005199

Chanvorachote, P., and Luanpitpong, S. (2016). Iron induces cancer stem cells and aggressive phenotypes in human lung cancer cells. *Am. J. Physiol. Cell Physiol.* 310, C728–C739. doi: 10.1152/ajpcell.00322.2015

Chen, T., Li, Q., Wu, J., Wu, Y., Peng, W., Li, H., et al. (2018). Fusobacterium nucleatum promotes M2 polarization of macrophages in the microenvironment of colorectal tumours

via a TLR4-dependent mechanism. *Cancer Immunol. Immunother.* 67, 1635–1646. doi: 10.1007/s00262-018-2233-x

Chen, J., Qiao, Y., Chen, G., Chang, C., Dong, H., Tang, B., et al. (2021). Salmonella flagella confer anti-tumor immunological effect *via* activating Flagellin/TLR5 signalling within tumor microenvironment. *Acta Pharm. Sin. B* 11, 3165–3177. doi: 10.1016/j.apsb.2021.04.019

Chen, J., Yao, Y., Gong, C., Yu, F., Su, S., Chen, J., et al. (2011). CCL18 from tumor-associated macrophages promotes breast cancer metastasis *via* PITPNM3. *Cancer Cell* 19, 541–555. doi: 10.1016/j.ccr.2011.02.006

Christoffersen, T. E., Hult, L. T., Kuczkowska, K., Moe, K. M., Skeie, S., Lea, T., et al. (2014). *In vitro* comparison of the effects of probiotic, commensal and pathogenic strains on macrophage polarization. *Probiotics Antimicrob Proteins.* 6, 1–10. doi: 10.1007/s12602-013-9152-0

Christofides, A., Strauss, L., Yeo, A., Cao, C., Charest, A., and Boussiotis, V. A. (2022). The complex role of tumor-infiltrating macrophages. *Nat. Immunol.* 23, 1148–1156. doi: 10.1038/s41590-022-01267-2

Codolo, G., Toffoletto, M., Chemello, F., Coletta, S., Soler Teixidor, G., Battaggia, G., et al. (2019). Helicobacter pylori dampens HLA-II expression on macrophages *via* the up-regulation of miRNAs targeting CIITA. *Front. Immunol.* 10:2923. doi: 10.3389/fimmu.2019.02923

Cohen, R. J., Shannon, B. A., McNeal, J. E., Shannon, T., and Garrett, K. L. (2005). Propionibacterium acnes associated with inflammation in radical prostatectomy specimens: a possible link to cancer evolution? *J. Urol.* 173, 1969–1974. doi: 10.1097/01.ju.0000158161.15277.78

Coker, O. O., Dai, Z., Nie, Y., Zhao, G., Cao, L., Nakatsu, G., et al. (2018). Mucosal microbiome dysbiosis in gastric carcinogenesis. *Gut* 67, 1024–1032. doi: 10.1136/gutjnl-2017-314281

Coletta, S., Battaggia, G., Della Bella, C., Furlani, M., Hauke, M., Faass, L., et al. (2021). ADP-heptose enables helicobacter pylori to exploit macrophages as a survival niche by suppressing antigen-presenting HLA-II expression. *FEBS Lett.* 595, 2160–2168. doi: 10.1002/1873-3468.14156

Contreras, A., Doan, N., Chen, C., Rusitanonta, T., Flynn, M. J., and Slots, J. (2000). Importance of Dialister pneumosintes in human periodontitis. *Oral Microbiol. Immunol.* 15, 269–272. doi: 10.1034/j.1399-302x.2000.150410.x

Coussens, L. M., and Werb, Z. (2002). Inflammation and cancer. *Nature* 420, 860–867. doi: 10.1038/nature01322

Coutzac, C., Jouniaux, J. M., Paci, A., Schmidt, J., Mallardo, D., Seck, A., et al. (2020). Systemic short chain fatty acids limit antitumor effect of CTLA-4 blockade in hosts with cancer. *Nat. Commun.* 11:2168. doi: 10.1038/s41467-020-16079-x

Cremer, T. J., Ravneberg, D. H., Clay, C. D., Piper-Hunter, M. G., Marsh, C. B., Elton, T. S., et al. (2009). MiR-155 induction by F. novicida but not the virulent F. tularensis results in SHIP down-regulation and enhanced pro-inflammatory cytokine response. *PLoS One* 4:e8508. doi: 10.1371/journal.pone.0008508

Croft, A. J., Metcalfe, S., Honma, K., and Kay, J. G. (2018). Macrophage polarization alters Postphagocytosis survivability of the commensal Streptococcus gordonii. *Infect. Immun.* 86:e00858-17. doi: 10.1128/IAI.00858-17

Curiel, T. J., Coukos, G., Zou, L., Alvarez, X., Cheng, P., Mottram, P., et al. (2004). Specific recruitment of regulatory T cells in ovarian carcinoma fosters immune privilege and predicts reduced survival. *Nat. Med.* 10, 942–949. doi: 10.1038/nm1093

Daisley, B. A., Chanyi, R. M., Abdur-Rashid, K., Al, K. F., Gibbons, S., Chmiel, J. A., et al. (2020). Abiraterone acetate preferentially enriches for the gut commensal Akkermansia muciniphila in castrate-resistant prostate cancer patients. *Nat. Commun.* 11:4822. doi: 10.1038/s41467-020-18649-5

de Martel, C., Plummer, M., Parsonnet, J., van Doorn, L. J., and Franceschi, S. (2009). Helicobacter species in cancers of the gallbladder and extrahepatic biliary tract. *Br. J. Cancer* 100, 194–199. doi: 10.1038/sj.bjc.6604780

de Queiroz, N., Marinho, F. V., de Araujo, A., Fahel, J. S., and Oliveira, S. C. (2021). MyD88-dependent BCG immunotherapy reduces tumor and regulates tumor microenvironment in bladder cancer murine model. *Sci. Rep.* 11:15648. doi: 10.1038/s41598-021-95157-6

Dejea, C. M., Fathi, P., Craig, J. M., Boleij, A., Taddese, R., Geis, A. L., et al. (2018). Patients with familial adenomatous polyposis harbor colonic biofilms containing tumorigenic bacteria. *Science* 359, 592–597. doi: 10.1126/science.aah3648

Derosa, L., Hellmann, M. D., Spaziano, M., Halpenny, D., Fidelle, M., Rizvi, H., et al. (2018). Negative association of antibiotics on clinical activity of immune checkpoint inhibitors in patients with advanced renal cell and non-small-cell lung cancer. *Ann. Oncol.* 29, 1437–1444. doi: 10.1093/annonc/mdy103

Desnues, B., Raoult, D., and Mege, J. L. (2005). IL-16 is critical for *Tropheryma whipplei* replication in Whipple's disease. *J. Immunol.* 175, 4575–4582. doi: 10.4049/jimmunol.175.7.4575

Di Paola, M., Sani, C., Clemente, A. M., Iossa, A., Perissi, E., Castronovo, G., et al. (2017). Characterization of cervico-vaginal microbiota in women developing persistent high-risk human papillomavirus infection. *Sci. Rep.* 7:10200. doi: 10.1038/s41598-017-09842-6

Dias-Jacome, E., Libanio, D., Borges-Canha, M., Galaghar, A., and Pimentel-Nunes, P. (2016). Gastric microbiota and carcinogenesis: the role of non-helicobacter pylori bacteria – a systematic review. *Rev. Esp. Enferm. Dig.* 108, 530–540. doi: 10.17235/reed.2016.4261/2016

Dickson, R. P., Erb-Downward, J. R., Martinez, F. J., and Huffnagle, G. B. (2016). The microbiome and the respiratory tract. *Annu. Rev. Physiol.* 78, 481–504. doi: 10.1146/annurev-physiol-021115-105238

Dickson, R. P., and Huffnagle, G. B. (2015). The lung microbiome: new principles for respiratory bacteriology in health and disease. *PLoS Pathog.* 11:e1004923. doi: 10.1371/journal.ppat.1004923

Donders, G. G. G., Bellen, G., Grinceviciene, S., Ruban, K., and Vieira-Baptista, P. (2017). Aerobic vaginitis: no longer a stranger. *Res. Microbiol.* 168, 845–858. doi: 10.1016/j.resmic.2017.04.004

Dornand, J., Gross, A., Lafont, V., Liautard, J., Oliaro, J., and Liautard, J. P. (2002). The innate immune response against Brucella in humans. *Vet. Microbiol.* 90, 383–394. doi: 10.1016/S0378-1135(02)00223-7

Duan, B., Shao, L., Liu, R., Msuthwana, P., Hu, J., and Wang, C. (2021). Lactobacillus rhamnosus GG defense against salmonella enterica serovar typhimurium infection through modulation of M1 macrophage polarization. *Microb. Pathog.* 156:104939. doi: 10.1016/j.micpath.2021.104939

Duluc, D., Delneste, Y., Tan, F., Moles, M. P., Grimaud, L., Lenoir, J., et al. (2007). Tumor-associated leukemia inhibitory factor and IL-6 skew monocyte differentiation into tumor-associated macrophage-like cells. *Blood* 110, 4319–4330. doi: 10.1182/blood-2007-02-072587

Dutta, U., Garg, P. K., Kumar, R., and Tandon, R. K. (2000). Typhoid carriers among patients with gallstones are at increased risk for carcinoma of the gallbladder. *Am. J. Gastroenterol.* 95, 784–787. doi: 10.1111/j.1572-0241.2000.01860.x

Ehrt, S., Schnappinger, D., Bekiranov, S., Drenkow, J., Shi, S., Gingeras, T. R., et al. (2001). Reprogramming of the macrophage transcriptome in response to interferon-gamma and mycobacterium tuberculosis: signaling roles of nitric oxide synthase-2 and phagocyte oxidase. *J. Exp. Med.* 194, 1123–1140. doi: 10.1084/jem.194.8.1123

Eisele, N. A., Ruby, T., Jacobson, A., Manzanillo, P. S., Cox, J. S., Lam, L., et al. (2013). Salmonella require the fatty acid regulator PPARdelta for the establishment of a metabolic environment essential for long-term persistence. *Cell Host Microbe* 14, 171–182. doi: 10.1016/j.chom.2013.07.010

Eklof, V., Lofgren-Burstrom, A., Zingmark, C., Edin, S., Larsson, P., Karling, P., et al. (2017). Cancer-associated fecal microbial markers in colorectal cancer detection. *Int. J. Cancer* 141, 2528–2536. doi: 10.1002/ijc.31011

Elliott, D. R. F., Walker, A. W., O'Donovan, M., Parkhill, J., and Fitzgerald, R. C. (2017). A non-endoscopic device to sample the oesophageal microbiota: a case-control study. *Lancet Gastroenterol. Hepatol.* 2, 32–42. doi: 10.1016/S2468-1253(16)30086-3

Erreni, M., Mantovani, A., and Allavena, P. (2011). Tumor-associated macrophages (TAM) and inflammation in colorectal cancer. *Cancer Microenviron.* 4, 141–154. doi: 10.1007/s12307-010-0052-5

Fallows, D., Peixoto, B., Kaplan, G., and Manca, C. (2016). Mycobacterium leprae alters classical activation of human monocytes *in vitro*. *J. Inflamm (Lond).* 13:8. doi: 10.1186/s12950-016-0117-4

Fang, W., Zhou, T., Shi, H., Yao, M., Zhang, D., Qian, H., et al. (2021). Progranulin induces immune escape in breast cancer *via* up-regulating PD-L1 expression on tumor-associated macrophages (TAMs) and promoting CD8(+) T cell exclusion. *J. Exp. Clin. Cancer Res.* 40:4. doi: 10.1186/s13046-020-01786-6

Farrell, J. J., Zhang, L., Zhou, H., Chia, D., Elashoff, D., Akin, D., et al. (2012). Variations of oral microbiota are associated with pancreatic diseases including pancreatic cancer. *Gut* 61, 582–588. doi: 10.1136/gutjnl-2011-300784

Fernandes, D. M., Jiang, X., Jung, J. H., and Baldwin, C. L. (1996). Comparison of T cell cytokines in resistant and susceptible mice infected with virulent *Brucella abortus* strain 2308. *FEMS Immunol. Med. Microbiol.* 16, 193–203. doi: 10.1111/j.1574-695X.1996.tb00136.x

Fischer, K., Hoffmann, P., Voelkl, S., Meidenbauer, N., Ammer, J., Edinger, M., et al. (2007). Inhibitory effect of tumor cell-derived lactic acid on human T cells. *Blood* 109, 3812–3819. doi: 10.1182/blood-2006-07-035972

Fredricks, D. N., Fiedler, T. L., and Marrazzo, J. M. (2005). Molecular identification of bacteria associated with bacterial vaginosis. *N. Engl. J. Med.* 353, 1899–1911. doi: 10.1056/NEJMoa043802

Fu, A., Mo, Q., Wu, Y., Wang, B., Liu, R., Tang, L., et al. (2019). Protective effect of bacillus amyloliquefaciens against salmonella *via* polarizing macrophages to M1 phenotype directly and to M2 depended on microbiota. *Food Funct.* 10, 7653–7666. doi: 10.1039/C9FO01651A

Fu, X., Zeng, L., Liu, Z., Ke, X., Lei, L., and Li, G. (2016). MicroRNA-206 regulates the secretion of inflammatory cytokines and MMP9 expression by targeting TIMP3 in mycobacterium tuberculosis-infected THP-1 human macrophages. *Biochem. Biophys. Res. Commun.* 477, 167–173. doi: 10.1016/j.bbrc.2016.06.038

Gan, Z., Tang, X., Wang, Z., Li, J., Wang, Z., and Du, H. (2019). Regulation of macrophage iron homeostasis is associated with the localization of bacteria. *Metallomics* 11, 454–461. doi: 10.1039/C8MT00301G

Garrett, W. S. (2019). The gut microbiota and colon cancer. *Science* 364, 1133–1135. doi: 10.1126/science.aaw2367

Geller, L. T., Barzily-Rokni, M., Danino, T., Jonas, O. H., Shental, N., Nejman, D., et al. (2017). Potential role of intratumor bacteria in mediating tumor resistance to the chemotherapeutic drug gemcitabine. *Science* 357, 1156–1160. doi: 10.1126/science.aah5043

Glowacka, P., Zakowska, D., Naylor, K., Niemcewicz, M., and Bielawska-Drozd, A. (2018). Brucella – virulence factors, pathogenesis and treatment. *Pol. J. Microbiol.* 67, 151–161. doi: 10.21307/pjm-2018-029

Goldmann, O., von Kockritz-Blickwede, M., Holtje, C., Chhatwal, G. S., Geffers, R., and Medina, E. (2007). Transcriptome analysis of murine macrophages in response to infection with streptococcus pyogenes reveals an unusual activation program. *Infect. Immun.* 75, 4148–4157. doi: 10.1128/IAI.00181-07

Golombos, D. M., Ayangbesan, A., O'Malley, P., Lewicki, P., Barlow, L., Barbieri, C. E., et al. (2018). The role of gut microbiome in the pathogenesis of prostate cancer: a prospective. *Pilot Study. Urology.* 111, 122–128. doi: 10.1016/j.urology.2017.08.039

Gomes, S., Cavadas, B., Ferreira, J. C., Marques, P. I., Monteiro, C., Sucena, M., et al. (2019). Profiling of lung microbiota discloses differences in adenocarcinoma and squamous cell carcinoma. *Sci. Rep.* 9:12838. doi: 10.1038/s41598-019-49195-w

Gondwe, T., Ness, R., Totten, P. A., Astete, S., Tang, G., Gold, M. A., et al. (2020). Novel bacterial vaginosis-associated organisms mediate the relationship between vaginal douching and pelvic inflammatory disease. *Sex. Transm. Infect.* 96, 439–444. doi: 10.1136/sextrans-2019-054191

Greathouse, K. L., White, J. R., Vargas, A. J., Bliskovsky, V. V., Beck, J. A., von Muhlinen, N., et al. (2018). Interaction between the microbiome and TP53 in human lung cancer. *Genome Biol.* 19:123. doi: 10.1186/s13059-018-1501-6

Haas, R., Smith, J., Rocher-Ros, V., Nadkarni, S., Montero-Melendez, T., D'Acquisto, F., et al. (2015). Lactate regulates metabolic and pro-inflammatory circuits in control of T cell migration and effector functions. *PLoS Biol.* 13:e1002202. doi: 10.1371/journal.pbio.1002202

Hashemi Goradel, N., Heidarzadeh, S., Jahangiri, S., Farhood, B., Mortezaee, K., Khanlarkhani, N., et al. (2019). Fusobacterium nucleatum and colorectal cancer: a mechanistic overview. *J. Cell. Physiol.* 234, 2337–2344. doi: 10.1002/jcp.27250

He, Z., Gharaibeh, R. Z., Newsome, R. C., Pope, J. L., Dougherty, M. W., Tomkovich, S., et al. (2019). Campylobacter jejuni promotes colorectal tumorigenesis through the action of the cytolethal distending toxin. *Gut* 68, 289–300. doi: 10.1136/gutjnl-2018-317200

Heim, C. E., Bosch, M. E., Yamada, K. J., Aldrich, A. L., Chaudhari, S. S., Klinkebiel, D., et al. (2020). Lactate production by Staphylococcus aureus biofilm inhibits HDAC11 to reprogramme the host immune response during persistent infection. *Nat. Microbiol.* 5, 1271–1284. doi: 10.1038/s41564-020-0756-3

Hosgood, H. D. 3rd, Sapkota, A. R., Rothman, N., Rohan, T., Hu, W., Xu, J., et al. (2014). The potential role of lung microbiota in lung cancer attributed to household coal burning exposures. *Environ. Mol. Mutagen.* 55, 643–651. doi: 10.1002/em.21878

Hsieh, Y. Y., Tung, S. Y., Pan, H. Y., Yen, C. W., Xu, H. W., Lin, Y. J., et al. (2018). Increased abundance of clostridium and fusobacterium in gastric microbiota of patients with gastric cancer in Taiwan. *Sci. Rep.* 8:158. doi: 10.1038/s41598-017-18596-0

Hu, L., Liu, Y., Kong, X., Wu, R., Peng, Q., Zhang, Y., et al. (2021). Fusobacterium nucleatum facilitates M2 macrophage polarization and colorectal carcinoma progression by activating TLR4/NF-kappaB/S100A9 Cascade. *Front. Immunol.* 12:658681. doi: 10.3389/fimmu.2021.658681

Huang, Z., Luo, Q., Guo, Y., Chen, J., Xiong, G., Peng, Y., et al. (2015). Mycobacterium tuberculosis-induced polarization of human macrophage orchestrates the formation and development of tuberculous granulomas *in vitro*. *PLoS One* 10:e0129744. doi: 10.1371/journal.pone.0129744

Im, S. S., Yousef, L., Blaschitz, C., Liu, J. Z., Edwards, R. A., Young, S. G., et al. (2011). Linking lipid metabolism to the innate immune response in macrophages through sterol regulatory element binding protein-1a. *Cell Metab.* 13, 540–549. doi: 10.1016/j.cmet.2011.04.001

Italiani, P., and Boraschi, D. (2014). From monocytes to M1/M2 macrophages: phenotypical vs functional differentiation. *Front. Immunol.* 5:514. doi: 10.3389/fimmu.2014.00514

Jin, C., Lagoudas, G. K., Zhao, C., Bullman, S., Bhutkar, A., Hu, B., et al. (2019). Commensal microbiota promote lung cancer development *via* gammadelta T cells. *Cells* 176, 998–1013.e16. doi: 10.1016/j.cell.2018.12.040

Jin, Z., Tian, Y., Yan, D., Li, D., and Zhu, X. (2017). BCG increased membrane expression of TRIM59 through the TLR2/TLR4/IRF5 pathway in RAW264.7 macrophages. *Protein Pept. Lett.* 24, 765–770. doi: 10.2174/0929866524666170818155524

Jung, M., Mertens, C., and Brune, B. (2015). Macrophage iron homeostasis and polarization in the context of cancer. *Immunobiology* 220, 295–304. doi: 10.1016/j.imbio.2014.09.011

Kadioglu, A., and Andrew, P. W. (2004). The innate immune response to pneumococcal lung infection: the untold story. *Trends Immunol.* 25, 143–149. doi: 10.1016/j.it.2003.12.006

Kaufmann, S. H. (2016). Immunopathology of mycobacterial diseases. *Semin. Immunopathol.* 38, 135–138. doi: 10.1007/s00281-015-0547-8

Keay, S., Zhang, C. O., Baldwin, B. R., and Alexander, R. B. (1999). Polymerase chain reaction amplification of bacterial 16s rRNA genes in prostate biopsies from men without chronic prostatitis. *Urology* 53, 487–491. doi: 10.1016/S0090-4295(98)00553-6

Khan, J., Sharma, P. K., and Mukhopadhaya, A. (2015). Vibrio cholerae porin OmpU mediates M1-polarization of macrophages/monocytes *via* TLR1/TLR2 activation. *Immunobiology* 220, 1199–1209. doi: 10.1016/j.imbio.2015.06.009

Kim, J., Ochoa, M. T., Krutzik, S. R., Takeuchi, O., Uematsu, S., Legaspi, A. J., et al. (2002). Activation of toll-like receptor 2 in acne triggers inflammatory cytokine responses. *J. Immunol.* 169, 1535–1541. doi: 10.4049/jimmunol.169.3.1535

Kim, K. S., Rowlinson, M. C., Bennion, R., Liu, C., Talan, D., Summanen, P., et al. (2010). Characterization of Slackia exigua isolated from human wound infections, including abscesses of intestinal origin. *J. Clin. Microbiol.* 48, 1070–1075. doi: 10.1128/JCM.01576-09

Kiszewski, A. E., Becerril, E., Aguilar, L. D., Kader, I. T., Myers, W., Portaels, F., et al. (2006). The local immune response in ulcerative lesions of Buruli disease. *Clin. Exp. Immunol.* 143, 445–451. doi: 10.1111/j.1365-2249.2006.03020.x

Kostic, A. D., Chun, E., Robertson, L., Glickman, J. N., Gallini, C. A., Michaud, M., et al. (2013). Fusobacterium nucleatum potentiates intestinal tumorigenesis and modulates the tumor-immune microenvironment. *Cell Host Microbe* 14, 207–215. doi: 10.1016/j.chom.2013.07.007

Kostic, A. D., Gevers, D., Pedamallu, C. S., Michaud, M., Duke, F., Earl, A. M., et al. (2012). Genomic analysis identifies association of fusobacterium with colorectal carcinoma. *Genome Res.* 22, 292–298. doi: 10.1101/gr.126573.111

Krakowiak, M. S., Noto, J. M., Piazuelo, M. B., Hardbower, D. M., Romero-Gallo, J., Delgado, A., et al. (2015). Matrix metalloproteinase 7 restrains helicobacter pylori-induced gastric inflammation and premalignant lesions in the stomach by altering macrophage polarization. *Oncogene* 34, 1865–1871. doi: 10.1038/onc.2014.135

Kusaka, Y., Kajiwara, C., Shimada, S., Ishii, Y., Miyazaki, Y., Inase, N., et al. (2018). Potential role of gr-1+ CD8+ T lymphocytes as a source of interferon-gamma and M1/M2 polarization during the acute phase of murine legionella pneumophila pneumonia. *J. Innate Immun.* 10, 328–338. doi: 10.1159/000490585

Kwong, T. N. Y., Wang, X., Nakatsu, G., Chow, T. C., Tipoe, T., Dai, R. Z. W., et al. (2018). Association between bacteremia from specific microbes and subsequent diagnosis of colorectal cancer. *Gastroenterology* 155, 383–390.e8. doi: 10.1053/j.gastro.2018.04.028

Laniewski, P., Barnes, D., Goulder, A., Cui, H., Roe, D. J., Chase, D. M., et al. (2018). Linking cervicovaginal immune signatures, HPV and microbiota composition in cervical carcinogenesis in non-Hispanic and Hispanic women. *Sci. Rep.* 8:7593. doi: 10.1038/s41598-018-25879-7

Lara-Tejero, M., and Galan, J. E. (2000). A bacterial toxin that controls cell cycle progression as a deoxyribonuclease I-like protein. *Science* 290, 354–357. doi: 10.1126/science.290.5490.354

Laroumagne, S., Lepage, B., Hermant, C., Plat, G., Phelippeau, M., Bigay-Game, L., et al. (2013). Bronchial colonisation in patients with lung cancer: a prospective study. *Eur. Respir. J.* 42, 220–229. doi: 10.1183/09031936.00062212

Lauterbach, M. A., Hanke, J. E., Serefidou, M., Mangan, M. S. J., Kolbe, C. C., Hess, T., et al. (2019). Toll-like receptor signaling rewires macrophage metabolism and promotes histone acetylation *via* ATP-citrate Lyase. *Immunity* 51, 997–1011.e7. doi: 10.1016/j.immuni.2019.11.009

Laviron, M., and Boissonnas, A. (2019). Ontogeny of tumor-associated macrophages. *Front Immunol.* 10:1799. doi: 10.3389/fimmu.2019.01799

Lax, A. J., and Thomas, W. (2002). How bacteria could cause cancer: one step at a time. *Trends Microbiol.* 10, 293–299. doi: 10.1016/S0966-842X(02)02360-0

Le Noci, V., Guglielmetti, S., Arioli, S., Camisaschi, C., Bianchi, F., Sommariva, M., et al. (2018). Modulation of pulmonary microbiota by antibiotic or probiotic aerosol therapy: a strategy to promote immunosurveillance against lung metastases. *Cell Rep.* 24, 3528–3538. doi: 10.1016/j.celrep.2018.08.090

Lee, J. E., Lee, S., Lee, H., Song, Y. M., Lee, K., Han, M. J., et al. (2013). Association of the vaginal microbiota with human papillomavirus infection in a Korean twin cohort. *PLoS One* 8:e63514. doi: 10.1371/journal.pone.0063514

Lee, S. H., Sung, J. Y., Yong, D., Chun, J., Kim, S. Y., Song, J. H., et al. (2016). Characterization of microbiome in bronchoalveolar lavage fluid of patients with lung cancer comparing with benign mass like lesions. *Lung Cancer* 102, 89–95. doi: 10.1016/j.lungcan.2016.10.016

Leskinen, M. J., Rantakokko-Jalava, K., Manninen, R., Leppilahti, M., Marttila, T., Kylmala, T., et al. (2003). Negative bacterial polymerase chain reaction (PCR) findings in prostate tissue from patients with symptoms of chronic pelvic pain syndrome (CPPS) and localized prostate cancer. *Prostate* 55, 105–110. doi: 10.1002/pros.10218

Li, J. J., Liu, Y., Song, L. T., Li, C. Y., and Jiang, S. Y. (2022). Regulation of microRNA-126 on the polarization of human macrophages stimulated by Porphyromonas gingivalis lipopolysaccharide. *Zhonghua Kou Qiang Yi Xue Za Zhi* 57, 390–396. doi: 10.3760/cma.j.cn112144-20210701-00310

Li, Q., Peng, W., Wu, J., Wang, X., Ren, Y., Li, H., et al. (2019). Autoinducer-2 of gut microbiota, a potential novel marker for human colorectal cancer, is associated with the activation of TNFSF9 signaling in macrophages. *Onco. Targets. Ther.* 8:e1626192. doi: 10.1080/2162402X.2019.1626192

Li, S. J., Sun, S. J., Gao, J., and Sun, F. B. (2016). Wogonin induces Beclin-1/PI3K and reactive oxygen species-mediated autophagy in human pancreatic cancer cells. *Oncol. Lett.* 12, 5059–5067. doi: 10.3892/ol.2016.5367

Li, Q., Wu, W., Gong, D., Shang, R., Wang, J., and Yu, H. (2021). Propionibacterium acnes overabundance in gastric cancer promote M2 polarization of macrophages *via* a TLR4/PI3K/Akt signaling. *Gastric Cancer* 24, 1242–1253. doi: 10.1007/s10120-021-01202-8

Liang, M. D., Bagchi, A., Warren, H. S., Tehan, M. M., Trigilio, J. A., Beasley-Topliffe, L. K., et al. (2005). Bacterial peptidoglycan-associated lipoprotein: a naturally occurring toll-like receptor 2 agonist that is shed into serum and has synergy with lipopolysaccharide. *J. Infect. Dis.* 191, 939–948. doi: 10.1086/427815

Lin, Y., Xu, J., and Lan, H. (2019). Tumor-associated macrophages in tumor metastasis: biological roles and clinical therapeutic applications. *J. Hematol. Oncol.* 12:76. doi: 10.1186/s13045-019-0760-3

Liss, M. A., White, J. R., Goros, M., Gelfond, J., Leach, R., Johnson-Pais, T., et al. (2018). Metabolic biosynthesis pathways identified from fecal microbiome associated with prostate cancer. *Eur. Urol.* 74, 575–582. doi: 10.1016/j.eururo.2018.06.033

Liu, J., Luo, M., Zhang, Y., Cao, G., and Wang, S. (2020). Association of high-risk human papillomavirus infection duration and cervical lesions with vaginal microbiota composition. *Ann. Transl. Med.* 8:1161. doi: 10.21037/atm-20-5832

Liu, L., Shi, W., Xiao, X., Wu, X., Hu, H., Yuan, S., et al. (2021). BCG immunotherapy inhibits cancer progression by promoting the M1 macrophage differentiation of THP1 cells *via* the Rb/E2F1 pathway in cervical carcinoma. *Oncol. Rep.* 46:245. doi: 10.3892/or.2021.8196

Liu, H. X., Tao, L. L., Zhang, J., Zhu, Y. G., Zheng, Y., Liu, D., et al. (2018). Difference of lower airway microbiome in bilateral protected specimen brush between lung cancer patients with unilateral lobar masses and control subjects. *Int. J. Cancer* 142, 769–778. doi: 10.1002/ijc.31098

Liu, P. S., Wang, H., Li, X., Chao, T., Teav, T., Christen, S., et al. (2017). Alpha-ketoglutarate orchestrates macrophage activation through metabolic and epigenetic reprogramming. *Nat. Immunol.* 18, 985–994. doi: 10.1038/ni.3796

Liu, C. Y., Xu, J. Y., Shi, X. Y., Huang, W., Ruan, T. Y., Xie, P., et al. (2013). M2-polarized tumor-associated macrophages promoted epithelial-mesenchymal transition in pancreatic cancer cells, partially through TLR4/IL-10 signaling pathway. *Lab. Investig.* 93, 844–854. doi: 10.1038/labinvest.2013.69

Lizotte, P. H., Baird, J. R., Stevens, C. A., Lauer, P., Green, W. R., Brockstedt, D. G., et al. (2014). Attenuated listeria monocytogenes reprograms M2-polarized tumor-associated macrophages in ovarian cancer leading to iNOS-mediated tumor cell lysis. *Onco. Targets. Ther.* 3:e28926. doi: 10.4161/onci.28926

Long, K. B., Collier, A. I., and Beatty, G. L. (2019). Macrophages: key orchestrators of a tumor microenvironment defined by therapeutic resistance. *Mol. Immunol.* 110, 3–12. doi: 10.1016/j.molimm.2017.12.003

Lopes, R. L., Borges, T. J., Zanin, R. F., and Bonorino, C. (2016). IL-10 is required for polarization of macrophages to M2-like phenotype by mycobacterial DnaK (heat shock protein 70). *Cytokine* 85, 123–129. doi: 10.1016/j.cyto.2016.06.018

Lu, L., Ling, W., and Ruan, Z. (2021). TAM-derived extracellular vesicles containing microRNA-29a-3p explain the deterioration of ovarian cancer. *Mol. Ther. Nucleic. Acids* 25, 468–482. doi: 10.1016/j.omtn.2021.05.011

Lunn, R. M., Mehta, S. S., Jahnke, G. D., Wang, A., Wolfe, M. S., and Berridge, B. R. (2022). Cancer Hazard evaluations for contemporary needs: highlights from new National Toxicology Program Evaluations and methodological advancements. *J. Natl. Cancer Inst.* 114, 1441–1448. doi: 10.1093/jnci/djac164

Luo, F., Sun, X., Qu, Z., and Zhang, X. (2016). Salmonella typhimurium-induced M1 macrophage polarization is dependent on the bacterial O antigen. *World J. Microbiol. Biotechnol.* 32:22. doi: 10.1007/s11274-015-1978-z

Ma, Z., Li, R., Hu, R., Deng, X., Xu, Y., Zheng, W., et al. (2020). Brucella abortus BspJ is a Nucleomodulin that inhibits macrophage apoptosis and promotes intracellular survival of Brucella. *Front. Microbiol.* 11:599205. doi: 10.3389/fmicb.2020.599205

Mantovani, A., Allavena, P., Sica, A., and Balkwill, F. (2008). Cancer-related inflammation. *Nature* 454, 436–444. doi: 10.1038/nature07205

Mantovani, A., Sica, A., Sozzani, S., Allavena, P., Vecchi, A., and Locati, M. (2004). The chemokine system in diverse forms of macrophage activation and polarization. *Trends Immunol.* 25, 677–686. doi: 10.1016/j.it.2004.09.015

Mantovani, A., Sozzani, S., Locati, M., Allavena, P., and Sica, A. (2002). Macrophage polarization: tumor-associated macrophages as a paradigm for polarized M2 mononuclear phagocytes. *Trends Immunol.* 23, 549–555. doi: 10.1016/S1471-4906(02)02302-5

Mima, K., Nishihara, R., Qian, Z. R., Cao, Y., Sukawa, Y., Nowak, J. A., et al. (2016). Fusobacterium nucleatum in colorectal carcinoma tissue and patient prognosis. *Gut* 65, 1973–1980. doi: 10.1136/gutjnl-2015-310101

Mima, K., Sukawa, Y., Nishihara, R., Qian, Z. R., Yamauchi, M., Inamura, K., et al. (2015). Fusobacterium nucleatum and T cells in colorectal carcinoma. *JAMA Oncol.* 1, 653–661. doi: 10.1001/jamaoncol.2015.1377

Miquel, S., Martin, R., Rossi, O., Bermudez-Humaran, L. G., Chatel, J. M., Sokol, H., et al. (2013). Faecalibacterium prausnitzii and human intestinal health. *Curr. Opin. Microbiol.* 16, 255–261. doi: 10.1016/j.mib.2013.06.003

Mitra, A., MacIntyre, D. A., Lee, Y. S., Smith, A., Marchesi, J. R., Lehne, B., et al. (2015). Cervical intraepithelial neoplasia disease progression is associated with increased vaginal microbiome diversity. *Sci. Rep.* 5:16865. doi: 10.1038/srep16865

Molinero, N., Ruiz, L., Milani, C., Gutierrez-Diaz, I., Sanchez, B., Mangifesta, M., et al. (2019). The human gallbladder microbiome is related to the physiological state and the biliary metabolic profile. *Microbiome* 7:100. doi: 10.1186/s40168-019-0712-8

Monack, D. M., Raupach, B., Hromockyj, A. E., and Falkow, S. (1996). Salmonella typhimurium invasion induces apoptosis in infected macrophages. *Proc. Natl. Acad. Sci. U. S. A.* 93, 9833–9838. doi: 10.1073/pnas.93.18.9833

Moratalla, A., Caparros, E., Juanola, O., Portune, K., Puig-Kroger, A., Estrada-Capetillo, L., et al. (2016). Bifidobacterium pseudocatenulatum CECT7765 induces an M2 anti-inflammatory transition in macrophages from patients with cirrhosis. *J. Hepatol.* 64, 135–145. doi: 10.1016/j.jhep.2015.08.020

Murata, H., Tsuji, S., Tsujii, M., Fu, H. Y., Tanimura, H., Tsujimoto, M., et al. (2004). Helicobacter bilis infection in biliary tract cancer. *Aliment. Pharmacol. Ther.* 20, 90–94. doi: 10.1111/j.1365-2036.2004.01972.x

Murphy, J. T., Sommer, S., Kabara, E. A., Verman, N., Kuelbs, M. A., Saama, P., et al. (2006). Gene expression profiling of monocyte-derived macrophages following infection with Mycobacterium avium subspecies avium and Mycobacterium avium subspecies paratuberculosis. *Physiol. Genomics* 28, 67–75. doi: 10.1152/physiolgenomics.00098.2006

Murray, P. J., Allen, J. E., Biswas, S. K., Fisher, E. A., Gilroy, D. W., Goerdt, S., et al. (2014). Macrophage activation and polarization: nomenclature and experimental guidelines. *Immunity* 41, 14–20. doi: 10.1016/j.immuni.2014.06.008

Murray, P. J., and Wynn, T. A. (2011). Protective and pathogenic functions of macrophage subsets. *Nat. Rev. Immunol.* 11, 723–737. doi: 10.1038/nri3073

Myers, D. R., Abram, C. L., Wildes, D., Belwafa, A., Welsh, A. M. N., Schulze, C. J., et al. (2020). Shp1 loss enhances macrophage effector function and promotes anti-tumor immunity. *Front. Immunol.* 11:576310. doi: 10.3389/fimmu.2020.576310

Nagano, T., Otoshi, T., Hazama, D., Kiriu, T., Umezawa, K., Katsurada, N., et al. (2019). Novel cancer therapy targeting microbiome. *Onco. Targets. Ther.* 12, 3619–3624. doi: 10.2147/OTT.S207546

Nagaraja, V., and Eslick, G. D. (2014). Systematic review with meta-analysis: the relationship between chronic salmonella typhi carrier status and gall-bladder cancer. *Aliment. Pharmacol. Ther.* 39, 745–750. doi: 10.1111/apt.12655

Nath, G., Singh, Y. K., Kumar, K., Gulati, A. K., Shukla, V. K., Khanna, A. K., et al. (2008). Association of carcinoma of the gallbladder with typhoid carriage in a typhoid endemic area using nested PCR. *J. Infect. Dev. Ctries.* 2, 302–307. doi: 10.3855/jidc.226

Nath, G., Singh, Y. K., Maurya, P., Gulati, A. K., Srivastava, R. C., and Tripathi, S. K. (2010). Does salmonella Typhi primarily reside in the liver of chronic typhoid carriers? *J. Infect. Dev. Ctries.* 4, 259–261. doi: 10.3855/jidc.820

Nejman, D., Livyatan, I., Fuks, G., Gavert, N., Zwang, Y., Geller, L. T., et al. (2020). The human tumor microbiome is composed of tumor-type-specific intracellular bacteria. *Science* 368, 973–980. doi: 10.1126/science.aay9189

Oishi, Y., Spann, N. J., Link, V. M., Muse, E. D., Strid, T., Edillor, C., et al. (2017). SREBP1 contributes to resolution of pro-inflammatory TLR4 signaling by reprogramming fatty acid metabolism. *Cell Metab.* 25, 412–427. doi: 10.1016/j.cmet.2016.11.009

Onderdonk, A. B., Delaney, M. L., and Fichorova, R. N. (2016). The human microbiome during bacterial vaginosis. *Clin. Microbiol. Rev.* 29, 223–238. doi: 10.1128/CMR.00075-15

Parhi, L., Alon-Maimon, T., Sol, A., Nejman, D., Shhadeh, A., Fainsod-Levi, T., et al. (2020). Breast cancer colonization by fusobacterium nucleatum accelerates tumor growth and metastatic progression. *Nat. Commun.* 11:3259. doi: 10.1038/s41467-020-16967-2

Paynich, M. L., Jones-Burrage, S. E., and Knight, K. L. (2017). Exopolysaccharide from *Bacillus subtilis* induces anti-inflammatory M2 macrophages that prevent T cell-mediated disease. *J. Immunol.* 198, 2689–2698. doi: 10.4049/jimmunol.1601641

Pearce, M. M., Hilt, E. E., Rosenfeld, A. B., Zilliox, M. J., Thomas-White, K., Fok, C., et al. (2014). The female urinary microbiome: a comparison of women with and without urgency urinary incontinence. *MBio* 5, e01283–e01214. doi: 10.1128/mBio.01283-14

Peng, K. T., Hsieh, C. C., Huang, T. Y., Chen, P. C., Shih, H. N., Lee, M. S., et al. (2017). Staphylococcus aureus biofilm elicits the expansion, activation and polarization of myeloid-derived suppressor cells *in vivo* and *in vitro*. *PLoS One* 12:e0183271. doi: 10.1371/journal.pone.0183271

Peters, B. A., Hayes, R. B., Goparaju, C., Reid, C., Pass, H. I., and Ahn, J. (2019). The microbiome in lung cancer tissue and recurrence-free survival. *Cancer Epidemiol. Biomark. Prev.* 28, 731–740. doi: 10.1158/1055-9965.EPI-18-0966

Pidwill, G. R., Gibson, J. F., Cole, J., Renshaw, S. A., and Foster, S. J. (2020). The role of macrophages in Staphylococcus aureus infection. *Front. Immunol.* 11:620339. doi: 10.3389/fimmu.2020.620339

Pinheiro da Silva, F., Aloulou, M., Skurnik, D., Benhamou, M., Andremont, A., Velasco, I. T., et al. (2007). CD16 promotes Escherichia coli sepsis through an FcR gamma inhibitory pathway that prevents phagocytosis and facilitates inflammation. *Nat. Med.* 13, 1368–1374. doi: 10.1038/nm1665

Pittet, M. J., Michielin, O., and Migliorini, D. (2022). Clinical relevance of tumour-associated macrophages. *Nat. Rev. Clin. Oncol.* 19, 402–421. doi: 10.1038/s41571-022-00620-6

Pleguezuelos-Manzano, C., Puschhof, J., Rosendahl Huber, A., van Hoeck, A., Wood, H. M., Nomburg, J., et al. (2020). Mutational signature in colorectal cancer caused by genotoxic pks(+) E. coli. *Nature* 580, 269–273. doi: 10.1038/s41586-020-2080-8

Polak, D., Yaya, A., Levy, D. H., Metzger, Z., and Abramovitz, I. (2021). Enterococcus faecalis sustained infection induces macrophage pro-resolution polarization. *Int. Endod. J.* 54, 1840–1849. doi: 10.1111/iej.13574

Poore, G. D., Kopylova, E., Zhu, Q., Carpenter, C., Fraraccio, S., Wandro, S., et al. (2020). Microbiome analyses of blood and tissues suggest cancer diagnostic approach. *Nature* 579, 567–574. doi: 10.1038/s41586-020-2095-1

Pore, D., Mahata, N., Pal, A., and Chakrabarti, M. K. (2010). 34 kDa MOMP of Shigella flexneri promotes TLR2 mediated macrophage activation with the engagement of NF-kappaB and p38 MAP kinase signaling. *Mol. Immunol.* 47, 1739–1746. doi: 10.1016/j.molimm.2010.03.001

Pradhan, S. B., and Dali, S. (2004). Relation between gallbladder neoplasm and helicobacter hepaticus infection. *Kathmandu Univ Med J (KUMJ).* 2, 331–335.

Pushalkar, S., Hundeyin, M., Daley, D., Zambirinis, C. P., Kurz, E., Mishra, A., et al. (2018). The pancreatic cancer microbiome promotes oncogenesis by induction of innate and adaptive immune suppression. *Cancer Discov.* 8, 403–416. doi: 10.1158/2159-8290.CD-17-1134

Ridlon, J. M., Ikegawa, S., Alves, J. M., Zhou, B., Kobayashi, A., Iida, T., et al. (2013). Clostridium scindens: a human gut microbe with a high potential to convert glucocorticoids into androgens. *J. Lipid Res.* 54, 2437–2449. doi: 10.1194/jlr.M038869

Riquelme, E., Zhang, Y., Zhang, L., Montiel, M., Zoltan, M., Dong, W., et al. (2019). Tumor microbiome diversity and composition influence pancreatic cancer outcomes. *Cells* 178, 795–806.e12. doi: 10.1016/j.cell.2019.07.008

Roberts, P. J., Dickinson, R. J., Whitehead, A., Laughton, C. R., and Foweraker, J. E. (2002). The culture of lactobacilli species in gastric carcinoma. *J. Clin. Pathol.* 55:477. doi: 10.1136/jcp.55.6.477

Rosenberger, C. M., and Finlay, B. B. (2003). Phagocyte sabotage: disruption of macrophage signalling by bacterial pathogens. *Nat. Rev. Mol. Cell Biol.* 4, 385–396. doi: 10.1038/nrm1104

Routy, B., Le Chatelier, E., Derosa, L., Duong, C. P. M., Alou, M. T., Daillere, R., et al. (2018). Gut microbiome influences efficacy of PD-1-based immunotherapy against epithelial tumors. *Science* 359, 91–97. doi: 10.1126/science.aan3706

Rubinstein, M. R., Wang, X., Liu, W., Hao, Y., Cai, G., and Han, Y. W. (2013). Fusobacterium nucleatum promotes colorectal carcinogenesis by modulating E-cadherin/beta-catenin signaling *via* its FadA adhesin. *Cell Host Microbe* 14, 195–206. doi: 10.1016/j.chom.2013.07.012

Ruffell, B., Chang-Strachan, D., Chan, V., Rosenbusch, A., Ho, C. M., Pryer, N., et al. (2014). Macrophage IL-10 blocks CD8+ T cell-dependent responses to chemotherapy by suppressing IL-12 expression in intratumoral dendritic cells. *Cancer Cell* 26, 623–637. doi: 10.1016/j.ccell.2014.09.006

Russell, D. G., Cardona, P. J., Kim, M. J., Allain, S., and Altare, F. (2009). Foamy macrophages and the progression of the human tuberculosis granuloma. *Nat. Immunol.* 10, 943–948. doi: 10.1038/ni.1781

Sakamoto, R., Kajihara, I., Mijiddorj, T., Otsuka-Maeda, S., Sawamura, S., Nishimura, Y., et al. (2021). Existence of Staphylococcus aureus correlates with the progression of extramammary Paget's disease: potential involvement of interleukin-17 and M2-like macrophage polarization. *Eur. J. Dermatol.* 31, 48–54. doi: 10.1684/ejd.2021.3972

Salazar, C. R., Sun, J., Li, Y., Francois, F., Corby, P., Perez-Perez, G., et al. (2013). Association between selected oral pathogens and gastric precancerous lesions. *PLoS One* 8:e51604. doi: 10.1371/journal.pone.0051604

Sanchez-Lopez, E., Zhong, Z., Stubelius, A., Sweeney, S. R., Booshehri, L. M., Antonucci, L., et al. (2019). Choline uptake and metabolism modulate macrophage IL-1beta and IL-18 production. *Cell Metab.* 29, 1350–1362.e7. doi: 10.1016/j.cmet.2019.03.011

Schulte, L. N., Eulalio, A., Mollenkopf, H. J., Reinhardt, R., and Vogel, J. (2011). Analysis of the host microRNA response to salmonella uncovers the control of major cytokines by the let-7 family. *EMBO J.* 30, 1977–1989. doi: 10.1038/emboj.2011.94

Schulz, C., Schutte, K., Mayerle, J., and Malfertheiner, P. (2019). The role of the gastric bacterial microbiome in gastric cancer: helicobacter pylori and beyond. *Ther. Adv. Gastroenterol.* 12:1756284819894062. doi: 10.1177/1756284819894062

Scott, A. J., Alexander, J. L., Merrifield, C. A., Cunningham, D., Jobin, C., Brown, R., et al. (2019). International cancer microbiome consortium consensus statement on the role of the human microbiome in carcinogenesis. *Gut* 68, 1624–1632. doi: 10.1136/gutjnl-2019-318556

Seow, S. W., Cai, S., Rahmat, J. N., Bay, B. H., Lee, Y. K., Chan, Y. H., et al. (2010). Lactobacillus rhamnosus GG induces tumor regression in mice bearing orthotopic bladder tumors. *Cancer Sci.* 101, 751–758. doi: 10.1111/j.1349-7006.2009.01426.x

Sepich-Poore, G. D., Zitvogel, L., Straussman, R., Hasty, J., Wargo, J. A., and Knight, R. (2021). The microbiome and human cancer. *Science* 371:6536. doi: 10.1126/science.abc4552

Sfanos, K. S., Sauvageot, J., Fedor, H. L., Dick, J. D., De Marzo, A. M., and Isaacs, W. B. (2008). A molecular analysis of prokaryotic and viral DNA sequences in prostate tissue from patients with prostate cancer indicates the presence of multiple and diverse microorganisms. *Prostate* 68, 306–320. doi: 10.1002/pros.20680

Sha, S., Shi, Y., Tang, Y., Jia, L., Han, X., Liu, Y., et al. (2021). Mycobacterium tuberculosis Rv1987 protein induces M2 polarization of macrophages through activating the PI3K/Akt1/mTOR signaling pathway. *Immunol. Cell Biol.* 99, 570–585. doi: 10.1111/imcb.12436

Shapouri-Moghaddam, A., Mohammadian, S., Vazini, H., Taghadosi, M., Esmaeili, S. A., Mardani, F., et al. (2018). Macrophage plasticity, polarization, and function in health and disease. *J. Cell. Physiol.* 233, 6425–6440. doi: 10.1002/jcp.26429

Shaughnessy, L. M., and Swanson, J. A. (2007). The role of the activated macrophage in clearing listeria monocytogenes infection. *Front. Biosci.* 12, 2683–2692. doi: 10.2741/2364

Shi, Y., Zheng, W., Yang, K., Harris, K. G., Ni, K., Xue, L., et al. (2020). Intratumoral accumulation of gut microbiota facilitates CD47-based immunotherapy *via* STING signaling. *J. Exp. Med.* 217:e20192282. doi: 10.1084/jem.20192282

Shrestha, E., White, J. R., Yu, S. H., Kulac, I., Ertunc, O., De Marzo, A. M., et al. (2018). Profiling the urinary microbiome in men with positive versus negative biopsies for prostate cancer. *J. Urol.* 199, 161–171. doi: 10.1016/j.juro.2017.08.001

Smith, M. W., Schmidt, J. E., Rehg, J. E., Orihuela, C. J., and McCullers, J. A. (2007). Induction of pro- and anti-inflammatory molecules in a mouse model of pneumococcal pneumonia after influenza. *Comp. Med.* 57, 82–89. PMID: 17348295

So, K. A., Yang, E. J., Kim, N. R., Hong, S. R., Lee, J. H., Hwang, C. S., et al. (2020). Changes of vaginal microbiota during cervical carcinogenesis in women with human papillomavirus infection. *PLoS One* 15:e0238705. doi: 10.1371/journal.pone.0238705

Sohn, W., Jun, D. W., Lee, K. N., Lee, H. L., Lee, O. Y., Choi, H. S., et al. (2015). Lactobacillus paracasei induces M2-dominant Kupffer cell polarization in a mouse model of nonalcoholic steatohepatitis. *Dig. Dis. Sci.* 60, 3340–3350. doi: 10.1007/s10620-015-3770-1

Sokol, H., Pigneur, B., Watterlot, L., Lakhdari, O., Bermudez-Humaran, L. G., Gratadoux, J. J., et al. (2008). Faecalibacterium prausnitzii is an anti-inflammatory commensal bacterium identified by gut microbiota analysis of Crohn disease patients. *Proc. Natl. Acad. Sci. U. S. A.* 105, 16731–16736. doi: 10.1073/pnas.0804812105

St Jean, A. T., Zhang, M., and Forbes, N. S. (2008). Bacterial therapies: completing the cancer treatment toolbox. *Curr. Opin. Biotechnol.* 19, 511–517. doi: 10.1016/j.copbio.2008.08.004

Stapels, D. A. C., Hill, P. W. S., Westermann, A. J., Fisher, R. A., Thurston, T. L., Saliba, A. E., et al. (2018). Salmonella persisters undermine host immune defenses during antibiotic treatment. *Science* 362, 1156–1160. doi: 10.1126/science.aat7148

Su, P., Wang, Q., Bi, E., Ma, X., Liu, L., Yang, M., et al. (2020). Enhanced lipid accumulation and metabolism are required for the differentiation and activation of tumor-associated macrophages. *Cancer Res.* 80, 1438–1450. doi: 10.1158/0008-5472.CAN-19-2994

Suarez, G., Romero-Gallo, J., Piazuelo, M. B., Sierra, J. C., Delgado, A. G., Washington, M. K., et al. (2019). Nod1 imprints inflammatory and carcinogenic responses toward the gastric pathogen helicobacter pylori. *Cancer Res.* 79, 1600–1611. doi: 10.1158/0008-5472.CAN-18-2651

Suzuki, M., Mimuro, H., Kiga, K., Fukumatsu, M., Ishijima, N., Morikawa, H., et al. (2009). Helicobacter pylori CagA phosphorylation-independent function in epithelial proliferation and inflammation. *Cell Host Microbe* 5, 23–34. doi: 10.1016/j.chom.2008.11.010

Tamura, R., Tanaka, T., Yamamoto, Y., Akasaki, Y., and Sasaki, H. (2018). Dual role of macrophage in tumor immunity. *Immunotherapy* 10, 899–909. doi: 10.2217/imt-2018-0006

Tan, S., Xia, L., Yi, P., Han, Y., Tang, L., Pan, Q., et al. (2020). Exosomal miRNAs in tumor microenvironment. *J. Exp. Clin. Cancer Res.* 39:67. doi: 10.1186/s13046-020-01570-6

Tannahill, G. M., Curtis, A. M., Adamik, J., Palsson-McDermott, E. M., McGettrick, A. F., Goel, G., et al. (2013). Succinate is an inflammatory signal that induces IL-1beta through HIF-1alpha. *Nature* 496, 238–242. doi: 10.1038/nature11986

Templeton, D. M., and Liu, Y. (2003). Genetic regulation of cell function in response to iron overload or chelation. *Biochim. Biophys. Acta* 1619, 113–124. doi: 10.1016/S0304-4165(02)00497-X

Thomas, A. M., Manghi, P., Asnicar, F., Pasolli, E., Armanini, F., Zolfo, M., et al. (2019). Metagenomic analysis of colorectal cancer datasets identifies cross-cohort microbial diagnostic signatures and a link with choline degradation. *Nat. Med.* 25, 667–678. doi: 10.1038/s41591-019-0405-7

Thurlow, L. R., Hanke, M. L., Fritz, T., Angle, A., Aldrich, A., Williams, S. H., et al. (2011). Staphylococcus aureus biofilms prevent macrophage phagocytosis and attenuate inflammation *in vivo*. *J. Immunol.* 186, 6585–6596. doi: 10.4049/jimmunol.1002794

Tian, Y., Jin, Z., Zhu, P., Liu, S., Zhang, D., Tang, M., et al. (2019). TRIM59: a membrane protein expressed on bacillus Calmette-Guerin-activated macrophages that induces apoptosis of fibrosarcoma cells by direct contact. *Exp. Cell Res.* 384:111590. doi: 10.1016/j.yexcr.2019.111590

Trinchieri, G. (2012). Cancer and inflammation: an old intuition with rapidly evolving new concepts. *Annu. Rev. Immunol.* 30, 677–706. doi: 10.1146/annurev-immunol-020711-075008

Tsay, J. J., Wu, B. G., Badri, M. H., Clemente, J. C., Shen, N., Meyn, P., et al. (2018). Airway microbiota is associated with upregulation of the PI3K pathway in lung cancer. *Am. J. Respir. Crit. Care Med.* 198, 1188–1198. doi: 10.1164/rccm.201710-2118OC

Tsay, J. J., Wu, B. G., Sulaiman, I., Gershner, K., Schluger, R., Li, Y., et al. (2021). Lower airway Dysbiosis affects lung cancer progression. *Cancer Discov.* 11, 293–307. doi: 10.1158/2159-8290.CD-20-0263

Tsuchiya, Y., Loza, E., Villa-Gomez, G., Trujillo, C. C., Baez, S., Asai, T., et al. (2018). Metagenomics of microbial communities in gallbladder bile from patients with gallbladder cancer or Cholelithiasis. *Asian Pac. J. Cancer Prev.* 19, 961–967. doi: 10.22034/APJCP.2018.19.4.961

Tuohy, J. L., Somarelli, J. A., Borst, L. B., Eward, W. C., Lascelles, B. D. X., and Fogle, J. E. (2020). Immune dysregulation and osteosarcoma: *Staphylococcus aureus* downregulates TGF-beta and heightens the inflammatory signature in human and canine macrophages suppressed by osteosarcoma. *Vet. Comp. Oncol.* 18, 64–75. doi: 10.1111/vco.12529

Umezu, D., Okada, N., Sakoda, Y., Adachi, K., Ojima, T., Yamaue, H., et al. (2019). Inhibitory functions of PD-L1 and PD-L2 in the regulation of anti-tumor immunity in murine tumor microenvironment. *Cancer Immunol. Immunother.* 68, 201–211. doi: 10.1007/s00262-018-2263-4

Urbaniak, C., Gloor, G. B., Brackstone, M., Scott, L., Tangney, M., and Reid, G. (2016). The microbiota of breast tissue and its association with breast cancer. *Appl. Environ. Microbiol.* 82, 5039–5048. doi: 10.1128/AEM.01235-16

Vitale, I., Manic, G., Coussens, L. M., Kroemer, G., and Galluzzi, L. (2019). Macrophages and metabolism in the tumor microenvironment. *Cell Metab.* 30, 36–50. doi: 10.1016/j.cmet.2019.06.001

Wang, L., Johnson, E. E., Shi, H. N., Walker, W. A., Wessling-Resnick, M., and Cherayil, B. J. (2008). Attenuated inflammatory responses in hemochromatosis reveal a role for iron in the regulation of macrophage cytokine translation. *J. Immunol.* 181, 2723–2731. doi: 10.4049/jimmunol.181.4.2723

Wang, Y., Li, Y., Li, H., Song, H., Zhai, N., Lou, L., et al. (2017). Brucella dysregulates monocytes and inhibits macrophage polarization through LC3-dependent autophagy. *Front. Immunol.* 8:691. doi: 10.3389/fimmu.2017.00691

Wang, T. R., Peng, J. C., Qiao, Y. Q., Zhu, M. M., Zhao, D., Shen, J., et al. (2014). Helicobacter pylori regulates TLR4 and TLR9 during gastric carcinogenesis. *Int. J. Clin. Exp. Pathol.* 7, 6950–6955. PMID: 25400780

Wang, X., Wu, Y., Jiao, J., and Huang, Q. (2018). Mycobacterium tuberculosis infection induces IL-10 gene expression by disturbing histone deacetylase 6 and histonedeacetylase 11 equilibrium in macrophages. *Tuberculosis (Edinb.)* 108, 118–123. doi: 10.1016/j.tube.2017.11.008

Wang, B., Wu, Y., Liu, R., Xu, H., Mei, X., Shang, Q., et al. (2020). Lactobacillus rhamnosus GG promotes M1 polarization in murine bone marrow-derived macrophages by activating TLR2/MyD88/MAPK signaling pathway. *Anim. Sci. J.* 91:e13439. doi: 10.1111/asj.13439

Wang, Y., Xi, J., Yi, J., Meng, C., Zhao, X., Sun, Z., et al. (2022). Brucella induces M1 to M2 polarization of macrophages through STAT6 signaling pathway to promote bacterial intracellular survival. *Res. Vet. Sci.* 145, 91–101. doi: 10.1016/j.rvsc.2022.02.006

Wang, L. L., Yu, X. J., Zhan, S. H., Jia, S. J., Tian, Z. B., and Dong, Q. J. (2014). Participation of microbiota in the development of gastric cancer. *World J. Gastroenterol.* 20, 4948–4952. doi: 10.3748/wjg.v20.i17.4948

Weng, M. T., Chiu, Y. T., Wei, P. Y., Chiang, C. W., Fang, H. L., and Wei, S. C. (2019). Microbiota and gastrointestinal cancer. *J. Formos. Med. Assoc.* 118, S32–S41. doi: 10.1016/j.jfma.2019.01.002

Wilson, M. R., Jiang, Y., Villalta, P. W., Stornetta, A., Boudreau, P. D., Carra, A., et al. (2019). The human gut bacterial genotoxin colibactin alkylates DNA. *Science* 363:eaar7785. doi: 10.1126/science.aar7785

Wirbel, J., Pyl, P. T., Kartal, E., Zych, K., Kashani, A., Milanese, A., et al. (2019). Meta-analysis of fecal metagenomes reveals global microbial signatures that are specific for colorectal cancer. *Nat. Med.* 25, 679–689. doi: 10.1038/s41591-019-0406-6

Wu, J., Li, K., Peng, W., Li, H., Li, Q., Wang, X., et al. (2019). Autoinducer-2 of fusobacterium nucleatum promotes macrophage M1 polarization *via* TNFSF9/IL-1beta signaling. *Int. Immunopharmacol.* 74:105724. doi: 10.1016/j.intimp.2019.105724

Wu, N., Yang, X., Zhang, R., Li, J., Xiao, X., Hu, Y., et al. (2013). Dysbiosis signature of fecal microbiota in colorectal cancer patients. *Microb. Ecol.* 66, 462–470. doi: 10.1007/s00248-013-0245-9

Wynn, T. A., and Vannella, K. M. (2016). Macrophages in tissue repair, regeneration, and fibrosis. *Immunity* 44, 450–462. doi: 10.1016/j.immuni.2016.02.015

Xu, C., Fan, L., Lin, Y., Shen, W., Qi, Y., Zhang, Y., et al. (2021). Fusobacterium nucleatum promotes colorectal cancer metastasis through miR-1322/CCL20 axis and M2 polarization. *Gut Microbes* 13:1980347. doi: 10.1080/19490976.2021.1980347

Yachida, S., Mizutani, S., Shiroma, H., Shiba, S., Nakajima, T., Sakamoto, T., et al. (2019). Metagenomic and metabolomic analyses reveal distinct stage-specific phenotypes of the gut microbiota in colorectal cancer. *Nat. Med.* 25, 968–976. doi: 10.1038/s41591-019-0458-7

Yamamura, K., Baba, Y., Nakagawa, S., Mima, K., Miyake, K., Nakamura, K., et al. (2016). Human microbiome fusobacterium Nucleatum in esophageal cancer tissue is associated with prognosis. *Clin. Cancer Res.* 22, 5574–5581. doi: 10.1158/1078-0432.CCR-16-1786

Yan, X., Yang, M., Liu, J., Gao, R., Hu, J., Li, J., et al. (2015). Discovery and validation of potential bacterial biomarkers for lung cancer. *Am. J. Cancer Res.* 5, 3111–3122. PMID: 26693063

Yang, Y., Weng, W., Peng, J., Hong, L., Yang, L., Toiyama, Y., et al. (2017). Fusobacterium nucleatum increases proliferation of colorectal cancer cells and tumor development in mice by activating toll-like receptor 4 signaling to nuclear factor-kappaB, and up-regulating expression of MicroRNA-21. *Gastroenterology* 152, 851–866.e24. doi: 10.1053/j.gastro.2016.11.018

Yang, M., Xu, J., Wang, Q., Zhang, A. Q., and Wang, K. (2018). An obligatory anaerobic salmonella typhimurium strain redirects M2 macrophages to the M1 phenotype. *Oncol. Lett.* 15, 3918–3922. doi: 10.3892/ol.2018.7742

Yao, Y., Li, G., Wu, J., Zhang, X., and Wang, J. (2015). Inflammatory response of macrophages cultured with helicobacter pylori strains was regulated by miR-155. *Int. J. Clin. Exp. Pathol.* 8, 4545–4554. PMID: 26191144

Yao, R. R., Li, J. H., Zhang, R., Chen, R. X., and Wang, Y. H. (2018). M2-polarized tumor-associated macrophages facilitated migration and epithelial-mesenchymal transition of HCC cells *via* the TLR4/STAT3 signaling pathway. *World J. Surg. Oncol.* 16:9. doi: 10.1186/s12957-018-1312-y

Yerneni, S. S., Werner, S., Azambuja, J. H., Ludwig, N., Eutsey, R., Aggarwal, S. D., et al. (2021). Pneumococcal extracellular vesicles modulate host immunity. *MBio* 12:e0165721. doi: 10.1128/mBio.01657-21

Yin, Z., Ma, T., Huang, B., Lin, L., Zhou, Y., Yan, J., et al. (2019). Macrophage-derived exosomal microRNA-501-3p promotes progression of pancreatic ductal adenocarcinoma through the TGFBR3-mediated TGF-beta signaling pathway. *J. Exp. Clin. Cancer Res.* 38:310. doi: 10.1186/s13046-019-1313-x

Yoshikawa, M., Yamada, S., Sugamata, M., Kanauchi, O., and Morita, Y. (2021). Dectin-2 mediates phagocytosis of lactobacillus paracasei KW3110 and IL-10 production by macrophages. *Sci. Rep.* 11:17737. doi: 10.1038/s41598-021-97087-9

Yu, G., Gail, M. H., Consonni, D., Carugno, M., Humphrys, M., Pesatori, A. C., et al. (2016). Characterizing human lung tissue microbiota and its relationship to epidemiological and clinical features. *Genome Biol.* 17:163. doi: 10.1186/s13059-016-1021-1

Yu, T., Guo, F., Yu, Y., Sun, T., Ma, D., Han, J., et al. (2017). Fusobacterium nucleatum promotes Chemoresistance to colorectal cancer by modulating autophagy. *Cells* 170, 548–563.e16. doi: 10.1016/j.cell.2017.07.008

Zarza, S. M., Mezouar, S., and Mege, J. L. (2021). From Coxiella burnetii infection to pregnancy complications: key role of the immune response of placental cells. *Pathogens* 10:627. doi: 10.3390/pathogens10050627

Zhang, Z., Amorosa, L. F., Coyle, S. M., Macor, M. A., Lubitz, S. E., Carson, J. L., et al. (2015). Proteolytic cleavage of AMPKalpha and intracellular MMP9 expression are both required for TLR4-mediated mTORC1 activation and HIF-1alpha expression in leukocytes. *J. Immunol.* 195, 2452–2460. doi: 10.4049/jimmunol.1500944

Zhang, Y., Li, S., Liu, Q., Long, R., Feng, J., Qin, H., et al. (2020a). Mycobacterium tuberculosis heat-shock protein 16.3 induces macrophage M2 polarization through CCRL2/CX3CR1. *Inflammation* 43, 487–506. doi: 10.1007/s10753-019-01132-9

Zhang, Y., Meng, W., Yue, P., and Li, X. (2020b). M2 macrophage-derived extracellular vesicles promote gastric cancer progression *via* a microRNA-130b-3p/MLL3/GRHL2 signaling cascade. *J. Exp. Clin. Cancer Res.* 39:134. doi: 10.1186/s13046-020-01626-7

Zhao, Q., Hu, H., Wang, W., Peng, H., and Zhang, X. (2015). Genome sequence of Sphingobium yanoikuyae B1, a polycyclic aromatic hydrocarbon-degrading strain. *Genome Announc.* 3:e01522-14. doi: 10.1128/genomeA.01522-14

Zheng, P., Chen, L., Yuan, X., Luo, Q., Liu, Y., Xie, G., et al. (2017). Exosomal transfer of tumor-associated macrophage-derived miR-21 confers cisplatin resistance in gastric cancer cells. *J. Exp. Clin. Cancer Res.* 36:53. doi: 10.1186/s13046-017-0528-y

Zheng, J. H., Nguyen, V. H., Jiang, S. N., Park, S. H., Tan, W., Hong, S. H., et al. (2017). Two-step enhanced cancer immunotherapy with engineered *Salmonella typhimurium* secreting heterologous flagellin. *Sci. Transl. Med.* 9:eaak9537. doi: 10.1126/scitranslmed.aak9537

Zhou, J., Li, X., Wu, X., Zhang, T., Zhu, Q., Wang, X., et al. (2018). Exosomes released from tumor-associated macrophages transfer miRNAs that induce a Treg/Th17 cell imbalance in epithelial ovarian cancer. *Cancer Immunol. Res.* 6, 1578–1592. doi: 10.1158/2326-6066.CIR-17-0479

Zhou, Z., Peng, Y., Wu, X., Meng, S., Yu, W., Zhao, J., et al. (2019). CCL18 secreted from M2 macrophages promotes migration and invasion *via* the PI3K/Akt pathway in gallbladder cancer. *Cell. Oncol. (Dordr.)* 42, 81–92. doi: 10.1007/s13402-018-0410-8

Zhou, Y., Wang, L., Pei, F., Ji, M., Zhang, F., Sun, Y., et al. (2019). Patients with LR-HPV infection have a distinct vaginal microbiota in comparison with healthy controls. *Front. Cell. Infect. Microbiol.* 9:294. doi: 10.3389/fcimb.2019.00294

Zhu, X., Shen, H., Yin, X., Long, L., Chen, X., Feng, F., et al. (2017). IL-6R/STAT3/miR-204 feedback loop contributes to cisplatin resistance of epithelial ovarian cancer cells. *Oncotarget* 8, 39154–39166. doi: 10.18632/oncotarget.16610

Zhu, Q., Wu, X., Tang, M., and Wu, L. (2020). Observation of tumor-associated macrophages expression in gastric cancer and its clinical pathological relationship. *Medicine (Baltimore)* 99:e19839. doi: 10.1097/MD.0000000000019839

Zhu, Q., Wu, X., Wu, Y., and Wang, X. (2016). Interaction between Treg cells and tumor-associated macrophages in the tumor microenvironment of epithelial ovarian cancer. *Oncol. Rep.* 36, 3472–3478. doi: 10.3892/or.2016.5136

10.3389/fmicb.2023.1115556

Glossary

TAMs	Tumor-associated macrophages
ROS	Reactive oxygen species
TNF-α	Tumor necrosis factor-α
IL-	Interleukin-
CXCL	C-X-C motif chemokine ligand
CCL	C-C motif chemokine ligand
TGF-β	Transforming growth factor β
TLRs	Toll-like receptors
STAT3	Signal transducer and activator of transcription 3
c-MYC	Cellular myelocytomatosis viral oncogene
NF-κB	Nuclear factor kappa-B
MRP14/S100A9	Myeloid-related protein-14
MyD88	Myeloid differentiation factor 88
AI-2	Autoinducer-2
TNFSF9	TNF receptor superfamily member 9
SCARI1/CD163	Scavenger receptor cysteine-rich type 1 protein M130
PRRs	Pattern recognition receptors
NLRs	NOD-like Receptors
MMPs	Matrix metalloproteinases
MHC	Major histocompatibility complex
miRNAs	micro-RNAs
CIITA	Major histocompatibility complex (MHC) class II transactivator
HLAII	Human leukocyte antigen (HLA) class II
PI3K	Phosphatidylinositide 3-kinases
AKT/PKB	Protein kinase B
LPS	Lipopolysaccharides
iNOS	Inducible nitric oxide synthase
HDAC	Histone deacetylase

HLA-DR	Human leukocyte antigen DR
MR/CD206	Mannose receptor
TCA cycle	Tricarboxylic acid cycle
VEGF	Vascular endothelial growth factor
ARG-1	Arginase 1
HIF-1α	Hypoxia-inducible factor-1α
MAPK	Mitogen-activated protein kinase
Lcn-2	Lipocalin 2
SOX9	Sex-determining region of the Y chromosome (SRY)-box transcription factor 9
COX-2	Cyclooxygenase-2
SREBP-1a	Sterol regulatory element binding proteins transcription factor 1a
SHP-1/PTPN6	Protein tyrosine phosphatase
Th	T helper cell
Tregs	Regulatory T cells
PITPNM3	PITPNM family member 3
PD-L1	Programmed death-ligand 1
PD-L2	Programmed death-ligand 2
SHIP1	Src homology 2-containing inositol-5′-phosphatase 1
TAB2	TGF-β activated kinase 1 (MAP3K7) binding protein 2
SOCS1	Suppressors of cytokine signaling 1
TIMP3	TIMP Metallopeptidase Inhibitor 3
TGFBR3	Transforming growth factor beta receptor 3
MLL3	Myeloid/lymphoid or mixed lineage leukemia 3
GRHL2	Grainy head-like transcription factor 2
FOXO3	Forkhead box O3
GSK-3β	Glycogen synthase kinase-3β
MMAC1/PTEN	Mutated in multiple advanced cancers 1

frontiers | Frontiers in Microbiology

TYPE Original Research
PUBLISHED 22 February 2023
DOI 10.3389/fmicb.2023.1129690

OPEN ACCESS

EDITED BY
Yuan Xiao,
Shanghai Jiao Tong University,
China

REVIEWED BY
Xuhui Zheng,
University of Washington,
United States
Sunil Banskar,
University of Arizona,
United States

*CORRESPONDENCE
Hongbin Song
✉ hongbinsong@263.net
Peng Li
✉ jiekenlee@126.com
Hao Guo
✉ h.guo@foxmail.com

†These authors have contributed equally to this work

SPECIALTY SECTION
This article was submitted to Infectious Agents and Disease, a section of the journal Frontiers in Microbiology

RECEIVED 22 December 2022
ACCEPTED 30 January 2023
PUBLISHED 22 February 2023

CITATION
Chen Q, Liu M, Lin Y, Wang K, Li J, Li P, Yang L, Jia L, Zhang B, Guo H, Li P and Song H (2023) Topography of respiratory tract and gut microbiota in mice with influenza A virus infection.
Front. Microbiol. 14:1129690.
doi: 10.3389/fmicb.2023.1129690

Topography of respiratory tract and gut microbiota in mice with influenza A virus infection

Qichao Chen[1,2†], Manjiao Liu[3,4†], Yanfeng Lin[1,2], Kaiying Wang[2], Jinhui Li[2], Peihan Li[2], Lang Yang[2], Leili Jia[2], Bei Zhang[3,4], Hao Guo[3,4]*, Peng Li[2]* and Hongbin Song[1,2]*

[1]Academy of Military Medical Sciences, Academy of Military Sciences, Beijing, China, [2]Chinese PLA Center for Disease Control and Prevention, Beijing, China, [3]State Key Laboratory of Translational Medicine and Innovative Drug Development, Jiangsu Simcere Diagnostics Co., Ltd., Nanjing, Jiangsu Province, China, [4]Nanjing Simcere Medical Laboratory Science Co., Ltd., Nanjing, Jiangsu Province, China

Introduction: Influenza A virus (IAV)-induced dysbiosis may predispose to severe bacterial superinfections. Most studies have focused on the microbiota of single mucosal surfaces; consequently, the relationships between microbiota at different anatomic sites in IAV-infected mice have not been fully studied.

Methods: We characterized respiratory and gut microbiota using full-length 16S rRNA gene sequencing by Nanopore sequencers and compared the nasopharyngeal, oropharyngeal, lung and gut microbiomes in healthy and IAV-infected mice.

Results: The oropharyngeal, lung and gut microbiota of healthy mice were dominated by *Lactobacillus* spp., while nasopharyngeal microbiota were comprised primarily of *Streptococcus* spp. However, the oropharyngeal, nasopharyngeal, lung, and gut microbiota of IAV-infected mice were dominated by *Pseudomonas, Escherichia*, *Streptococcus*, and *Muribaculum* spp., respectively. *Lactobacillus murinus* was identified as a biomarker and was reduced at all sites in IAV-infected mice. The microbiota composition of lung was more similar to that of the nasopharynx than the oropharynx in healthy mice.

Discussion: These findings suggest that the main source of lung microbiota in mice differs from that of adults. Moreover, the similarity between the nasopharyngeal and lung microbiota was increased in IAV-infected mice. We found that IAV infection reduced the similarity between the gut and oropharyngeal microbiota. *L. murinus* was identified as a biomarker of IAV infection and may be an important target for intervention in post-influenza bacterial superinfections.

KEYWORDS

influenza A virus infection, respiratory tract microbiota, gut microbiota, oropharynx, nasopharynx, lung

Introduction

The risk of a novel influenza A virus (IAV) pandemic looms as a major global public health threat (Iuliano et al., 2018). Secondary bacterial infection following influenza is a prevalent cause of severe pneumonia and death (McCullers, 2014). The normal host microbiome resists colonization by pathogens through niche competition and host immune regulation, and plays an important role in post-influenza bacterial superinfection (Dominguez-Bello et al., 2019).

The intestinal microbiome includes 10^{14} bacteria representing 1,000 species, which are closely related to host metabolism, immunity and mental health (Lynch and Pedersen, 2016). Patients with

IAV infection exhibited significantly decreased diversity and abundance of gut microbiota, including a significant reduction in the relative abundance of *Actinomycetes* and *Firmicutes* at the phylum level and anaerobic butyrate-producing bacteria (*Racinobacteriaceae* and *Ruminococcaceae*) at the family level (Gu et al., 2020). Intestinal dysbiosis dysregulates host CD4+ and CD8+ T cell generation and antibody response, and aggravates IAV-induced lung pathology (Ichinohe et al., 2011). In addition to the gut microbiome, respiratory microbiota also plays an important role in IAV infection. Due to differences in anatomy and development, the human respiratory tract can be divided into the upper and lower respiratory tracts (URT and LRT, respectively). IAV infection can significantly alter the URT microbiome, including oropharyngeal and nasopharyngeal microbiota. For example, IAV-infected children had lower abundance of *Moraxella*, *Staphylococcus*, *Clostridium* and *Duchenne* spp. in the nasopharynx, and *Streptococcus*, *Neisseria* and *Hemophilus spp.* in the oropharynx than healthy children (Wen et al., 2018). In healthy adults, lung microbiota originates primarily from the oropharynx by direct mucosal dispersion and micro-aspiration (Bassis et al., 2015). A murine model demonstrated that IAV infection induced a long-term LRT dysbiosis that featured a clear shift from *Alphaproteobacteria* to *Gammaproteobacteria* and a significant increase in the relative abundance of *Streptococcus* and *Staphylococcus* spp. (Gu et al., 2019). Although multiple studies have characterized the changes of respiratory tract and gut microbiota after IAV infection, most have focused on specific anatomic sites. Correlations between URT, LRT and gut microbiota during IAV infection have not been studied fully. In addition, due to the read length limitation of second-generation sequencing, few species-level studies of host dysbiosis during IAV infection have been conducted.

To further understand the changes and correlation between URT, LRT and gut microbiota during IAV infection, we performed full length 16sRNA gene sequencing of nasopharyngeal, oropharyngeal, lung and gut microbiota using Nanopore sequencing technology in a murine model. We found that IAV infection altered the microbiota structures of the URT, LRT and gut. The lung microbiota was more similar to nasopharyngeal than oropharyngeal microbiota in healthy mice. However, the similarity between nasopharyngeal and lung microbiota deceased during IAV-infection. We also observed that IAV infection reduced the similarity between gut and oropharyngeal microbiota. In addition, we found representative species responses to IAV infection. For example, IAV infection decreased the relative abundance of *Lactobacillus murinus* in the respiratory tract and gut.

Materials and methods

Animal model and sample collection

Twenty C57BL/6 N female mice (6 weeks of age) were purchased from Beijing Vital River Laboratory Animal Technology Co., Ltd. (China) and adapted in specific pathogen-free conditions (5 mice/cage) for 1 week. Mice were randomly divided into two groups ($n = 10$): a PBS mock infected (Mock) group and an IAV-infected (IAV) group. To establish a murine model of IAV infection, mice of the IAV group were anesthetized with 0.3% pentobarbital sodium (intraperitoneal injection, 50 mg/kg) and infected intranasally with 25 μl sterile PBS containing strain A/Puerto Rico/8/34 (60 PFU). Control mice were mock infected with 25 μl sterile PBS. One nasal drip experiment for each mouse. All mice in the IAV group and Mock group were infected in the same day. All mice had access to water and food under a strict 12 h light/dark cycle. All animal procedures for animal raising and handling were approved by the Animal Care and Use Committee of Chinese PLA Center for Disease Control and Prevention. All animals were euthanized with 0.3% pentobarbital sodium (intraperitoneal injection, 150 mg/kg) on post-infection day-4. After weighing the fresh lungs, left lungs were stored at-80°C and right lungs were fixed in 4% paraformaldehyde for hematoxylin and eosin (H&E) staining. The lung index was calculated with the formula: lung index = [(lung weight/g)/(bodyweight/g)] × 100% (Gao et al., 2020). Nasopharyngeal lavage fluid (NLF) was collected as reported previously (Puchta et al., 2014). Oropharyngeal samples were collected using swabs and placed in 1 ml sterile PBS at 4°C. Bronchoalveolar lavage fluid (BALF) was collected by washing the bronchoalveolar tree three times using 1 ml sterile PBS. Fecal samples were collected and stored at-80°C for further experiments.

Hematoxylin and eosin staining

Fresh right lung tissues were fixed in 4% paraformaldehyde and embedded in paraffin. Prepared embedded lung tissues were cut into 3–5 μm-thick sections and stained with H&E. Pathological scores were evaluated as reported previously (Renne et al., 2009).

Nucleic acid extraction and qPCR

Bacterial genomic DNA of fresh NLF, BALF and oropharyngeal swabs was extracted using the QIAamp DNA Microbiome Kit (QIAGEN, Germany). Total RNA of fresh NLF, BALF and oropharyngeal swabs was extracted using QIAamp® MinElute® Virus Spin (QIAGEN, Germany). Genomic DNA and total RNA of fecal samples were extracted using AllPrep® PowerFecal® DNA/RNA Kit (QIAGEN, Germany). A control extraction with no sample was performed for each kit. IAV titers of NLF, BALF, oropharyngeal swab and fecal samples were assayed with Luna® Universal Probe One-Step RT-qPCR Kit (NEB, United States). The following primers were used: 5'-GACCRATCCTGTCACCTCTGAC-3′ (Forward primer), 5'-GGGCATTYTGGACAAAKCGTCTACG-3′ (Reverse primer) and 5'-FAM-TGCAGTCCTCGCTCACTGGGCACG-BHQ1-3′ (Probe). Copies of IAV were calculated using the standard curve method.

Full length 16S rRNA gene sequencing and bioinformatics pipeline

Genomic DNA of NLF, BALF, oropharyngeal swab and fecal samples was used for full length 16S rRNA gene sequencing. In addition to the samples, library preparation contained a negative control (Control extraction with no sample) and a positive control (mock community). PCR reactions were conducted using KAPA HiFi HotStart ReadyMix (KAPA Biosystems, United States) and 0.5 μM of Universal-27F (5′-TTTCTGTTGGTGCT GATATTGCAGAGTTTGAT CCTGGCT CAG-3′) and Universal-1492R (5′- ACTTGCC TGTCGCTCTATCTT CTACGACTTAACCCCAATCGC-3′). Cycling conditions were set as 95°C for 3 min; 10 cycles of 98°C for 30 s, 55°C for 1 min and 72°C for 1 min; and 72°C for 5 min. The amplification products were purified using 0.8 × AgencourtAMPure XP Beads (Beckman, United States). Cleaned DNA was barcoded and pooled using PCR Barcoding Expansion Pack

1–96 (EXP-PBC096; Oxford Nanopore Technologies, United Kingdom). A library was prepared for sequencing using Ligation Sequencing Kit (SQK-LSK109; Oxford Nanopore Technologies, United Kingdom) and sequenced on the MinION Mk1B (Oxford Nanopore Technologies, United Kingdom) with R10 flow cell (Oxford Nanopore Technologies, United Kingdom). Raw reads were base-called and demultiplexed using Guppy (V 5.0.11+) to obtain high-quality reads with min_score = 8. The filtered reads were within a size range of 1.2–1.8 kb. Read numbers and mapping rates for each sample are presented in Supplementary Table S1. Emu software was used to estimates species composition distribution based on the Emu v3.0 + database (Curry et al., 2022). Alpha diversity (Shannon and Chao1 indices) and Bray Curtis Distance were calculated by R package vegan (v2.5.7). The principal coordinate analysis (PCoA) was formed by R package ape (v5.6.2). Functional composition and KEGG pathway abundance of microbiota was predicted using PICRUST2 software (Douglas et al., 2022). LEfse analysis was used to identify biomarkers by comparing abundance between groups (Wilcoxon test $p < 0.01$ and $|\log10(LDA)| > 3$).

Statistics

Body weight, IAV titer and histologic scoring were analyzed with unpaired t tests. Shannon index, Chao1 index and bacterial taxa abundance among groups were analyzed with the Mann–Whitney test. $^{***}p \leq 0.001$, $^{**}p \leq 0.01$, $^{*}p \leq 0.05$.

Results

IAV induced severe respiratory tract infection and lung injury

To validate our murine infection model, we compared body weight, IAV titer and lung pathology between mock and IAV groups. A significant increase in lung index but a significant decrease in body weight were observed in the IAV group compared to the mock group (Figure 1A). We also observed significantly increased IAV titers in the oropharynx, nasopharynx, lung and fecal samples of the IAV group and found the highest IAV titers in the lung (Figure 1B). H&E staining showed that pulmonary injury was induced by IAV infection and featured alveolar wall thickening (Yellow arrow), mononuclear cell infiltration (Black arrows) and bronchial epithelial cell injury (Red arrow). The mean histologic score of the IAV group was significantly higher than that of the mock group (Figure 1C).

IAV infection altered the composition of respiratory tract microbial communities

The diversity (Shannon diversity index) and richness (Chao1 index) of the oropharyngeal, nasopharyngeal and lung microbiota were similar between the two groups (Figure 2A). PCoA analysis showed clearly different oropharyngeal and nasopharyngeal microbiota in IAV group compared with the mock group; however, lung microbiota structures were not significantly different (Figure 2B; Supplementary Figures S1A,B,C).

We further examined taxonomic profiles at different classification levels. The most prominent phyla of all samples in the mock group were *Proteobacteria* and *Firmicutes*, while the IAV group had a relatively reduced abundance of *Firmicutes* but increased abundance of *Proteobacteria* in the oropharynx and nasopharynx. However, these changes were not observed in the lung. At the genus level, *Lactobacillus* was most abundant in oropharynx and lung, whereas *Streptococcus* was predominant in the nasopharynx of the mock group. However, the IAV group exhibited different dominant genera at all locations. *Pseudomonas* was dominant in the oropharynx, whereas *Escherichia* was most abundant in nasopharynx and *Streptococcus* was predominant in the lung (Figure 2C). We also investigated species-level changes of respiratory tract microbiota during IAV infection. For the mock group, *L. murinus* was predominant in oropharynx and lung, whereas *Streptococcus respiraculi* was most abundant in nasopharynx. For the IAV group, *Pseudomonas fluorescens* was predominant in oropharynx, *Escherichia coli* was predominant in nasopharynx, whereas *Streptococcus respiraculi* was most abundant in lung (Figure 3A). The metabolic function prediction of microbiota showed that IAV infection decreased D-glutamine, D-glutamate and D-Alanine metabolism in the oropharynx and reduced peptidoglycan biosynthesis in the nasopharynx, while increasing pantothenate and CoA biosynthesis in the lung (Figure 3B).

Comparison of microbiota structures of respiratory tract sites during IAV infection

We found that the lung microbiota was more similar to nasopharyngeal than oropharyngeal microbiota in the mock group. Moreover, the similarity between lung and nasopharyngeal microbiota was increased in the IAV group compared to the mock group (Figure 4A). These results suggest that IAV infection increased the influence of nasopharyngeal microbiota on lung microbiota. We screened the species with significant differences between the IAV group and the mock group by the Mann–Whitney test and showed the changes at each location on the heat map. Compared with respective locations in mock group, the oropharynx showed a significant difference of 18 species, the nasopharynx displayed a significant difference of 7 species and the lung exhibited a significant difference of 13 species. We identified some species with synchronous alterations at multiple respiratory tract locations in response to IAV infection. For example, compared with mock group, the relative abundance of *Lactobacillus animalis*, *Lactobacillus johnsonii* and *L. murinus* decreased, while the relative abundance of *Enterococcus faecalis* increased in the oropharynx, nasopharynx and lungs in IAV group. In addition, we found that some species of the URT and LRT responded differently to IAV infection. For example, the relative abundance of *S. danieliae*, *S. respiraculi and Streptococcus suis* decreased in the URT but increased in the LRT in the IAV group (Figure 4B).

IAV infection reduced the similarity between oropharyngeal and gut microbiota

IAV infection significantly increased the diversity (Shannon diversity index) and richness (Chao1 index) of gut microbiota (Figure 5A). Beta diversity showed that IAV infection strongly influenced the gut microbiota, as results of the mock and IAV groups clustered away from each other (Figure 5B; Supplementary Figure S1D). *Firmicutes* and *Bacteroidetes* were the dominant gut bacteria in both the IAV and mock groups. However, IAV infection resulted in an

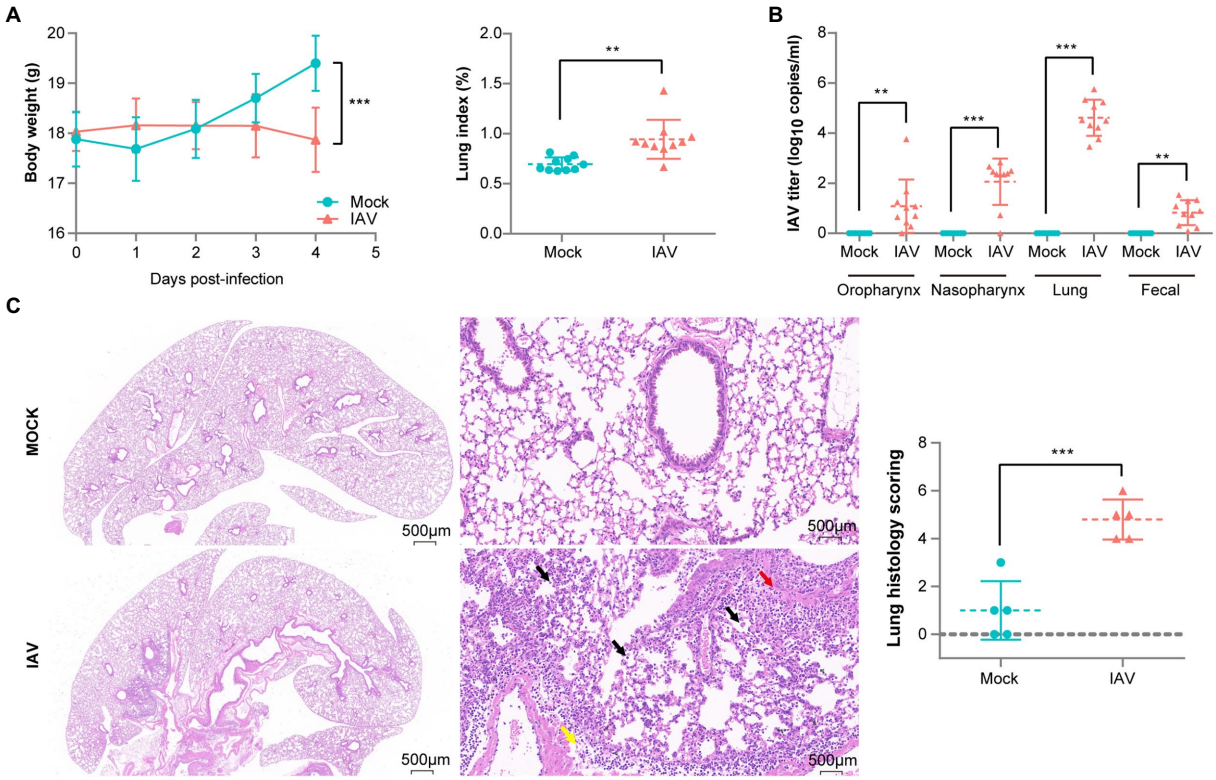

FIGURE 1
Pathological difference between mock-and IAV-infected mice. **(A)** Body weight and lung index (n=10 per group). **(B)** IAV titers of oropharynx, nasopharynx, lung and fecal samples (n=10 per group). **(C)** H&E staining and histologic scoring of right lungs (n=5 per group). Body weight, IAV titer and histologic scoring were compared by using unpaired t tests *p<0.05, ** p<0.01, ***p<0.001.

increase in the relative abundance of *Bacteroidetes* and a decrease in the relative abundance of *Firmicutes* in gut. At the genus level, IAV infection caused a decrease in the relative abundance of *Lactobacillus* and an increase in the relative abundance of *Muribaculum and Parasutterella* (Figure 5C). LEfSe analysis to identify species-level bacteria associated with IAV infection identified 7 species that were differentially abundant between the mock and IAV groups. *Lactobacillus intestinalis*, *Lactobacillus reuteri*, *L. animalis*, *L. johnsonii*, *Helicobacter japonicus* and *L. murinus* were enriched in the mock group, while *Parasutterella excrementihominis* was significantly more abundant in IAV group (Figure 5D). The metabolic function prediction of microbiota showed that IAV infection decreased D-glutamine and D-glutamate metabolism in gut (Figure 5E). Considering the habitual coprophagy of mice, we analyzed the correlation between gut microbiota and oropharyngeal microbiota in mock and IAV groups and found that the diversity and richness of the gut microbiota were significantly higher than those of the oropharynx in both the IAV and mock groups (Figure 6A). In addition, the oropharyngeal microbiota was more similar to the gut microbiota in mock group than in the IAV group (Figure 6B). We observed the same changes in the relative abundance of some species in the gut and oropharynx after IAV infection. For example, the relative abundance of *L. murinus*, *L. reuteri*, *L. animalis* and *L. johnsonii* were decreased, while the relative abundance of *Phocaeicola sartorii* increased in both gut and oropharynx in IAV group (Figure 6C).

Discussion

IAV infection can alter respiratory tract and gut microbiota (Lv et al., 2021; Rattanaburi et al., 2022). As murine models are the most commonly used *in vivo* systems in influenza research, many experiments have described long-or short-term dysbiosis in IAV-infected mice (Yildiz et al., 2018; Sencio et al., 2021). However, most studies have focused on a single mucosal surface, and have rarely studied the association of microbiota among multiple locations systematically. Therefore, we compared the respiratory and gut microbiota of normal and IAV-infected mice using full-length 16srRNA gene sequencing and analyzed the correlation of microbiota among different anatomic sites in normal and infected mice.

As expected, we successfully established a murine IAV infection model. Previous murine studies have reported that influenza infection decreases body weight and increases lung index (An et al., 2018; Ling et al., 2020). We observed the same results in our experiments. In addition to the respiratory tract, we also detected IAV in the feces of the IAV-infected group. Concordant with our results, virus was also identified in fecal samples from IAV/IBV-infected patients (Hirose et al., 2016). Our histopathologic findings of robust leukocytic infiltration and edema in IAV-infected lung tissue were also observed in a previous study and were associated with protease-activated receptor 4 (Kim et al., 2021).

The respiratory tract is complex, and each segment has its own unique microbiota, which respond similarly or differently to IAV

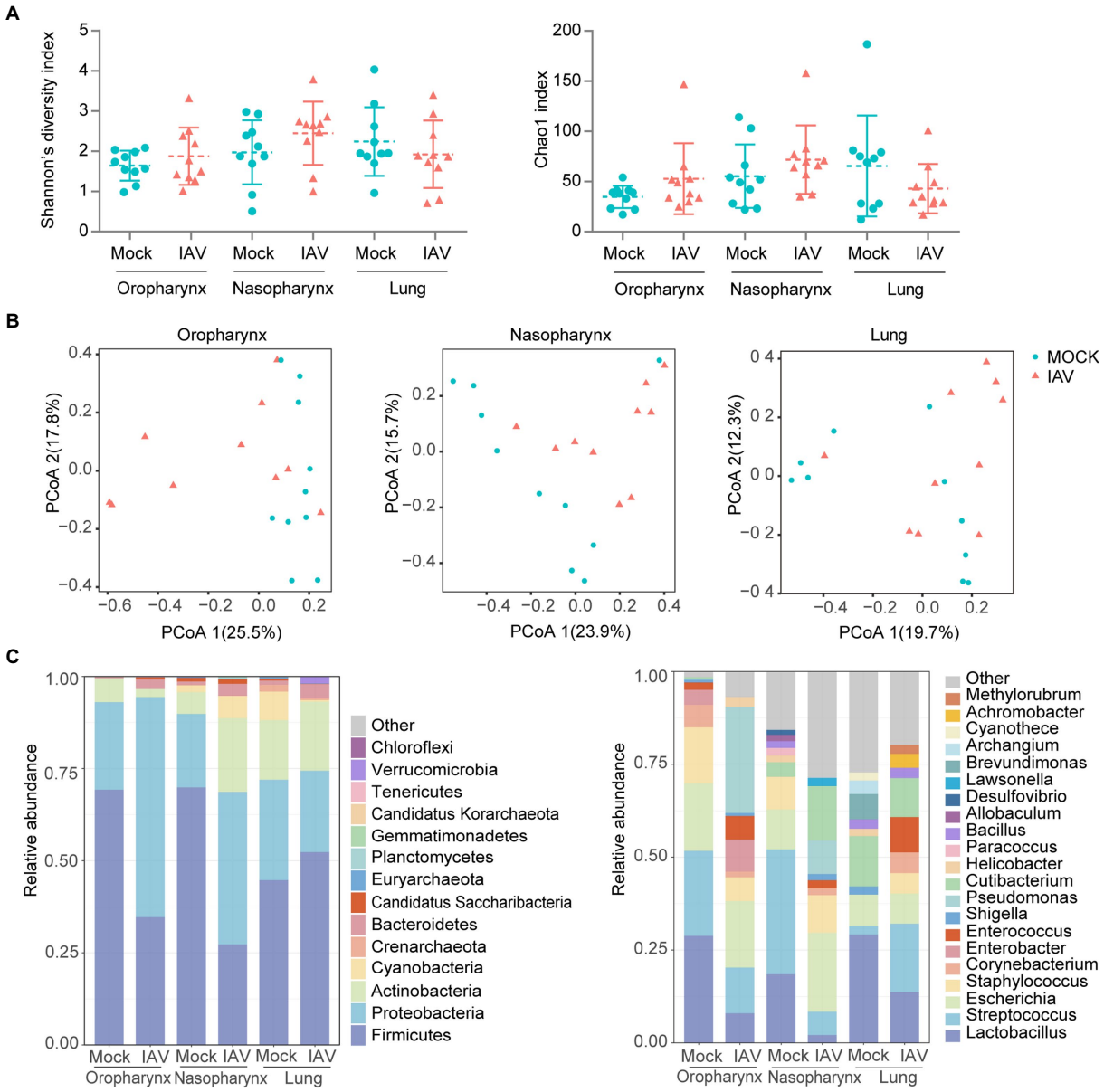

FIGURE 2
Respiratory tract dysbiosis during IAV infection. **(A)** Shannon diversity and Chao1 indices of oropharyngeal, nasopharyngeal and lung microbiota. **(B)** 2D-PCoA plots of oropharyngeal, nasopharyngeal and lung microbiota. Relative abundance of the top 10 bacteria at the phylum and genus levels **(C)**. Shannon and Chao1 indices were analyzed with Mann–Whitney test. *p<0.05, ** p<0.01, ***p<0.001. n=10 per group.

infection. In this study, species diversity and richness of oropharyngeal, nasopharyngeal and pulmonary microbiota in IAV-infected mice were similar to those of normal mice. Consonant with our findings, several studies have shown no significant changes in microbial diversity and richness in the URT and LRT of IAV-infected mice (Planet et al., 2016; Yildiz et al., 2018). However, the composition of the microbiota of the different sites responded differently to IAV infection.

The reduction of relative abundance of *L. murinus* at all three respiratory tract sites may have altered host immune response and may have also reduced colonization resistance, as evidenced by the increased relative abundance of oropharyngeal and nasopharyngeal *P. fluorescens*. *L. murinus* belong to *Lactobacillus* genus which induces Th17 and RORγt+ regulatory T cells and reduces pulmonary inflammation in tuberculosis (Bernard-Raichon et al., 2021). Moreover, *L. murinus* provides a barrier against pneumococcal colonization in a respiratory dysbiosis model (Yildiz et al., 2020). *P. fluorescens* belongs to *Pseudomonadales*, which typically subsist at low levels in the indigenous microbiota of various body sites, but are related to cystic fibrosis, chronic airway diseases, asthma and non-cystic fibrosis-related bronchiectasis (Scales et al., 2014). The relative abundance of *Pseudomonadales* also increased in the URT of IAV-infected patients (Kaul et al., 2020).

Interestingly, we found that the relative abundance of *S. danieliae* was increased in the URT and decreased in the LRT. *S. danieliae* is a major component of the URT microbiome of healthy mice and is involved in the establishment of oral microbiota (Joseph et al., 2021). However, oral administration of *Staphylococcus aureus* and *S. danieliae* aggravated experimental psoriasis in a murine model (Okada et al., 2020). There have been few other reports of *S. danieliae* to date. Our

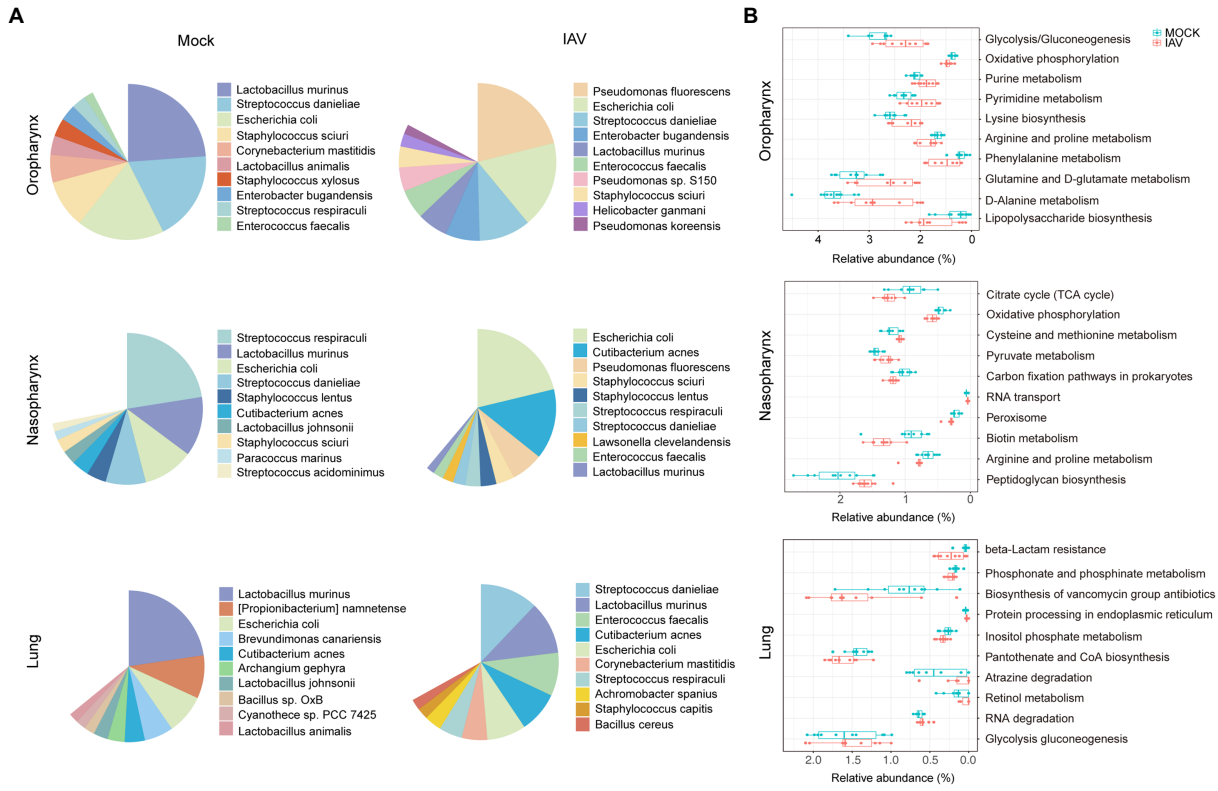

FIGURE 3
Characterization of species-level bacteria and functional composition of respiratory tract microbiota during IAV infection. **(A)** Relative abundance of the top 10 bacterial species of oropharyngeal, nasopharyngeal and lung microbiota in mock and IAV groups. **(B)** Top 10 significantly altered metabolic pathways of oropharyngeal, nasopharyngeal and lung microbiota between mock and IAV groups. Pathway abundance prediction by PICRUSt2. *n* =10 per group. The relative abundance on the x-axis represents the ratio of the corresponding functional abundance to all predicted functional abundances.

research showed that the lung microbiota was more like that of the nasopharynx than the oropharynx, which suggests that the nasopharynx may serve as the primary reservoir of lung microbiota in mice. In contrast, the oropharynx is the origin of lung microbiota in human adults (Bassis et al., 2015). The nasopharyngeal microbiota is most similar to the lung microbiota in healthy cattle (McMullen et al., 2020). Moreover, IAV infection increased the similarity between nasopharyngeal and lung microbiota in this study. This may have been related to host innate and adaptive immune responses to IAV (Liong et al., 2020; Wang et al., 2021).

IAV infection can decrease the species diversity of gut microbiota in H7N9-infected humans (Qin et al., 2015). However, our results showed that IAV infection increased intestinal species diversity in mice. This could be due to different viral strains, host responses, or sample collection methods. The relative abundance of *Lactobacillus* spp. (*L. intestinalis*, *L. reuteri*, *L. animalis*, *L. johnsonii* and *L. murinus*) was decreased in IAV-infected mice. Considering the absolute abundance can be estimated from the sequencing counts (Yang et al., 2022), we also evaluated the absolute abundance of *Lactobacillus* in the genus and species levels between the IAV and Mock groups, and found that change of *Lactobacillus* was consistent in the absolute and relative abundance (Supplementary Table S2). In general, the decreased abundance of Lactobacillus species may be an important phenomenon of IAV infection. *Lactobacillus* plays an important role in anti-viral immunity. For example, a previous study showed that *Lactobacillus johnsonii* supplementation attenuates respiratory viral infection *via* immune cell modulation (Fonseca et al., 2017). Moreover, the relative abundance of *L. murinus* was not only decreased in the gut, but also in all three segments of the respiratory tract (oropharynx, nasopharynx, lungs). Reduced relative abundance of *L. murinus* at all anatomic sites may have reduced colonization resistance. *L. murinus* maintained intestinal immune homeostasis and mediated anti-inflammatory effects in murine models (Tang et al., 2015; Pan et al., 2018). Probiotic administration of *L. murinus* prevented salt-sensitive hypertension by modulating TH17 cells in mice (Wilck et al., 2017). *Parasutterella excrementihominis* was significantly more abundant in gut microbiota in IAV infected mice, and was found in a higher relative abundance in older adults (Fart et al., 2020). Increased relative abundance of *P. excrementihominis* has been associated with fatty liver disease, chronic bowel inflammation and irritable bowel syndrome (Blasco-Baque et al., 2017; Chen et al., 2018). In addition, IAV infection reduced the similarity of oropharyngeal and gut microbiota. The correlation between murine oropharyngeal and intestinal microbiota may be due to coprophagy (Bogatyrev et al., 2020). Because IAV infection reduces murine alimentation (Bartley et al., 2017), decreased fecal feeding may have lowered the similarity between oropharyngeal and gut microbiota in our infected mice. The murine behavior of coprophagy and subsequent respiratory colonization by enteric microflora brings into question the utility of murine models of post-viral bacterial superinfections.

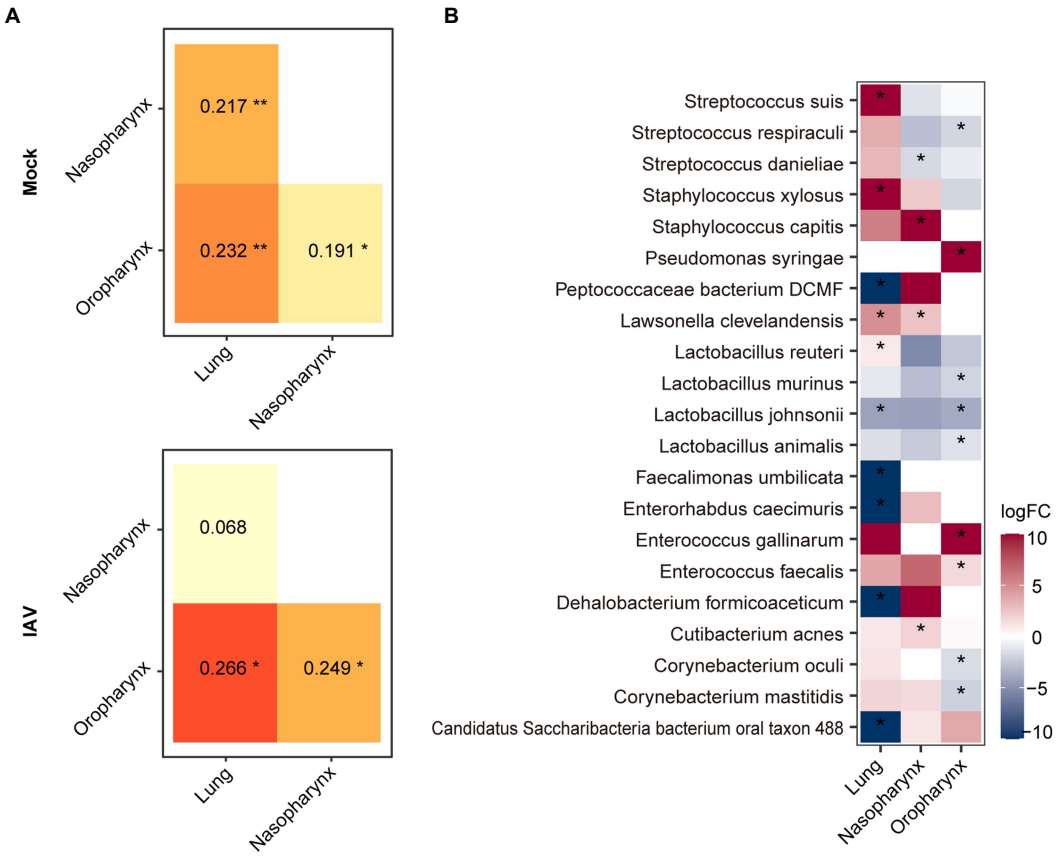

FIGURE 4
Comparison of oropharyngeal, nasopharyngeal and lung microbiota during IAV infection. **(A)** Similarity analysis of the microbiota of different locations in the IAV and mock groups. **(B)** Distribution of significantly different species between mock and IAV groups in different sampling locations. Shannon and Chao1 indices among different sampling locations were analyzed with the Mann–Whitney test. Similarity of microbiota of different locations was analyzed with ANOSIM. Bacterial taxa abundance between mock and IAV group was also analyzed with the Mann–Whitney test. ***p<0.001, **p<0.01, *p<0.05. n=10 per group.

Conclusion

We characterized the oropharyngeal, nasopharyngeal, lung and gut microbiota and compared the microbiota structure of different mucosal surfaces in normal and IAV-infected mice. In addition, we determined that the nasopharynx is the primary reservoir of lung microbiota in healthy mice. IAV infection increased the similarity between lung and nasopharyngeal microbiota. However, IAV infection reduced the similarity between oropharyngeal and gut microbiota. The relative abundance of *L. murinus* may serve as a biomarker of IAV infection because it was reduced in all locations.

Data availability statement

The data presented in the study are deposited in the NCBI Bio-project repository (https://www.ncbi.nlm.nih.gov/bioproject/), accession number PRJNA910300.

Ethics statement

The animal study was reviewed and approved by Animal Care and Use Committee of Chinese PLA Center for Disease Control and Prevention.

Author contributions

PenL and HS conceived and designed the experiments. QC, KW, LJ, YL, and JL performed the experiments. ML, HG, BZ, PeiL, and LY analyzed the full length 16s rRNA gene sequencing data. QC and PenL wrote the manuscript. All authors contributed to the article and approved the submitted version.

Funding

This study was supported by National Key Research and Development Program of China (2021YFC2301000), the National Science and Technology Major Project (2018ZX10201001 and 2018ZX10305410).

Conflict of interest

ML, BZ, and HG were employed by the companies Jiangsu Simcere Diagnostics Co., Ltd. and Nanjing Simcere Medical Laboratory Science Co., Ltd.

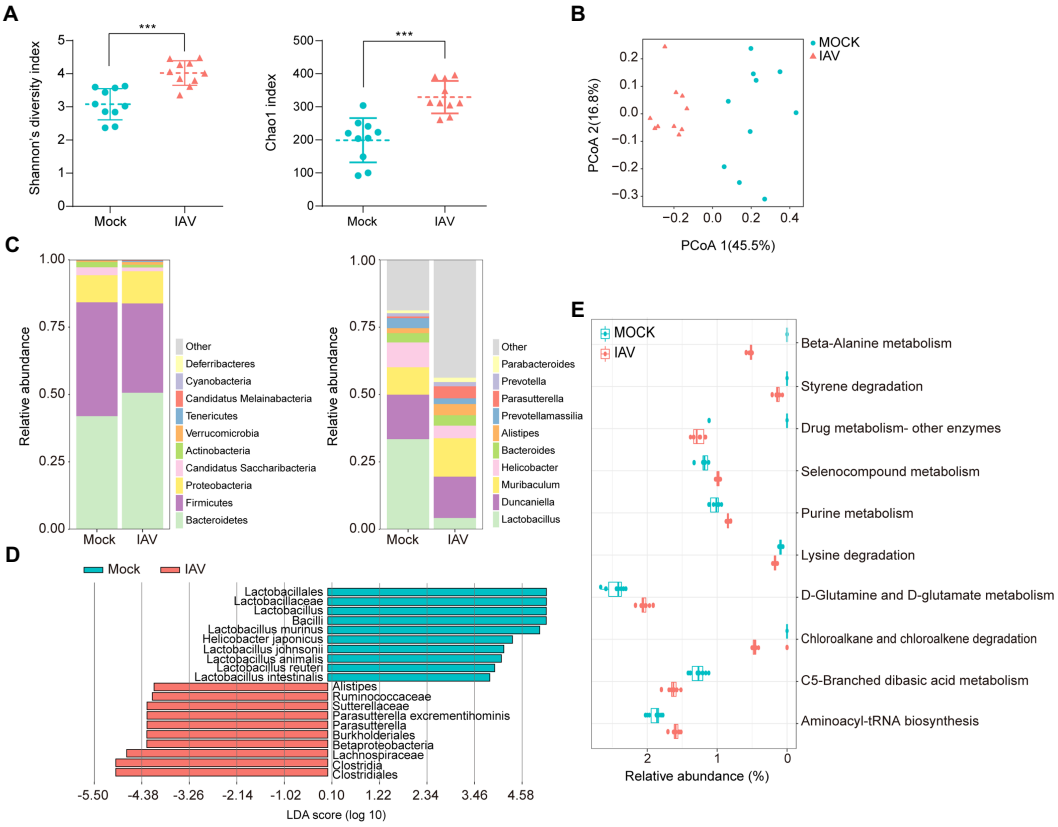

FIGURE 5
Characterization of gut microbiota and correlation between gut and oropharyngeal microbiota during IAV infection. **(A)** Shannon diversity and Chao1 indices of gut microbiota in IAV and mock groups. **(B)** 2D-PCoA plots of gut microbiota in mock and IAV groups **(C)** Relative abundance of the top 10 bacteria at the phylum and genus levels of gut microbiota in mock and IAV groups. **(D)** LEfSe analysis at the species level of gut microbiota in mock and IAV groups. **(E)** Top 10 significantly altered metabolic pathways of gut microbiota between mock and IAV groups. Pathway abundance prediction by PICRUSt2. Statistical analyses of Shannon index, Chao1 index and bacterial taxa abundance were conducted by using the Mann–Whitney test. *p<0.05, ** p<0.01, ***p<0.001.

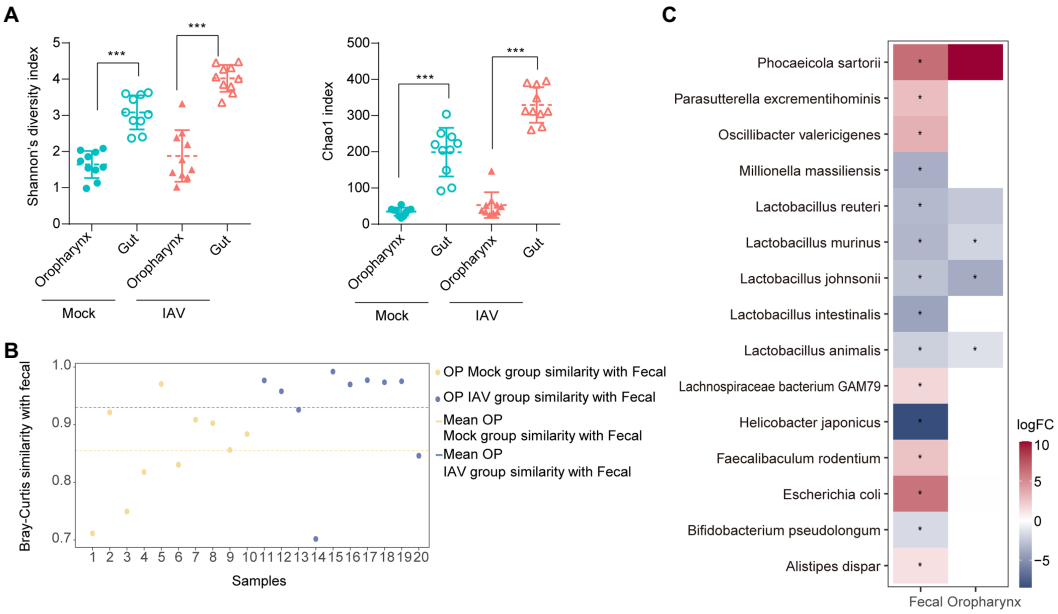

FIGURE 6
Comparison of oropharyngeal and gut microbiota during IAV infection **(A)** Comparison of the Shannon diversity and Chao1 indices between gut and oropharyngeal microbiota in IAV and mock groups. **(B)** Similarity analysis between gut and oropharyngeal microbiota in IAV and mock groups. **(C)** Distribution of gut and oropharyngeal differential species between mock and IAV groups screened by Lefse analysis. Statistical analyses of Shannon index, Chao1 index and bacterial taxa abundance were conducted by using the Mann–Whitney test. *p<0.05, ** p<0.01, ***p<0.001.

The remaining authors declare that the research was conducted in the absence of any commercial or financial relationships that could be construed as a potential conflict of interest.

Publisher's note

All claims expressed in this article are solely those of the authors and do not necessarily represent those of their affiliated organizations, or those of the publisher, the editors and the reviewers. Any product that may be evaluated in this article, or claim that may be made by its manufacturer, is not guaranteed or endorsed by the publisher.

Supplementary material

The Supplementary material for this article can be found online at: https://www.frontiersin.org/articles/10.3389/fmicb.2023.1129690/full#supplementary-material

References

An, S., Jeon, Y. J., Jo, A., Lim, H. J., Han, Y. E., Cho, S. W., et al. (2018). Initial influenza virus replication can be limited in allergic asthma through rapid induction of type III interferons in respiratory epithelium. *Front. Immunol.* 9:986. doi: 10.3389/fimmu.2018.00986

Bartley, J. M., Zhou, X., Kuchel, G. A., Weinstock, G. M., and Haynes, L. (2017). Impact of age, caloric restriction, and influenza infection on mouse gut microbiome: An exploratory study of the role of age-related microbiome changes on influenza responses. *Front. Immunol.* 8:1164. doi: 10.3389/fimmu.2017.01164

Bassis, C. M., Erb-Downward, J. R., Dickson, R. P., Freeman, C. M., Schmidt, T. M., Young, V. B., et al. (2015). Analysis of the upper respiratory tract microbiotas as the source of the lung and gastric microbiotas in healthy individuals. *MBio* 6:e00037. doi: 10.1128/mBio.00037-15

Bernard-Raichon, L., Colom, A., Monard, S. C., Namouchi, A., Cescato, M., Garnier, H., et al. (2021). A pulmonary lactobacillus murinus strain induces Th17 and RORγt+ regulatory T cells and reduces lung inflammation in tuberculosis. *J. Immunol.* 207, 1857–1870. doi: 10.4049/jimmunol.2001044

Blasco-Baque, V., Coupé, B., Fabre, A., Handgraaf, S., Gourdy, P., Arnal, J. F., et al. (2017). Associations between hepatic miRNA expression, liver triacylglycerols and gut microbiota during metabolic adaptation to high-fat diet in mice. *Diabetologia* 60, 690–700. doi: 10.1007/s00125-017-4209-3

Bogatyrev, S. R., Rolando, J. C., and Ismagilov, R. F. (2020). Self-reinoculation with fecal flora changes microbiota density and composition leading to an altered bile-acid profile in the mouse small intestine. *Microbiome.* 8:19. doi: 10.1186/s40168-020-0785-4

Chen, Y. J., Wu, H., Wu, S. D., Lu, N., Wang, Y. T., Liu, H. N., et al. (2018). Parasutterella, in association with irritable bowel syndrome and intestinal chronic inflammation. *J. Gastroenterol. Hepatol.* 33, 1844–1852. doi: 10.1111/jgh.14281

Curry, K. D., Wang, Q., Nute, M. G., Tyshaieva, A., Reeves, E., Soriano, S., et al. (2022). Emu: species-level microbial community profiling of full-length 16S rRNA Oxford Nanopore sequencing data. *Nat. Methods* 19, 845–853. doi: 10.1038/s41592-022-01520-4

Dominguez-Bello, M. G., Godoy-Vitorino, F., Knight, R., and Blaser, M. J. (2019). Role of the microbiome in human development. *Gut* 68, 1108–1114. doi: 10.1136/gutjnl-2018-317503

Douglas, G. M., Maffei, V. J., Zaneveld, J. R., Yurgel, S. N., Brown, J. R., Taylor, C. M., et al. (2022). PICRUSt2 for prediction of metagenome functions. *Nat. Biotechnol.* 38, 685–688. doi: 10.1038/s41587-020-0548-6

Fart, F., Rajan, S. K., Wall, R., Rangel, I., Ganda-Mall, J. P., Tingö, L., et al. (2020). Differences in gut microbiome composition between senior orienteering athletes and community-dwelling older adults. *Nutrients* 12:2610. doi: 10.3390/nu12092610

Fonseca, W., Lucey, K., Jang, S., Fujimura, K. E., Rasky, A., Ting, H. A., et al. (2017). Lactobacillus johnsonii supplementation attenuates respiratory viral infection via metabolic reprogramming and immune cell modulation. *Mucosal Immunol.* 10, 1569–1580. doi: 10.1038/mi.2017.13

Gao, D., Niu, M., Wei, S. Z., Zhang, C. E., Zhou, Y. F., Yang, Z. W., et al. (2020). Identification of a pharmacological biomarker for the bioassay-based quality control of a thirteen-component TCM formula (Lianhua Qingwen) used in treating influenza a virus (H1N1) infection. *Front. Pharmacol.* 11:746. doi: 10.3389/fphar.2020.00746

Gu, S., Chen, Y., Wu, Z., Chen, Y., Gao, H., Lv, L., et al. (2020). Alterations of the gut microbiota in patients with coronavirus disease 2019 or H1N1 influenza. *Clin. Infect. Dis.* 71, 2669–2678. doi: 10.1093/cid/ciaa709

Gu, L., Deng, H., Ren, Z., Zhao, Y., Yu, S., Guo, Y., et al. (2019). Dynamic changes in the microbiome and mucosal immune microenvironment of the lower respiratory tract by influenza virus infection. *Front. Microbiol.* 10:2491. doi: 10.3389/fmicb.2019.02491

Hirose, R., Daidoji, T., Naito, Y., Watanabe, Y., Arai, Y., Oda, T., et al. (2016). Long-term detection of seasonal influenza RNA in faeces and intestine. *Clin. Microbiol. Infect.* 22, 813.e1–813.e7. doi: 10.1016/j.cmi.2016.06.015

Ichinohe, T., Pang, I. K., Kumamoto, Y., Peaper, D. R., Ho, J. H., Murray, T. S., et al. (2011). Microbiota regulates immune defense against respiratory tract influenza a virus infection. *Proc. Natl. Acad. Sci. U. S. A.* 108, 5354–5359. doi: 10.1073/pnas.1019378108

Iuliano, A. D., Roguski, K. M., Chang, H. H., Muscatello, D. J., Palekar, R., Tempia, S., et al. (2018). Estimates of global seasonal influenza-associated respiratory mortality: a modelling study. *Lancet* 391, 1285–1300. doi: 10.1016/S0140-6736(17)33293-2.27

Joseph, S., Aduse-Opoku, J., Hashim, A., Hanski, E., Streich, R., Knowles, S. C. L., et al. (2021). A 16S rRNA gene and draft genome database for the murine oral bacterial community. *mSystems.* 6, e01222–e01220. doi: 10.1128/mSystems.01222-20

Kaul, D., Rathnasinghe, R., Ferres, M., Tan, G. S., Barrera, A., Pickett, B. E., et al. (2020). Microbiome disturbance and resilience dynamics of the upper respiratory tract during influenza a virus infection. *Nat. Commun.* 11:2537. doi: 10.1038/s41467-020-16429-9

Kim, S. J., Carestia, A., McDonald, B., Zucoloto, A. Z., Grosjean, H., Davis, R. P., et al. (2021). Platelet-mediated NET release amplifies coagulopathy and drives lung pathology during severe influenza infection. *Front. Immunol.* 12:772859. doi: 10.3389/fimmu.2021.772859

Ling, L. J., Lu, Y., Zhang, Y. Y., Zhu, H. Y., Tu, P., Li, H., et al. (2020). Flavonoids from Houttuynia cordata attenuate H1N1-induced acute lung injury in mice via inhibition of influenza virus and toll-like receptor signaling. *Phytomedicine* 67:153150. doi: 10.1016/j.phymed.2019.153150

Liong, S., Oseghale, O., To, E. E., Brassington, K., Erlich, J. R., Luong, R., et al. (2020). Influenza a virus causes maternal and fetal pathology via innate and adaptive vascular inflammation in mice. *Proc. Natl. Acad. Sci. U. S. A.* 117, 24964–24973. doi: 10.1073/pnas.2006905117

Lv, L., Gu, S., Jiang, H., Yan, R., Chen, Y., Chen, Y., et al. (2021). Gut mycobiota alterations in patients with COVID-19 and H1N1 infections and their associations with clinical features. *Commun Biol.* 4:480. doi: 10.1038/s42003-021-02036-x

Lynch, S. V., and Pedersen, O. (2016). The human intestinal microbiome in health and disease. *N. Engl. J. Med.* 375, 2369–2379. doi: 10.1056/NEJMra1600266

McCullers, J. A. (2014). The co-pathogenesis of influenza viruses with bacteria in the lung. *Nat. Rev. Microbiol.* 12, 252–262. doi: 10.1038/nrmicro3231

McMullen, C., Alexander, T. W., Léguillette, R., Workentine, M., and Timsit, E. (2020). Topography of the respiratory tract bacterial microbiota in cattle. *Microbiome.* 8:91. doi: 10.1186/s40168-020-00869-y

Okada, K., Matsushima, Y., Mizutani, K., and Yamanaka, K. (2020). The role of gut microbiome in psoriasis: oral administration of *Staphylococcus aureus* and *streptococcus danieliae* exacerbates skin inflammation of imiquimod-induced psoriasis-like dermatitis. *Int. J. Mol. Sci.* 21:3303. doi: 10.3390/ijms21093303

Pan, F., Zhang, L., Li, M., Hu, Y., Zeng, B., Yuan, H., et al. (2018). Predominant gut *lactobacillus murinus* strain mediates anti-inflammaging effects in calorie-restricted mice. *Microbiome.* 6:54. doi: 10.1186/s40168-018-0440-5

Planet, P. J., Parker, D., Cohen, T. S., Smith, H., Leon, J. D., Ryan, C., et al. (2016). Lambda interferon restructures the nasal microbiome and increases susceptibility to Staphylococcus aureus superinfection. *MBio* 7, e01939–e01915. doi: 10.1128/mBio.01939-15

Puchta, A., Verschoor, C. P., Thurn, T., and Bowdish, D. M. (2014). Characterization of inflammatory responses during intranasal colonization with Streptococcus pneumoniae. *J. Vis. Exp.* 83:e50490. doi: 10.3791/50490

Qin, N., Zheng, B., Yao, J., Guo, L., Zuo, J., Wu, L., et al. (2015). Influence of H7N9 virus infection and associated treatment on human gut microbiota. *Sci. Rep.* 5:14771. doi: 10.1038/srep14771

Rattanaburi, S., Sawaswong, V., Chitcharoen, S., Sivapornnukul, P., Nimsamer, P., Suntronwong, N., et al. (2022). Bacterial microbiota in upper respiratory tract of COVID-19 and influenza patients. *Exp. Biol. Med.* 247, 409–415. doi: 10.1177/15353702211057473

Renne, R., Brix, A., Harkema, J., Herbert, R., Kittel, B., Lewis, D., et al. (2009). Proliferative and nonproliferative lesions of the rat and mouse respiratory tract. *Toxicol. Pathol.* 37, 5S–73S. doi: 10.1177/0192623309353423

Scales, B. S., Dickson, R. P., LiPuma, J. J., and Huffnagle, G. B. (2014). Microbiology, genomics, and clinical significance of the *Pseudomonas fluorescens* species complex, an unappreciated colonizer of humans. *Clin. Microbiol. Rev.* 27, 927–948. doi: 10.1128/CMR.00044-14

Sencio, V., Gallerand, A., Gomes Machado, M., Deruyter, L., Heumel, S., Soulard, D., et al. (2021). Influenza virus infection impairs the gut's barrier properties and favors

secondary enteric bacterial infection through reduced production of short-chain fatty acids. *Infect. Immun.* 89:e0073420. doi: 10.1128/IAI.00734-20

Tang, C., Kamiya, T., Liu, Y., Kadoki, M., Kakuta, S., Oshima, K., et al. (2015). Inhibition of dectin-1 signaling ameliorates colitis by inducing lactobacillus-mediated regulatory T cell expansion in the intestine. *Cell Host Microbe* 18, 183–197. doi: 10.1016/j.chom.2015.07.003

Wang, R., Zhu, Y., Ren, C., Yang, S., Tian, S., Chen, H., et al. (2021). Influenza a virus protein PB1-F2 impairs innate immunity by inducing mitophagy. *Autophagy* 17, 496–511. doi: 10.1080/15548627.2020.1725375

Wen, Z., Xie, G., Zhou, Q., Qiu, C., Li, J., Hu, Q., et al. (2018). Distinct nasopharyngeal and oropharyngeal microbiota of children with influenza a virus compared with healthy children. *Biomed. Res. Int.* 2018:6362716. doi: 10.1155/2018/6362716

Wilck, N., Matus, M. G., Kearney, S. M., Olesen, S. W., Forslund, K., Bartolomaeus, H., et al. (2017). Salt-responsive gut commensal modulates TH17 axis and disease. *Nature* 551, 585–589. doi: 10.1038/nature24628

Yang, Y., Che, Y., Liu, L., Wang, C., Yin, X., Deng, Y., et al. (2022). Rapid absolute quantification of pathogens and ARGs by nanopore sequencing. *Sci. Total Environ.* 809:152190. doi: 10.1016/j.scitotenv.2021.152190

Yildiz, S., Mazel-Sanchez, B., Kandasamy, M., Manicassamy, B., and Schmolke, M. (2018). Influenza a virus infection impacts systemic microbiota dynamics and causes quantitative enteric dysbiosis. *Microbiome.* 6:9. doi: 10.1186/s40168-017-0386-z

Yildiz, S., Pereira Bonifacio Lopes, J. P., Bergé, M., González-Ruiz, V., Baud, D., Kloehn, J., et al. (2020). Respiratory tissue-associated commensal bacteria offer therapeutic potential against pneumococcal colonization. *elife* 9:e53581. doi: 10.7554/eLife.53581

Frontiers in Microbiology

Explores the habitable world and the potential of microbial life

The largest and most cited microbiology journal which advances our understanding of the role microbes play in addressing global challenges such as healthcare, food security, and climate change.

Discover the latest Research Topics

See more →

Frontiers

Avenue du Tribunal-Fédéral 34
1005 Lausanne, Switzerland
frontiersin.org

Contact us

+41 (0)21 510 17 00
frontiersin.org/about/contact